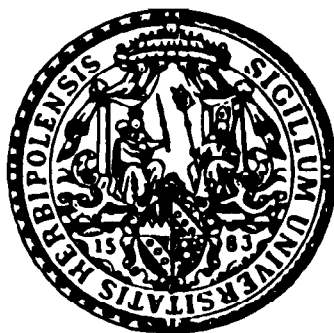# Infrared photodissociation spectroscopy of ionic hydrocarbons: microsolvation and protonation sites

Dissertation zur Erlangung des

naturwissenschaftlichen Doktorgrades

der Julius-Maximilians-Universität Würzburg

vorgelegt von

Dipl.-Phys. Horia - Sorin Andrei

aus Bukarest

Würzburg 2007

Eingericht am:_____

bei der Fakultät für Chemie und Pharmazie

1.
Gutachter:_____

2.
Gutachter:_____

der Dissertation

1. Prüfer:_____

2. Prüfer:_____

3. Prüfer:_____

des Öffentlichen Promotionskolloquiums

Tag des Öffentlichen Promotionskolloquiums:_____

Doktorurkunde ausgehändigt am:_____

Table of contents

1. Introduction

1.1. Ions and ionic radicals

Molecular ions (cations of stable molecules, protonated or deprotonated molecules, radical cations) play key roles in chemical reactions. Such species are considered to be highly relevant, because their long-distance interaction with the environment is much more significant than the one of the neutrals. It results that their detailed characterization is an important step for understanding and controlling the reactions in which they appear. A key element in explaining the physical and chemical properties of molecules, ions, and molecular complexes is their structure. This is a topic of great experimental and theoretical significance as it provides the basis for predicting the properties of complex molecular systems.

To this end, spectroscopic investigations are probably the most convenient experimental approaches. Done either in condensed phase or in gaseous phase, spectroscopy provides reliable fingerprinting, allowing for positive identification and separation of various isomers of the same molecular formula. Spectroscopic fingerprinting techniques have been already successfully used for identification of unknown species. A category of such unknown species whose properties are highly relevant in chemistry are transient species (ions, radicals).

Spectroscopic investigations of unknown species have been successful, for example in astrophysics. More than 146 different molecules and highly reactive ions and radicals have already been identified via infrared spectroscopic observations of nebulae, interstellar clouds and circumstellar envelopes.[1],[2],[3] Such species can also be found in planetary atmospheres, where they play an important role in the chemical processes occurring there.[4],[5],[6] Other environments rich in radicals and charged species are combustion flames; here, they are believed to play key roles in processes like soot formation.[7],[8],[9]

Knowledge about structure of molecules is of great relevance also for understanding biological processes.[10] Intermolecular interaction like H-bonding or molecular stacking

provide key information for understanding the conformation and function of amino acids, peptides, proteins, and DNA.[11] Ion-molecule interactions are encountered when studying the helical structure of DNA in solution, which is influenced by its dense cationic atmosphere.[12] Such information can be provided, for example, via gas-phase investigations of neutral, ionized, or protonated molecular complexes. Thus, spectroscopy can be used not only for obtaining clues about the equilibrium structures of the reactants and reaction products, but also for revealing details of the chemical reactions mechanisms.

It is relevant to note that all the examples presented above are dealing with radicals and charged species investigated either isolated or surrounded by well-controlled environments. Given the easiness with which such reactive species undergo changes (via chemical reactions, charge or proton transfer, and so on), this type of studies appears as the only reliable option.

1.2. State of the art in gas-phase spectroscopy

Gas-phase investigations come to complement the condensed-phase NMR, IR and UV-VIS spectroscopy and X-ray crystallography studies which, until recently, have provided the majority of information about molecular entities.[13],[14],[15] Although these methods have yielded valuable data about the properties of ions, radicals and molecular complexes, they all share the disadvantage that their results are distorted because of the strong perturbation caused by the environment (solvent, other radicals or ions). Complementary to these studies, gas-phase investigations of isolated molecules, radicals or cations offer a wealth of information about their intrinsic properties. For example, high pressure mass spectrometry (HPMS) studies are excelling all other ascertainments of binding energies of molecular species toward ligands.

The greatest problem faced by gas-phase experiments is the low density of the investigated species. This makes direct methods like radiation absorption at best hard to apply and, quite often, unable to yield meaningful results. A workaround is to measure not the reduction in intensity of the excitation beam but to use a consequence of the photon absorption (such as electronic emission, dissociation of a molecule or a complex, a chemical reaction, etc.). All the spectroscopic methods enumerated in the following belong to this category of action spectroscopy.[16]

The most widely used spectroscopic techniques for studying molecular aggregates in gas phase are the zero kinetic energy photoelectron spectroscopy (ZEKE),[17],[18],[19] the mass-analyzed threshold ionization (MATI),[20],[21] the autoionization detected IR

spectroscopy (ADIR),[22],[23] the photoionization efficiency spectroscopy (PIE), and the IR (multi)photodissociation spectroscopy (IRPD and IRMPD). The methods based on the use of IR radiation are especially interesting. As the IR spectroscopic methods probe directly the vibrational energy levels, they provide results closely connected with the structure of the investigated species. The alterations of the IR spectra that occur together with changes in the environment can reveal fundamental parameters of the intermolecular interactions as well as details of the reactivity of the investigated species. Control over the number and species of molecules or atoms surrounding the investigated species also opens the way toward understanding fundamental mechanisms like proton transfer and about the solvation onset.[24],[25],[26],[27],[28],[29],[30]

As mentioned above, a number of gas-phase spectroscopic methods are available to the present-day scientist for investigating properties of isolated ions or weakly bound complexes. In the present work, single photon IR photodissociation is used in conjunction with an electron impact ion source for investigating weakly bound complexes. In the following, some spectroscopic methods which yield similar or complementary results will be described. As beside the spectroscopic technique, also the ionization technique and the cluster aggregation path employed are relevant for the outcome of such a gas-phase experiment, few important cation cluster production techniques will be shortly presented.

ZEKE & MATI Both these methods originate in the basic photoelectron spectroscopy. There, a light source is tuned over the ionization threshold of a molecule (A) and the vibrational energy levels of the resulting cation (A$^+$) are extracted by analyzing the kinetic energy distribution of the electrons ejected from A. The basic idea behind ZEKE was to delay by few μs (with respect to the light pulse) the pulsed extraction field used to feed the electrons into the kinetic energy analyzer.[18],[19],[21] The delay allows the kinetic electrons to leave the interaction volume and the pulsed extraction field is then responsible for ionizing long-lived Rydberg states, placed between 1-2 cm^{-1} and 6-8 cm^{-1} below the ionization threshold. As the electron transferred by the light pulse into a Rydberg state has little influence over the molecule around which orbits, it follows that the vibrational properties extracted are essentially linked with A$^+$. MATI follows the same scheme, but is based on the detection of the resulting ions.[20] As the ions are characterized by much lower mobility, a small field is used for separating the ions produced by the light pulse from the near-threshold neutrals. As implied by its name, the method is useful for investigations requiring species identification (clusters, radicals). Specially designed shapes of the electrical pulses and narrow band lasers essential for improving the resolution of the

method (reference [31] quotes a resolution of 0.06 cm^{-1}). Such high-resolution spectra allow for determination of highly accurate value for the ionization energy of a molecule, of frequencies for vibrational modes of a molecule or a cluster, and, for small A$^+$ ions, of rotational constants. Dissociation energy of a complex between a cation and a ligand (A$^+\cdots$L) can be determined using MATI spectroscopy, by monitoring the intensity of the signal corresponding to A$^+$ as a function of the excess internal energy of the complex. Both methods are reaching their limits when dealing with proton stretch vibrations (O-H, N-H, C-H). This difficulty comes partly from poor Franck-Condon factors between the ground and Rydberg states and also from band congestion in electronic transitions used as the final step of the measurement.[22]

Recently, reports have been published regarding the use of these spectroscopic schemes for investigating many molecules. Among the reported experimental results on substituted arenes, one can find MATI investigations of H-bonded 3-methylindole$\cdots$C$_6$H$_6$ complexes,[32] of p-methylphenol, p-ethylphenol, and p-n-propylphenol[33],[34] as well as ZEKE investigations of indole-3-ethanol,[35] 4-aminopyridine,[36] pyrazine,[37] of the p-aminobenzoic acid,[38] and the m-aminobenzoic acid.[39]

ADIR This method is an enhancement of ZEKE and MATI. While in the standard ZEKE and MATI the elimination of the Rydberg electron is assisted by an electric field, ADIR uses a purely optic approach. Thus, after excitation of the ground vibrational state of a high Rydberg state (via the standard two-color double-resonance technique - see below), an IR source is scanned over vibrational range of the ion core. Resonant vibrational excitation results then in autoionization.[22],[23] The method is valuable as it yields directly the IR spectrum of the ion core, including weaker combination bands.[40],[41]

IRPD This method is based on the dissociation of a weakly bound complex upon resonant absorption of one IR photon. In the following, it will be shown an outline of the IRPD scheme applied to cationic complexes (A$^+\cdots$L$_n$). As there are many ways for producing cationic complexes, few of the methods will be presented in the following paragraphs. The IRPD process implies the absorption of an IR photon via excitation of an IR active vibration of the complex; this is followed by internal vibrational energy redistribution (IVR) and leads to the evaporation of (some of) the ligands, resulting in the production of a A$^+\cdots$L$_m$ fragment.[42],[43],[44] The primary consequence of this single photon absorption approach is that only weak intermolecular bonds are broken. Thus, the IR spectrum of the A$^+\cdots$L$_n$ complex is obtained by monitoring the yield of A$^+\cdots$L$_m$ fragments as a function of the IR wavelength. The experiment is usually done in a mass spectrometric

setup which allows mass selection of both the parent and the fragment species. The IRPD scheme has specially been devised in order to provide enhanced detection, low background, and high species selectivity. Despite its simplicity, IRPD spectroscopy can provide detailed molecular structure of the investigated species, as well as valuable information regarding the way solvent molecules aggregate around and interact with the investigated ion. If only a very weakly bound ligand is attached to the target ion (for example a rare gas atom), the resulting IR spectrum is essentially the same with the one of the bare ion (messenger technique).

Worldwide, a number of research teams are using this method for exploring the structure of weakly bound charged complexes. Among the most fascinating results are the recent investigations of protonated water clusters[45],[46] and the equally recent monitoring of the dynamic of the photoionization-induced hydrophobic-to-hydrophilic switching in phenol···Ar_n clusters.[47] Other subjects investigated using IRPD are proton wires,[48],[49] microsolvation of metal ions,[50],[51] or biologically-relevant molecules.[52],[53],[54]

IRMPD This technique is similar with the single photon induced dissociation technique described above, the main difference being that in the present case a large number of photons are pumped into the same vibrational mode. The de-excitation of the pumped vibrational mode occurs via IVR in less that 1 ns after excitation; thus, the method is best described as multiple photon excitation, in contrast to the coherent multiphoton excitation.[55] The internal energy thus accumulated is spent into the breaking of intramolecular covalent bonds. Thus, the method allows the recording of an IR spectrum with detection sensitivity, background level, and species selectivity similar with the one of the obtained via IRPD of weakly bound clusters. At the same time, as this method is applicable directly on bare ions, there is no messenger anymore, thus eliminating the (small) distortion induced by the ligand.

The multiple photon excitation approach avoids the anharmonicity bottleneck of the coherent multiphoton excitation which would otherwise limit the use of one controlled, monochromatic light source for exciting the ion. To this end, the best suited light source is the free electron laser (FEL). The FEL allows not only for high-intensity, tunable, narrow-band beams to be produced, but also has the advantage of operating over a broad range in the IR domain (either via fundamental emission or via harmonic generation). Recently, FEL were used for recording the IR spectra of model protonated dipeptides like N-acetyl-alanine and alanyl-histidine,[56] of various protonated aromatic hydrocarbons,[55],[57] as well as of metal cations binding to organic molecules.[58]

A critical aspect of gas phase studies of charged complexes is the way the investigated species are produced. Often, complexes between a charged moiety and one or more ligands ($A^+ \cdots L_n$) are generated in a supersonic expansion. Spectroscopic information of $A^+ \cdots L_n$ is then extracted via one of the methods presented above (PIE, MATI, ZEKE, IRPD, ADIR, etc).

The methods of ionizing or producing molecules in high-lying Rydberg states via photon absorption(s) have both advantages and downturns. Basically, one can use direct one photon excitation for pumping one molecule from its ground electronic state to a Rydberg state. This approach is not easily applicable, as in implies the use of a narrow-band tunable light source in the UV range (usually at 7 ... 9 eV or higher). Another approach is to use non resonant multiple photon absorption, which would again require a powerful tunable light source in the range of 3.5 ... 4.5 eV (for non resonant two-photon absorption). Finally, the most successful method uses resonant excitation of the molecule to an electronically excited state placed at 3.5 ... 4.5 eV, followed by another resonant absorption process which brings the molecule into a Rydberg state. The method is appealing as the ions (ion cores) produced this way are readily produced in their ground vibrational state (vibrationally cold). However, this resonance enhanced multiphoton ionization (REMPI) method has a major drawback when applied to weakly bound complexes, as it often generates weakly bound $A^+ \cdots L$ complexes not in the global minimum of their intermolecular potential energy surface (PES). This limitation is the result of the specific sequencing of the events leading to the production of $A^+ \cdots L$. Having the cluster aggregation take place before ionization is likely to result in a complex having its structure "frozen" in an arrangement similar with the one corresponding to the global minimum on the PES of the precursor $A \cdots L$. It follows that, if the preferred ligand binding site changes from $A \cdots L$ to $A^+ \cdots L$, the spectroscopic studies of $A^+ \cdots L$ prepared by photoionization of $A \cdots L$ will be limited by the Franck-Condon principle. This sets limits for the population of the most stable structure of $A^+ \cdots L$ if this structure is largely different from the global minimum of $A \cdots L$. Unfortunately, such a situation is quite common for $A \cdots L$ / $A^+ \cdots L$ dimers with both polar and nonpolar L.

A different approach, which overcomes this limitation, can be used for producing ro-vibrationally cold $A^+ \cdots L_n$ complexes. The $A^+ \cdots L_n$ complexes are produced in a supersonic plasma expansion by electron ionization (EI) of A followed by cluster aggregation. This method predominantly produces of the most stable isomer of a given $A^+ \cdots L_n$ complex, independent of the most stable structure of neutral $A \cdots L_n$. The excellent

performance of this method has been proven via comparisons of the IR spectra of Ph(enol)$^+$···Ar$_n$,[25] An(iline)$^+$···Ar$_n$,[29] and In(dole)$^+$···Ar$_n$[26] obtained via EI followed by cluster aggregation with their corresponding photoionization (PIE, ZEKE, MATI) or REMPI-IR spectra. The IR spectra of these EI-generated cations have evidenced the existence of isomers which previously have completely escaped detection and which were interpreted as global minimum structures. The major drawback of the method is the considerably larger molecular fragmentation produced by the colision of the precursor A with the ~100 eV electrons used for ionization.

Other widespread methods for generation of ions and weakly bound complexes in gas phase are:

* the matrix-assisted laser desorption/ionization (MALDI), which brings into gas-phase ions of molecules frozen into a matrix which strongly absorbs in the UV output of a laser;[59],[60]

* electrospray;[59],[61]

* laser ablation.[50]

A highly attractive aspect of spectroscopic studies of isolated species is that they can directly be compared with theoretical results obtained via quantum chemical calculations. Such comparisons are valuable both for theoreticians and for experimentalists. For theoreticians, they provide feedback on how well a theory is able to reproduce the features observed in experimental investigations. For experimentalists, a good match between experiment and quantum chemical predictions increases the usability of the theoretical evaluations. For example, theoretical information which cannot be directly derived from experiment (like atomic charge distributions, details of the potential energy surface - PES, etc.) can further be used to give insight in the structure and reactivity of molecules. Also spectral information which, for fundamental or practical reasons, cannot be experimentally obtained, can be extrapolated from quantum chemical calculations. Results obtained on the experimental setup used in the present work have been successfully matched by high-level calculations, resulting over the last 13 years in comprehensive IR spectroscopic studies of small cations and protonated species.[62],[63],[64] More recently, such experimental and theoretical characterization were combined in studies of larger systems.[65]

1.3. Structure and objectives of this work

The experimental results presented in this work have all been obtained via single photon IRPD. In particular, the experimental setup presented here is used to study the dissociation of positively charged complexes upon excitation with a single IR photon with

the frequency in the range of proton stretch vibrations (ν_{C-H}, ν_{N-H}, ν_{O-H} $\equiv$ 2500 ... 4000 cm^{-1}). This setup was previously used to obtain IR spectra of small cations and protonated species,[62],[63],[64] as well as of larger cations.[65] The production of complexes is based on EI, which, as seen above, has the clear advantage of predominantly generating the most stable complexes over the method based on REMPI. Indeed, having the cluster aggregation take place after ionization is more likely to produce global minimum structures than clustering ligands around a neutral molecule followed by resonant ionization of that molecule. This latter approach is usually producing complexes with structures similar with the global minimum in the PES of the corresponding neutral complex.

The present work deals with two major topics. First of all, cations of aromatic molecules (A$^+$) are identified and characterized via IRPD spectroscopy of their complexes with nonpolar ligands (**Chapter 3** and **Chapter 5**). Following these experiments, similar investigations are done on the protonated forms of the same molecules (**Chapter 4** and **Chapter 6**). Finally, continuing the line of spectral investigations on protonated species, the structure and properties of the ethyl cation are identified and characterized via its complexation and microsolvation (**Chapter 7**).

(Substituted) aromatic molecules and their cations play an important role in biological and chemical recognition as well as organic reaction mechanisms.[66],[67],[68],[69] Their protonation and deprotonation are also important processes in organic chemistry and biochemistry; for example, protonated aromatic molecules (AH$^+$) are short-lived reaction intermediates which appear in electrophilic aromatic substitutions where they determine reaction rates and product selectivities,[70] in combustion flames,[9] and in models of extraterrestrial hydrocarbon plasmas.[71] In the present work, two aromatic molecules are investigated: 1-naphthalenole (1-Np) and imidazole (Im). They have been chosen based on their chemical relevance and for expanding previous studies made on the same experimental setup. Both 1-Np and Im can be encompassed in the same group of aromatic molecules with acidic YH$_k$ groups. Researching the topology of the interaction potential of such aromatic cations with nonpolar and polar ligands (A$^+\cdots$L) is relevant, as it was demonstrated to differ qualitatively from that of neutral A$\cdots$L. The difference stems from the significant additional electrostatic and inductive attraction arising from the positive charge.[17],[66],[72],[73],[74] As a consequence, the equilibrium structures and interaction energies of A$^+\cdots$L are often different from the ones of A$\cdots$L. Illustrative examples are Ph$^+\cdots$Ar,[25],[75],[76],[77] An$^+\cdots$Ar,[29] and In$^+\cdots$Ar;[26] they all have H-bound global minima in the ground electronic state of the cation, whereas the π-bound isomers (which were identified as global minima in the ground electronic state of the corresponding neutral complexes) are only local

minima. This change will trigger changes in both the chemical activity and the solvation mechanisms. Such a switch in the ligand recognition motif occurs also upon the protonation of aromatic molecules with acidic YH_k groups (AH^+): in this case both complexes of protonated phenol with Ar and with N_2 ($PhH^+\cdots Ar$ and $PhH^+\cdots N_2$)[24],[78],[79] favor H-bonds over π-bonds. This is not true for arenes without YH_k groups (such as benzene - Bz): the most stable dimers of their cation or protonated forms with Ar and N_2 ($Bz^+\cdots L$ and $BzH^+\cdots L$, L = Ar, N_2)[27],[28],[80],[81] feature π-bonds, because CH protons are only weakly acidic even in the ground state of the cation or protonated species.[28]

The experimental results presented in *Chapter 3*, regarding the size-selected $1\text{-}Np^+\cdots L_n$ complexes (L = Ar, N_2) have been published in reference [82]. This study of $1\text{-}Np^+\cdots L_n$ complexes (L = Ar, N_2) is an extension of studies done already on Bz^+ and on Ph^+. Indeed, $1\text{-}Np^+\cdots L_n$ complexes (L = Ar, N_2) serve as a suitable model for solvation of $1\text{-}Np^+$ in a nonpolar solvent. From this viewpoint, the competition between H-bonding and π-bonding and its consequences on the cluster growth are particularly interesting. Another aspect which has prompted this investigation is that 1-Np is a strong photoacid (the acidity of the OH group increases drastically upon electronic excitation or ionization). Its photoacidity may eventually promote proton transfer to a suitable solvent;[83],[84],[85] such proton transfer processes are among the most fundamental reactions occurring in chemical and biological systems. As the properties of the proton transfer process depend sensitively on the environment, the nonpolar environments used here are a first step toward understanding the unfolding of these processes.

The protonation of 1-Np (*Chapter 4*) has been previously observed in superacid solutions[86] by means of NMR spectroscopy and it has been found to occur exclusively at the ring hosting the OH group, in para position with respect to the OH group. This is at odds with studies done for PhH^+ in superacid solutions,[87] that prove the existence of at least of one O-bound and at least one C-bound isomer. The aim of the investigation presented here is to give support to the idea that, like Ph, 1-Np can be protonated at more than one site and that IRPD techniques can be used to select well-defined isomers of $1\text{-}NpH^+$. Analysis of theoretical data allows to first estimates for site-sensitive proton affinity of 1-Np.

Chapter 5 presents experimental and theoretical results of an IRPD study of $Im^+\cdots L_n$ complexes (L = Ar, N_2); the experimental results have been published in reference [88]. Im is a heterocyclic aromatic molecule which occurs as an essential constituent in many

biomolecular building blocks, such as the DNA bases adenine and guanine, and the histidine residue of proteins.[89] In aqueous biological environments, Im, Im[+], as well as ImH[+] are involved in electron transfer during photosynthesis, in many biologically important enzymatic processes, and in protein structure determination.[89],[90],[91],[92] Im[(+)] is interesting also from technological viewpoints, as it can simultaneously protonate at one N atom and deprotonate at the other N atom, thus acting as a proton shuttle. Indeed, there are studies regarding the use of Im in the proton exchange membranes of modern fuel cells as a proton wire - building molecule. The aim of the present spectroscopic study is to elucidate the interaction of the radical cation of this basic biomolecular building block with a hydrophobic environment. Thus, the investigations are selectively focused on the microsolvation of Im[+] by a well-defined number of nonpolar ligands (L = Ar, N_2).

Fundamental understanding of processes like proton shuttling in Im requires the detailed knowledge of the intermolecular potential of Im, Im[+] and ImH[+] interacting with the surrounding environment. In this light, in *Chapter 6* is studied the microsolvation of ImH[+] in an nonpolar environment (Ar or N_2) as well as its microhydration. Part of the experimental results presented here have been published in reference [93]. The interaction of ImH[+] with solvent molecules takes place via well-defined families of binding sites: ligand molecules can interact with the π-electron system of the aromatic ring (π-bond) or form H-bonds to the acidic protons of Im (N-H$\cdots$L or C-H$\cdots$L). The preferred binding motif of all dimers strongly depends on the protonation state of Im as well as on fundamental properties of L, such as its proton donor and proton acceptor abilities. This work aims to elucidate the interaction of ImH[+] with a hydrophobic or hydrophilic environment. Thus, the investigations are selectively focused on the microsolvation of ImH[+] by a well-defined number of nonpolar ligands (L = Ar, N_2) as well as on its interaction with a controlled number of H_2O molecules.

Chapter 7 is presenting an experimental and theoretical analysis pertaining to the structure of the ethyl cation ($C_2H_5^+$). This is an alkyl cation fundamental for hydrocarbon mass spectrometry,[94] which has recently been identified in the mass spectra recorded in the atmosphere of Saturn's moon Titan.[95] In laboratory environments it is frequently used as chemical ionization reagent for investigating proton transfer toward a wealth of molecules.[96] Despite its ubiquity, there is still a lack of direct evidence of its structure. Indeed, two largely different geometries are conceptually being considered for its structure: the classical open geometry ($[H_2CCH_3]^+$) and the nonclassical geometry, where one proton bridges the double C=C bond of an ethylene molecule (H_2CCH_2). The viewpoint of the classical chemistry is based on the structure of the ethyl radical; indeed, for this entity

there is a large experimental body showing that its equilibrium structure is an open one ($C_2H_5 = H_2CCH_3$).[97],[98],[99],[100],[101] At the same time, theoretical studies of $C_2H_5^+$[102] and of the related $C_2H_7^+$[103],[104],[105] and $C_3H_9^+$[106] suggest that in its equilibrium structure, $C_2H_5^+$ has, indeed, one proton bridging the double C=C bond. These studies are supported by photoelectron spectra which exhibit a gradual onset of the photoionization signal, possibly indicating a significant change in geometry upon ionization.[107],[108],[109] In the present work, unique IRPD spectroscopic results obtained on $C_2H_5^+\cdots L_n$ complexes with nonpolar ligands (Ar, N_2, CO_2, CH_4) are presented. The aim of this investigation is to elucidate the structure of $C_2H_5^+$ and its dependence on the solvation environment.

References

[1] Stutzki J., Winnewisser G., The Cologne Database for Molecular Spectroscopy, 2007, http://www.ph1.uni-koeln.de/vorhersagen/

[2] Mueller H.S.P., Schlöder F., Stutzki J., Winnewisser G. *J. Mol. Struct.* **742** (2005) 215

[3] Mueller H.S.P., Thorwirth S., Roth D.A., Winnewisser G. *Astronomy and Astrophysics* **370** (2001) 49

[4] Levine J.S., The photochemistry of atmospheres: Earth, the other planets, and comets, Academic Press, Orlando (1985)

[5] Ausloos P., Kinetics of the ion-molecule reactions, Plenum Press, New York (1979)

[6] Ausloos P., Interactions between ions and molecules, Plenum Press, New York (1975)

[7] Richter H., Howard J.B. *Prog. Energ. Combust.* **26** (2000) 565

[8] Calcote H.F. *Combust. Flames* **126** (2001) 1607

[9] Fialkov A.B., Dennenbaum J., Homann K.H. *Combust. Flame* **125** (2001) 763

[10] Weinkauf R., Schermann J.P., de Vries M.S., Kleinermanns K. *Eur.Phys. J. D* **20** (2002) 309

[11] Jurecka P., Hobza P. *J. Am. Chem. Soc.* **125** (2003) 15608

[12] Orozco M., Luque F.J. *Chem. Rev.* **100** (2000) 4187

[13] Reed C.A., Kim K.C., Stoyanov E.S., Stasko D., Tham F.S., Mueller L.J., Boyd P.D.W. *J. Am. Chem. Soc.* **125** (2003) 1796

[14] Perkampus H.H., Baumgarten E. *Angew. Chem. - Intl. Ed.* **3** (1964) 776

[15] Olah G.A., White A.M., O'Brien D.H. *Chem. Rev.* **70** (1970) 561

[16] Duncan M. *Int. J. Mass Spectrom.* **200** (2000) 545

[17] Mueller-Dethlefs K., Dopfer O., Wright T.G. *Chem. Rev.* **94** (1994) 1845

[18] Cockett M.C.R. *Chem. Soc. Rev.* **34** (2005) 935

[19] Fischer I. *Int. J. Mass. Spectrom.* **216** (2002) 131

[20] Zhu L.C., Johnson P. *J. Chem. Phys.* **94** (1991) 5769

[21] Merkt F. *Annu. Rev. Phys. Chem.* **48** (1997) 675

[22] Fujii A., Iwasaki A., Ebata T., Mikami N. *J. Phys. Chem. A* **101** (1997) 5963

[23] Ebata T., Fujii A., Mikami N. *Int. Rev. Phys. Chem.* **17** (1998) 331

[24] Solca N., Dopfer O. *J. Chem. Phys.* **120** (2004) 10470

[25] Solca N., Dopfer O. *J. Phys. Chem. A* **105** (2001) 5637

[26] Solca N., Dopfer O. *Phys. Chem. Chem. Phys.* **6** (2004) 2732

[27] Dopfer O., Olkhov R.V., Maier J.P. *J. Chem. Phys.* **111** (1999) 10754

[28] Solca N., Dopfer O. *Chem. Eur. J.* **9** (2003) 3154

[29] Solca N., Dopfer O. *Eur. Phys. J. D* **20** (2002) 469

[30] Solca N., Dopfer O. *J. Phys. Chem. A* **106** (2002) 7261

[31] Hollenstein U., Seiler R., Schmutz H., Andrist M., Merkt F. *J. Chem. Phys.* **115** (2001) 5461

[32] Georgiev S., Neusser H.J. *J. Electr. Spectr. Rel. Phenom.* **142** (2005) 207

[33] Li C.Y., Lin J.L., Tzeng W.B. *J. Chem. Phys.* **120** (2004) 10513

[34] Li C.Y., Lin J.L., Tzeng W.B. *J. Chem. Phys.* **122** (2005) art.no.44311

[35] Gu Q.L., Basu S., Knee J.L. *J. Phys. Chem. A* **111** (2007) 1808

[36] He Y.G., Wu C.Y., Kong W. *J. Chem. Phys.* **120** (2004) 7497

[37] Riese M., Gaber A., Grotemeyer J. *Z. Phys. Chem.* **221** (2007) 663

[38] He Y.G., Wu C.Y., Kong W. *J. Chem. Phys.* **121** (2004) 3533

[39] He Y.G., Wu C.Y., Kong W. *J. Chem. Phys.* **121** (2004) 8321

[40] Gerhards M., Unterberg C. *Appl. Phys. A* **72** (2001) 273

[41] Gerhards M., Schiwek M., Unterberg C., Kleinermanns K. *Chem. Phys. Lett.* **297** (1998) 515

[42] Solca N., Dopfer O. *J. Am. Chem. Soc.* **125** (2003) 1421

[43] Solca N., Dopfer O. *Chem. Phys. Lett.* **347** (2001) 59

[44] Dopfer O. *J. Phys. Org. Chem.* **19** (2006) 540

[45] Headrick J.M., Diken E.G., Walters R.S., Hammer N.I., Christie R.A., Cui J., Myshakin E.M., Duncan M.A., Johnson M.A., Jordan K.D. *Science* **308** (2005) 1765

[46] Shin J.W., Hammer N.I., Diken E.G., Johnson M.A., Walters R.S., Jaeger T.D., Duncan M.A., Christie R.A., Jordan K.D. *Science* **304** (2004) 1137

[47] Ishiuchi S.-I., Sakai M., Tsuchida Y., Takeda A., Kawashima Y., Dopfer O., Mueller-Dethlefs K., Fujii M. *J. Am. Chem. Soc.* **0** (2007) 0

[48] Solca N., Dopfer O. *J. Phys. Chem. A* **109** (2005) 6174

[49] Larsen R.W., Zielke P., Suhm M.A. *J. Chem. Phys.* **126** (2007) art.no.194307

[50] Duncan M.A. *Ann. Rev. Phys. Chem.* **48** (1997) 69

[51] Cabarcos O.M., Weinheimer C.J., Lisy J.M. *J. Chem. Phys.* **110** (1999) 8429

[52] Macleod N.A., Simons J.P. *Mol. Phys.* **104** (2006) 3317

[53] Macleod N.A., Simons J.P. *Phys. Chem. Chem. Phys.* **6** (2004) 2821

[54] Kamariotis A., Boyarkin O.V., Mercier S.R., Beck R.D., Bush M.F., Williams E.R., Rizzo T.R. *J. Am. Chem. Soc.* **128** (2006) 905

[55] Oomens J., Sartakov B.G., Meijer G., von Helden G. *Int. J. Mass Spectr.* **254** (2006) 1

[56] Lucas B., Gregoire G., Lemaire J., Maitre P., Glotin F., Schermann J.P., Desfrancois C. *Int. J. Mass Spectr.* **243** (2005) 105

[57] Chiavarino B., Crestoni M.E., Fornarini S., Dopfer O., Lemaire J., Maitre P. *J. Phys. Chem. A* **110** (2006) 9352

[58] Valle J.J., Eyler J.R., Oomens J., Moore D.T., van der Meer A.F.G., von Helden G., Meijer G., Hendrickson C.L., Marshall A.G., Blakney G.T. *Rev. Sci. Instr.* **76** (2005) 23103

[59] Nordhoff E., Kirpekar F., Roepstorff P. *Mass Spectr. Rev.* **15** (1996) 67

[60] Harvey D.J. *Mass Spectr. Rev.* **18** (1999) 349

[61] Gaskell S.J. *J. Mass Spectr.* **32** (1997) 677

[62] Nizkorodov S.A., PhD thesis, Basel, 1997

[63] Olkhov R.V., PhD thesis, Basel, 1999

[64] Roth D., PhD thesis, Basel, 2001

[65] Solca N., PhD thesis, Basel, 2003

[66] Brutschy B. *Chem. Rev.* **100** (2000) 3891

[67] Brutschy B. *Chem. Rev.* **92** (1992) 1567

[68] Kim K.S., Tarakeshwar P., Lee J.Y. *Chem. ReV.* **100** (2000) 4145

[69] Meyer E.A., Castellano R.K., Diederich F. *Angew. Chem., Int. Ed.* **42** (2003) 1210

[70] March J., Advanced Organic Chemistry: Reactions, Mechanisms, and Structure, 1982

[71] Snow T.P, Le Page V., Keheyan Y., Bierbaum M. *Nature* **391** (1998) 259

[72] Ebata T., Fujii A., Mikami N. *Int. Rev. Phys. Chem.* **17** (1998) 331

[73] Braun J.E., Mehnert T., Neusser H.J. *Int. J. Mass Spectrom.* **203** (2000) 1

[74] Bieske E.J, Dopfer O. *Chem. Rev.* **100** (2000) 3963

[75] Solca N., Dopfer O. *Chem. Phys. Lett.* **325** (2000) 354

[76] Solca N., Dopfer O. *J. Mol. Struct.* **563** (2001) 241

[77] Solca N., Dopfer O. *Chem. Phys. Lett.* **369** (2003) 68

[78] Solca N., Dopfer O. *Chem. Phys. Lett.* **342** (2001) 191

[79] Solca N., Dopfer O. *J. Am. Chem. Soc.* **126** (2004) 1716

[80] Neusser H.J., Krause H. *Chem. Rev.* **94** (1994) 1829

[81] Solca N., Dopfer O. *Angew. Chem. Int. Ed.* **41** (2002) 3628

[82] Andrei H.S., Solca N, Dopfer O. *Phys. Chem. Chem. Phys.* **6** (2004) 3801

[83] Rappoport Z. *The Chemistry of Phenols* (2003)

[84] Forster T. *Z. Elektrochem.* **54** (1950) 42

[85] Forster T. *Z. Elektrochem.* **54** (1950) 531

[86] Olah G.A., Mateescu Gh.D., Mo Y.K. *J. Am. Chem. Soc.* **95** (1973) 1865

[87] Olah G.A., Mo Y.K. *J. Org. Chem.* **38** (1973) 353

[88] Andrei H.S., Solca N., Dopfer O. *J. Phys. Chem. A* **109** (2005) 3598

[89] Stryer, I., Biochemistry, Freeman, New York (1996)

[90] Noguchi T., Inoue Y., Tang X. *Biochemistry* **38** (1999) 399

[91] Kyte, J. *Mechanisms in Protein Chemistry* (1995)

[92] Bachovchin W.W. *Biochemistry* **25** (1986) 7751

[93] Andrei H.S., Solca N., Dopfer O. *Chem. Phys. Chem.* **7** (2006) 107

[94] Surya Prakash G.K., Schleyer P.v.R., Stable Carbocation Chemistry, John Wiley & Sons, New York (1997)

[95] Cravens T.E., Robertson I.P., Waite J.H., Yelle R.V., Kasprzak W.T., Keller C.N., Ledvina S.A., Niemann H.B., Luhmann J.G., McNutt R.L., Ip W.-H., De La Haye V., Mueller-Wodarg I., Wahlund J.-E., Anicich V.G., and Vuitton V. *Geophys. Res. Lett.* **33** (2006) 7105

[96] Tsuji M., Arikawa T., Nishimura Y. *Bull. Chem. Soc. Jpn.* **72** (1999) 293

[97] Pacansky J., Dupuis M. *J. Am. Chem. Soc.* **104** (1982) 415

[98] Pacansky J., Dupuis M. *J. Chem. Phys.* **68** (1978) 4276

[99] Sears T.J., Johnson P.M., BeeBe-Wang J. *J. Chem. Phys.* **111** (1999) 9213

[100] Kim E., Yamamoto S. *J. Chem. Phys.* **120** (2004) 3265

[101] Sears T.J., Johnson P.M., Jin P., Oatis S. *J. Chem. Phys.* **104** (1996) 781

[102] Quapp W., Heidrich D. *J. Mol. Struct. (Theochem)* **585** (2002) 105

[103] Carneiro J.W.M., Schleyer P.v.R., Saunders M., Remington R., Schaefer H.F., Rauk A., Sorensen T.S. *J. Am. Chem. Soc.* **116** (1994) 3483

[104] East A.L.L., Liu Z.F., McCague C., Cheng K., Tse T.S. *J. Phys. Chem. A* **102** (1998) 10903

[105] Obata S., Hirao K. *Bull. Chem. Soc. Jpn.* **66** (1993) 3271

[106] Esteves P.M., Mota C.J.A., Ramirez-Solis A., and Hernandez-Lamoneda R. *J. Am. Chem. Soc.* **120** (1998) 3213

[107] Houle F. A. and Beauchamp J.L *J. Am. Chem. Soc.* **101** (1979) 4067

[108] Dyke J.M., Ellis A.R., Keddar N., and Morris A. *J. Phys. Chem.* **88** (1984) 2565

[109] Ruscic B., Berkowitz J.,Curtiss L.A., Pople J.A. *J. Chem. Phys.* **91** (1989) 114

2. Experimental setup

The $XH^+\cdots L_n$ complexes have been investigated by gas phase IR photodissociation spectroscopy (IRPD) in a tandem quadrupole - octopole - quadrupole (QOQ) mass spectrometric apparatus.[1],[2],[3],[4] The cations and their weakly bound complexes have been produced in an ion source (IS) which combines the electron impact ionization (EI) with three-body associations in the high-pressure region of a supersonic molecular beam. The tunable IR radiation source used in the experiments is an optical parametric oscillator (OPO) laser pumped by the fundamental and the second harmonic of a Nd:YAG laser. A brief description of the experimental setup (both mass spectrometry and laser systems) is presented in the following pages. Figure 1 shows a block schematic of the mass spectrometric apparatus. A number of electrostatic aperture lenses are distributed along the path of the ion beam, assisting the collimation of the beam and the proper coupling between the various devices used. The positions of these control elements are presented in Figure 2. Finally, Figure 3 shows a block schematic of the OPO laser system.

2.1. Precursors

The systems investigated in the present work can be broadly classified as either open or closed shell cations. The group of open shell cations, including 1-naphthalenole$^+$ (1-Np$^+$) and imidazole$^+$ (Im$^+$), are systems obtained by electron impact ionization of neutral molecules. The second group consists of systems obtained by protonation of neutral molecules; in the following are presented IRPD studies on protonated 1-naphthalenole (1-NpH$^+$), protonated imidazole (ImH$^+$), and protonated ethylene (C$_2$H$_5^+$). All these protonated species are obtained via chemical ionization, by adding a suitable protonation agent (H$_2$ or CH$_4$) to the carrier gas mixture.

In all cases, the ion production starts with a suitable mixture of precursors in gas phase. Special care is required to ensure that the gas mixture has the proper composition, as some of the substances used have too low or too high vapor pressure at room temperature. Gases (Ar, N$_2$, H$_2$, CH$_4$, CO$_2$) are mixed in a buffer gas bottle in various

15

ratios, depending on their destination: carrier, ligand or protonation agents. Overall static gas pressure, both before and inside the buffer gas bottle ranges between 2 and 9 bar and proves to be an important parameter in the optimization of clusters production. As H_2O is sometimes used as a ligand, a small flask is inserted in the gas line; the vapor pressure of H_2O is controlled by heating or cooling the flask accordingly. The substances which are solid at room temperature are placed in a small container, whose temperature (< 150ºC) can be altered with a heating circuit. Thus, the control parameter list for the precursors include: gas pressures after the regulators, mixing ratio of the used gases, static pressure of the mixture, vapor pressure on top of the liquid and solid samples (via their temperature).

2.2. Ion source

The gaseous mixture of precursors is injected into a vacuum chamber, where the average pressure is kept under 10^{-4} mbar during operation (10^{-7} mbar without gas injection) by a 2 m^3/s diffusion pump backed by a rotary pump. A liquid nitrogen trap is used to stop oil vapor backstreaming from the diffusion pump from reaching the mass spectrometry system. The injection system consists of a pulsed valve (nozzle diameter 0.5 ... 0.8 mm), electromagnetically actuated at a repetition rate of 40 Hz. The valve opening duration (50 ... 250 μs) influences the background pressure in the ion source chamber. Two electron beams, accelerated to about 100 eV by a pulsed electric field, are crossing the gas jet less than 1 mm from the nozzle. The small distance is paramount here, as it ensures that the targets of the ionization process are molecules (not clusters!) and it maximizes the volume of the high pressure range where complexes can grow in size (number of ligands). The gas is thus excited and / or ionized via electron impact and a series of reactions (Penning ionization, chemical reaction, etc) yields the species to be investigated. The most probable reaction path for generating cations (X^+) or protonated species (XH^+) is presented in each chapter. Still in the high-pressure range of the expansion, the weakly bound complexes are created by incremental three-body collisions:

$$X(H)^+ \cdots L_{n-1} + L + M \rightarrow X(H)^+ \cdots L_n + M \qquad M = L, X \qquad (1)$$
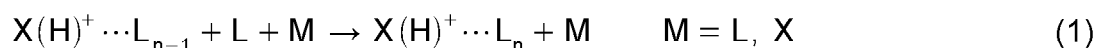
The entire setup is placed inside a metallic cage which shields the particles from external electrical fields. This cage defines the body of the ion source and its potential (+40 V with respect to the walls of the vacuum vessel) is used as reference.

The central part of the supersonic beam is sliced with a skimmer placed at a static

potential of ~-4 V with respect to the body of the ion source. A small cylinder placed inside the skimmer (02 in Figure 2, static potential, typically around -35 V with respect to ground) insures that only a small amount of ionized complexes passing through the skimmer opening are lost. Finally, a plate (03) placed at -180 V with respect to ground accelerates the ions toward the mass spectrometry stage. Briefly, the IS control parameters are: valve position with respect to the electron beams, valve opening duration, the duration and the position in time of the electric pulse used for electron acceleration with respect to the gas pulse, magnitude of accelerating field for electrons, skimmer and extractor potentials with respect to the shell of the ion source (which acts as shield and reference).

2.3. Ion selection, steering, and detection

The output of the ion source is directed through the opening of lens 04 toward the high vacuum chamber which houses the mass spectrometry stage. The species of interest must be separated from the wealth of ions and ionic complexes produced by the source. This is done with a quadrupole mass filter (QMF) which operates by destabilizing the trajectories of all particles entering the device, bar the selected m/q. The ion beam which exits QMF1 is overlapping with a flow of neutral gas (mainly gas ejected from the nozzle and not ionized by the electron beams). These molecules can become trapped in the volume of the machine and their possible collisions with the ion beam can give rise later on to unwanted background signals. In order to avoid this, the ion beam is separated from the neutrals flow using electrostatic fields (10 and 11) and the neutrals are pumped out of the enclosure. Another beneficial effect of this "bending" of the ion beam is that the region in which IR photodissociation occurs is separated optically from the production and the selection ranges.

The ion beam is injected afterwards into an octopole ion guide, whose offset potential is used to control the kinetic energy of the ions. Here the ions undergo dissociation following either IR vibrational excitation

$$XH^+ \cdots L_n + h \cdot \nu \rightarrow [XH^+ \cdots L_n]^* \rightarrow XH^+ \cdots L_m + (n-m) \cdot L \qquad (2)$$
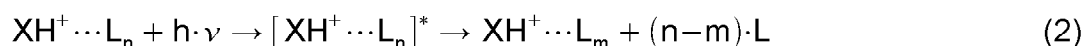
or collision with background gas. While the laser-induced dissociation (LID) is the targeted process during spectra recording, collision-induced dissociation (CID) is required for optimization of the ion production, selection, and transmission. The former process requires as little as possible collisions with the background gas, while the latter process requires a certain amount of background gas. The pressure in the volume housing the

17

octopole ranges between ~10^{-7} mbar (background pressure during maintenance pumping and during IRPD spectra recording) and ~10^{-5} mbar for CID. The gas used for CID is air and the pressure of the background gas is fine-tuned using a regulating valve.

The next device in the chain is a second quadrupole mass filter - QMF2 - which offers the ability to mass-select only one product of the reactions taking place in the octopole (this ability can be extended to more than one mass channel by switching the selected mass between various channels to be monitored).

Figure 1. *Block schematic of the QOQ mass spectrometric apparatus, coupled with the tunable OPO laser system.*
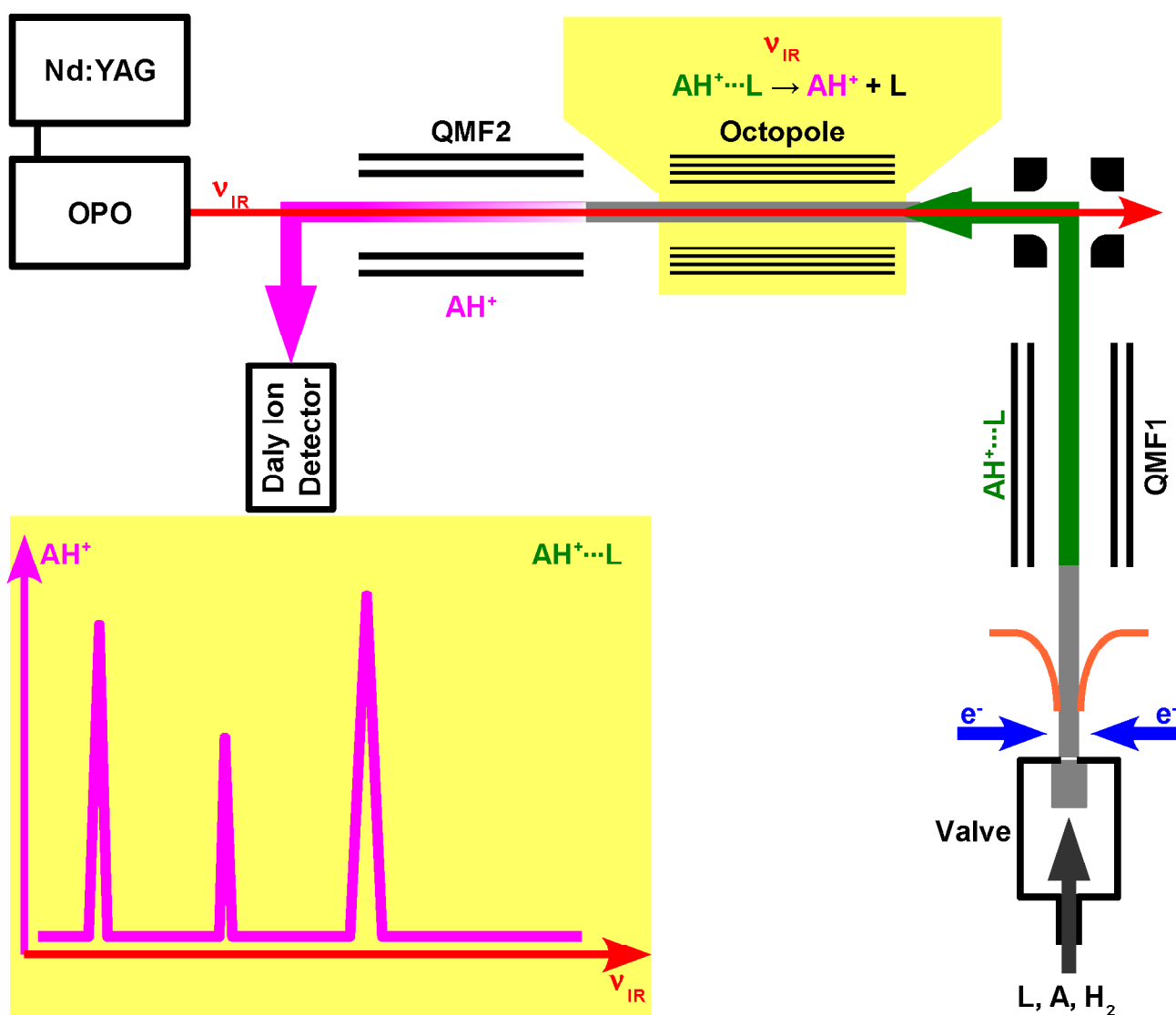
Finally, the detection of the ions is done using a Daly cation detector.[5] Here, the ions enter an electrical field perpendicular to the ion beam axis. The electrical field is produced by applying a potential difference larger than -20 kV (with respect to ground) across two electrodes. The ions collide with the cathode of the device where secondary emission

processes are responsible for creating electron pulses; these electron pulses are collected by the anode, which is a thin metallic layer on top of a scintillator plate. The photons emitted by the scintillator plate upon electron impact are collected by a photomultiplier. The chain is designed so that the detection efficiency is close to 100%.

Three turbomolecular pumps are used for evacuating the high vacuum chamber housing the mass spectrometry stage. The pump placed close to the quadrupole bender is mainly used for evacuating the neutrals that have drifted through QMF1. Another pump is used to evacuate the volume of the octopole. This serves the double purpose of eliminating the background gas during IRPD investigations and of stabilizing the background pressure during CID investigations. The last turbomolecular pump maintains the low pressure required for a low-noise operation of the Daly detector.

Figure 2. *The positions of the electrostatic lenses along the path of the ion beam.*

potentials (with respect to ground ≡ wall of the vessel)

skimmer ≅ +35 V (variable)

IS body = +40 V

QMF1 ≅ +32 V (variable)

Octopole = +35 V

QMF2 ≅ +32 V (variable)
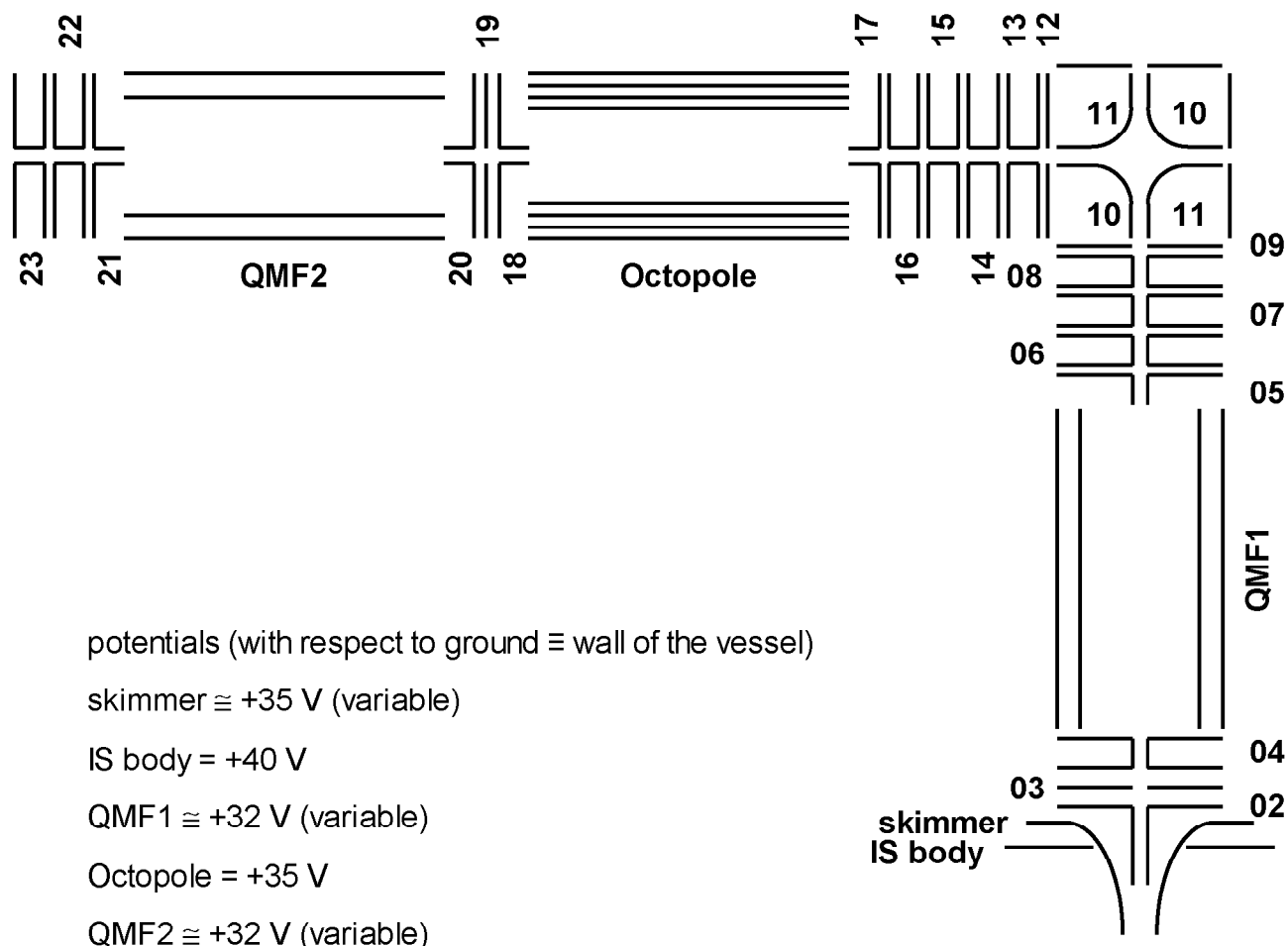
Along the ion path there are a number of electrostatic lenses whose potentials (with respect to ground) can be controlled independently and are used to adjust the path of the ions and the collimation of the ion beam. The positions of these lenses are shown in Figure 2, while typical values of the potentials are listed in the table below. It must be

stressed that all these potentials are tuned during optimization and that their values depend on many parameters (gas pressure, gas species, investigated species, etc.).

02	-35 V	08	-90 V	14	-90 V	20	+18 V
03	-180 V	09	0 V	15	-80 V	21	-20 V
04	-6 V	10	-33 V	16	-10 V	22	+17 V
05	-12 V	11	+33 V	17	-40 V	23	-17 V
06	floating	12	-4 V	18	+18 V		
07	-17 V	13	-20 V	19	-39 V		

Overall, the control parameters for the ion selection, steering, and detection are: the offset voltages of the two QMFs and the one of the octopole and the voltages of the electrostatic elements. The voltage applied on the Daly detector and the one applied on the photomultiplier are used as elements adjusting the intensity of the current in the detection circuit and thus preventing the saturation of the signals during recordings.

2.4. Laser system

The OPO laser is a Continuum Mirage 3000 which must be pumped by linearly polarized, near Gaussian laser beams. The pump laser is a seeded Continuum PowerLite PL8020 which operates at a repetition rate of 20 Hz and delivers the following performance:

fundamental wavelength	9394.492 cm^{-1} (further denoted 1064 nm)	
energy @ 1064 nm	~750 mJ (no SHG)	~400 mJ (with SHG)
linewidth @ 1064 nm	1.0 cm^{-1} (unseeded)	0.003 cm^{-1} (seeded)
pulsewidth @ 1064 nm	8 ... 9 ns	
temporal jitter @ 1064 nm	±1 ns	
energy @ SHG (532 nm)	~100 mJ	
pulsewidth @ SHG (532 nm)	6 ... 8 ns	

The OPO laser system is used to convert the pump laser radiation into mid-IR light continuously tunable in the range 2500 ... 6900 cm^{-1}. The layout of the three stages of the OPO laser system is presented in Figure 3. It consists of one laser stage (master oscillator - MO) followed by two amplification stages (one non-resonant oscillator - NRO and one

optical parametric amplifier - OPA).

The MO stage is using about 20% from the 532 nm pump beam, which is separated via a beamsplitter. This beam is injected into a laser cavity built with two planar mirrors, where it is used for pumping the active medium (a potassium titanyl phosphate - KTP - crystal). A grating inserted in the cavity is used as tuning element. The tunable output of this laser is used primarily as seed for the NRO stage. At the same time, a small part of the MO output is separated using a beamsplitter and is used to monitor the performance of the MO cavity. The use of the MO stage is required and sensible only if the Nd:YAG pump laser operates in single longitudinal mode (seeded mode). In this case, the bandwidth of all the outputs of the OPO laser system is <0.017 cm^{-1} (<500 MHz).

Figure 3. *Block schematic of the OPO laser system.*

532 nm (pump MO and NRO)
710 ... 840 nm (output MO and signal NRO)
1064 nm (pump OPA)
6900 ... 4700 cm^{-1} (idler NRO and signal OPA)
4700 ... 2500 cm^{-1} (idler OPA)
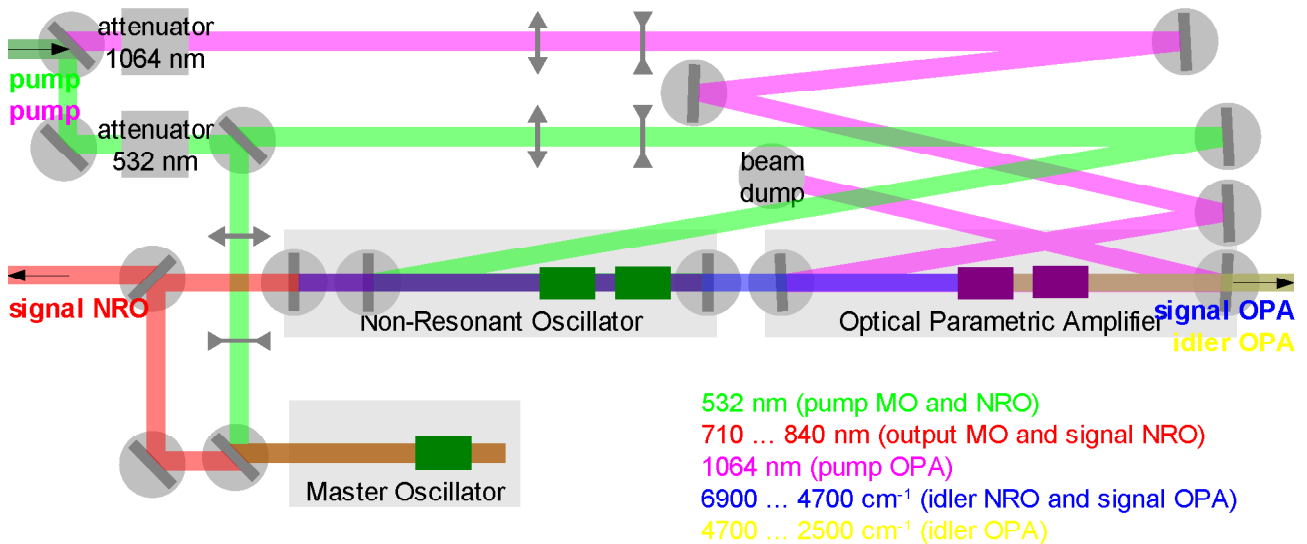
The NRO stage consists of two KTP crystals which are seeded by the MO output and pumped by the remaining 532 nm beam. This stage acts as amplifier for the MO output. The output of the NRO stage consists of two components; their photon energies are linked via the following equation:

$$\nu_{532nm} = \nu_{signal}^{NRO} + \nu_{idler}^{NRO} \tag{3}$$

This equation is also valid for the output of the MO stage. The two mirrors encompassing the NRO stage are directing these two outputs in opposite directions: the *signal* output (11900 ... 14100 cm^{-1} ≡ 710 ... 840 nm) is directed outside the laser system and the *idler* output (6900 ... 4700 cm^{-1}) is directed toward the OPA stage, where it is used as seed.

The OPA stage also uses two KTP crystals seeded by the NRO *idler* output and pumped by the 1064 nm beam. Like in the case of the NRO stage, the output of this stage

consists of two components (*signal* - 6900 ... 4700 cm^{-1} and *idler* - 2500 ... 4700 cm^{-1}) linked via an equation similar with **(3)**:

$$\nu_{1064nm} = \nu_{signal} + \nu_{idler} \tag{4}$$

Apart from the NRO stage, OPA is a simple amplifier: there is only one mirror which simply deflects the remaining 1064 nm pump into a beam dump. Both outputs of the OPA stage are extracted via the same output port of the laser.

For all three stages of the OPO laser system, the wave vectors of the photons involved in the nonlinear processes must conserve momentum:

$$\vec{k}_{pump} = \vec{k}_{signal} + \vec{k}_{idler} \tag{5}$$

Simultaneously, the energies of the pump and output photons of the OPO laser system are linked via the following equations:

pump: $$\nu_{532nm} = 2 \cdot \nu_{1064nm} \tag{6}$$

MO and NRO: $$\nu_{532nm} = \nu_{signal}^{NRO} + \nu_{idler}^{NRO} \qquad \left(\begin{matrix} \nu_{signal}^{MO} = \nu_{signal}^{NRO} \\ \nu_{idler}^{MO} = \nu_{idler}^{NRO} \end{matrix} \right) \tag{7}$$

OPA: $$\nu_{1064nm} = \nu_{signal}^{OPA} + \nu_{idler}^{OPA} \qquad \left(\nu_{signal}^{OPA} = \nu_{idler}^{NRO} \right) \tag{8}$$

The OPO laser system is tuned to a certain wavelength if **(5)** is true for all three stages; this is achieved by adjusting the angles between the pump beams and all five active media as well as the tuning mirror. The scanning of a spectral domain thus involves continuous angular matching between the afore-mentioned elements; this is achieved via a dedicated computer. It must be noted that the two outputs of the OPA travel in slightly different, frequency-dependent directions. Such displacement is not significant for scans of less than 300 cm^{-1}. For longer scans, the laser beam might be shifting enough to be clipped by the apertures of the electrostatic lenses. To prevent this, the overlap of the laser beam with the ion beam is optimized as close as possible to the maximum of each observed band. Thus, ratios between the strength of various observed bands are reliable to within a factor 2; this factor decreases toward unity as the distance between the considered bands drops below 300 cm^{-1}.

2.5. Laser frequency calibration

As the driving computer is able to reliably compute only the displacement of the

tuned wavelength with respect to the beginning of a scan but offers no absolute wavelength control, additional measurements must be used to properly establish the position of the observed IRPD spectra features. In the present experiment, these measurements take the form of opto-acoustic spectra recorded together with every IRPD spectrum. Given the direct relationship between the *signal* and the *idler* outputs, either of them can be used for calibration purposes.

The opto-acoustic spectra are recorded in a long, narrow tube filled with a substance whose ro-vibrational spectrum is known from literature[6],[7] and matches the investigated range. If the wavelength of one output of the OPO laser matches a ro-vibrational line of this substance, absorption of the IR laser radiation occurs. It is followed by de-excitation, resulting in a small shockwave which is recorded via a microphone placed on the wall of the tube. The wavelength evaluated by the driving computer is then shifted so that at the beginning of the scan the recorded and the etalon opto-acoustic spectra are overlapping. The recorded spectrum is then stretched / compressed so that the recorded opto-acoustic lines match in position the etalon spectrum. This procedure is giving better than 0.2 cm^{-1} accuracy. Extensive analysis shows that, during apparently smooth continuous scans, the computer-evaluated wavelength of the laser output oscillates with an amplitude of maximum 2 cm^{-1} with respect to the opto-acoustically calibrated value.

The substance used for calibrating the range above 3500 cm^{-1} is H_2O. This is done not by using opto-acoustic spectra but by monitoring the drops in intensity of the OPO laser, which occur as the *idler* laser beam is absorbed by atmospheric water. The etalon substance used for calibrating the range under 3200 cm^{-1} is HDO; in this case, the opto-acoustic spectra are recorded by using the *signal* laser beam. The $3300 \dots 3500 \text{ cm}^{-1}$ range is covered by the ro-vibrational spectrum of NH_3.

If the recorded IRPD spectra contain fully rotationally-resolved features, the calibration described above is repeated using the output of a Fabry-Perot interferometer. In this case, each interval between successive opto-acoustic lines is checked and adjusted knowing that the interference fringes seen through the Fabry-Perot interferometer are equally spaced in wavelength.

References

[1] Dopfer O., *Z. Phys. Chem.* **219** (2005) 125
[2] Dopfer O., *Int. Rev. Phys. Chem.* **22** (2003) 437
[3] Bieske E.J, Dopfer O., *Chem. Rev.* **100** (2000) 3963
[4] Nizkorodov S.A., PhD thesis, Universitaet Basel (1997)

[5] Daly N.R., *Rev. Sci. Instr.* **31** (1960) 264

[6] Camy-Peyret C., Flaud J.M., Guelachvili G., Amiot C., *Mol. Phys.* **26** (1973) 825

[7] Guelachvili G., Rao K.N., *Handbook of Infrared Standards*, Academic Press (London, 1993)

3. IRPD spectroscopy of 1-Naphthol$^+$···L$_n$ complexes (L = Ar, N$_2$; n = 1...5)

Abstract The two rotamers of the 1-naphthol cation are investigated and their interaction with nonpolar ligands (Ar, N$_2$) in the ground electronic state is characterized by IR photodissociation spectra of isolated 1-Np$^+$···L$_n$ complexes (L = Ar, N$_2$) and by density functional calculations at the UB3LYP/6-311G(2df,2pd) level. The complexes are created in an electron impact cluster ion source, which predominantly produces the most stable isomers of a given cluster ion. The behaviour of the investigated dimers points toward a competition between H-bonding and π-bonding. The dependence of the OH stretch vibration shifts (Δv_{OH}) on the number of ligands and the photofragmentation branching ratios provide information about the stepwise microsolvation of both 1-Np$^+$ rotamers in a nonpolar hydrophobic environment. Estimations for the ligand binding energies and the acidities of both rotamers are also obtained. Finally, analysis of the Δv_{OH} shifts of the H-bound dimers yields a first experimental estimate for the proton affinity of the t-1-naphthoxy radical.

3.1. Introduction

Arenes and substituted arenes are fundamental molecules in chemistry and biology. The properties of benzene (C$_6$H$_6$ = Bz, Figure 1a), one of the simplest aromatic hydrocarbon, and of the substituted benzenes have been studied for a long time. The interest for the substituted benzenes stems from the variety of interesting properties which result from both the substituent functional groups and the aromatic π-electron system.[1],[2] Naphthalene (C$_{10}$H$_8$ = Np, Figure 1b), with its two fused benzene rings, is an appealing molecule for extending the exploration from monocyclic to polycyclic aromatic hydrocarbons.

Because of the symmetry of the molecule, monosubstitution of naphthalene yields two nonequivalent isomeric products: α (or 1, close to the fusing bond) and β (or 2, away from the fusing bond). Usually, the major product of the monosubstitution has the functional group in α-position. 1-Naphthol (1-C$_{10}$H$_8$O = 1-hydroxynaphthalene =

α-hydroxynaphthalene = 1-Np), obtained by the substitution of an H atom by an OH group, is of particular interest. Depending on the orientation of the OH group with respect to the aromatic rings system, two rotamers of 1-Np are known: *trans* (*anti*, further denoted as t-1-Np, Figure 1d), having the OH group pointing away from the rings and *cis* (*syn*, further denoted as c-1-Np, Figure 1e), having the OH group pointing toward the rings.

Figure 1. *Structures of the calculated monomers and H-bound dimers: **a** Bz; **b** Np; **c** Ph*$^+$*; **d** t-1-Np*$^+$*; **e** c-1-Np*$^+$*; **f** Ph*$^+$*···Ar; **g** t-1-Np*$^+$*···Ar; **h** c-1-Np*$^+$*···Ar; **i** Ph*$^+$*···N₂*... wait

Figure 1. *Structures of the calculated monomers and H-bound dimers: **a** Bz; **b** Np; **c** Ph*$^+$*; **d** t-1-Np*$^+$*; **e** c-1-Np*$^+$*; **f** Ph*$^+$*···Ar; **g** t-1-Np*$^+$*···Ar; **h** c-1-Np*$^+$*···Ar; **i** Ph*$^+$*···N_2*; **j** t-1-Np*$^+$*···N_2*; **k** c-1-Np*$^+$*···N_2*. All geometries are evaluated at the UB3LYP/6-311++G(2df,2pd).*
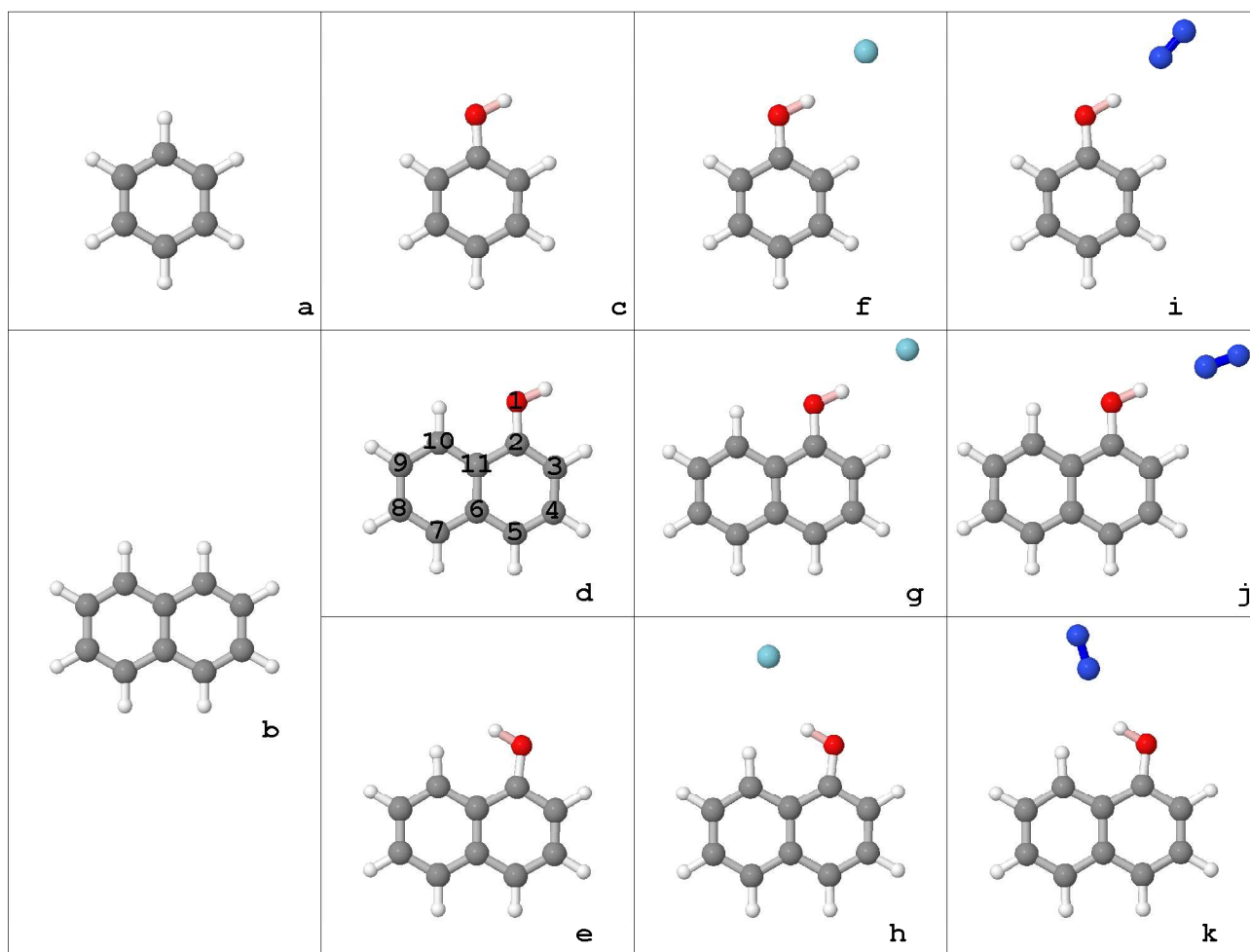
This bicyclic monohydroxyarene is a strong photoacid, that is the acidity of the OH group increases drastically upon electronic excitation or by ionization, which eventually may promote proton transfer to a suitable solvent.[2],[3],[4] The properties of such proton transfer processes, which are among the most fundamental reactions occurring in chemical and biological systems, depend sensitively on the environment. Thus, the controlled solvation of such a molecule is seen as a valuable model for studying the energetics and the dynamics of photo-induced proton transfer in both isolated complexes and in solution

under controlled solvation conditions. Consequently, a study of the solvation of the 1-Np$^+$ cation by a well-defined number of non-polar ligands can be seen as providing direct information on the acidity of the OH group in the cation ground state and its dependence on stepwise solvation in a hydrophobic environment.

In general, aromatic molecules (A) offer two major types of recognition sites for inert ligands L. Ligands can bind to the aromatic π-electron system (π-bond) or to one of the aromatic CH protons (H-bonds). It should be noted that such H-bonds are usually less stable. This situation can change dramatically upon substitution: the aromatic molecules (A) with acidic functional YH_k groups (e.g., Y = N, O) offer the k acidic protons of YH_k as more favourable binding sites than the aliphatic or aromatic CH protons. The preferred binding site in A⋯L dimers (π-bonding or H-bonding) depends on several factors, including the degree of electronic excitation and charge state of A, the acidity of the YH_k group, and the ligand type (polar or nonpolar).

Complexes of neutral A with rare gas atoms have π-bound equilibrium structures in the singlet electronic ground state (S$_0$): Ar complexes of benzene (Bz⋯Ar),[5] phenol (Ph⋯Ar, YH_k = OH),[6],[7] aniline (An⋯Ar, YH_k = NH$_2$),[8] and indole (In⋯Ar, YH_k = NH)[9] are all π-bonded. The attraction in the π-bonded A⋯Ar dimer is the result of dispersion interaction between Ar and the π-electron system of A. In fact, H-bound isomers have not been detected for any aromatic A⋯Ar complex in S$_0$. This situation changes for A⋯N$_2$ dimers, because the quadrupole moment of N$_2$ leads to additional electrostatic interactions with the polar YH_k group of A with such magnitude that the H-bond may energetically compete with the π-bond. The presence of a YH_k group is crucial here: N$_2$ favors H-bonding to Ph[6],[10] but π-bonding to less acidic Bz[11],[12] or An.[13]

In general, the topology of the interaction potential of A$^+$⋯L radical cation dimers differs qualitatively from that of neutral A⋯L, because of the significant additional electrostatic and inductive attraction arising from the positive charge.[14],[15],[16],[17],[18] As a consequence, the equilibrium structures and interaction energies of A$^+$⋯L are often rather different from the ones of A⋯L. Illustrative examples are Ph$^+$⋯Ar,[19],[20], [21],[22] An$^+$⋯Ar,[23] and In$^+$⋯Ar;[24] they all have H-bound global minima in the ground electronic state of the cation (D$_0$), whereas the π-bound isomers (global minima in S$_0$) are only local minima. Similarly, Ph$^+$⋯N$_2$,[6],[19],[20],[25] An$^+$⋯N$_2$,[26] and In$^+$⋯N$_2$[24] prefer H-bonds over π-bonds in D$_0$; a major difference between the Ar- and N$_2$-based dimers stems from the additional charge-quadrupole interaction which increases the strength of both H- and π-bonds in A$^+$⋯N$_2$ with respect to their A$^+$⋯Ar equivalents. Such a change in the ligand recognition

motif occurs also upon the protonation of aromatic molecules (AH$^+$) with acidic YH$_k$ groups: the PhH$^+\cdots$Ar and PhH$^+\cdots$N$_2$[27],[28],[29] dimers also favor H-bonds over π-bonds. This is not true for arenes without YH$_k$ groups (such as Bz): the most stable dimers of their cation or protonated forms with Ar and N$_2$ (Bz$^+\cdots$L and BzH$^+\cdots$L, L = Ar, N$_2$)[5],[30],[31],[32] feature π-bonds, because CH protons are only weakly acidic even in the ground state of the cation or protonated species.[31]

Often, A$^+\cdots$L are generated by resonance enhanced multiphoton ionization (REMPI) of A$\cdots$L formed in a supersonic expansion. Spectroscopic information of A$^+\cdots$L may then be extracted from photoionization efficiency spectra (PIE), mass analyzed threshold ionization (MATI), zero kinetic energy photoelectron (ZEKE) spectra, IR photodissociation (IRPD), etc. The fact that the preferred ligand binding site changes from A$\cdots$L to A$^1\cdots$L is limiting the spectroscopic studies of A$^+\cdots$L prepared by photoionization of A$\cdots$L. More exactly, the Franck-Condon principle sets limits for the population of the most stable structure of A$^+\cdots$L if this structure is largely different from the global minimum of A$\cdots$L. Unfortunately, such a situation is quite common for A$\cdots$L / A$^+\cdots$L dimers with both polar and nonpolar L. The present study has employed a method for producing "cold" A$^+\cdots$L$_n$ complexes which overcomes this obstacle. The A$^+\cdots$L$_n$ complexes are produced in a supersonic plasma expansion by electron ionization of A followed by cluster aggregation. This results predominantely in the production of the most stable isomer of a given A$^+\cdots$L$_n$ complex, independent of the most stable structure of neutral A$\cdots$L$_n$. The excellent performance of this method has been proven via comparisons of the EI-IRPD spectra of Ph$^+\cdots$Ar$_n$, An$^+\cdots$Ar$_n$, and In$^+\cdots$Ar$_n$ with their corresponding photoionization (PIE, ZEKE, MATI) or REMPI-IR spectra. The EI-IRPD spectra have evidenced the existence of isomers which previously have completely escaped detection and which were interpreted as global minimum structures.

Spectroscopic information about the structures and relative energies of both c-1-Np and t-1-Np rotamers is available from a variety of techniques, including (dispersed) laser-induced fluorescence, REMPI, and IR spectra. Information on the corresponding x-1-Np$^+$ cation rotamers is provided by ZEKE, MATI, and REMPI-IR spectra. The results relevant for the present work can be summarized as follows. In S$_0$, t-1-Np is slightly more stable than c-1-Np ($\Delta E = 220 \pm 50$ cm^{-1}) and its OH group is somewhat more acidic as demonstrated by the smaller OH stretch frequency ($\nu_{OH} = 3655$ cm^{-1} vs. 3663 cm^{-1}). Interestingly, the energy order of both rotamers is reversed in S$_1$ ($\Delta E = -59$ cm^{-1}). In D$_0$, t-1-Np$^+$ is again more stable than c-1-Np$^+$ ($\Delta E = 495$ cm^{-1}), indicating that the potential for OH rotation is quite sensitive to both electronic excitation and ionization. The acidity of

t-1-Np is substantially increased upon ionization, as revealed by the large decrease in ν_{OH} from 3655 cm^{-1} to 3579 cm^{-1}. No spectroscopic information is available for the acidity of c-1-Np$^+$.

Spectroscopic and theoretical information about neutral and ionic complexes of 1-Np (1-Np$\cdots$L$_n$ and 1-Np$^+\cdots$L$_n$, L = Ar, N$_2$) is rather limited. REMPI, hole-burning, and IR spectra of t-1-Np$\cdots$Ar are consistent with a π-bound structure in S$_0$, in agreement with the quantum chemical calculations. Similarly, the REMPI-IR spectrum of t-1-Np$^+\cdots$Ar in the OH stretch range was interpreted with a π-bound isomer in D$_0$. No evidence has been reported for H-bound 1-Np$\cdots$Ar or 1-Np$^+\cdots$Ar dimers. Calculations predict π-bound t-1-Np$\cdots$N$_2$ to be more stable than the H-bound isomer in S$_0$, and preliminary REMPI and hole-burning spectra appear to be consistent with this view. Extensive literature searches failed to identify spectroscopic information for c-1-Np$\cdots$L$_n$ or c-1-Np$^+\cdots$L$_n$ complexes. Such information is diffcult to obtain because of the usually low population of the less stable c-1-Np rotamer in molecular beams and steric hindrance involved in the formation of H-bound c-1-Np$\cdots$L or c-1-Np$^+\cdots$L complexes.

Several aspects motivated the present EI-IRPD and theoretical study on size-selected 1-Np$^+\cdots$L$_n$ complexes (L = Ar, N$_2$). First of all, these clusters serve as a suitable model for solvation of the highly acidic 1-Np$^+$ cations in a nonpolar solvent. The competition between H-bonding and π-bonding and its consequences on the cluster growth are particularly interesting. As Ar and N$_2$ are weak proton acceptors, proton transfer from 1-Np$^+$ to the solvent may not be expected in D$_0$ even for complete solvation. Second, the ability of the OH group to form H-bonds to a ligand is correlated with its acidity. This means that the IR spectra of H-bound 1-Np$^+\cdots$L dimers directly probe the acidity of the 1-Np$^+$ rotamers and eventually enable a first estimate of the unknown proton affinity (PA) of the 1-naphthoxy radical. Finally, the comparison of 1-Np$^+\cdots$L$_n$ with Ph$^+\cdots$L$_n$ and H$_2$O$^+\cdots$L$_n$ reveals the influence of substitution of a monocyclic and bicyclic aromatic system on the acidity of ROH$^+$ cations. The acidity is expected to decrease in the order H$_2$O$^+$ > Ph$^+$ > 1-Np$^+$ because of increasing charge delocalization in the aromatic rings.

3.2. Density functional calculations

In order to support the characterization of the intramolecular O-H and intermolecular H$\cdots$L bonds, density functional theory (DFT) quantum chemical calculations were carried out for a number of monomers (Ph$^{(+)}$, t-1-Np$^{(+)}$ and c-1-Np$^{(+)}$ - see Figures 1c, 1d, and 1e) and for the corresponding OH-bound dimers (Ph$^+\cdots$L, x-1-Np$^+\cdots$L) at the

UB3LYP/6-311++G(2df,2pd) level of theory, using the Gaussian 03 quantum chemistry package.[33] The geometrical and energetical properties relevant for the present study are summarized in Table 1. The listed parameters are:

* intramolecular O-H bond length (r_{OH}), stretch frequency (ν_{OH}), and ν_{OH} IR intensity (I_1)

* intermolecular H$\cdots$L bond length (r_{HL}), angle (θ_{OHL}), stretch frequency (ν_s), ν_s IR intensity (I_s), and the dissociation energy of the dimers (D_0).

Table 1. *The geometrical and energetical parameters relevant for the description of the intramolecular O-H bond and the intermolecular OH$\cdots$L bond in $A^{(+)}\cdots L$ complexes (A = Ph, t-1-Np, c-1-Np; L= Ar, N_2), as calculated at the UB3LYP/6-311++G(2df,2pd) level of theory; the harmonic frequencies have been scaled by 0.9503.*

	r_{OH}, Å	ν_{OH}, cm^{-1} (I_1, km/mol)	r_{HL}, Å	θ_{OHL}, °	ν_s, cm^{-1} (I_s, km/mol)	D_0, cm^{-1}
Ph	0.9617	3643 (63)				
Ph$^+$	0.9713	3533 (269)				
Ph$^+\cdots$Ar	0.9755	3445 (780)	2.38	167	68 (7)	446
Ph$^+\cdots$N$_2$	0.9803	3353 (1239)	1.98	167	107 (10)	1274
t-1-Np	0.9617	3644 (74)				
c-1-Np	0.9604	3659 (46)				
t-1-Np$^+$	0.9673	3580 (294)				
c-1-Np$^+$	0.9665	3587 (123)				
t-1-Np$^+\cdots$Ar	0.9700	3524 (722)	2.48	172	49 (5)	274
t-1-Np$^+\cdots$N$_2$	0.9737	3454 (1184)	2.05	170	88 (8)	927
c-1-Np$^+\cdots$Ar	0.9681	3553 (297)	2.62	148	42 (4)	212
c-1-Np$^+\cdots$N$_2$	0.9708	3504 (522)	2.15	150	80 (6)	803

The relative stabilities of the monomers and the transition states between them are including zero-point energy contributions. The calculations of the dimer properties were all counterpoise corrected for basis set superposition error (BSSE).[34],[35] As the vibrational frequencies were computed as harmonic, they were scaled by an average scaling factor of 0.9503 to bring the calculated ν_{OH} frequencies of both t-1-Np$^+$ and Ph$^+$ in agreement with the experimental value, ν_{OH} = 3579 cm^{-1} (3534 cm^{-1}).[36],[37]

3.2.1. DFT calculations of monomers

The optimized geometries of the monomers (x-1-Np$^{(+)}$ and Ph$^{(+)}$) were found to be planar for both neutral and cation ground states; this result is consistent with available spectroscopic data.[38],[39] Transition states between the *cis* and *trans* minima of 1-Np$^{(+)}$ and

around the equilibrium geometry of $Ph^{(+)}$ are best described by a rotation motion of the O-H bond around the C_2-O bond (see Figure 1d for identification of atoms). Figure 2 compares the relative stabilities of these monomers and the potential barriers for the internal OH rotation.

In the neutral ground state (S_0), t-1-Np is predicted to be more stable than c-1-Np by 322 cm⁻¹, in reasonable agreement with the 220 ± 50 cm⁻¹ estimated from the analysis of the UV spectrum recorded in an absorption cell.[40] In the cation ground electronic state (D_0), the *trans* rotamer is also the most stable isomer, c-1-Np⁺ being 730 cm⁻¹ less stable than t-1-Np⁺; this difference in stability is more than twice as large as in S_0. The difference in stability of both rotamers in D_0 and S_0 corresponds to the difference in their adiabatic ionization potentials; owing to the harmonic character of the calculations, the predicted value (408 cm⁻¹) is slightly larger than the experimental measurement (281 cm⁻¹).[39]

Figure 2. *Relative stabilities and OH rotation barriers for the considered monomers.*
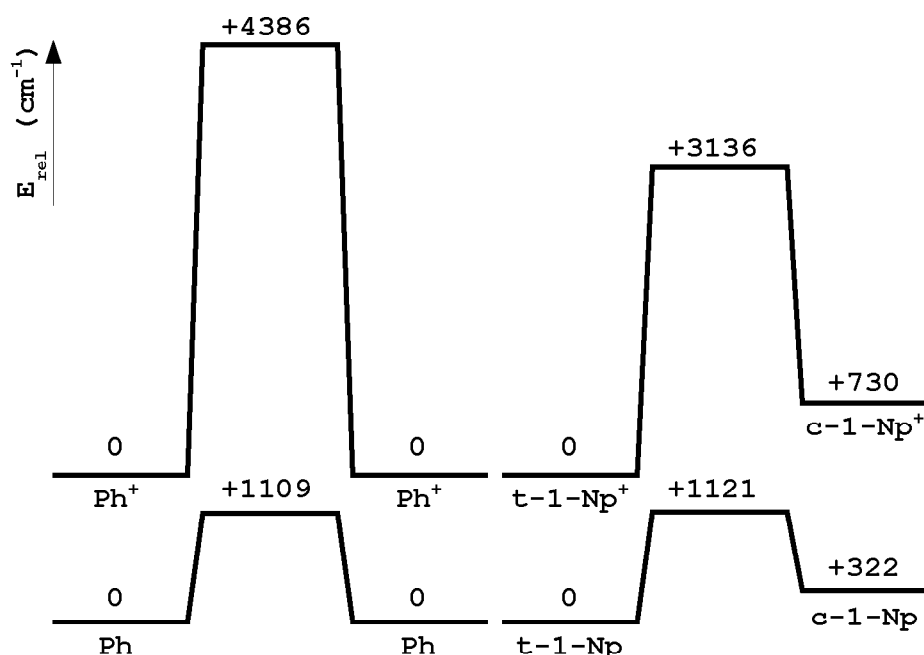
The experimental barrier for OH rotation in Ph ($E^{Ph}_{bar,exp}$ = 1215 ± 10 cm⁻¹, determined by rotationally resolved UV spectroscopy in a molecular beam)[41] compares very well with the calculated one ($E^{Ph}_{bar,calc}$ = 1109 cm⁻¹). This means that the level of the theory is appropriate for energetic calculations related to the internal OH rotation. As no value has been yet experimentally found for the OH rotation barrier of 1-Np, one must rely on the calculated value ($E^{1-Np}_{bar,calc}$ = 1121 cm⁻¹). In the D_0 state, the OH rotation barrier of Ph⁺ is almost four times larger than the one encountered in the neutral, $E^{Ph+}_{bar,calc}$ = 4386 cm⁻¹;

similarly, the barrier for OH rotation from t-1-Np' toward c-1-Np' ($E_{bar,calc}^{1-Np+}$ = 3136 cm^{-1}) is significantly larger than in S_0. The OH rotation barrier of hydroxyarenes is usually correlated with their C_2-O bond strength.[38],[41] In general, the stronger (and shorter) the C_2-O bond, the more hindered the internal rotation. This correlation between the length of the C_2-O bond and the OH rotation barrier can be seen in Table 2.

Table 2. *The correlation between the length of the C_2-O bond and the OH rotation barrier computed for Ph$^{(+)}$ and 1-Np$^{(+)}$.*

isomer	r_{C-O} (Å)	$E_{bar,calc}$ (cm^{-1})	TS
Ph$^+$	1.3076	4386	Ph$^+$ $\longleftrightarrow$ Ph$^+$
t-1-Np$^+$	1.3196	3136	t-1-Np$^+$ $\longleftrightarrow$ c-1-Np$^+$
t-1-Np	1.3655	1121	t-1-Np $\longleftrightarrow$ c-1-Np
Ph	1.3897	1109	Ph $\longleftrightarrow$ Ph

It is remarkable that not only the OH rotation barrier, but also the O-H bond strength varies along the same line, as is signaled by the changes in bond length and stretch vibration frequency (see Table 3). In general, the differences between the t-1-Np$^+$ and c-1-Np$^+$ rotamers are significantly smaller than between any of them and Ph$^+$. Interestingly, the steric hindrance in the c-1-Np$^+$ is reducing the IR oscillator strength for ν_{OH} by a factor of 2.4 with respect to t-1-Np$^+$ (I_1 = 123 km/mol vs. 294 km/mol).

Table 3. *The correlation between the O-H bond parameters of various monomers; the sequence of the monomers in the table is similar with the sequence in Table 2, linking the changes in the C_2-O and the O-H bond characteristics.*

isomer	r_{O-H} (Å)	ν_{OH} (cm^{-1})
c-1-Np	0.9604	3659
t-1-Np	0.9617	3644
Ph	0.9617	3643
c-1-Np$^+$	0.9665	3587
t-1-Np$^+$	0.9673	3580
Ph$^+$	0.9713	3533

3.2.2. DFT calculations of H-bound dimers

The H-bound 1-Np$^+$···L dimers feature quasi-linear H-bonds of L to the acidic OH group of 1-Np$^+$, leading to planar equilibrium geometries with C_s symmetry (Figures 1g, 1h,

1j, and 1k as well as Table 1). The linearity of the intermolecular bonds is more visible in the t-1-Np$^+$···L dimers ($\theta_{OH···L} \geq 170°$). The steric hindrance arising from the interaction of the ligand with the proximal proton on the second aromatic ring ($C_{11}H$), is "bending" the intermolecular bonds created by c-1-Np$^+$ ($\theta_{OH···L} \geq 148°$). The deviation from linearity registered by the angle made by the N≡N molecular axis with the intermolecular H···N bond is a good indication of this steric hindrance. It is known that the anisotropy of the long-range charge-quadrupole and charge-induced dipole interactions aligns the N_2 ligand in such a way that the molecular axis points toward the positive charge.[17],[19],[24],[26],[28],[31],[42],[43],[44],[45],[46] The H···N≡N configuration of t-1-Np$^+$···N_2 is closer to the ideal linear bond than the configuration of c-1-Np$^+$···N_2 (180° > 170° > 150°). Another indication of the steric hindrance in c-1-Np'···L results from the $C_{11}H$···N≡N separation; this value is slightly larger than the sums of the van der Waals radii of the bonded atoms (2.71 Å ≅ 1.1 Å + 1.5 Å).[47] The $C_{11}H$···Ar intermolecular separation obeys the same rule: 3.07 Å ≅ 1.1 Å + 1.9 Å.[47] The increase in the acidity along the series c-1-Np$^+$ < t-1-Np$^+$ < Ph$^+$ is directly correlated with the intermolecular interaction strength, leading to shorter H···L bonds, larger intermolecular stretch frequencies and higher dissociation energies. This trend is summarized in Table 4.

Table 4. *The variation of geometrical and energetical intermolecular bond parameters as a function of the cation acidity.*

		L = Ar			L = N$_2$		
		r_{HL} (Å)	v_s (cm^{-1})	D_0 (cm^{-1})	r_{HL} (Å)	v_s (cm^{-1})	D_0 (cm^{-1})
c-1-Np$^+$···L	↓	2.62	42	212	2.15	80	803
t-1-Np$^+$···L		2.48	49	274	2.05	88	927
Ph$^+$···L		2.38	68	446	1.98	107	1274

The effects of H-bonding on the intramolecular O-H bonds are an elongation (Δr_{OH}), a reduction in the stretch frequency (Δv_{OH}), and an enhancement in the IR oscillator strength (ΔI_1). Again, the magnitude of these effects is correlated with the H-bond strength and increases along the same series c-1-Np$^+$ < t-1-Np$^+$ < Ph$^+$ (see Table 5). These theoretical results demonstrate that IR spectroscopy in the OH stretch range is a suitable tool to probe both the acidity of the x-1-Np$^+$ rotamers and their ability to form H-bonds.

Similar to previous studies on (*para*-halogenated) Ph(H)$^+$···Ar$_n$ and Ph(H)$^+$···(N_2)$_n$, it will be shown that the EI-IRPD spectra of the corresponding 1-Np$^+$···Ar$_n$ and 1-Np$^+$···(N_2)$_n$

complexes demonstrate that the H-bonds are more stable than the π-bonds.[19],[20],[28],[29] Hence, the energetically most favorable 1-Np$^+$···L$_n$ cluster growth begins with the

Table 5. *The variation of geometrical and energetical parameters of the complexated OH bond as a function of the cation acidity.*

		L = Ar			L = N$_2$		
		Δr_{OH} (Å)	Δv_{OH} (cm^{-1})	ΔI_1 (km/mol)	Δr_{OH} (Å)	Δv_{OH} (cm^{-1})	ΔI_1 (km/mol)
c-1-Np$^+$···L		0.0016	34	174	0.0043	83	399
t-1-Np$^+$···L		0.0027	56	428	0.0064	126	890
Ph$^+$···L		0.0042	88	511	0.0090	180	970

formation of a H-bound 1-Np$^+$···L dimer, to which further π-bound ligands are attached. The exact position of the π-bound ligands is however not easy to specify (e.g., over the first or the second aromatic ring) and dificult to determine from both the present spectroscopic and theoretical approaches. As DFT calculations do not properly describe dispersion forces, π-bound 1-Np$^+$···L isomers were not investigated theoretically.[19] On the other hand, previous studies revealed that π-bound ligands have only very minor effects on the OH bond properties.[19],[36],[22]

3.3. Experimental details

The IRPD spectra of 1-Np$^+$···L$_n$ complexes (L = Ar, N$_2$, n ≤ 5) were recorded over the O-H and C-H stretch ranges using the QOQ tandem mass spectrometer coupled to the electron impact ion source (EI + QMF1 + OP + QMF2) described in the **Experimental setup** chapter of this work; only the details specific to the 1-Np$^+$···L$_n$ IRPD experiment are presented here. The expanding gas mixture was produced by injecting the ligand / buffer gas (Ar or N$_2$ at static pressures of 3...10 bar) through a cell containing molten 1-Np (T ≅ 350 K). 1-Np$^+$···L$_n$ clusters were produced by EI of 1-Np and subsequent three-body association reactions in the high pressure region of the expansion:[20]
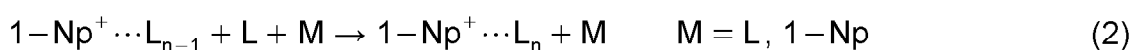
$$1-Np + e^- \rightarrow 1-Np^+ + 2 \cdot e^- \tag{1}$$

$$1-Np^+ \cdots L_{n-1} + L + M \rightarrow 1-Np^+ \cdots L_n + M \qquad M = L, 1-Np \tag{2}$$

Previous experiments of small (substituted and / or protonated) arenes are showing that this reaction sequence produces the most stable A(H)$^+$···L$_n$ complexes and to smaller

extent less stable isomers.[20],[21],[22],[23],[24],[42],[48] Alternative mechanisms involve the formation of neutral 1-Np···L_n complexes and their subsequent electron impact ionization or the formation of a neutral L_n cluster followed by its attachment to a 1-Np$^+$ cation. These mechanisms are known to play only a minor role in the production of complexes in the ion source used here.[20]

Figure 3. *Mass spectrum of the output of the EI ion source, obtained after optimization for 1-Np$^+$···(N$_2$)$_n$ generation; N$_2$ (at 3 bar) was used as carrier gas; the 1-Np sample was heated at $\cong$ 350 K. The inset shows a vertically expanded version of the spectrum (X50) to ease the identification of weak peaks.* ▲ *marks the sequence of 1-Np$^+$···(N$_2$)$_n$ (144 + n·28 u);* ▲ *marks the sequence of N$_n^+$;* ▲ *marks the sequence of H$_2$O$^+$···(N$_2$)$_n$, H$_2$O being a contaminant coming from the gas inlet system. Integration over the peaks of 1-Np$^+$···(N$_2$)$_n$ yields an abundance of 80 : 8 : 2 : 1 for n = 0...3.*
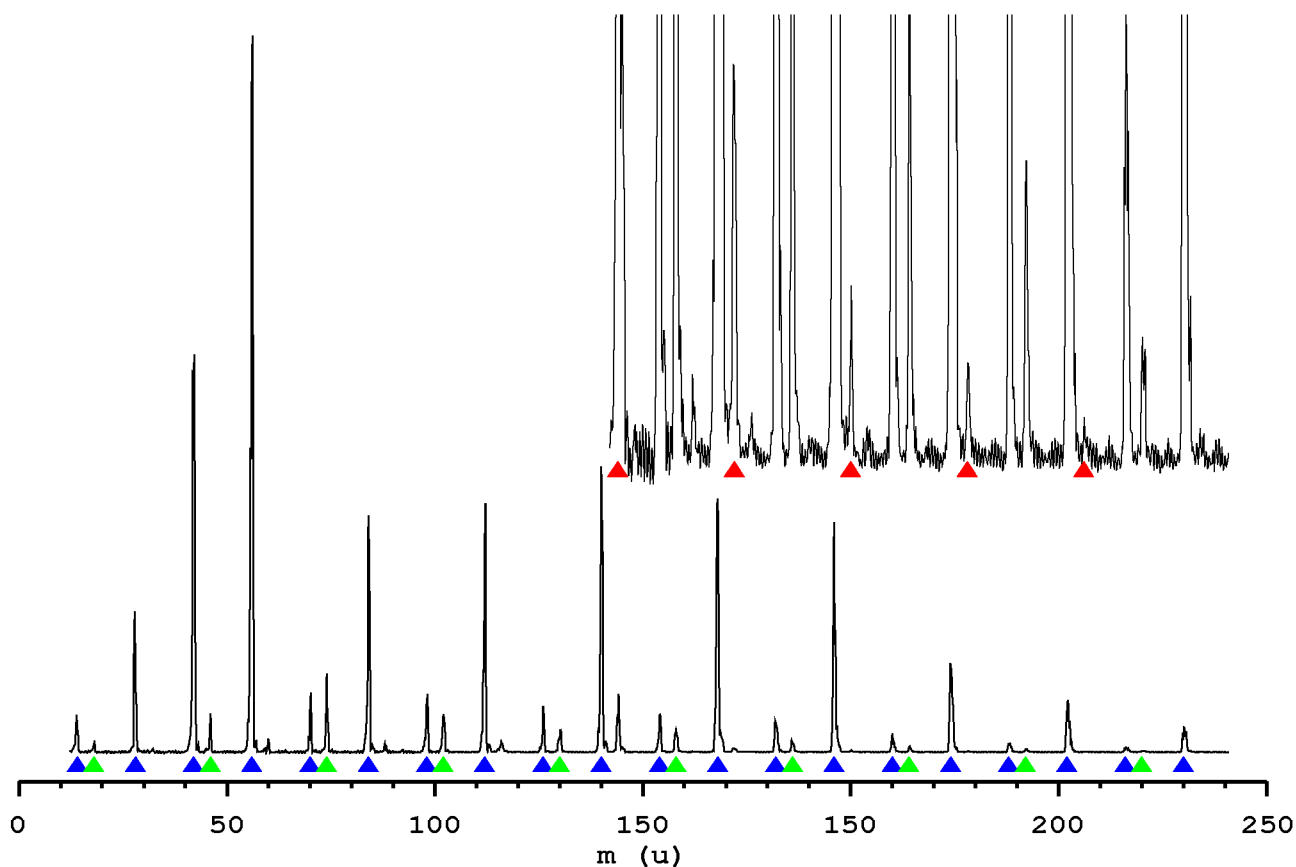

Figure 3 shows a mass spectrum of the ion source recorded after optimization for 1-Np$^+$···(N$_2$)$_n$ generation. The spectrum is dominated by N$_n^+$ ions; the sequence of [1-Np···(N$_2$)$_n$]$^+$ cluster ions is clearly visible; also a sequence of [H$_2$O···(N$_2$)$_n$]$^+$ ions can be seen, due to the contamination of the gas feeding lines with H$_2$O. The intensity ratios of 1-Np$^+$···(N$_2$)$_n$ are of the order of 80 : 8 : 2 : 1 for n = 0...3, indicating the sequential

formation of weakly-bound noncovalent complexes.

The IR spectra of $1\text{-Np}^+\cdots L_n$ are obtained by monitoring the amount of $1\text{-Np}^+\cdots L_m$ fragments generated in the octopole by the absorption of the IR laser beam by $1\text{-Np}^+\cdots L_n$ as a function of the wavelength of the excitation laser:
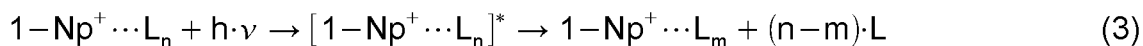
$$1-\text{Np}^+\cdots L_n + h\cdot\nu \rightarrow [1-\text{Np}^+\cdots L_n]^* \rightarrow 1-\text{Np}^+\cdots L_m + (n-m)\cdot L \qquad (3)$$

As the energy density of the excitation laser beam was too low ($I < 200$ kW/cm^2) for multiple photon absorption to occur, no photodissociation channels involving the fragmentation of the 1-Np^+ cation were observed.

For certain $1\text{-Np}^+\cdots(N_2)_n$ parent complexes ($n > 3$), several concurrent fragment channels (m) are appearing. In this situation, the IR spectra were recorded simultaneously in the two highest-intensity fragment channels. As the spectra recorded in different fragment channels are similar, only the spectra obtained in the dominant channels will be shown. The wavelength of the laser was calibrated to an accuracy of better than 1 cm^{-1} using the absorption of the laser beam by atmospheric water.
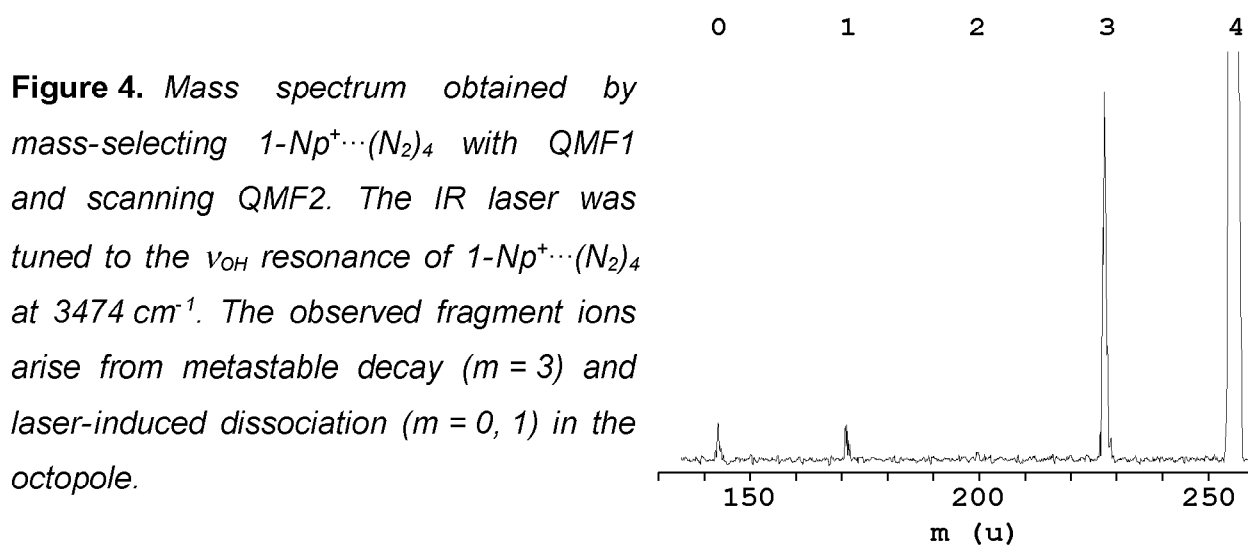
Figure 4. *Mass spectrum obtained by mass-selecting $1\text{-Np}^+\cdots(N_2)_4$ with QMF1 and scanning QMF2. The IR laser was tuned to the ν_{OH} resonance of $1\text{-Np}^+\cdots(N_2)_4$ at 3474 cm^{-1}. The observed fragment ions arise from metastable decay (m = 3) and laser-induced dissociation (m = 0, 1) in the octopole.*

As an example of the photofragmentation process, in Figure 4 are presented mass spectra recorded with QMF2, as QMF1 was filtering only the mass of $1\text{-Np}^+\cdots(N_2)_4$. The large signal in the m = 3 fragment channel is the result of the metastable decay of the hot complexes. The signals in the m = 0 and m = 1 channels are the results of the laser-induced dissociation of $1\text{-Np}^+\cdots(N_2)_4$.

3.4. Results and discussion

A comparison of the EI-IRPD spectra of $1\text{-Np}^+\cdots N_2$ and $1\text{-Np}^+\cdots Ar$ with the REMPI-IR

spectrum of t-1-Np$^+$···Ar is presented in Figure 5. The strong dependence of the spectra on the parameters of the ion source is underlined in Figure 6, which presents two spectra of 1-Np$^+$···N$_2$ recorded under "cold" (Figure 6a) and "warm" (Figure 6b) expansion conditions. Finally, the EI-IRPD spectra of 1-Np$^+$···Ar$_n$ (n = 1, 2) and 1-Np$^+$···(N$_2$)$_n$ (n = 1...5) recorded in the OH stretch range are shown in together in Figure 7. Table 6 summarizes the band maxima and widths of the ν_{OH} transitions observed (A-C), along with their isomer assignments.

3.4.1. 1-Np$^+$···L dimers

The EI-IRPD spectrum of 1-Np$^+$···Ar (Figure 5b) displays two transitions, which are attributed to the ν_{OH} fundamentals of the H-bound (A) and π-bound (B) isomers of t-1-Np$^+$···Ar, respectively. These assignments are based on the band positions, relative IR intensities, and band profiles, as well as the comparison with the DFT calculations and the REMPI-IR spectrum.

The more intense band at 3538 cm^{-1} (A) is assigned to ν_{OH} of H-bound t-1-Np$^+$···Ar (Figure 1e). The derived complexation-induced red-shift of -41 cm^{-1} from the corresponding t-1-Np$^+$ transition (3579 cm^{-1})[36] is consistent with the calculated value (-57 cm^{-1}). The blue-shaded band contour with a sharp P branch head is characteristic for excitation of a proton donor stretch vibration, because the intermolecular H-bond becomes stronger and shorter in the excited state, resulting in larger rotational constants.[17],[19],[45],[48]

Band B (3580 cm^{-1}) is assigned to ν_{OH} of π-bound t-1-Np$^+$···Ar complexes. The position is in good agreement with the REMPI-IR spectrum (Figure 5c).[36] The modest complexation-induced blue shift of +1 cm^{-1} and the rather symmetric band profile support this assignment, because intermolecular π-bonding has almost no influence on the OH bond. It must be noted that there are actually other binding sites, which also have little impact on the OH bond, such as H-bonding to aromatic CH groups. Although these alternative binding sites cannot be completely ruled out from both the experimental and the theoretical point of view, the presently favored assignment for B is to a π-bound isomer. This scenario is supported by theoretical and spectroscopic data obtained for BzH$^+$···Ar[31],[32], Bz$^+$···Ar[30],[49], and PhH$^+$···Ar[29], which indicate that intermolecular CH···Ar bonds in A(H)$^+$···Ar are less stable than π-bonds. The assignment of band B to a π-bound isomer is used as working hypothesis for further discussion in this chapter.

The EI-IRPD spectrum of t-1-Np$^+$···Ar clearly demonstrates that the H-bound isomer is the global minimum on the intermolecular potential, whereas the π-bound structure is a less stable local minimum. Nonetheless, the H-bound isomer could not be detected in the

Figure 5. *EI-IRPD spectra of 1-Np$^{+}\cdots$L dimers with L = N$_2$ (a) and Ar (b) over the O-H stretch range compared to the REMPI-IRPD spectrum of t-1-Np$^{+}\cdots$Ar (c*). All EI-IRPD spectra were recorded in the 1-Np^{+} fragment channel. The line indicates the v_{OH} position of free t-1-Np^{+} (3579 cm^{-1*}). The vibrational and isomer assignments of the transitions observed are listed in Table 6.*
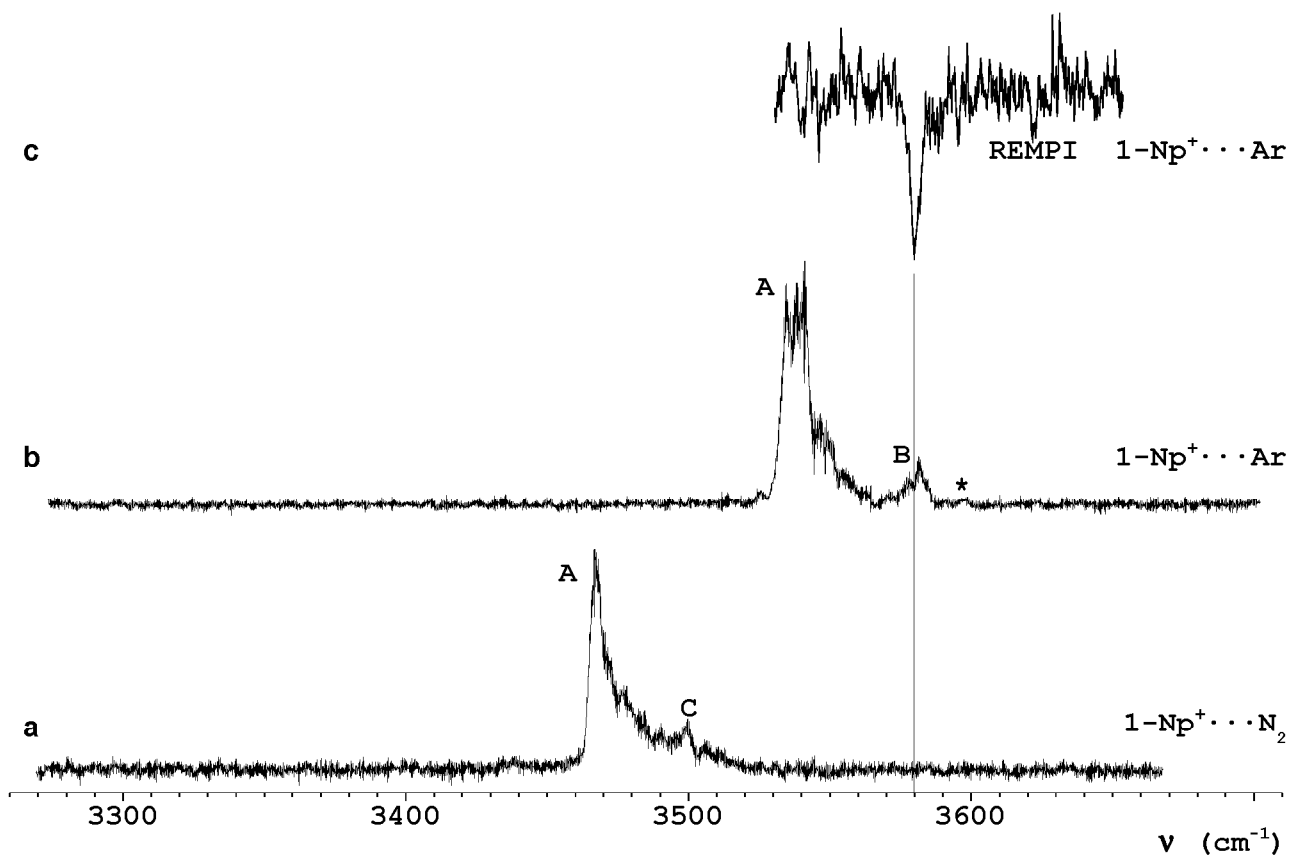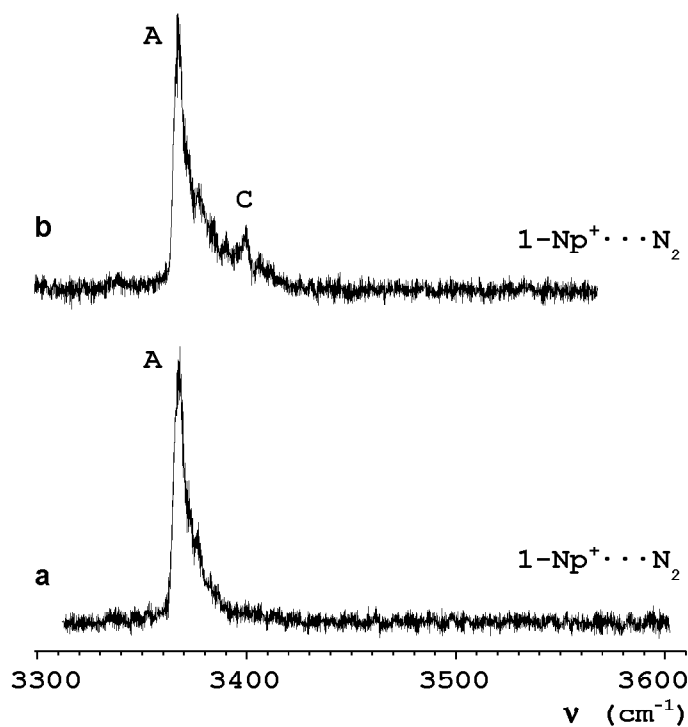

Figure 6. *EI-IRPD spectra of 1-Np$^{+}\cdots$N$_2$ obtained under warm (a) and cold (b) expansion conditions.*

38

REMPI-IR spectrum (Figure 5c)[36], because it was obtained through resonant ionization of π-bound t-1-Np$^+$···Ar. In contrast to both H- and π-bound t-1-Np$^+$···Ar dimers, spectroscopic indication of the corresponding c-1-Np$^+$···Ar complexes in the EI-IRPD spectra is uncertain. As the ν_{OH} frequency of bare c-1-Np$^+$ has not been measured[36], one must rely on the calculated value which is slightly larger than for t-1-Np$^+$ (+8 cm^{-1}). Some of the EI-IRPD spectra recorded for 1-Np$^+$···Ar actually reveal a very weak band at 3595 cm^{-1} (indicated by an asterisk in Figure 5b) appearing about 15 cm^{-1} to the blue of π-bound t-1-Np$^+$···Ar. At first glance, this signal may be attributed to ν_{OH} of π-bound c-1-Np$^+$···Ar, which could occur in detectable abundance only under certain experimental conditions. If this interpretation were correct, a minor part of the blue wing of band A may arise from ν_{OH} of H-bound c-1-Np$^+$···Ar (Figure 1e). However, according to the analysis of the 1-Np$^+$···N$_2$ spectra (vide infra), the abundances of c-1-Np$^+$ and its Ar complex are probably too small for observing ν_{OH} of π-bound c-1-Np$^+$···Ar even under favorable (e.g., warm) expansion conditions. Thus, the interpretation of the weak 3595 cm^{-1} band remains open.

Table 6. *Band maxima and widths (FWHM, in parentheses) of the ν_{OH} transitions observed in the EI-IRPD spectra of 1-Np$^+$···L$_n$, recorded in the dominant fragment channels, along with their isomer assignments; (H/xπ) denotes an isomer with one H-bound and x π-bound ligands (1 + x = n).*

ν_{OH} (cm^{-1})	band	isomer
3538 (10)	A	t-1-Np$^+$···Ar (H)
3580 (10)	B	t-1-Np$^+$···Ar (π)
3539 (10)	A	t-1-Np$^+$···Ar (H)
3467 (6)	A	t-1-Np$^+$···N$_2$(H)
3499 (5)	C	c-1-Np$^+$···N$_2$ (H/π)
3469 (5)	A	t-1-Np$^+$···(N$_2$)$_2$ (H/π)
3499 (5)	C	c-1-Np$^+$···(N$_2$)$_2$ (H/π)
3472 (8)	A	t-1-Np$^+$···(N$_2$)$_3$ (H/2π)
3500 (5)	C	c-1-Np$^+$···(N$_2$)$_3$ (H/2π)
3474 (7)	A	t-1-Np$^+$···(N$_2$)$_4$ (H/3π)
3501 (6)	C	c-1-Np$^+$···(N$_2$)$_4$ (H/3π)
3476 (16)	A	t-1-Np$^+$···(N$_2$)$_5$ (H/4π)
3502 (13)	C	c-1-Np$^+$···(N$_2$)$_5$ (H/4π)

The spectrum of 1-Np$^+$···N$_2$ was recorded under two different supersonic expansion

conditions: "cold" (Figure 6a), characterized by a narrow rotational contour and "warm" (Figure 6b), exhibiting a slightly larger FWHM. To facilitate the comparison with $1\text{-Np}^+\cdots\text{Ar}$, the "cold" spectrum was plotted also in Figure 5a. The "cold" spectrum displays a single blue-shaded band at 3467 cm^{-1} (A), which is assigned to ν_{OH} of H-bound $t\text{-}1\text{-Np}^+\cdots\text{N}_2$ (Figure 1h). The measured red-shift of -112 cm^{-1} upon H-bonding is slightly smaller than the calculated value of -134 cm^{-1}. Moreover, it is roughly three times larger than the one for $t\text{-}1\text{-Np}^+\cdots\text{Ar}$ (-41 cm^{-1}) because of the stronger H-bond. In addition to band A, the "warm" $1\text{-Np}^+\cdots\text{N}_2$ spectrum shows a transition at 3499 cm^{-1} (C), which is absent in the "cold" spectrum. This band is attributed to ν_{OH} of H-bound $c\text{-}1\text{-Np}^+\cdots\text{N}_2$ (Figure 1i). The -88 cm^{-1} shift from calculated ν_{OH} of $c\text{-}1\text{-Np}^+$ (3587 cm^{-1}) agrees with the prediction (-91 cm^{-1}). Both EI-IRPD spectra of $1\text{-Np}^+\cdots\text{N}_2$ do not show any absorption near 3580 cm^{-1}, implying that the abundances of the π-bound $x\text{-}1\text{-Np}^+\cdots\text{N}_2$ isomers were below the detection limit under both "warm" and "cold" conditions.

The spectra of $1\text{-Np}^+\cdots\text{L}$ can yield information about the relative abundance of the H-bound and π-bound $t\text{-}1\text{-Np}^+\cdots\text{L}$ dimers in the plasma expansion, via the ratio of the integrated intensities of bands A and B. The integrated intensity of each band depends on the IR oscillator strength of the vibration responsible for the band and on the abundance of the dimer responsible for the band. Thus, for a given ligand, the ratio of the integrated intensities of bands A and B is proportional to the relative abundance of the H-bound and π-bound $t\text{-}1\text{-Np}^+\cdots\text{L}$ dimers. The constant of proportionality is the ratio between the IR intensities of the ν_{OH} vibrations of the H-bound and π-bound $t\text{-}1\text{-Np}^+\cdots\text{L}$ dimers (Table 6). However, no calculations have been made for the π-bound $t\text{-}1\text{-Np}^+\cdots\text{L}$ dimers; in this situation their IR intensity is approximated by the IR intensity of the $t\text{-}1\text{-Np}^+$ monomer.[19],[23],[26] This approximation is considered appropriate because previous studies have shown that π-bonding has little effect on the properties of a functional group. For $t\text{-}1\text{-Np}^+\cdots\text{Ar}$, this procedure results in an abundance ratio of $N_H : N_\pi \approx 1.6$, on the basis of the experimental ν_{OH} intensity ratio of ≈ 4 and the theoretical ratio $I_H : I_\pi \approx 2.5$. For $t\text{-}1\text{-Np}^+\cdots\text{N}_2$, a lower limit for $N_H : N_\pi > 10$ can be estimated from the achieved signal-to-noise ratio (≈ 40) and $I_H : I_\pi \approx 4$. The larger abundance of the H-bound $t\text{-}1\text{-Np}^+\cdots\text{L}$ isomers suggests that they are more stable than the π-bound dimers, because the EI source produces predominantly the most stable isomer of a given complex.[20],[50] Moreover, the energy difference between both isomers appears to be significantly larger for $t\text{-}1\text{-Np}^+\cdots\text{N}_2$ than for $t\text{-}1\text{-Np}^+\cdots\text{Ar}$, resulting in a less eficient production of the π-bound isomer for the N_2 complex. Similar to previous studies on $\text{Ph}^+\cdots\text{Ar}$[21] and $\text{In}^+\cdots\text{Ar}$[24], the relative intensity ratio of the ν_{OH} bands of H-bound

and π-bound t-1-Np$^+$···Ar depended on the expansion conditions, confirming that both transitions arise indeed from two different isomers. The spectrum in Figure 5b was obtained when the conditions were optimized for the production of π-bound t-1-Np$^+$···Ar. As the relative population of the H-bound isomer increased for decreasing effective source temperature, this isomer corresponds to the global minimum of the t-1-Np$^+$···Ar potential, whereas the π-bound structure is a less stable local minimum.

In a similar fashion, the "warm" spectrum of 1-Np$^+$···N$_2$ (Figure 6b) yields $N_t : N_c \approx 8$ for the ratio between the H-bound x-1-Np$^+$···N$_2$ populations (the integrated band strengths ratio is ~18 and the predicted IR intensity ratio is ~2.3). As the N$_2$ complexation energies are similar for both t-1-Np$^+$ and c-1-Np$^+$ (927 cm^{-1} and 803 cm^{-1} respectively), the c-1-Np$^+$ concentration in the plasma expansion is estimated to be roughly one order of magnitude smaller than that of t-1-Np$^+$. This result can be checked for consistency with the production mechanism described in the experimental details section and the internal rotation potentials in Figure 2. Assuming for the gas mixture a temperature of $T \cong 350$ K at nozzle level and knowing the experimental difference between the ground level energies of c-1-Np and t-1-Np ($\Delta E \cong 220$ cm^{-1}) the thermal population ratio is estimated to be $N_t : N_c \approx 2.5$.[40] Adiabatic cooling in the supersonic expansion increases this ratio only slightly because both isomers are separated by a significant barrier ($E_{bar,calc}^{1-Np} = 1121$ cm^{-1}, corresponding to $T = 1610$ K).[51] Assuming that the EI process described in (1) is mainly a vertical ionization process, a similar ratio is obtained for the x-1-Np$^+$ rotamers because isomerization is hindered in D$_0$ by a barrier ($E_{bar,calc}^{1-Np+} = 3198$ cm^{-1}) even larger than $E_{bar,calc}^{1-Np}$. Owing to comparable complexation energies for H-bonding and also π-bonding for both 1-Np$^+$ rotamers, the t/c-1-Np$^+$···L dimer population ratios should be similar to the t/c-1-Np$^+$ monomer ratios, (2), i.e. $N_t : N_c \approx 3...10$ depending on the eficiency of adiabatic cooling of neutral t/c-1-Np. Thus, the deduced ratio of $N_t : N_c \approx 8$ for the H-bound x-1-Np$^+$···N$_2$ isomers is within the expected range. If the weak 3595 cm^{-1} band in the 1-Np$^+$···Ar spectrum were indeed due to ν_{OH} of π-bound c-1-Np$^+$···Ar, the relative abundance of π-bound x-1-Np$^+$···Ar (and also x-1-Np$^+$) would be derived as $N_t : N_c \approx 2.1$ from the experimental (≈ 5) and predicted (≈ 2.4) ν_{OH} intensity ratios. This rather small ratio would imply an unexpectedly high population of both c-1-Np$^+$ and π-bound c-1-Np$^+$···Ar and makes this tentative assignment questionable.

3.4.2. Larger 1-Np$^+$···L$_n$ complexes

Figure 7 reproduces the EI-IRPD spectra of 1-Np$^+$···Ar$_n$ (n = 1, 2) and 1-Np$^+$···(N$_2$)$_n$

Figure 7. *EI-IRPD spectra of 1-Np$^+$···L$_n$ for L = Ar (n = 1,2) and L = N$_2$ (n = 1...5), recorded in the dominant 1-Np$^+$···L$_m$ fragment channel (Table 7). The vibrational and isomer assignments of the transitions observed are listed in Table 6.*
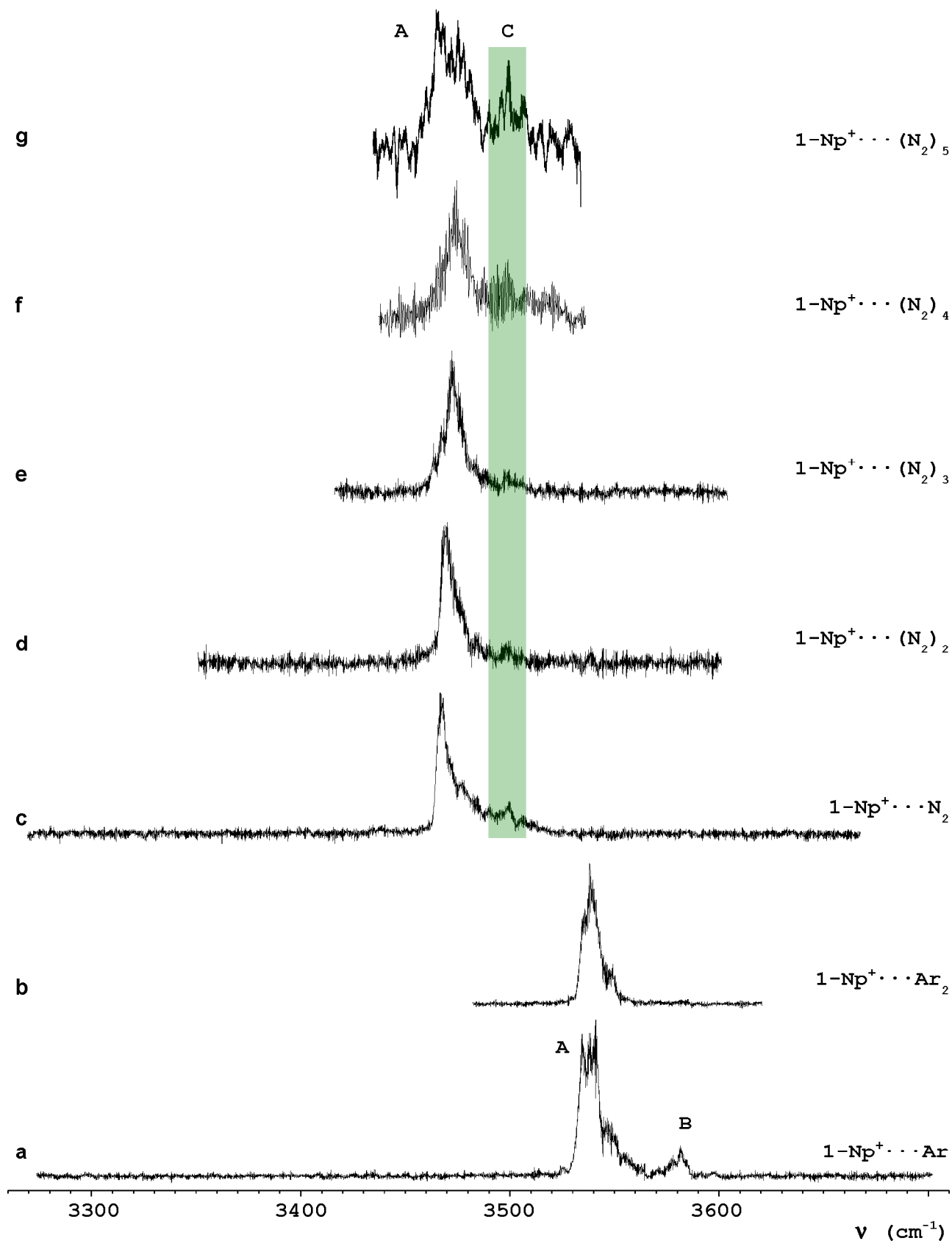
(n = 1...5) recorded in the dominant fragment channels; the photofragmentation ratio is listed in Table 7. As seen before, the 1-Np$^+\cdots$Ar spectrum (Figure 7a) is dominated by two transitions at 3538 cm^{-1} (A) and 3580 cm^{-1} (B) assigned to ν_{OH} of H-bound and π-bound t-1-Np$^+\cdots$Ar. The 1-Np$^+\cdots$Ar$_2$ spectrum (Figure 7b) reveals only a single band at 3539 cm^{-1} (A), which is blue-shifted by +1 cm^{-1} from band A of H-bound t-1-Np$^+\cdots$Ar. Consequently, this band is assigned to ν_{OH} of a t-1-Np$^+\cdots$Ar$_2$ isomer, which is obtained by adding a π-bound ligand to the H-bound t-1-Np$^+\cdots$Ar dimer; this trimer will further be denoted t-1-Np$^+\cdots$Ar$_2$ (H/π). It should be noted that the +1 cm^{-1} blue-shifting has also been observed for the attachment of a π-bound Ar ligand to bare t-1-Np$^+$. Obviously, it is interesting to search for the t-1-Np$^+\cdots$Ar$_2$ isomers with two π-bound ligands, t-1-Np$^+\cdots$Ar$_2$ (2π); the ν_{OH} transitions of these isomers are expected near 3580 cm^{-1}. As the 1-Np$^+\cdots$Ar$_2$ spectrum lacks any signal in that frequency range, it is reasonable to consider the abundance of t-1-Np$^+\cdots$Ar$_2$ (2π) isomers as being below the detection limit; consequently, the abundance ratio of t-1-Np$^+\cdots$Ar$_2$ (2π) and t-1-Np$^+\cdots$Ar$_2$ (H/π) is estimated to be less than 5%. A direct implication is that the H-bond between Ar and t-1-Np$^+$ is stronger than the π-bond; this means that the preferred solvation sequence in small t-1-Np$^+\cdots$Ar$_n$ complexes begins with the formation of an H-bound t-1-Np$^+\cdots$Ar dimer core, which is further solvated by (n-1) π-bound ligands.

The 1-Np$^+\cdots$N$_2$ spectrum (Figure 7c) displays two transitions at 3467 cm^{-1} (A) and 3499 cm^{-1} (C), which, as discussed above, are assigned to ν_{OH} of the H-bound isomers of x-1-Np$^+\cdots$N$_2$. Figure 7d ... f shows the effects resulting from the attachment of four further N$_2$ ligands. The observed small incremental blue-shifts suggest that the dominant x-1-Np$^+\cdots$(N$_2$)$_n$ complexes have one H-bound and (n-1) π-bound ligands. Figure 8 shows a plot of the ν_{OH} frequencies of x-1-Np$^+\cdots$L$_n$ as a function of the cluster size n.

3.4.3. Ligand binding energies

Table 7 lists the photofragmentation branching ratios obtained upon resonant excitation of the OH stretch vibration of t-1-Np$^+\cdots$(N$_2$)$_n$. In agreement with previous studies on related systems, the range of photoinduced fragment channels (m) for a given parent cluster size (n) is rather narrow (Figure 4).[21],[24],[26],[29] The photofragmentation branching ratios can be used to extract rough estimates of the binding energies of the ligands. For this, several assumptions about the evaporation process have to be made. First, one has to consider that all the energy of the absorbed photon (ν_{OH}) is available for ligand evaporation.[21] Also, only one ligand is considered to be H-bound while the others are

π-bound; no other binding sites will be included in this simple model. The relative intensities of bands A and B of the t-1-$Np^+ \cdots Ar$ spectrum suggest that the H-bond of Ar to t-1-Np^+ is more stable than the π-bond, $(D_0(H) > D_0(\pi))$; as band B is below the detection limit for the 1-$Np^+ \cdots N_2$ dimers, the $D_0(H) > D_0(\pi)$ inequality is expected to be valid also for the 1-$Np^+ \cdots (N_2)_n$ complexes. In order to further simplify the model, one can assume that the weakest bound ligands evaporate first and that all π-bound ligands have the same binding energy. Table 7 shows that the complexes with 6 and 7 N_2 ligands are shedding mainly 5 ligands upon excitation with a photon of about 3500 cm^{-1}; thus, the estimated dissociation energy of the π-bound ligands is $D_0(\pi) \approx 640 \pm 60$ cm^{-1}. This evaluation of $D_0(\pi)$ can further be used together with the branching ratio observed for the complex with 5 N_2 ligands to extract an estimation for $D_0(H)$. The fact that ~3500 cm^{-1} are enough for the evaporation of three π-bound and one H-bound ligands from t-1-$Np^+ \cdots (N_2)_4$ sets the upper limit for $D_0(H)$ at 2000 cm^{-1}. The lower limit (500 cm^{-1}) is given by the fact that the H-bound ligands are stronger bound than the π-bound ones. These limits can be translated into $D_0(H) \approx 1210 \pm 530$ cm^{-1}, which agrees with the predicted value, $D_0(H) = 927$ cm^{-1}. Within the cluster size range investigated, the ν_{OH} bands assigned to c-1-$Np^+ \cdots (N_2)_n$ display photofragmentation branchings similar to the ν_{OH} bands of t-1-$Np^+ \cdots (N_2)_n$, confirming that $D_0(\pi)$ and $D_0(H)$ are roughly comparable for both 1-Np^+ rotamers.

Table 7. *Photofragmentation branching ratios (in percents) of t-1-$Np^+ \cdots L_n$ complexes for the reaction presented in* **(3)** *as measured at the ν_{OH} band maxima of the most stable isomers; only channels with contributions larger than 5% are listed; uncertainties are estimated as 5%.*

Ligand	n	m = 0	m = 1	m = 2	m = 3
Ar	1,2	100			
N_2	1,2,3	100			
N_2	4	60	40		
N_2	5		70	30	
N_2	6		45	30	25
N_2	7		15	50	35

As the t-1-$Np^+ \cdots Ar_2$ (H/π) trimer evaporates both ligands upon ν_{OH} excitation, the only information which can be extracted from the photofragmentation is that $D_0(H) + D_0(\pi) < 3540$ cm^{-1}. Fortunately, further refinement of these numbers is possible via comparisons with previously investigated similar systems. The binding energies of the

π-bound dimers of Bz$^+$···Ar, para-difluorobenzene$^+$···Ar, In$^+$···Ar, and Ph$^+$···Ar were accurately measured as 512 ± 3 cm^{-1}[16], 572 ± 6 cm^{-1}[7], 537 ± 10 cm^{-1}[52], and 535 ± 3 cm^{-1}[53], respectively. This suggests that the strength of the π-bond of Ar to an aromatic cation (A$^+$) is rather insensitive to the detailed structure of A$^+$[31], contrasting with the neutral A···Ar dimers, where $D_0(\pi)$ increases with the number of aromatic rings.[16] Thus, one can assume for the x-1-Np$^+$···Ar dimers a binding energy $D_0(\pi) = 550 \pm 50$ cm^{-1}, setting upper and lower limits for $D_0(H)$ of x-1-Np$^+$···Ar: 500 cm^{-1} < $D_0(H)$ < 3040 cm^{-1}. Further comparisons of the Ph$^+$···Ar with the t-1-Np$^+$···Ar spectra offers reasons for further reducing the upper limit of $D_0(H)$ of x-1-Np$^+$···Ar to something smaller than $D_0(H)$ of Ph$^+$···Ar (670 $\pm$ 140 cm^{-1})[20]. First, Δv_{OH} of H-bound t-1-Np$^+$···Ar is much smaller than Δv_{OH} of H-bound Ph$^+$···Ar (1.15% vs. 2.0%)[20], because t-1-Np$^+$ is less acidic than Ph$^+$. Second, the $N_H : N_\pi$ ratio of t-1-Np$^+$···Ar in the EI source is lower than for Ph$^+$···Ar under comparable conditions. When the conditions are optimized for the generation of the π-bound isomers, $N_H : N_\pi \approx 1.6$ for t-1-Np$^+$···Ar and $N_H : N_\pi \approx 4$ for Ph$^+$···Ar[22]. This comparison suggests that $D_0(H) - D_0(\pi)$ is larger for Ph$^+$···Ar than for t-1-Np$^+$···Ar. Because $D_0(\pi)$ of Ph$^+$···Ar and t-1-Np$^+$···Ar are comparable, $D_0(H)$ of Ph$^+$···Ar provides an upper limit for $D_0(H)$ of t-1-Np$^+$···Ar: 500 cm^{-1} < $D_0(H)$ < 800 cm^{-1} or $D_0(H) \approx 650 \pm 150$ cm^{-1}. Thus, the calculated dissociation energy of $D_0 = 274$ cm^{-1} substantially underestimates the true interaction energy, in line with conclusions previously drawn for UB3LYP/6-311G(2df,2pd) calculations of related Ar complexes.[19],[22],[23],[28]

3.4.4. Microsolvation of t-1-Np$^+$ by N$_2$

As seen above, the calculations are yielding two types of minima on the intermolecular PES of x-1-Np$^+$···N$_2$, namely H-bound global minima and less stable π-bound dimers. The lack of absorptions of π-bound t/c-Np$^+$···N$_2$ in the recorded IR spectra demonstrates that indeed, π-bound dimers are substantially less stable local minima. The absence of absorptions over the range of π-bound dimers has also been witnessed for Ph$^+$···N$_2$,[19] PhH$^+$···N$_2$,[29] and An$^+$···N$_2$;[26] at the same time, a weak band was assigned to the π-bound In$^+$···N$_2$[24] isomer. It is notable that the PA of In is the smallest of all other investigated dimers; the connection between PA and the preferred ligand binding motif can easily be extended by adding A(H)' without acidic functional groups, such as Bz(H)', which also prefer π-bonds with N$_2$ over H-bonds.[30],[31]

The ligand binding energies extracted from the photofragmentation data show that the dissociation energies of π-bound A(H)$^+$···N$_2$ are relatively insensitive to the detailed

structure of A(H)$^+$.[31] Indeed, IRPD of 1-Np$^+$···(N$_2$)$_n$ yields D$_0$(π) = 640± 60 cm^{-1} for the dominant t-1-Np$^+$ rotamer, similar to the dissociation energies of the π-bound Ph$^+$···N$_2$ - 750 ± 150 cm^{-1},[20] An$^+$···N$_2$ - 700 ± 200 cm^{-1},[26] BzH$^+$···N$_2$ - 800 cm^{-1},[31] and the carbenium isomers of PhH$^+$···N$_2$ - 750 ± 150 cm^{-1}. [29] In contrast, the strength of the H-bonds in A(H)$^+$···N$_2$ depends heavily on the acidity of the proton donor group of A(H)$^+$. It should be noted that for all A(H)$^+$ with acidic groups D$_0$(H) » D$_0$(π). Also the optimal 1-Np$^+$···L interaction is significantly stronger than the L-L attraction, (D$_0$ ~ 100 cm^{-1} for both Ar···Ar and N$_2$···N$_2$).[54],[55] Thus, the 1-Np$^+$···L$_n$ cluster growth is mainly driven by the 1-Np$^+$···L dimer potential, because three-body forces are small for ion complexes with nonpolar ligands. Consequently, the solvation sequence for the most stable 1-Np$^+$···L$_n$ complexes starts with the formation of H-bound 1-Np$^+$···L, which is further solvated by (n-1) π-bound ligands. A similar cluster growth was deduced for Ph(H)$^+$···L$_n$ and An$^+$···L$_n$ with L = Ar and N$_2$, which also starts with the solvation of the acidic protons of the OH$_{(2)}$ and NH$_2$ groups by H-bound ligands, before further π-bound ligands are attached to the aromatic ring.[20],[24],[26],[29]

Figure 8. *Position of the maxima of the v_{OH} bands of the most stable isomers observed in the EI-IRPD spectra of various A(H)$^+$···Ar$_n$ and A(H)$^+$···(N$_2$)$_n$ as a function of the number of ligands (n). A(H)$^+$ = t-1-Np$^+$ (●), c-1-Np$^+$ (●), Ph$^+$ (●),[20] and the carbenium ions (ortho and / or para protonation) of PhH$^+$ (●).[29] As no experimental value is available for $v_{OH}^{c-1-Np^+}$, the value plotted here is derived from calculations.*
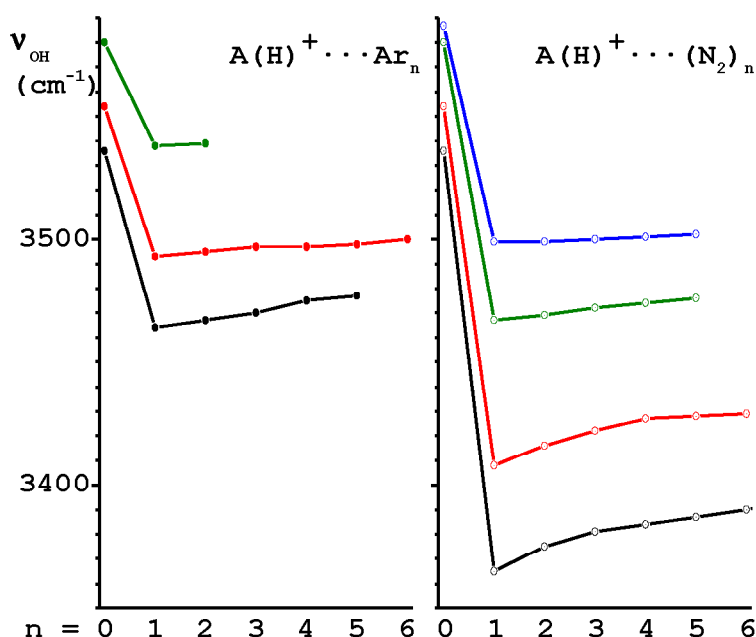

Figure 8 plots the v_{OH} frequencies of the most stable isomers for some A(H)$^+$···Ar$_n$ and A(H)$^+$···(N$_2$)$_n$ complexes as a function of the cluster size n. The A(H)$^+$ ions include monohydroxyarene radical cations (A$^+$ = Ph$^+$, t-1-Np$^+$, c-1-Np$^+$) as well as carbenium ions of PhH$^+$, which all possess a single OH group. The plots mirror the preferred evolution of the solvation subshells in these clusters:

* the first H-bound ligand induces a large v_{OH} red shift because of the destabilization

of the O-H bond upon intermolecular H-bonding. The size of Δv_{OH} is correlated with the strength of the intermolecular interaction: $|\Delta v_{OH}|$ is larger for N_2 dimers than for Ar dimers and increases for rising OH acidity in the order c-1-Np$^+$ < t-1-Np$^+$ < PhH$^+$ < Ph$^+$, which is also reflected by decreasing v_{OH} frequencies of the bare monomers n = 0.

* the H-bound dimers (n = 1) are further solvated by π-bound ligands, which induce small incremental blue shifts of v_{OH}. Thus, π-bound ligands slightly destabilize the intermolecular H-bond to the first ligand via noncooperative three-body forces, which in turn stabilize the intramolecular O-H bond. As expected, the v_{OH} frequencies are not converged at the largest cluster size investigated (n ≤ 7), because the first solvent shell around A(H)$^+$ is not complete yet.

3.4.5. Proton affinity of 1-naphthoxy radical

As the PA of the t-1-naphthoxy radical has not been measured so far, one may try to evaluate it using the complexation-induced red-shift in the proton donor stretch vibration, Δv_{XH}. For of H-bound XH$^+$···L dimers, Δv_{XH} is correlated with the difference in the PA of the two bases X and L: the smaller PA(X) - PA(L), the stronger the intermolecular H···L bond and the larger Δv_{XH}.[17],[20],[45],[56],[57] This relation may be used to estimate unknown PA values of bases X from IR spectra of their XH$^+$···L dimers. Recently, this procedure was applied to XH$^+$ = In$^+$ to obtain the first experimental determination of the PA of the indolyl radical.[24] The relative red shifts measured for a series of H-bound Ar- and N_2-based dimers show a decrease correlated with the increase in PAs:

XH$^+$···N_2	SiOH$^+$	Ph$^+$	t-1-Np$^+$	In$^+$	An$^+$
$\dfrac{\Delta v_{XH}}{v_{XH}}\Big|_{L=Ar}$	5.9%	2.0%	1.15%	0.84%	0.31%
$\dfrac{\Delta v_{XH}}{v_{XH}}\Big|_{L=N2}$	14.1%	4.8%	3.13%	2.2%	0.57%
PA (kJ/mol)	778	873	908±5	923±3	950

The shifts are larger for L = N_2 compared to L = Ar, because PA(N_2) > PA(Ar) (494 kJ/mol vs. 369 kJ/mol).[58] Linear extrapolation using the data for Ph$^+$ and An$^+$ (measured independently), yields for the t-1-naphthoxy radical PA $\cong$ 908 kJ/mol. As the uncertainty of this method for determining PA values is not well documented, the error should be enlarged to ±30 kJ/mol. The PA of c-1-naphthoxy is predicted to be larger by around 10 kJ/mol according to the smaller Δv_{OH} values. These evaluations demonstrate that IR

spectroscopy of cluster ions can be used to selectively probe thermochemical properties, such as the PA, of specific conformers of transient radicals.

3.5. Conclusions

The acidity of the x-1-Np$^+$ rotamers and their microsolvation in nonpolar hydrophobic solvents have been investigated by DFT calculations and IR spectra of size-selected 1-Np$^+\cdots$Ar$_n$ (n = 1, 2) and 1-Np$^+\cdots$(N$_2$)$_n$ (n = 1...5) complexes. The shifts in the frequency as well as the enhancement in the intensity of the OH stretch vibration (Δv_{OH}) which result from the complexation have been studied yielding dependences on both the species of the ligands (L) and the number of ligands (n). The photofragmentation branching ratios of 1-Np$^+\cdots$L$_n$ provides information about the microsolvation of both 1-Np$^+$ rotamers in Ar and N$_2$. The IR spectra demonstrate that the preferred ion-ligand binding motif between 1-Np$^+$ and L is H-bonding to the acidic OH group, whereas π-bonding to the aromatic ring is less favorable. Consequently, the preferred 1-Np$^+\cdots$L$_n$ cluster growth begins with the formation of H-bound 1-Np$^+\cdots$L dimers, which are further solvated by (n-1) π-bound ligands. In general, the H/π-bonds in 1-Np$^+\cdots$(N$_2$)$_n$ are stronger than those in 1-Np$^+\cdots$Ar$_n$, mainly because of the additional charge-quadrupole interaction in the N$_2$ complexes. The detection of c-1-Np$^+\cdots$(N$_2$)$_n$ corresponds to the first observation of c-1-Np$^+$ complexes and enables thus direct comparison of both 1-Np$^+$ rotamers.

t-1-Np$^+$ is found to be slightly more acidic than c-1-Np$^+$ but both 1-Np$^+$ rotamers are considerably less acidic than Ph$^+$. Increasing charge delocalization causes the acidity of ROH$^+$ cations to decrease along the order H$_2$O$^+$ > Ph$^+$ > 1-Np$^+$, a trend opposite to the one observed for the corresponding neutral ROH molecules. The Δv_{OH} shifts of H-bound t-1-Np$^+\cdots$L yield a first experimental estimate for the proton affinity of the t-1-naphoxy radical as ~908 ± 30 kJ/mol demonstrating that IR spectroscopy of cluster ions can be used to probe thermochemical properties of transient radicals. The most stable 1-Np$^+\cdots$Ar structure (H-bound) differs qualitatively from that of the neutral dimer (π-bound), emphasizing the large impact of ionization on the interaction potential and the preferred recognition motif between aromatic molecules and nonpolar ligands. The ionization-induced switch in the preferred binding site from π-bonding in A$\cdots$Ar to H-bonding in A$^+\cdots$Ar has now been established for a large variety of A molecules with acidic functional YH$_k$ groups (Y = O, N) and seems to be a general phenomenon.

The mechanism for clusters generation is shown to be of paramount importance: the x-1-Np$^+\cdots$L$_n$ complexes were generated in an EI cluster ion source, which predominantly

produces the most stable structure of a given cluster ion, resulting in the investigation of the global minimum structure of x-1-Np$^+\cdots$Ar (H-bound). The spectroscopic results differ from the previously recorded photoionization spectra, which are able to probe only the π-bound structures - global minima of x-1-Np$\cdots$Ar. This demonstrates that the EI source is more generally applicable than photoionization for the spectroscopic characterization of global minima of cation complexes.

References

[1] Borges dos Santos R.M., Simoes J.A.M., *J. Phys. Chem. Ref. Data* **27** (1998) 707

[2] Rappoport Z., *The Chemistry of Phenols* John Wiley & Sons (New York, 2003)

[3] Forster T., *Z. Elektrochem.* **54** (1950) 42

[4] Forster T., *Z. Elektrochem.* **54** (1950) 531

[5] Neusser H.J., Krause H., *Chem. Rev.* **94** (1994) 1829

[6] Fujii A., Miyazaki M., Ebata T., Mikami N., *J. Chem. Phys.* **110** (1999) 11125

[7] Dessent C.E.H., Haines S.R., Muller-Dethlefs K., *Chem. Phys. Lett.* **315** (1999) 103

[8] Sinclair W.E., Pratt D.W., *J. Chem. Phys.* **105** (1996) 7942

[9] Korter T.M., Kupper J., Pratt D.W., *J. Chem. Phys.* **111** (1999) 3946

[10] Schmitt M., Ratzer C., Meerts L., *J. Chem. Phys.* **120** (2004) 2752

[11] Hobza P., Selzle H.L., Schlag E.W.S., *Chem. Rev.* **94** (1994) 1767

[12] Weber T., Smith A.M., Riedle E., Neusser H.J., Schlag E.W., *Chem. Phys. Lett.* **175** (1990) 79

[13] Schafer M., Pratt D.W., *J. Chem. Phys.* **115** (2001) 11147

[14] Ebata T., Fujii A., Mikami N., *Int. Rev. Phys. Chem.* **17** (1998) 331

[15] Muller-Dethlefs K., Dopfer O., Wright T.G., *Chem. Rev.* **94** (1994) 1845

[16] Braun J.E., Mehnert T., Neusser H.J., *Int. J. Mass Spectrom.* **203** (2000) 1

[17] Bieske E.J., Dopfer O., *Chem. Rev.* **100** (2000) 3963

[18] Brutschy B., *Chem. Rev.* **100** (2000) 3891

[19] Solca N., Dopfer O., *Chem. Phys. Lett.* **325** (2000) 354

[20] Solca N., Dopfer O., *J. Phys. Chem. A* **105** (2001) 5637

[21] Solca N., Dopfer O., *J. Mol. Struct.* **563** (2001) 241

[22] Solca N., Dopfer O., *Chem. Phys. Lett.* **369** (2003) 68

[23] Solca N., Dopfer O., *Eur. Phys. J. D* **20** (2002) 469

[24] Solca N., Dopfer O., *Phys. Chem. Chem. Phys.* **6** (2004) 2732

[25] Haines S.R., Geppert W.D., Chapman D.M., Watkins M.J., Dessent C.E.H., Cockett M.C.R., Muller-Dethlefs K., *J. Chem. Phys.* **109** (1998) 9244

[26] Solca N., Dopfer O., *J. Phys. Chem. A* **106** (2002) 7261

[27] Solca N., Dopfer O., *Chem. Phys. Lett.* **342** (2001) 191

[28] Solca N., Dopfer O., *J. Am. Chem. Soc.* **126** (2004) 1716

[29] Solca N., Dopfer O., *J. Chem. Phys.* **120** (2004) 10470

[30] Dopfer O., Olkhov R.V., Maier J.P., *J. Chem. Phys.* **111** (1999) 10754

[31] Solca N., Dopfer O., *Chem. Eur. J.* **9** (2003) 3154

[32] Solca N., Dopfer O., *Angew. Chem. Int. Ed.* **41** (2002) 3628

[33] M.J. Frisch, G.W. Trucks, H.B. Schlegel, G.E. Scuseria, M.A. Robb, J.R. Cheeseman, J.A. Montgomery Jr., T. Vreven, K.N. Kudin, J.C. Burant, J.M. Millam, S.S. Iyengar, J. Tomasi, V. Barone, B. Mennucci, M. Cossi, G. Scalmani, N. Rega, G.A. Petersson, H. Nakatsuji, M. Hada, M. Ehara, K. Toyota, R. Fukuda, J. Hasegawa, M. Ishida, T. Nakajima, Y. Honda, O. Kitao, H. Nakai, M. Klene, X. Li, J.E. Knox, H.P. Hratchian, J.B. Cross, V. Bakken, C. Adamo, J. Jaramillo, R. Gomperts, R.E. Stratmann, O. Yazyev, A.J. Austin, R. Cammi, C. Pomelli, J.W. Ochterski, P.Y. Ayala, K. Morokuma, G.A. Voth, P. Salvador, J.J. Dannenberg, V.G. Zakrzewski, S. Dapprich, A.D. Daniels, M.C. Strain, O. Farkas, D.K. Malick, A.D. Rabuck, K. Raghavachari, J.B. Foresman, J.V. Ortiz, Q. Cui, A.G. Baboul, S. Clifford, J. Cioslowski, B.B. Stefanov, G. Liu, A. Liashenko, P. Piskorz, I. Komaromi, R.L. Martin, D.J. Fox, T. Keith, M.A. Al-Laham, C.Y. Peng, A. Nanayakkara, M. Challacombe, P.M.W. Gill, B. Johnson, W. Chen, M.W. Wong, C. Gonzalez, J.A. Pople, *Gaussian 03, Revision D.01 Gaussian, Inc., Wallingford CT* (2004)

[34] Boys S.F., Bernardi F., *Mol. Phys.* **19** (1970) 553

[35] Chalasinski G., Szczesniak M.M., *Chem. Rev.* **94** (1994) 1723

[36] Fujimaki E., Matsumoto Y., Fujii A., Ebata T., Mikami N., *J. Phys. Chem. A* **104** (2000) 7227

[37] Fujii A., Sawamura T., Tanabe S., Ebata T., Mikami N., *Chem. Phys. Lett.* **225** (1994) 104

[38] Johnson J.R., Jordan K.D., Plusquellic D.F., Pratt D.W., *J. Chem. Phys.* **93** (1990) 2258

[39] Lakshminarayan C., Smith J., Knee J.L., *Chem. Phys. Lett.* **182** (1991) 656

[40] Hollas J.M., Hussein M.Z.B., *J. Mol. Spec.* **127** (1988) 497

[41] Berden G., Meerts W.L., *J. Chem. Phys.* **104** (1996) 972

[42] Dopfer O., Roth D., Maier J.P., *Int. J. Mass Spectrom.* **218** (2002) 281

[43] Olkhov R.V., Nizkorodov S.A., Dopfer O., *J. Chem. Phys.* **107** (1997) 8229

[44] Roth D., Dopfer O., *Phys. Chem. Chem. Phys.* **4** (2002) 4855

[45] Olkhov R.V., Dopfer O., *Chem. Phys. Lett.* **314** (1999) 215

[46] Dopfer O., Roth D., Maier J.P., *J. Am. Chem. Soc.* **124** (2002) 494

[47] Israelachvili J., *Intermolecular and Surface Forces* Academic Press (1992)

[48] Olkhov R.V., Nizkorodov S.A., Dopfer O., *Chem. Phys.* **239** (1998) 393

[49] Fujii A., Fujimaki E., Ebata T., Mikami N., *J. Chem. Phys.* **112** (2000) 6275

[50] Dopfer O., *Int. Rev. Phys. Chem.* **22** (2003) 437

[51] Oikawa A., Abe H., Mikami N., Ito M., *J. Phys. Chem.* **88** (1984) 5180

[52] Bellm S.M., Moulds R.J., Lawrance W.D., *J. Chem. Phys.* **115** (2001) 10709

[53] Gascooke J.R., Lawrance W.D., *J. Phys. Chem. A* **104** (2000) 10328

[54] Hutson J.M., *Annu. Rev. Phys. Chem.* **41** (1990) 123

[55] Aquilanti V., Bartolomei M., Cappelletti D., Carmona-Novillo E., Pirani F., *J. Chem. Phys.* **117** (2002) 615

[56] Fujii A., Ebata T., Mikami N., *J. Phys. Chem. A* **106** (2002) 8554

[57] Jacox M.E., *Chem. Soc. Rev.* **31** (2002) 108

[58] Hunter E.P., Lias S.G., *J. Phys. Chem. Ref. Data* **27** (1998) 413

4. IRPD investigation of (protonated 1-Naphthol)$^+$···L$_n$ complexes (L = Ar, N$_2$; n = 1...6)

Abstract The following chapter presents the analysis of the IRPD spectra of protonated 1-naphthol tagged with weakly bound nonpolar ligands (1-NpH$^+$···L$_n$, L = Ar, N$_2$; n = 1...6). The spectra were recorded over the O-H stretch vibration range of the complexes produced in the electron impact cluster source. Mass selectivity was provided by the tandem quadrupole - octopole - quadrupole mass spectrometry system (QOQ). The assignment of the spectra was assisted by quantum chemical calculations of the 1-NpH$^+$, 1-NpH$^+$···Ar and 1-NpH$^+$···N$_2$ isomers at the B3LYP/6-311++(2df,2pd) level of theory. As naphthalenoles are closely related to phenol ($\equiv$ Ph), the previously reported IRPD studies of PhH$^+$···Ar$_n$ and PhH$^+$···(N$_2$)$_n$ were used to support the assignment of the bands. Based on the calculations and on the 1-NpH$^+$···L$_n$: PhH$^+$···L$_n$ comparison, a number of isomers arising from protonation at the O atom (*oxonium*) and at certain C atoms (*carbenium*) were identified in the recorded spectrum. The *carbenium* isomers were divided in few groups, depending on the position of the protonation sites with respect to the OH functional group. It was demonstrated that protonation on the ring hosting the OH group occurs only in the *ortho* and *para* positions and, on the second ring, in positions similar with *ortho* and *para*, mirrored by the C-C bond common to the two rings. Proton affinities of all the observed protonation sites were derived from previous experiments and were confirmed by quantum chemical calculations and by analysis of the O-H stretch vibrations shifts.

4.1. Introduction

Arenes and substituted arenes are basic molecules in organic chemistry. Their protonation and deprotonation are important processes in organic chemistry and biochemistry; for example, protonated aromatic molecules (AH$^+$) are short-lived reaction intermediates of large interest in physical and organic chemistry. They appear in electrophilic aromatic substitutions where they determine reaction rates and product selectivities,[1] in combustion (flames),[2] and in models of extraterrestrial hydrocarbon

plasmas.[3] Until recently, experimental techniques used for characterizing them involved condensed-phase NMR, IR and UV-VIS spectroscopy and X-ray crystallography.[4],[5],[6] Although these methods have yielded some properties of the solvated AH^+, they all have the disadvantage that they provide distorted information about the intrinsic properties of AH^+ because of the strong perturbation caused by the environment (solvent, other ions). Fortunately, gas-phase studies, done on bare molecules or on cations, offer a wealth of information about the intrinsic properties of AH^+. Even more, gas-phase experimental setups having the ability to monitor the number of solvent molecules are able to fill the gap by providing detailed images of the solvation onset.[7],[8],[9],[10],[11],[12],[13] Probably the most basic approach is the IR spectroscopy of these isolated species. Despite its simplicity, when combined with mass selection of the relevant species and - more recently - with high-level quantum chemical calculations, IR spectroscopy can provide a detailed picture of the way solvent molecules aggregate around the solvated species.

Naphthalene is one of the simplest bicyclic arenes and its study is seen as a key expansion from what is known about monocyclic arenes like benzene (Bz) toward larger systems. Naphthols (monohydroxynaphthalenes), are being known as strong photoacids, that is the acidity of the OH group increases drastically upon electronic excitation or by ionization, which eventually may promote proton transfer to a suitable solvent. Their protonation has been previously observed in superacid solutions[14] by means of NMR spectroscopy and it has been found that it occurs exclusively at the ring hosting the OH group, in *para* position with respect to the OH group. The experimental observation of only one, C-bound protonation site in 1-Np is at odds with studies done for the simpler PhH^+ in superacid solutions,[15] that prove the existence of at least of one O-bound and at least one C-bound isomer. More recently, quantum chemical calculations have been done to asses the proton affinities (PAs) of susbtituted naphthalenes; however, the lack of experimental support is making uncertain the results of such studies.

The aim of this chapter is to give experimental as well as theoretical support to the idea that, like Ph, 1-Np can be protonated not only at the ring hosting the OH group (ring A), but also at the oxygen atom, as well as at well-defined sites on the second ring (ring B). It will be shown that IRPD techniques are able to select well-defined isomers of $1-NpH^+$. In addition, experimentally- and computationally-derived values will be deduced for the binding energies of Ar and N_2 toward various isomers of $1-NpH^+$. As the binding energies are strongly dependent on the ligand attachement site (OH-bound and π-bound), their relative magnitudes help identifying the onset of the microsolvation.

Unless otherwise specified, all experimental results regarding the $PhH^+ \cdots L_n$

complexes were extracted from references [7], [16], and [17]. In order to allow for direct comparisons, the quantum chemistry results already known for $PhH^+(\cdots L)$[7],[16],[17] were repeated in the present work at the same level as the x-1-$NpH^+(\cdots L)$.

4.2. Quantum chemical calculations

4.2.1. DFT calculations of 1-NpH$^+$

Depending on the position of the OH functional group with respect to the conjoining C-C bond of naphthalene, two naphthol isomers can be identified. In the following only the one with the OH functional group attached in an *ortho* position with respect to this conjoining bond will be discussed (1-Naphthol ≡ 1-Np). Also, depending on the orientation of the OH functional group, *cis* and *trans* isomers of 1-Np can be identified. In Figure 1 is presented the atomic numbering of 1-Np and Ph and some of the studied isomers of 1-NpH$^+$. In the following, each isomer will be identified by a letter which denotes the species (***t*** = *trans*-1-Np, ***c*** = *cis*-1-Np, ***p*** = phenol), and a number which marks the atom at which the protonation occurs.

Figure 1. *Atomic numbering of 1-Np and Ph and geometry of some isomers of 1-NpH$^+$; the isomers are named **xk**, where **x** = **t**(-1-Np), **c**(-1-Np) or **p**(henol), and **k** marks the atom at which the protonation occurs.*
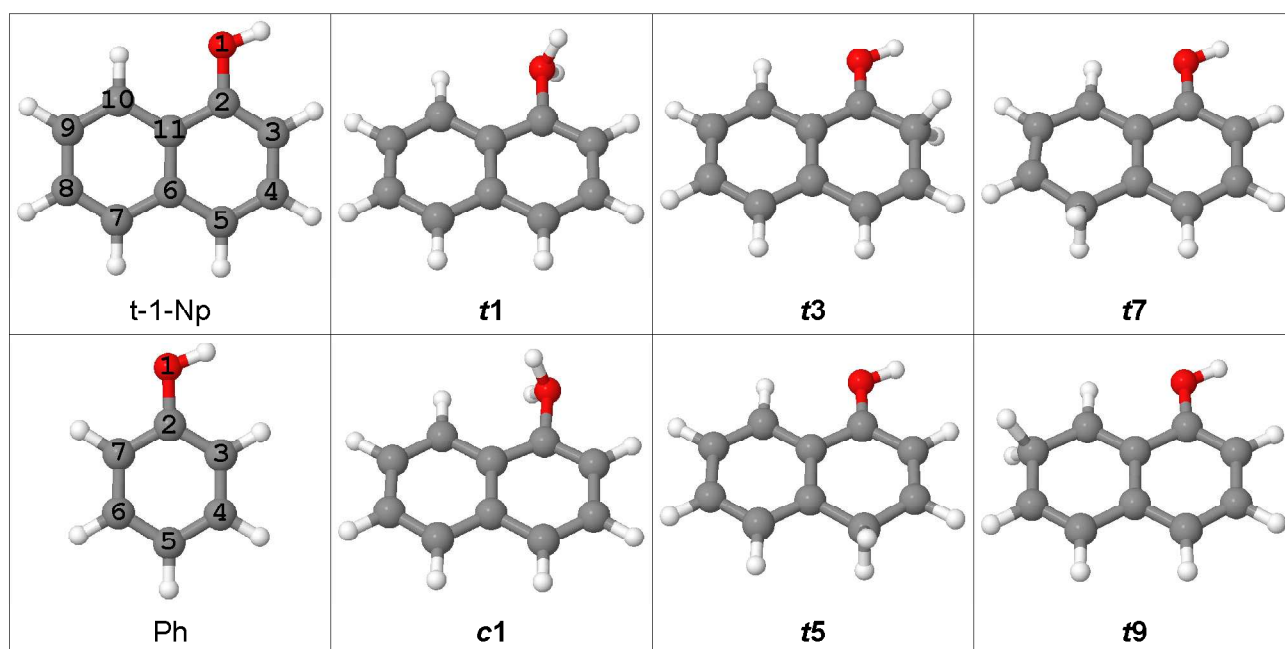
The protonation of the two rotamers of 1-Np was studied by means of density functional theory (DFT) calculations, using the Gaussian 03 quantum chemistry

Figure 2. *PES of t-1-NpH⁺ (a), c-1-NpH⁺ (b) and PhH⁺ (c) respectively, obtained at the B3LYP/6-311++G(2df,2pd) level (see also Figure 1).*
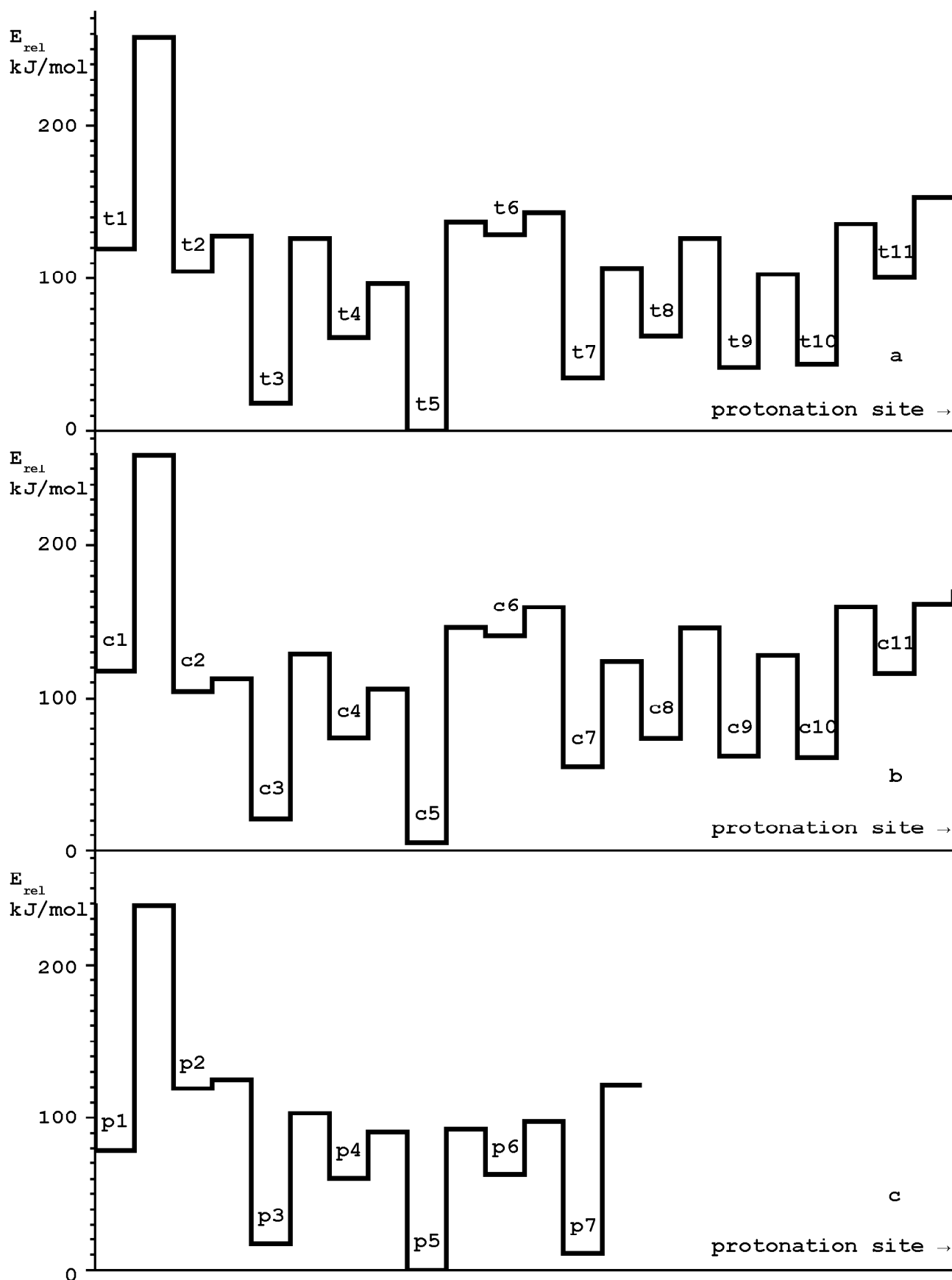
Table 1. Significant properties of x-1-Np, x-1-Np⁺ and x-1-NpH⁺ as obtained at the B3LYP/6-311++G(2df,2pd) level: the relative stabilization energy, E_{rel} (computed with respect to the most stable isomer of each species); the length of the O-H bond, r_{OH}; the frequency of the harmonic O-H stretch vibration(s), ω_{OH}.

species / isomer	E_{rel} (kJ/mol)	r_{OH} (Å)	ω_{OH} (cm⁻¹)	species / isomer	E_{rel} (kJ/mol)	r_{OH} (Å)	ω_{OH} (cm⁻¹)	species / isomer	E_{rel} (kJ/mol)	r_{OH} (Å)	ω_{OH} (cm⁻¹)
t-1-Np	0.00	0.9617	3834.9 (74)	*c*-1-Np	3.84	0.9604	3850.7 (46)	Ph		0.9617	3833.7 (63)
t-1-Np⁺	0.00	0.9673	3767.2 (294)	*c*-1-Np⁺	8.73	0.9665	3774.5 (123)	Ph⁺		0.9713	3717.3 (269)
t1	119.26	0.9733	3650.3 (265) / 3733.9 (282)	*c1*	117.72	0.9745	3630.8 (156) / 3704.7 (244)	*p1*	78.49	0.9740	3642.5 (239) / 3724.9 (300)
t5	0.00	0.9682	3754.7 (247)	*c5*	5.13	0.9678	3754.5 (123)	*p5*	0.00	0.9695	3738.5 (229)
t3	18.10	0.9682	3752.8 (255)	*c3*	21.13	0.9680	3749.1 (112)	*p3*	17.24	0.9687	3748.0 (226)
t7	34.78	0.9652	3795.0 (217)	*c7*	55.08	0.9626	3825.6 (93)				
t9	41.60	0.9659	3785.3 (224)	*c9*	61.57	0.9632	3816.5 (92)				
t10	43.37	0.9639	3813.2 (159)	*c10*	60.64	0.9618	3839.8 (69)				
t4	61.08	0.9642	3810.4 (152)	*c4*	73.95	0.9614	3846.6 (78)				
t8	61.97	0.9638	3814.0 (166)	*c8*	73.71	0.9620	3837.3 (79)	*p7*	11.13	0.9696	3736.1 (222)
t11	100.26	0.9676	3762.3 (231)	*c11*	116.33	0.9652	3789.4 (97)	*p4*	60.50	0.9650	3801.2 (159)
t2	104.33	0.9632	3820.6 (122)	*c2*	104.33	0.9632	3820.3 (122)	*p6*	63.06	0.9645	3806.4 (165)
t6	128.59	0.9643	3808.2 (172)	*c6*	140.60	0.9622	3833.6 (86)	*p2*	119.25	0.9644	3807.4 (134)

package[18]. Theoretical studies of small AH$^+$ ions (A = Bz, Ph, etc.) are showing that the isomers where the proton is bound on the π-electron system are actually saddle points on the potential energy surfaces (PES)[19]. Based on this observation, only the *carbenium* and *oxonium* σ-isomers are investigated. Figure 2 shows the relevant points on the PES of *t*-1-NpH$^+$, *c*-1-NpH$^+$ and PhH$^+$ respectively as they were obtained by relaxing all coordinates at the B3LYP/6-311++G(2df,2pd) level of theory. The basis set was chosen in such a way as to resonably describe the oxonium protonation of Ph[20],[16] and to give a good description of the diffuse interaction which dominates the *x*k$\cdots$Ar potential. All the equilibrium geometries (except *x*2, *x*6, and *x*11) have C_s symmetry, with the two protons present at each investigated site sticking symmetrically out of the molecular plane. The relative stabilization energies for *t*k and *c*k are given with respect to *t*5 (the lowmost isomer on the scale of absolute stabilization energy) while the reference point for *p*k is *p*5;[17],[7] all values are also zero point energy-corrected (ZPE-corrected). Generally speaking, the comparison between *t*k and *c*k on one hand and *p*k on the other hand should be made taking into account the position of the protonation site with respect to the position and orientation of the OH group. However, the strong similarities between *p*3 and *p*7 and between *p*4 and *p*6 respectively[21] are suggesting that comparisons can be done directly between *c*k and *p*k (k = 1...5). It should be noted that for both *x*2 input geometries considered, the equilibrium structure found was the same. The transition states (TS) depicted represent the barriers encountered by the proton as it hops between neighboring minima.

Checks of the harmonic vibrations are showing that all the *x*k and *p*k isomers labeled on the Figure 2 are minima on the PES. Table 1 summarizes the significant properties (relative stabilization energies - $E_{rel,xk}$, O-H bond length - $r_{OH,xk}$, and the O-H harmonic vibrations frequencies - $\omega_{OH,xk}$) of these isomers, together with the relevant information for the *x*-1-Np and *x*-1-Np$^+$ species. It can be seen that the listed properties are strongly isomer-dependent. Based on the properties presented in Table 1, the multitude of isomers of *x*-1-NpH$^+$ can be split into few categories.

*x*3 & *x*5 The first group of monomers to be considered comprises *t*5 and *t*3 (*c*5 and *c*3). They are characterized by similar r_{OH} and their $E_{rel,xn}$ are the lowest of all investigated isomers, being separated by just 18.10 kJ/mol (16.00 kJ/mol). The barriers that are isolating one from the other are 107.92 kJ/mol (107.81 kJ/mol) high - large enough to limit isomerization. It is interesting to note that the part of the PES of *x*k encompassing these isomers differs from the corresponding part of the PES of *p*k just by the height of the barrier, which rises at just 85.7 kJ/mol. It can be seen that, in terms of IR intensity, *t*k

dominate **ck** by a factor 2. It then makes sense to mainly investigate the **tk** monomers and their dimers. As $\omega_{OH,tk}$ are basically identical (their separation is of less than 2 cm^{-1}), they are probably indistinguishable in the conditions of the present experiment.

*x***7 &** *x***9** Similar reasoning allows us to group together **t7** and **t9** (**c7** and **c9**). Although these isomers have no equivalent among the isomers of PhH$^+$, their position with respect to the C_6-C_{11} bond and the location of the OH group makes them somehow similar with *ortho* and *para* PhH$^+$. It should be noted that in this last group the separation of the parameters is slightly larger which may translate in experimental observation of the individual bands.

Table 2. *Geometrical parameters (bond lengths and angles) most affected by the t-1-NpH$^+$↔c-1-NpH$^+$ isomerization.*

param.	t1 (Å)	c1 (Å)	Δ (Å)	param.	t1 (°)	c1 (°)	Δ (°)
R(1,2)	1.5101	1.5030	0.0071	A(12,1,20)	110.98	110.29	0.69
R(1,12)	0.9733	0.9745	-0.0012	A(1,2,3)	117.37	114.78	2.59
R(1,20)	0.9733	0.9745	-0.0012	A(1,2,11)	114.99	117.66	-2.67
R(2,3)	1.3586	1.3568	0.0018	A(2,3,13)	122.31	121.55	0.76
R(2,11)	1.4008	1.4024	-0.0016	A(4,3,13)	120.86	121.66	-0.80
R(3,13)	1.0817	1.0802	0.0015	A(9,10,19)	119.94	118.78	1.16
R(5,6)	1.4154	1.4165	-0.0011	A(11,10,19)	120.34	121.23	-0.89
R(6,11)	1.4355	1.4341	0.0014				
R(7,8)	1.3695	1.3704	-0.0009				
R(8,9)	1.4109	1.4094	0.0015				
R(9,10)	1.3707	1.3721	-0.0014				
R(10,19)	1.0802	1.0830	-0.0028				

*x***1** The **c1** and **t1** isomers will be analyzed apart from all other isomers, as they are characterized by almost identical E$_{rel}$ (E$_{rel,t1}$ - E$_{rel,c1}$ = 1.54 kJ/mol with ZPE, 1.94 kJ/mol without ZPE) and the lowest lying TS separating them, which is found on the path of the inversion of the OH$_2$ group, is extremely low (E$_{bar,t1c1}$ - E$_{rel,t1}$ = 1.62 kJ/mol ZPE-corrected, 4.88 kJ/mol without ZPE correction). The modifications of the geometry upon the **t1**↔**c1** isomerization are localized mainly at the O-H bonds and the neighboring atoms (see Table 2 for a list of the most significant changes). This isomerization barrier is consistent with the **p1**↔**p1** inversion barrier (1.93 kJ/mol ZPE-corrected, 5.15 kJ/mol without ZPE correction) at the same level of the theory. Previous studies on 1-Np$^+$[22], done at UB3LYP/6-311G(2df,2pd) and repeated here at the B3LYP/6-311++G(2df,2pd) level for the

sake of consistency, are showing that c-1-Np$^+$ is placed 8.73 kJ/mol higher than t-1-Np$^+$ and that they are separated by a barrier $E_{rel,tc}$ - $E_{rel,c}$ = 28.79 kJ/mol. The O-bound protons of **c1** are outside of the molecular plane, lowering their interaction with the C_{10}-bound proton and they are oriented in a way that facilitates their interaction with the π-electron system of the B ring. In the case of c-1-Np$^+$ the molecule is planar and the O-bound proton is repelled by the C_{10}-bound proton, accounting for the higher stabilization energy of c-1-Np$^+$ with respect to t-1-Np$^+$. It should be noted that the barrier heights cannot be directly compared as the isomerization processes are different: while the **t1**↔**c1** isomerization is an inversion process, the t-1-Np$^+$↔c-1-Np$^+$ isomerization occurs via the rotation of the O-H bond around the O-C_2 bond.

The almost identical E_{rel} values and the very low isomerization barrier found for **c1** and **t1** suggest similar populations for both isomers. Even more, they are surrounded by exceptionally high isomerization barriers ($E_{rel,t1t2}$ - $E_{rel,t1}$ = 138.70 kJ/mol and $E_{rel,c1c2}$ - $E_{rel,c1}$ = 141.63 kJ/mol), two orders of magnitude larger than the **t1**↔**c1** isomerization barrier, providing excellent isolation of **x1** from the neighboring stable isomers. The **x1** isomers are the most acidic ones as shown by $r_{OH,x1}$ (the longest) and their $\omega_{OH,x1}$ (the lowmost). This high acidity will be further translated in large red-shifts of the vibrations upon attachment of a tagging ligand, making them easily identifiable in the IR spectrum.

Protonation at C_2, C_6 or C_{11} atoms is quite improbable as it distorts the molecule, pushing E_{rel} close to the surrounding barriers and consequently making quite probable the depletion of the **x2**, **x6**, and **x11** populations via isomerization.

x4, x8, & x10 The remaining isomers (**x4**, **x8**, and **x10**) are characterized by rather similar values of $r_{OH,xk}$ and $\omega_{OH,xk}$. The values of their $\omega_{OH,xk}$ are well separated from other groups of vibrations (slightly tighter grouped for **tk** than for **ck**). At the same time, their $\omega_{OH,xk}$ are the highest ones from all investigated monomers, underlining the strength of the corresponding intramolecular O-H bonds. The strong intramolecular interaction results in a lowering of their OH-bonding ability. Also their IR intensities are only about 60% of the other $\omega_{OH,xk}$. It then results that the chances of seeing vibrations coming from these monomers in the spectrum are rather low. This way, all these 6 isomers can be placed into a mixed "group" which will not be analyzed further.

An observation which supports another reduction in the number of investigated isomers is that the IR intensities of $\omega_{OH,ck}$ are systematically smaller (50% or less) than the ones of the corresponding **tk** isomers. Knowing this, it is reasonable to selectively focus

the dimers' analysis, considering just **c1** and some **tk** isomers.

4.2.2. DFT calculations of 1-NpH$^+$···Ar

Following the analysis of the relative stability of the monomers, the attachment of an Ar ligand to the OH functional group of the most stable **tk** monomers (n = 5, 3, 7, 9) and to **x1** was investigated. Previous experimental studies of PhH$^+$···Ar obtained in the same EI ion source and in similar conditions[7],[16],[17] are showing that although the attachment of the Ar ligand to the π electron system is possible, it yields systematically lower binding energies and its impact on the OH acidic group is negligible. As the B3LYP method fails to properly describe the interaction between rare gases (Rg) and π electron systems, $\omega^{\pi}_{OH,xk\cdots Ar}$ will be considered to be roughly equal with the corresponding monomer's $\omega_{OH,xk}$.

The theoretical analysis of the dimers was done at the same level (B3LYP/6-311++(2df,2pd)) as the analysis of the monomers; the effect of the basis set superposition error (BSSE)[23],[24] was accounted for. Considering the fact that the intermolecular potential is flat, the geometry optimization has been enhanced by requesting tight convergence and the usage of GDIIS algorithm[25],[26] instead of the default algorithm (RFO).[27] To validate the results, geometry optimizations followed by frequency calculations have been done also using RFO for the dimers with the strongest intermolecular bond (**t1**···Ar, **t3**···Ar and **t5**···Ar). The differences in frequencies and IR intensities were found to be minor but slightly increasing with the distance between the protonation site and the complexation site. As the differences are appearing to come from faulty geometry optimizations due to the use of RFO, all the following dimer results were obtained using the enhanced geometry optimization method. The principal properties of the computed dimers are shown in Table 3.

Although Ar is a weakly perturbing ligand, its attachment to the OH group is inducing changes in the corresponding O-H bond: in all cases r_{OH} is increasing ($r^b_{OH,xk\cdots Ar} > r_{OH,xk}$) and the ω_{OH} is red-shifting ($\omega^b_{OH,xk\cdots Ar} < \omega^b_{OH,xk}$), showing that the O-H bonds become weaker. One can also see that together with the red-shifts of $\omega^b_{OH,xk\cdots Ar}$, their IR activities are also strongly enhanced: upon complexation, the IR intensity goes up by a factor 2...6, depending on the protonation site. Similar to the case of **pk**···Ar, the calculations predict that the O-H···Ar bonds are quasi-linear (165° < $\theta_{O-H\cdots Ar}$ < 177° for **xk**···Ar versus 166° < $\theta_{O-H\cdots Ar}$ < 178° for **pk**···Ar). A more detailed look reveals that while for each parameter the changes are occurring in the same direction, the exact amount depends on the protonation site and can be related to the isomers grouping established earlier.

Table 3. Significant parameters for selected **xn**···Ar dimers: the length of the O-H bond ($r_{OH,xn···Ar}$), the elongation of r_{OH} with respect to the corresponding monomer ($r_{OH,xn···Ar}$ - $r_{OH,xn}$), the harmonic frequency of the O-H vibration(s) ($\omega_{OH,xn···Ar}$), $\omega_{OH,xn}$ (as an approximation of the frequency of the corresponding π-bound isomer), the intermolecular bond length ($r_{H···Ar}$), the intermolecular bond angle ($\theta_{O-H···Ar}$), the binding energy (D_0) and the intermolecular stretch frequency (ω_s). For all the harmonic frequencies, the IR intensities (in km/mol) are listed in parentheses.

isomer	$r_{OH,xn···Ar}$ (Å)	Δr_{OH} (Å)	$\omega_{OH,xn···Ar}$ (cm⁻¹)	$\omega_{OH,xn}$ (cm⁻¹)	$r_{H···Ar}$ (Å)	$\theta_{O-H···Ar}$ (deg)	D_0 (cm⁻¹)	ω_s (cm⁻¹)
c1	0.9837	0.0092	3468.2 (911)	3630.8 (156)	2.2014	173.9	767	92.6 (6)
	0.9737	-0.0008	3681.6 (226)	3704.7 (244)				
t1	0.9831	0.0098	3477.0 (1063)	3650.3 (265)	2.1950	176.9	812	91.9 (5)
	0.9724	-0.0009	3709.4 (292)	3733.9 (282)				
t3	0.9713	0.0031	3684.4 (682)	3752.8 (255)	2.4497	165.9	345	53.8 (5)
t5	0.9710	0.0028	3690.7 (650)	3754.7 (247)	2.4678	165.1	316	51.8 (4)
t7	0.9671	0.0019	3755.3 (502)	3795.0 (217)	2.5613	165.9	176	42.9 (4)
t9	0.9680	0.0021	3739.5 (537)	3785.3 (224)	2.5365	166.3	212	45.3 (4)
p1	0.9847	0.0093	3452.8 (1066)	3642.5 (239)	2.1764	177.8	868	112.9 (15)
	0.9729	-0.0011	3703.7 (293)	3724.9 (300)				
p5	0.9730	0.0035	3662.7 (642)	3738.6 (229)	2.4222	165.8	363	65.7 (6)
p3	0.9722	0.0035	3671.3 (632)	3748.0 (226)	2.4202	166.9	378	66.9 (6)
p7	0.9731	0.0035	3659.7 (628)	3736.1 (222)	2.4230	167.1	371	65.7 (7)

***x*1···Ar** Similar to the case of ***p*1**···Ar, the largest changes in the properties of the O-H bond are observed in the case of the ***x*1**···Ar isomers. For both species, the O-H bond to which the ligand is bound ($r^b_{OH,x1\cdots Ar}$) expands by almost 1%. An analysis of the force constants shows that the corresponding vibration ($\omega^b_{OH,x1\cdots Ar}$) is derived from the symmetric vibration ($\omega^s_{OH,x1}$). This identification allows the estimation of the red-shifts (-163 cm^{-1} for ***t*1**···Ar and -173 cm^{-1} for ***c*1**···Ar), which are found to be lower than the red-shift exhibited by ***p*1**···Ar (-190 cm^{-1}). This seems to come against the finding that $r^b_{OH,t1\cdots Ar}$ expands slightly more than $r^b_{OH,p1-Ar}$, but one has to also take into account the dispersion of the charge across a larger molecular body. By contrast, the free O-H ($r^f_{OH,x1\cdots Ar}$) shrinks by a small amount and the corresponding $\omega^f_{OH,x1\cdots Ar}$ is shifting toward the average position for each rotamer ($\frac{\omega^b_{OH,x1\cdots Ar} + \omega^f_{OH,x1\cdots Ar}}{2}$). The IR activity of $\omega^b_{OH,c1\cdots Ar}$ is going up by a factor ~6 and the one of $\omega^b_{OH,t1\cdots Ar}$ goes up by a factor ~4 (rather similar with $\omega^b_{OH,p1\cdots Ar}$). As the two $\omega^b_{OH,x1\cdots Ar}$ bands are separated by just 10 cm^{-1} and their IR intensities are roughly the same, it is expected the experimental observation of only one feature in the range of $\omega^b_{OH,x1\cdots Ar}$. Despite their 28 cm^{-1} spacing, the chances of individual observation of the two $\omega^f_{OH,x1\cdots Ar}$ are poor, as their positions overlap with the much more IR active $\omega^f_{OH,t3\cdots Ar}$ and $\omega^f_{OH,t5\cdots Ar}$.

All these changes are closely related to the properties of the intermolecular bond. It can be seen that for both ***x*1**···Ar rotamers the intermolecular separation reaches the minimum value, while the O-H···Ar bond is closest to linearity ($\theta_{O-H\cdots Ar}$ > 174°). The binding energy of the dimers reaches the highest values of all studied ***x*n**···Ar dimers, being only slightly lower than the value evaluated via calculations for $D_0^{OH,p1\cdots Ar}$ (812 cm^{-1} for ***t*1**···Ar and 767 cm^{-1} for ***c*1**···Ar versus 868 cm^{-1} for ***p*1**···Ar). Comparing all three ***x*1**···Ar systems, it can clearly be seen that, while in the case of ***t*1**···Ar the ring B has little influence, ***c*1**···Ar is clearly affected by its presence: the IR intensity of the $\omega^b_{OH,c1\cdots Ar}$ is about 10% lower than the one of $\omega^b_{OH,t1\cdots Ar}$ and the ***c*1**···Ar isomer is weaker bound than ***t*1**···Ar by ~5%. As the amount of complexes that are created in the ion source is strongly correlated with their binding energy, it results that although ***c*1** is evaluated to be marginally more stable than ***t*1**, the ***c*1**···Ar dimers will be produced in lower amounts than ***t*1**···Ar. The IRPD signal depends on both the population of the isomer which is absorbing

and on the IR intensity of the vibration excited; thus, considering the lower values of both these parameters for $c1\cdots$Ar versus $t1\cdots$Ar, it can be predicted that the IRPD spectrum of 1-NpH$^+\cdots$Ar will show only one feature in the range of the bound OH vibration, which can clearly be associated with $\omega^b_{OH,t1\cdots Ar}$.

Finally, one more isomer related to $c1$ was investigated: the $c1\cdots$Ar dimer having the Ar atom held between the two O-bound protons and the C_{10}-bound proton was found to be a transition state for the transfer of the Ar from one OH binding site to the other.

$t3\cdots$Ar & $t5\cdots$Ar The $t3\cdots$Ar and $t5\cdots$Ar dimers are different from the $x1\cdots$Ar ones, as they exhibit far lower stretch vibration frequency of the O-H bond, longer OH$\cdots$Ar bonds and less linearity of the O-H$\cdots$Ar bond ($\theta_{O-H\cdots Ar} \cong 165°$). As they are deriving from monomers with very similar properties and the intermolecular interaction is almost the same, both the $\omega_{OH,tk\cdots Ar}$ vibrations have almost the same frequencies, making the discrimination between these two dimers impossible. Their IR intensities are almost equally enhanced by a factor ~2.5, slightly lower than the enhancement of the

corresponding $pn\cdots$Ar dimers ($\left.\dfrac{I^{OH}_{IR,pk\cdots Ar}}{I^{OH}_{IR,pk}}\right|_{k=3,5,7} \cong 2.8$).

The calculated $D_0^{OH,tk\cdots Ar}$ (345 cm^{-1} for $t3\cdots$Ar and 316 cm^{-1} for $t5\cdots$Ar) are smaller than $\left.\bar{D}_0^{OH,pk\cdots Ar}\right|_{k=3,5,7}$ = 371 cm^{-1}. It should be noted that experimental investigations[7],[16],[17] yielded $\left.\bar{D}_0^{OH,pk\cdots Ar}\right|_{k=3,5,7}$ = 650 ± 150 cm^{-1}, showing that the theoretical level seems to underestimate the interaction by a factor 1.4...2.2. Considering that the underestimation is similar for $t3\cdots$Ar and $t5\cdots$Ar, it results that 440 cm^{-1} < $D_0^{OH,tk\cdots Ar}$ < 760 cm^{-1} (k = 3, 5). Also from previous experiments^{citrings1np}, it is known that the binding energy of Ar to the cations or protonated forms of small arenes via a π-bond is rather insensitive to the structure of the arene molecule ($D_0^{\pi,A^+\cdots Ar}$ = 550 ± 50 cm^{-1}). A cursory comparison of these numbers shows that π-bound structures of $t3\cdots$Ar and $t5\cdots$Ar are quite possible; this was also the case for PhH$^+\cdots$Ar[7],[16],[17]: the recorded spectrum yielded one band which was assigned to such π-bound dimers.

$t7\cdots$Ar & $t9\cdots$Ar The last group of investigated dimers ($t7\cdots$Ar and $t9\cdots$Ar) are built from the least acidic monomers, as proven by the largely unperturbed O-H bond: the red-shifts of their $\omega^b_{OH,tk\cdots Ar}$ (k = 7, 9) as well as the frequencies of their intermolecular stretch vibrations are the smallest of all dimers. Any direct comparison of $tk\cdots$Ar (k = 7, 9) with the $pk\cdots$Ar systems must be carefully pondered as neither $t7$ nor $t9$ have equivalents among

pk; thus, if the underestimation of the intermolecular interaction found for *pk*···Ar (k = 3, 5, 7) would be common to all carbenium-based dimers, the calculated binding energies (176 cm^{-1} for *t7*···Ar and 212 cm^{-1} for *t9*···Ar) might be augmented to 240 cm^{-1} < $D_0^{OH, tk···Ar}$ < 470 cm^{-1}; such values are very low, lower even than the typical binding energy of a π-bound A$^+$···Ar. The idea that the calculations are indeed similarly underestimating the intermolecular interaction might be supported by the finding that both groups of carbenium dimers (k = 3, 5 as well as k = 7, 9) exhibit similar calculated enhancements (~2.5) of their $\omega_{OH, tk···Ar}^b$ IR intensities. Only the analysis of the experimental spectra can give further arguments for this discussion. However, it can be clearly seen that if $D_0^{OH, tk···Ar}$ (k = 7, 9) are at most slightly higher than the corresponding $D_0^{\pi, tk···Ar}$ (already evaluated to be 550 ± 50 cm^{-1}), the presence of four π-bonding sites versus only one OH-bonding site will tip the competition in favor of the π-bonded dimers, trimers and even tetramers. Thus, it is expected that the π-bonded *t7*···Ar and *t9*···Ar dimers may contribute in a noticeable manner to the spectrum.

Overall it can be seen that the effect of the ligand is stronger for the more acidic O···H bonds and that this isomer-dependence of the properties can be tracked even at the intermolecular level (intermolecular separation, bond angle, dissociation energy of the complex).

4.2.3. DFT calculations of 1-NpH$^+$···N$_2$

The attachment of a N$_2$ ligand was investigated for the same group of monomers (*tk*, k = 3, 5, 7, 9 and *x1*); again, the investigations were limited to OH-bound dimers. Like in the case of 1-NpH$^+$···Ar, the analysis was done at the same computational level as the analysis of the monomers, while considering the effects of BSSE. The results of the calculations are presented in Table 4; it can be seen that the complexation with N$_2$ replicates the complexation with Ar in terms of type of effects, at a scale greatly augmented by the higher PA of N$_2$ (493.8 kJ/mol versus 369.2 kJ/mol for Ar[28]). The higher strength of the intermolecular interaction transpires from every parameter listed: with respect to the results obtained for 1-NpH$^+$···Ar, the intramolecular O-H bonds are expanding more than twice as much, the intermolecular OH···N$_2$ bonds are almost 20% shorter, the red-shifts of the bound OH stretch vibrations are more than twice as large and the binding energies are almost three times larger. Similar with the case of 1-NpH$^+$···Ar, the intermolecular interaction occurs largely along the O-H bond axis: the range of values taken by the $\widehat{OHN}$ angle is identical with the range of values computed for $\widehat{OHAr}$. In the

63

Table 4. Significant parameters for selected **xn**···N2 dimers: the length of the O-H bond ($r_{OH,xm\cdots N2}$), the elongation of r_{OH} with respect to the corresponding monomer ($r_{OH,xn\cdots N2} - r_{OH,xn}$), the harmonic frequency of the O-H vibration(s) ($\omega_{OH,xn\cdots N2}$), $\omega_{OH,xn}$ (as an approximation of the frequency of the corresponding π-bound isomer), the intermolecular bond length ($r_{H\cdots N2}$), the intermolecular bond angle ($\theta_{O-H\cdots N2}$), the binding energy (D_0) and the intermolecular stretch frequency (ω_s). For all the harmonic frequencies, the IR intensities (in km/mol) are listed in parentheses.

isomer	$r_{OH,xm\cdots N2}$ (Å)	Δr_{OH} (Å)	$\omega_{OH,xm\cdots N2}$ (cm⁻¹)	$\omega_{OH,xn}$ (cm⁻¹)	$r_{H\cdots N2}$ (Å)	$\theta_{O-H\cdots N2}$ (°)	D_0 (cm⁻¹)	ω_s (cm⁻¹)
c1	0.9931	0.0186	3285.2 (1497)	3630.8 (156)	1.8130	172.5	1962	190.8 (16)
	0.9728	-0.0017	3691.7 (193)	3704.7 (244)				
t1	0.9933	0.0200	3281.6 (1636)	3650.3 (265)	1.8067	175.7	2019	191.7 (17)
	0.9714	-0.0019	3719.4 (270)	3733.9 (282)				
t3	0.9751	0.0069	3611.3 (1101)	3752.8 (255)	2.0386	165.2	1047	93.3 (8)
t5	0.9751	0.0069	3612.6 (1088)	3754.7 (247)	2.0351	164.4	991	94.8 (8)
t7	0.9698	0.0046	3700.7 (842)	3795.0 (217)	2.1176	165.5	727	81.6 (7)
t9	0.9706	0.0047	3688.2 (867)	3785.3 (224)	2.1184	167.8	784	80.4 (8)
p1	0.9952	0.0212	3248.3 (1669)	3642.5 (239)	1.7927	175.8	2143	160.7 (12)
	0.9719	-0.0021	3713.0 (265)	3724.9 (300)				
p5	0.9771	0.0076	3581.6 (1032)	3738.6 (229)	2.0167	165.9	1117	106.5 (9)
p3	0.9763	0.0076	3591.0 (1009)	3748.0 (226)	2.0173	166.4	1143	106.4 (9)
p7	0.9772	0.0076	3578.2 (1018)	3736.1 (222)	2.0156	166.5	1115	106.0 (10)

case of the 1-NpH$^+$···N$_2$ isomers the intermolecular interaction is a strongly oriented charge-quadrupole interaction, occurring along the N≡N molecular axis. This can be seen from the values taken by the $\widehat{HNN}$ angle, all of which are in the interval [174°...180°) with the exception of **c1**···N$_2$, for which the $\widehat{HNN}$ angle is just 170°; this last value is the result of the repulsion between the π electron systems of 1-NpH$^+$ and N$_2$.

The classification of the monomers established above and confirmed in the case of 1-NpH$^+$···Ar can still be easily identified. In the case of **x1**···N$_2$, the intramolecular O-H bond elongates by almost 2% (in contrast with the 1% computed for the **xk**···Ar dimers), while the intermolecular bond is shorter by 0.4 Å (~20%). The red-shifts of $\omega^b_{OH, x1···N_2}$ are -349 cm^{-1} for **t1**···N$_2$ and -365 cm^{-1} for **c1**···N$_2$, which represents more than twice the red-shifts of $\omega^b_{OH, x1···Ar}$. The IR activities of these bands are increasing ~9 and ~6 times, with respect to the monomer; these values represent circa 150% from the values predicted in the case of **x1**···Ar. All these results are in line with the predictions made for the PhH$^+$···N$_2$ dimers. In the case of the **t3**···N$_2$ and **t5**···N$_2$ there is practically no separation between the bound vibrations, making impossible their individual identification; like in the case of **x1**···N$_2$, the IR intensities are magnified due to the complexation by factors about 1.5 times larger than the ones of the corresponding **xk**···Ar isomers. Finally, the least acidic **t7**···N$_2$ and **t9**···N$_2$ are characterized, as expected, by the smallest O-H bond stretches and, consequently, by the smallest red-shifts (≅ -100 cm^{-1}). The binding energies of the OH-bound dimers are decreasing from **x1**···N$_2$ (~2000 cm^{-1}), through **t3**···N$_2$ & **t5**···N$_2$ (~1000 cm^{-1}), to **t7**···N$_2$ & **t9**···N$_2$ (~750 cm^{-1}). These numbers are all > 90 % than the corresponding computed **pk**···N$_2$ binding energies. Even more, the binding energies for all three groups of dimers (resulted from the quantum chemical calculations which are scaled to correct the underestimation of the interaction strength) are much larger than the corresponding $D_0^{\pi, pk···N_2}$ as evaluated from IRPD^{cit}. This is significant, because it implies that the IRPD spectrum of 1-NpH$^+$···N$_2$ will probably show no trace of π-bound complexes.

4.3. Experimental details

The IR spectra of 1-NpH$^+$···L$_n$ were recorded in the QOQ tandem mass spectrometer setup presented in the *Experimental setup* chapter and previously reported in literature[29]. The 1-Np sample is heated above melting point (T$_{sample}$ ≅ 380 K) and the vapors produced are seeded in a mixture of L (Ar or N$_2$) and H$_2$ (typical backing pressure - 3 bar; typical mixing ratio - 20:1). Electron impact reactions are producing a wealth of ions;

these particles are involved in chemical and physical processes leading to the formation of ionic clusters. One of the paths toward these ionic clusters, having high production rate, is described in the following. Brønsted acids[30] XH^+ ($X = H_2$, Ar, N_2) are formed in the high pressure range of the supersonic expansion via ion-molecule reactions **(1)** & **(2)**:

$$H_2 + e^- \rightarrow H_2^+ + 2e^- \tag{1}$$

$$H_2^+ + X \rightarrow XH^+ + H \tag{2}$$

The proton is afterwards transferred to the 1-Np molecule:[30]

$$1-Np + XH^+ \rightarrow 1-NpH^+ + X \tag{3}$$

The $1-NpH^+\cdots L_n$ complexes are produced in the supersonic expansion via three-body collisions as shown in **(4)**[8]

$$1-NpH^+\cdots L_n + L + M \rightarrow 1-NpH^+\cdots L_{n+1} + M \qquad M = \text{1-Np, L; L = Ar, } N_2 \tag{4}$$
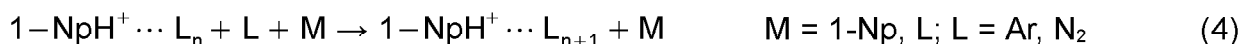
A typical mass spectrum of the ion source is presented in Figure 3; as it was recorded in the expansion of L = Ar, the major peaks are assigned to Ar^{2+}, Ar^+, $1-NpH^+$ and Ar_nH^+. The inset is a X50 vertical expansion of the mass scan, revealing the sequence of $1-NpH^+\cdots Ar_n$ complexes. It can be seen that the amount of complexes produced by the source is monotonically decreasing with the increasing in number of Ar atoms, thus supporting the sequential assembling of the clusters described in **(4)**.

An important aspect of the mechanism described above is that the molecular ions from **(3)** are "hot" (vibrationally excited). The energy from the excitation of one normal mode can "leak" into other normal modes via internal vibrational energy redistribution (IVR). This leads to the excitation of the intermolecular modes above the dissociation level, evaporating some of the ligands. This process occurs simultaneously with the three-body associations **(4)** and effectively drains the internal energy of the complex to a level lower than the binding energy of the weakest bound ligand.

The complexes can interact resonantly with the excitation laser beam, absorbing one IR photon via excitation of an IR active vibration (in the present case excitation of the O-H stretch vibration - ν_{OH}). This is followed by IVR and possibly by the evaporation of one or more ligands:[30],[31]

$$1-NpH^+\cdots Ar_n + h\cdot\nu_{IR} \rightarrow 1-NpH^+\cdots Ar_{n-m} + m\cdot Ar \tag{5}$$
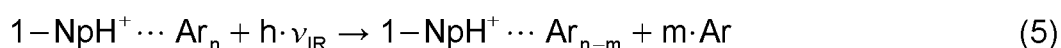
As detailed in the *Experimental setup* chapter, the charged fragment resulting from

the evaporation process described in **(5)** is filtered using the second QMF and enters in the Daly detector. Thus, the IR spectrum of 1-NpH$^+\cdots$L$_n$ is recorded by monitoring the ion current of 1-NpH$^+\cdots$L$_{n-m}$ versus the wavelength of the IR laser.

Figure 3. *A typical mass spectrum of the ion source, recorded by using a 20:1 mixture of Ar:H$_2$ at 3 bar, which flows over the 1-Np sample heated to ~380 K. The major peaks are assigned to Ar^{2+}, Ar$^+$, and Ar$_n$H$^+$ (▲) as well as to 1-NpH$^+$ (▲). The X50 vertical expansion of the scan (right hand) reveals the sequence of 1-NpH$^+\cdots$Ar$_n$ (▲).*
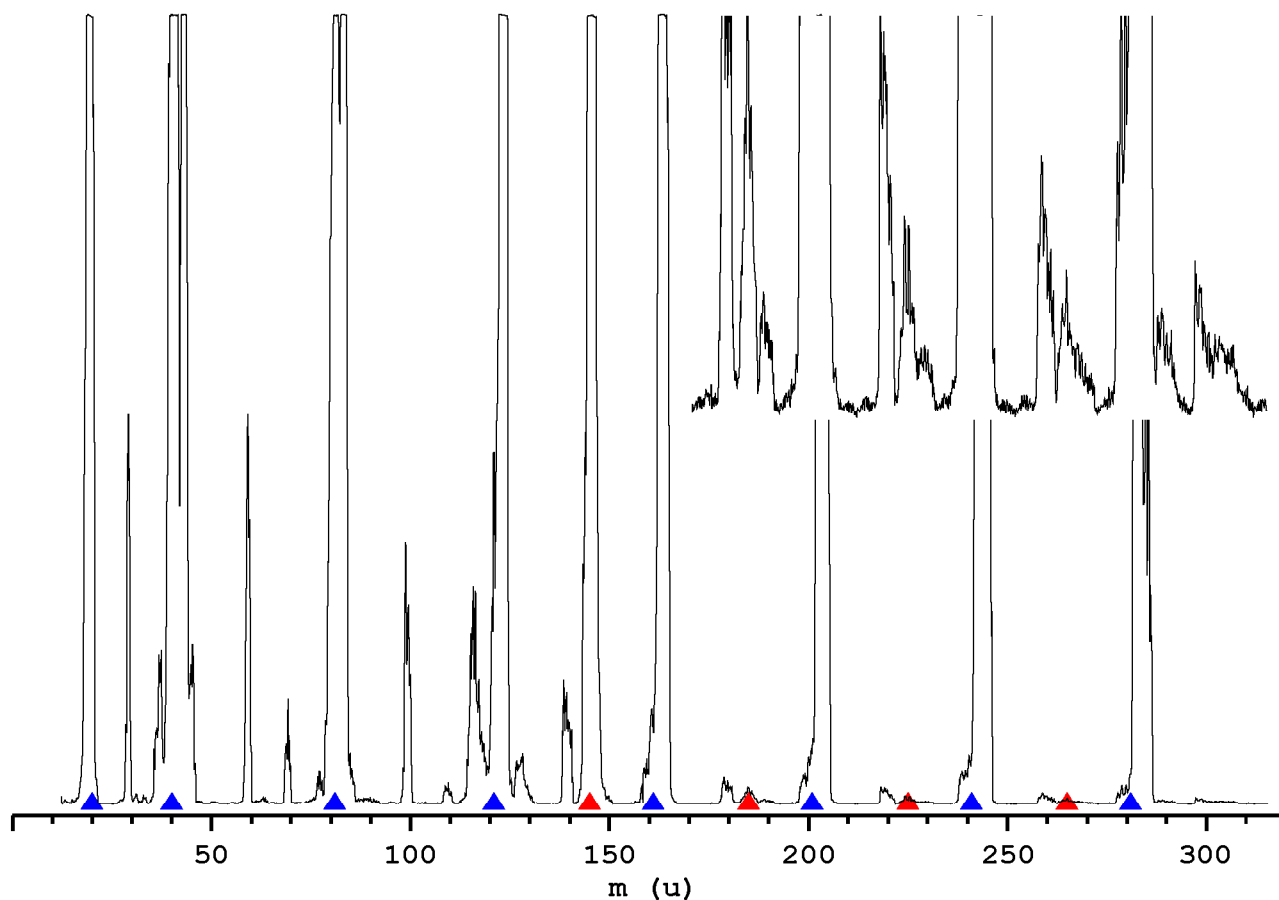
A recording of the laser power (done using an InSb IR detector) is used to eliminate the ion signal fluctuations caused by variable laser power; this is done by linearly normalizing the ion signal on the laser power. These absorptions of the laser output (caused mainly by the atmospheric water) are also used to calibrate the wavelength of the laser. The positions of these dips are compared with data from the literature[32],[33] and a linear stretching procedure is employed to match them, giving better than 1 cm^{-1} accuracy.

4.4. Results and discussion

Figure 4 and Figure 5 compare the IRPD spectra of 1-NpH$^+\cdots$Ar and 1-NpH$^+\cdots$N$_2$ with

Table 5. *Band maxima (in cm⁻¹), FWHM (in parentheses, in cm⁻¹) and proposed assignment for 1-NpH⁺···Arₙ and 1-NpH⁺···(N₂)ₙ. For comparison, the same information is listed for PhH⁺···Ar and PhH⁺···N₂.*

PhH⁺···Ar

	Band	Position (FWHM) (cm⁻¹)	Assignment
n=1, m=0	A₂	3329 (23)	ν_{p1}^{b} (H)
	H₁	3464 (10)	$\nu_{OH,PhH^+\cdots Ar}^{b}$, ¹³C
	B₁	3493 (12)	$\nu_{p3/5}^{b}$ (H)
	A₁	3534 (9)	ν_{p1}^{f} (H)
	B₁,π	3554 (13)	$\nu_{p3/5}^{\pi}$ (π)

PhH⁺···N₂

	Band	Position (FWHM) (cm⁻¹)	Assignment
n=1, m=0	A₂	3073 (36)	ν_{p1}^{b} (H)
	A₄	3252 (34)	ν_{p1}^{b} (H)
	H₁	3365 (4)	$\nu_{OH,PhH^+\cdots N_2}^{b}$, ¹³C
	B₁	3408 (6)	$\nu_{p3/5}^{b}$ (H)
	A₁	3543 (12)	ν_{p1}^{f} (H)

1-NpH⁺···Arₙ

	Band	Position (FWHM) (cm⁻¹)	Assignment
n=1, m=0	A₂	3331 (30)	ν_{x1}^{b} (H)
	B₁	3513 (11)	$\nu_{t3/5}^{b}$ (H)
	C₂	3573 (9)	ν_{t9}^{b} (H)
	D₂	3590 (7)	ν_{t7}^{b} (H)
	C₁	3620 (7)	ν_{t9}^{π} (π)
	D₁	3637 (4)	ν_{t7}^{π} (π)
n=2, m=0	A₂	3340 (20)	ν_{x1}^{b} (2H)
	A₁	3374 (27)	ν_{x1}^{b} (2H)
	B₁	3514 (10)	$\nu_{t3/5}^{b}$ (Hπ)
	C₂	3575 (10)	ν_{t9}^{b} (Hπ)
	D₂	3590 (5)	ν_{t7}^{b} (Hπ)
	C₁	3619 (14)	ν_{t9}^{π} (2π)
	D₁	3637 (4)	ν_{t7}^{π} (2π)
n=3, m=0	A₂	3347 (16)	ν_{x1}^{b} (2Hπ)
	A₁	3386 (19)	ν_{x1}^{b} (2Hπ)
	B₁	3515 (12)	$\nu_{t3/5}^{b}$ (H2π)
	C₂	3577 (10)	ν_{t9}^{b} (H2π)
	D₂	3590 (5)	ν_{t7}^{b} (H2π)
	C₁	3616 (11)	ν_{t9}^{f} (3π)
	D₁	3635 (4)	ν_{t7}^{f} (3π)

1-NpH⁺···(N₂)ₙ

	Band	Position (FWHM) (cm⁻¹)	Assignment
n=1, m=0	A₂	3096 (66)	ν_{x1}^{b} (H)
	B₁	3440 (8)	$\nu_{t3/5}^{b}$ (H)
	H₁	3466 (12)	$\nu_{t1Np^+\cdots N_2}^{b,OH}$, ¹³C
	C₂	3520 (8)	ν_{t9}^{b} (H)
	D₂	3541 (3)	ν_{t7}^{b} (H)
n=2, m=1	A₂	3162 (38)	ν_{x1}^{b} (2H)
	A₁	3199 (30)	ν_{x1}^{b} (2H)
n=2, m=0	B₁	3446 (11)	$\nu_{t3/5}^{b}$ (Hπ)
	H₁	3468 (9)	$\nu_{t1Np^+\cdots (N_2)_2}^{b,OH}$, ¹³C
	C₂	3525 (9)	ν_{t9}^{b} (Hπ)
	D₂	3546 (9)	ν_{t7}^{b} (Hπ)
n=3, m=2	A₂, A₁	3224 (29)	ν_{x1}^{b} (2Hπ)
n=3, m=1	B₁	3448 (10)	$\nu_{t3/5}^{b}$ (H2π)
	H₁	3471 (12)	$\nu_{t1Np^+\cdots (N_2)_3}^{b,OH}$, ¹³C
	C₂	3526 (8)	ν_{t9}^{b} (H2π)
	D₂	3546 (8)	ν_{t7}^{b} (H2π)

Table 5. (continued)

		Band	Position (FWHM) (cm⁻¹)	Assignment
n=4	m=1	A_2	3340 (6)	v^b_{x1} (2H2π)
		A_3	3362 (7)	v^b_{x1} (3Hπ)
		A_1	3382 (12)	v^b_{x1} (2H2π)
	m=0	B_1	3516 (10)	$v^b_{t3/5}$ (II3π)
		C_2	3575 (8)	v^b_{t9} (H3π)
		D_2	3590 (7)	v^b_{t7} (H3π)
		C_1	3615 (6)	v^f_{t9} (4π)
n=5	m=1	A_2	3344 (11)	v^b_{x1} (2H3π)
		A_3	3366 (7)	v^b_{x1} (3H2π)
		A_1	3385 (18)	v^b_{x1} (2H3π)
	m=0	B_1	3516 (10)	$v^b_{t3/5}$ (H4π)
		C_2	3575 (8)	v^b_{t9} (H4π)
		D_2	3590 (5)	v^b_{t7} (H4π)
		C_1	3613 (16)	v^f_{t9} (5π)
n=6	m=2	A_2	3345 (9)	v^b_{x1} (2H4π)
		A_3	3366 (3)	v^b_{x1} (3H3π)
		A_1	3385 3397 (20)	v^b_{x1} (2H4π)
	m=1	B_1	3516 (9)	$v^b_{t3/5}$ (H5π)
		C_2	3574 (7)	v^b_{t9} (H5π)
		D_2	3589 (6)	v^b_{t7} (H5π)
		C_1	3613 (5)	v^f_{t9} (6π)
	m=0	B_1	3516 (9)	$v^b_{t3/5}$ (H5π)
		C_2	3574 (7)	v^b_{t9} (H5π)
		D_2	3589 (6)	v^b_{t7} (H5π)
		C_1	3613 (5)	v^f_{t9} (6π)

Presently unassigned bands of the $1\text{-NpH}^+\cdots(\text{N}_2)_n$ spectra, together with their fragmentation channel.

		Band	Position (FWHM) (cm⁻¹)	Assignment
n=1	m=0	S_1	3432 (?)	shoulder
		X_1	3476 (9)	
		X_4	3581 (7)	
n=2	m=1	S_1	3436 (?)	shoulder
		X_1	3477 (9)	
		X_4	3582 (6)	
n=3	m=2	X_1	3480 (10)	
		X_4	3584 (6)	

Notes: The proposed geometries of the complexes are listed next to the assignment of the bands as *xHyπ* (*x* OH-bound ligands and *y* π-bound ligands).

The sharp dips seen in the $1\text{-NpH}^+\cdots Ar_n$ spectra at ~3519 cm⁻¹ and in the $1\text{-NpH}^+\cdots(N_2)_n$ spectra at ~3446 cm⁻¹ are artifacts generated by strong absorption of the IR excitation beam by atmosphere, thus they are not listed in the table.

Positions of bands A_1 (v^f_{x1}) could not be identified in the $1\text{-NpH}^+\cdots L$ spectra.

Bands H_1 are the result of IR absorption by $^{13}C^{12}C_5H_7O^+\cdots L$ and $^{13}C^{12}C_9H_9O^+\cdots L_n$ respectively.

69

the spectra of $PhH^+{\cdots}Ar$ and $PhH^+{\cdots}N_2$ recorded in the O-H stretch range. For comparison, the stick spectra resulting from the calculations of $x\mathbf{k}{\cdots}Ar$ and $x\mathbf{k}{\cdots}N_2$ are also plotted. In Figure 6 and Figure 7 are presented the IRPD spectra of $1\text{-}NpH^+{\cdots}Ar_n$ and $1\text{-}NpH^+{\cdots}(N_2)_n$. The positions of the maxima, their FWHM, and assignments of the transitions observed (identified with $v^y_{x\mathbf{k}{\cdots}L_m}$ or $v^y_{x\mathbf{k}}$ (**y** = **bound, free**) are listed in Table 5. The most probable geometries of the complexes are also listed near the assignment of the bands as $\mathbf{xHy\pi}$ (**x** OH-bound ligands and **y** π-bound ligands). The IRPD spectra of $1\text{-}NpH^+{\cdots}L_n$ (n > 2 for L = Ar and n ≠ 1 for L = N_2) were obtained by monitoring different $1\text{-}NpH^+{\cdots}L_m$ fragment channels; the dominant fragment channel is indicated in Table 5 and on each spectra by n → m.

4.4.1. Spectrum of 1-NpH⁺···Ar

The IRPD spectra of $1\text{-}NpH^+{\cdots}Ar$ and of $PhH^+{\cdots}Ar$ (for reference) are presented in Figure 4a and Figure 4b. Figures 4c … 4e show the stick spectra of the explored $x\mathbf{k}{\cdots}Ar$ dimers; the computed harmonic frequencies have been scaled (by 0.9527) as discussed below. The positions of the recorded bands, their FWHM and assignments are listed in Table 5. The bands will be identified by their positions, shapes, comparison with the computed vibrations of the dimers, and by comparing the $1\text{-}NpH^+{\cdots}Ar$ and $PhH^+{\cdots}Ar$ spectra.

Table 1 and Table 3 show the frequencies of the normal modes of $x\mathbf{k}$ and $x\mathbf{k}{\cdots}Ar$ respectively. It can be seen that these values are largely different from the positions of the observed bands centers (Table 5). This is due to the fact that the calculations are approximating the vibrations as harmonic. A scaling factor - whose value depends both on the method and on the basis set used[34] - is usually employed to bring the calculations in line with the experiment. Later it will be shown that its dependence on the ligand species (L) represents only a small part of the scaling factor. The scaling factor depends also on the species of the atom to which the proton is chemically bound (X), but this dependence will not be discussed any further. In the present case, the scaling factor will be calculated using the position of band B_1 and the harmonic frequencies of the vibrations to which this band can be associated with ($\omega^b_{t5{\cdots}Ar}$ and $\omega^b_{t3{\cdots}Ar}$). As neither of these vibrations can be considered dominant in their contribution to the IR activity of band B_1, their average value

$$\frac{\omega^b_{t3{\cdots}Ar} + \omega^b_{t5{\cdots}Ar}}{2}$$ will be used for calculating the scaling factor. The value thus obtained (0.9527) is virtually identical with the one calculated from the data regarding $PhH^+{\cdots}Ar$

Figure 4. *IRPD spectra of PhH$^+$$\cdots$Ar (a) and 1-NpH$^+$$\cdots$Ar (b). The stick spectra of **t7**$\cdots$Ar and **t9**$\cdots$Ar (c), **t3**$\cdots$Ar and **t5**$\cdots$Ar (d) and **x1**$\cdots$Ar (e), together with the stick spectra of the corresponding monomers are presented for comparison at the same scale of their calculated IR intensities; all harmonic frequencies have been scaled by a factor 0.9592. The black unmarked sticks show v^b_{xn} of OH-bound isomers while the gray ones marked with "▼" show v^f_{xn} of possible π-bound isomers (positions derived from corresponding monomers). The red-coloured band is a x10 enlargement of the band A$_2$.*
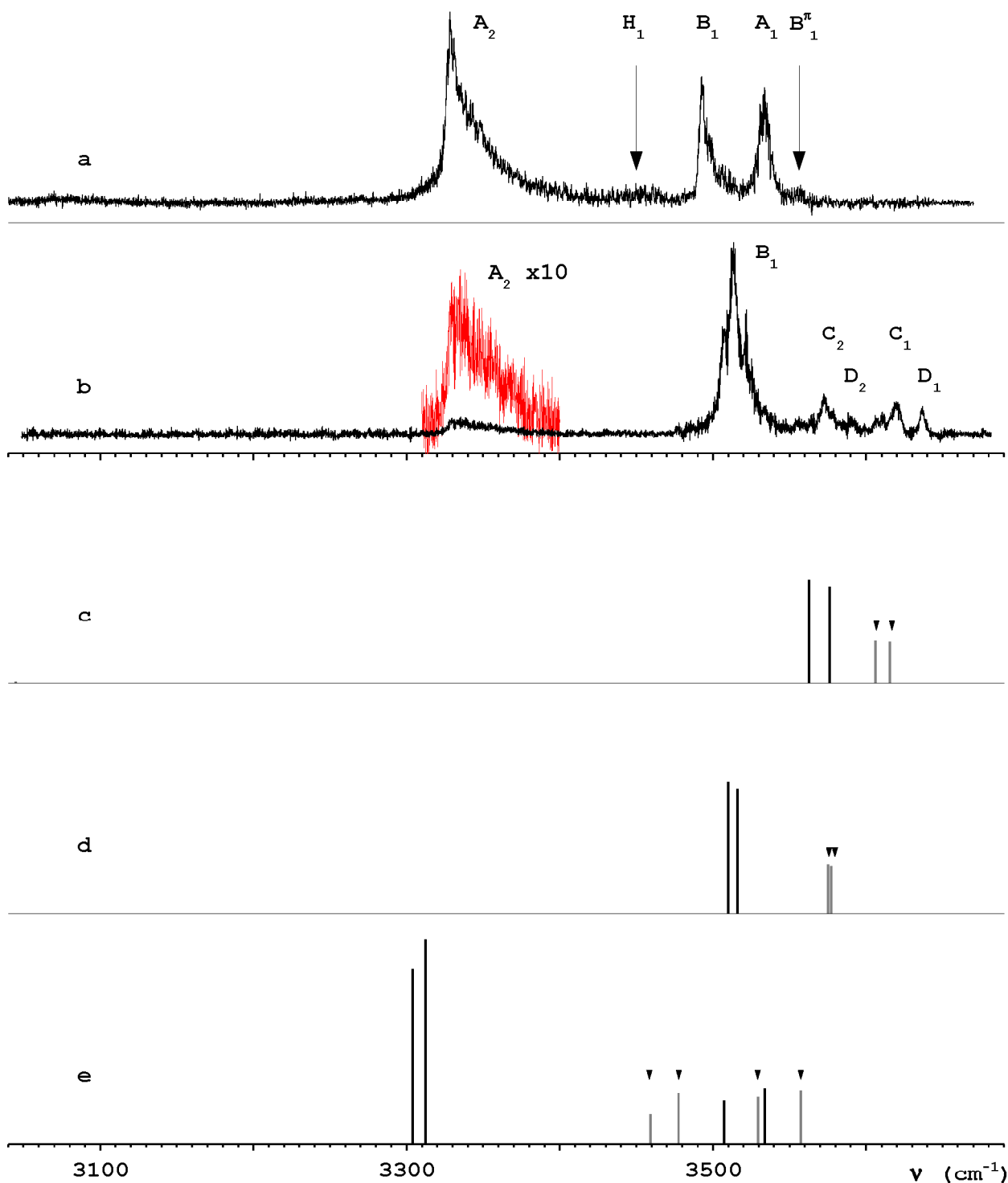
(0.9525). This scaling factor will be applied to the computed vibrations (see the stick spectra in Figure 4c ... 4e) which will further assist the identification of the observed bands.

The red-most feature of the spectrum is a rather weak, blue-shaded band (A$_2$, 3331 cm^{-1}), amply displaced with respect to the others. A similar band is present also in the spectrum of PhH$^+\cdots$Ar in a close position (3329 cm^{-1}). These two bands are similarly blue-shaded but they greatly differ in terms of relative strength. Both the position (red-shifted with respect to the normal position of an O-H stretch vibration, but different from the expected position of any C-H stretch vibration) and the asymmetric shape of this band suggest that the band corresponds to an Ar-bound O-H stretch vibration. A comparison between the position of this band with the calculated frequencies (Figure 4c ... 4e) leaves no doubt about the actual assignment: the only bands so largely red-shifted with respect to the others are the two $\nu^b_{x1\cdots Ar}$ (Figure 4e, 3304 cm^{-1} and 3313 cm^{-1}). These correspond to the dimers with the strongest intermolecular bond and, consequently, are expected to exhibit the most significant blue-shading of all observed bands. As seen above, the different binding energies of the two $x1\cdots$Ar suggest that the population of $c1\cdots$Ar is smaller than the one of $t1\cdots$Ar; the IR intensity of the $\nu^b_{c1\cdots Ar}$ vibration is also calculated to be smaller than the one of $\nu^b_{t1\cdots Ar}$. Adding to these facts the observation that the FWHM of band A$_2$ (30 cm^{-1}) is much larger than the computed separation between $\omega^b_{c1\cdots Ar}$ and $\omega^b_{t1\cdots Ar}$ (8 cm^{-1}), it results that the best assignment of band A$_2$ is $\nu^b_{t1\cdots Ar}$. This assignment is consistent with the one of band A$_2$ from the IRPD spectrum of PhH$^+\cdots$Ar. The most striking difference between the two experimental spectra is the apparently low IR activity of A$_2$ with respect to the other features of the 1-NpH$^+\cdots$Ar and PhH$^+\cdots$Ar spectra. This is solely the result of the low yield of $x1$ monomers from the ion source. In previous experiments[35] it had been found that, in the case of a mixture of isomers, it is possible to completely suppress the production of one isomer by just varying the parameters of the ion source (nozzle position, gas pressure, filament temperature, extraction potentials and timing).

With the position of $\nu^b_{t1\cdots Ar}$ pinpointed, the next step is to search for $\nu^f_{t1\cdots Ar}$ and possibly $\nu^f_{c1\cdots Ar}$ (marked with black lines above 3500 cm^{-1} in Figure 4e). The first aspect which should be noted is that the calculated separation between the free vibrations of the two $x1\cdots$Ar isomers ($\nu^f_{t1\cdots Ar} - \nu^f_{c1\cdots Ar}$ = 26 cm^{-1}) is much larger than the FWHM of all still unidentified bands in the spectrum, which means that it no longer makes sense to attempt to assign only one feature of the spectrum to both of them. Second, the PhH$^+\cdots$Ar investigation has demonstrated that the calculations are not only overestimating the

frequency of the bands (because of the harmonic approximation), but they are also overestimating the splitting caused by complexation by ~17%. Considering a similar overestimation of the red-shifts for $x1\cdots$Ar, the positions of $v^f_{t1\cdots Ar}$ and $v^f_{c1\cdots Ar}$ are evaluated to be 3521 cm^{-1} and 3505 cm^{-1} respectively. Finally, as seen in Table 3, the predicted ratios between the IR intensities of $v^b_{x1\cdots Ar}$ and $v^f_{x1\cdots Ar}$ are >3:1 in favor of the bound ones for both cis and trans isomers. These intensity ratios are virtually identical with the the similar intensity ratio predicted and found in the case of PhH$^+\cdots$Ar, proving that the calculations are accurate enough. The rather low signal recorded from A$_2$, together with the predicted IR activity ratios, put the bands corresponding to $v^f_{x1\cdots Ar}$ very close to the noise level of the spectrum. Analyzing the recorded spectrum over the predicted range for $v^f_{x1\cdots Ar}$, one can see that both these positions are covered by a strong band centered at 3513 cm^{-1}, which - as it will be shown later - can conclusively be assigned to other isomers. The association of π-bound $x1\cdots$Ar dimers with any band identified in the spectrum can be dismissed using the same arguments. The D$_0$ of the Ar ligands π-bonded toward $p1$ was shown to be just above half the D$_0$ of the OH-bounded ones, implying that the latter binding motif is the dominant one. As the O-H stretch vibration(s) of 1-NpH$^+$ are going to be largely unaffected by a π-bound ligand, one can use the calculations of the monomers as reference for searching these bands in the spectrum. The observations that their IR intensities are similar with the ones of $v^f_{x1\cdots Ar}$ and that the expected populations of π-bound $x1\cdots$Ar dimers are much smaller that the (barely observable) OH-bound $x1\cdots$Ar dimers are leading to the conclusion that, if present, signals from the π-bound $x1\cdots$Ar dimers will be well below the noise level.

The band B$_1$, centered on 3513 cm^{-1}, is the strongest feature of the spectrum. As seen above, only a tiny contribution to its IR activity may come from the two $v^f_{x1\cdots Ar}$ vibrations. A comparison between the PhH$^+\cdots$Ar and 1-NpH$^+\cdots$Ar spectra relates this band, both in position and in strength, with a band assigned to $v^b_{p3/5\cdots Ar}$ (B$_1$, 3493 cm^{-1}); the only significant difference is the shape of the band, which is only slightly blue-shaded, while in the case of PhH$^+\cdots$Ar the blue shading was more important. The more rounded shape and the apparent splitting of the band are actually artifacts resulting from parent ion flux oscillations and large IR laser power variations. The spacing between band B$_1$ of PhH$^+\cdots$Ar and band B$_1$ of 1-NpH$^+\cdots$Ar (20 cm^{-1}) is almost with the spacing between $\bar{\omega}^b_{pk\cdots Ar}\big|_{k=3,5}$ and $\bar{\omega}^b_{tk\cdots Ar}\big|_{k=3,5}$ (20.5 cm^{-1}). It can be seen that, within the 1 cm^{-1} precision in band position, the

two numbers are identical and that even by applying the anharmonic correction factor they will differ by at most 1 cm^{-1}. Adding to the similarities underlined above the fact that $t3$ and $t5$ are the most stable monomers and that $t3\cdots$Ar and $t5\cdots$Ar have similar D_0, it can safely be said that the band B_1 is mainly the result of an overlap between $\bar{v}^b_{t3\cdots Ar}$ and $\bar{v}^b_{t5\cdots Ar}$.

In the case of PhH$^+\cdots$Ar, the band denoted $B_{1,\pi}$ was assigned to isomers created by π-bonding the Ar atom to a $p3$ or $p5$ monomer. In order to search for the corresponding band in the spectrum of 1-NpH$^+\cdots$Ar, the same scaling procedure was applied. The calculated red-shifts are -63 cm^{-1} for $(\bar{v}^b_{tn\cdots Ar})_{n=3,5}$ with respect to $(\bar{v}^f_{tn\cdots Ar})_{n=3,5}$ and -73 cm^{-1} for $(\bar{v}^b_{pn-Ar})_{n=3,5}$ with respect to $(\bar{v}^f_{pn\cdots Ar})_{n=3,5}$. The red-shift thus calculated for the case of PhH$^+\cdots$Ar is ~19% larger than the one observed. Assuming that in the case of 1-NpH$^+\cdots$Ar the calculations are similarly overestimating the red-shift, the presumed position of $B_{1,\pi}$ is 3566 cm^{-1}. Investigation of the spectrum is rather inconclusive, as this range is framed by B_1 and another band (C_2) which will be shown to be related to other isomers.

The last four bands (C_2, D_2, C_1 and D_1) have no equivalent in the PhH$^+\cdots$Ar spectrum. Based on their positions, spacing and relative intensity, their primary assignment is to OH stretch vibrations of OH-bound and π-bound $t7\cdots$Ar and $t9\cdots$Ar dimers ($v^b_{t9\cdots Ar}$, $v^b_{t7\cdots Ar}$, $v^f_{t9\cdots Ar}$ and $v^f_{t7\cdots Ar}$ respectively). As shown in the calculations section, all these four vibrations are expected to occur in the presently investigated range of the spectrum, at a slightly higher frequency than $v^b_{t3/5\cdots Ar}$. The experimental red-shifts ($\Delta v^{exp}_{t9} = \Delta v^{exp}_{t7} = -47$ cm^{-1}) are close to the computed values ($\Delta v^{calc}_{t9} = -44$ cm^{-1} and $\Delta v^{calc}_{t7} = -39$ cm^{-1}). Considering the stability arguments from the calculations section, it results that the $t9\cdots$Ar isomers are giving rise to C_1 and C_2, while D_1 and D_2 are the result of IR activity of the $t7\cdots$Ar dimers.

Band H_1 from the PhH$^+\cdots$Ar spectrum was connected with the contamination of both IRPD parent and fragment mass channels with a Ph$^+\cdots$Ar complex having one ^{12}C atom substituted by ^{13}C ($m(^{12}C_6H_7O^+) = m(^{13}C^{12}C_5H_6O^+) = 95$ u). Such a contamination is to be expected, because the natural abundance of ^{13}C is a not negligible 1.07%, while the natural abundance of ^{12}C is 98.93%. As this contamination was clearly visible in the case of a molecule having six carbon atoms, it is expected that, in the present case of a molecule having ten carbon atoms, the contamination would be even more prominent. To identify such a contamination, one has to look for the strongest band in the spectrum of 1-Np$^+\cdots$Ar (attributed to the OH-bound dimer), which appears at 3538 cm^{-1}; the corresponding region of the 1-NpH$^+\cdots$Ar spectrum is fairly absorption-free. The absence of this band is probably the result of higher protonation rates in the present experiment

(resulting from larger amounts of H_2 in the gas mixture and / or from the higher PA of 1-Np versus the PA of Ph). A higher protonation rate can render this band invisible by decreasing the available amount of $^{13}C^{12}C_9H_8O^+$ on one hand and, on the other hand, by increasing the amount of $^{12}C_{10}H_9O^+$, which, in turn is increasing the absolute value of the noise level in the spectrum via higher metastable decay of the $^{12}C_{10}H_9O^+\cdots Ar$ dimers.

4.4.2. Spectrum of 1-NpH$^+$$\cdots$N$_2$

The features of the spectrum of 1-NpH$^+\cdots$N$_2$ (shown in Figure 5, together with the spectrum of PhH$^+\cdots$N$_2$) are similar with the spectrum of 1-NpH$^+\cdots$Ar; the positions, FWHM, and assignment of the observed bands are presented in Table 5. Stick spectra of the investigated dimers are also presented in Figure 5, using a scaling factor (0.9524) computed like in the case of 1-NpH$^+\cdots$Ar.

Table 1 and Table 4 show the frequencies of the normal modes of **xk** and **xk**$\cdots$N$_2$ respectively. Like in the case of **xk**$\cdots$Ar, the scaling factor will be calculated using the position of band B$_1$ and the harmonic frequency of the vibration to which this band can be associated with. As band B$_1$ is considered to originate from $\omega^b_{t5\cdots N_2}$ and $\omega^b_{t3\cdots N_2}$, their

average value $\dfrac{\omega^b_{t3\cdots N_2} + \omega^b_{t5\cdots N_2}}{2}$ will be used for calculating the scaling factor. It must be noted that the value obtained (0.9524) is slightly higher than the one calculated from the data regarding PhH$^+\cdots$N$_2$ (0.9503) but it is very close to the value previously used in the evaluation of the calculations done for the **xk**$\cdots$Ar dimers (0.9527). In fact, the **xk**$\cdots$Ar and **xk**$\cdots$N$_2$ scaling factors are so close, that if one would use their average for scaling all frequencies, the results would differ by at most 1 cm^{-1} from the ones calculated using the scaling factors specific to each species.

The scaling factor found here will be applied to the computed vibrations (see the stick spectra in Figure 5c ... 5e) which will further assist the identification of the observed bands.

The red-most feature of the spectrum is again a rather weak, blue-shaded band (A$_2$, 3107 cm^{-1}), amply red-shifted with respect to the others. Considering the characteristics of this band and the spectra of 1-NpH$^+\cdots$Ar, PhH$^+\cdots$Ar and PhH$^+\cdots$N$_2$, the only possible assignment is $\nu^b_{x1\cdots N_2}$.

Figure 5e shows the calculated positions of the four $\nu^b_{x1\cdots N_2}$ and $\nu^f_{x1\cdots N_2}$ bands. The lines above 3400 cm^{-1}, labeled with inverted triangles ($\blacktriangledown$), are marking the positions of the $\nu^{as}_{x1\cdots N_2}$ and $\nu^s_{x1\cdots N_2}$; these bands are regarded as approximations of the O-H stretch

Figure 5. *The IRPD spectra of PhH$^+$···N$_2$ (a) and of 1-NpH$^+$···N$_2$ (b). The stick spectra of **t7**···N$_2$ and **t9**···N$_2$ (c), **t3**···N$_2$ and **t5**···N$_2$ (d) and **x1**···N$_2$ (e), together with the stick spectra of the corresponding monomers are presented for comparison at the same scale of their calculated IR intensities; all harmonic frequencies have been scaled by a factor 0.9463. The black unmarked sticks show v^b_{xn} of OH-bound isomers while the gray ones marked with "▼" show v^f_{xn} of possible π-bound isomers (positions derived from corresponding monomers). The red-coloured band is a x20 enlargement of the band A$_2$.*

vibrations coming from possible π-bound dimers. However, three observations are leading to the conclusion that none of the presently recorded bands can be associated with any or all of these bands. First, the fact that π-bound dimers are weaker bound than their OH-bound counterparts implies that the amount of π-bound $x1\cdots N_2$ dimers is smaller than the amount of OH-bound $x1\cdots N_2$ dimers. Second, at equal populations of π- and OH-bound dimers, the predicted IR activities of the former are less than 1/6 of the predicted IR activities of $v^b_{x1\cdots N_2}$. These two facts are leading to the conclusion that although the presence of π-bound $x1\cdots N_2$ dimers in the ion beam cannot be excluded, IRPD signals from them will fall below the detection limit. Finally, the range in which these bands are expected is dominated by other far larger features, whose assignment is certain and different. A similar logical trail, applied to the $v^f_{x1\cdots N_2}$ bands, leads to the conclusion that also these bands cannot be conclusively identified in the spectrum.

The strongest band of the spectrum is B_1 (3440 cm^{-1}). Like in the case of 1-NpH$^+\cdots$Ar, it will be assigned to $v^b_{t5\cdots N_2}$ and $v^b_{t3\cdots N_2}$, its highly asymmetric shape, similar to band B_1 from the PhH$^+\cdots N_2$ spectrum, making this assignment even more obvious. The sharp dip near 3446 cm^{-1} is an artifact produced by the strong absorption of the IR laser beam in the atmosphere; as it is independent from the investigated species it will be seen at the same position in all 1-NpH$^+\cdots(N_2)_n$ spectra. Based on the observed position of $(\bar{v}^b_{tn\cdots N_2})_{n=3,5}$ and on the predicted red-shift of these vibration modes with respect to the $(\bar{v}^f_{tn})_{n=3,5}$ (-135 cm^{-1}) it appears that band X_4 (3581 cm^{-1}) can be assigned to $(\bar{v}^f_{tn\cdots N_2})_{n=3,5}$. However, as it will be shown later, the investigations of complexes with more than one ligand are disproving this assignment.

The positions identified in the 1-NpH$^+\cdots$Ar spectrum for v^f_{t9} and v^f_{t7} (band C_1 at 3620 cm^{-1} and D_1 at 3637 cm^{-1}) and the computed red-shifts of these vibrations upon complexation with N_2 (Δv^{calc}_{t9} = -93 cm^{-1} and Δv^{calc}_{t7} = -90 cm^{-1}) will support the identification of the $v^b_{t9\cdots N_2}$ and the $v^b_{t7\cdots N_2}$ bands in the 1-NpH$^+\cdots N_2$ spectrum. The evaluated positions of $v^b_{t9\cdots N_2}$ and $v^b_{t7\cdots N_2}$ (3527 cm^{-1} and 3547 cm^{-1}) are well matching the bands C_2 and D_2 observed at 3520 cm^{-1} and 3541 cm^{-1}. The absence of any evidence of π-bound 1-NpH$^+\cdots N_2$ dimers is connected to the binding energies of the OH-bound $t7\cdots N_2$ and $t9\cdots N_2$ which are evaluated to be larger than the binding energies of the corresponding π-bound dimers. Indeed, a comparison between the calculated binding energy of $p5\cdots N_2$ (1117 cm^{-1}) and the value evaluated from IRPD spectra (1300 ± 350 cm^{-1}) suggests that

the theoretical level slightly underestimates D_0. At the same time, $D_0^{\pi,p5\cdots N_2}$ was found to be 750 $\pm$ 150 cm^{-1}; this value is presumably larger than $D_0^{\pi,tn\cdots N_2}$ (n > 1) because the positive charge of the protonated species will be effectively distributed over two rings and not one like in the case of $pn\cdots N_2$ (n > 1).

The band H_1 (3466 cm^{-1}) originates from a contamination of both IRPD parent and fragment mass channels with 1-Np$^+\cdots N_2$ dimers having one ^{12}C atom substituted by a ^{13}C (1-NpH$^+$ = $^{12}C_{10}H_9O^+$ = 144 u = $^{13}C^{12}C_9H_8O^+$ = 1-Np$^+$). Such a contamination was observed in all PhH$^+\cdots Ar_n$ and PhH$^+\cdots(N_2)_n$ spectra. This band is found only 1 cm^{-1} away from the position observed in the 1-Np$^+\cdots N_2$ spectrum.[22]

Cursory scans done over the aliphatic C-H stretch vibration have shown no visible absorptions; consequently, the related bands observed in the PhH$^+\cdots N_2$ spectrum (B_2 at 2865 cm^{-1} and B_3 at 2877 cm^{-1} - not marked in Figure 5) have not been listed in Table 4. The bands which are yet unassigned will be discussed later.

The primary effect of the addition of one ligand to a XH-bound dimer is a slight blue-shift of the corresponding $\nu^b_{XH,AXH^+\cdots L}$. This is the result of the noncooperative three-body interactions, which are driving the H-bonds weaker. It is thus expected that the spectra of the complexes having at least one OH-bound ligand (2H(n-2)π or H(n-1)π for n = 2...6) will be characterized by blue-shifts of their O-H stretch vibrations.

4.4.3. Spectrum of 1-NpH$^+\cdots Ar_2$

The 1-NpH$^+\cdots Ar_2$ spectrum was recorded in the 2 $\rightarrow$ 0 fragmentation channel and no signal was seen upon laser excitation in the 2 $\rightarrow$ 1 fragmentation channel. This means that, like in the case of PhH$^+\cdots Ar_2$, the sum of the binding energies of both Ar ligands is smaller than the energy of the excitation photon for all isomers.

The features in the 1-NpH$^+\cdots Ar$ spectrum (Figure 4 and Figure 6a) are largely reproduced by the spectrum of 1-NpH$^+\cdots Ar_2$ (Figure 6b). The most notable differences are the +10 cm^{-1} blue-shift of band A_2 with respect to the position identified in the 1-NpH$^+\cdots Ar$ spectrum, as well as the appearance of a second amply red-shifted band (A_1, 3374 cm^{-1}). This band can be connected with the attachment of the second Ar ligand to the free OH group of $x1\cdots Ar$. Intuitively, such OH-bound $x1\cdots Ar_2$ represent the most stable trimer structures; the corresponding geometry of $p1\cdots Ar_2$ has been investigated via quantum chemical calculations and was found to be stable. This geometry is characterized by C_s symmetry, which implies that the two O-H bonds are equivalent, like in the case of the $x1$

Figure 6. *The IR spectra of 1-NpH$^+\cdots$Ar$_n$ (n = 1...6) obtained via the photodissociation process described in **(5)**; n and m are indicated on each spectrum (left hand and center respectively); the vertical bands are underlining related bands, as indicated on top of the figure. The dip at 3519 cm^{-1} is caused by an atmospheric absorption of the excitation laser.*

monomer; thus, the observed vibrations arise from the symmetric and antisymmetric combinations of these two equivalent O-H stretch oscillators. The assignments of these bands ($\nu^{s}_{x1\cdots Ar_2}$ at 3340 cm^{-1} and $\nu^{as}_{x1\cdots Ar_2}$ at 3374 cm^{-1}) are identical with the ones of bands A_2 and A_1 observed in the IRPD spectrum of PhH^{+}$\cdots$Ar$_2$ (3339 cm^{-1} and 3375 cm^{-1}); their very similar positions result in almost the same splitting of the two coupled vibrations (34 cm^{-1} for $x1$$\cdots$Ar$_2$ and 36 cm^{-1} for $p1$$\cdots$Ar$_2$).

The most prominent feature of the 1-NpH^{+}$\cdots$Ar$_2$ spectrum is band B_1 (3514 cm^{-1}). The similarly positioned and shaped band B_1 from the 1-NpH^{+}$\cdots$Ar spectrum was assigned to the spectroscopically indistinguishable OH-bound $t3$$\cdots$Ar and $t5$$\cdots$Ar. While band A_2 is blue-shifting by +10 cm^{-1} when adding a second ligand, band B_1 is shifting by merely 1 cm^{-1}. Given this minor blue-shift, the attachment of the second ligand must take place via π-bonding to one of the rings. There is no evidence for a trimer having both ligands π-bonded (no IR activity around the evaluated position of 3566 cm^{-1}), confirming that OH-bonding is by far the most stable binding motif for $t3$ and $t5$.

Similar to band B_1, the bands C_2 and D_2 are easily assigned to trimers built by π-bonding an Ar ligand to the OH-bonded $t9$$\cdots$Ar and $t7$$\cdots$Ar. Pretty much like band B_1, band C_2 exhibits a blue-shift of +2 cm^{-1}. It is interesting to note that band D_2 has no discernible shift; a cursory check of its position in all the 1-NpH^{+}$\cdots$Ar$_n$ spectra shows that, indeed, this band is not shifting upon complexation. Thus, it can be inferred that compexation via π-bonding of Ar has little effect on the properties of the O-H bond of $t7$. By far the most interesting features of the 1-NpH^{+}$\cdots$Ar$_2$ spectrum are the bands C_1 and D_1: in the 1-NpH^{+}$\cdots$Ar spectrum, similarly positioned bands were assigned to π-bonded $t9$$\cdots$Ar and $t7$$\cdots$Ar dimers. Their presence in the 1-NpH^{+}$\cdots$Ar$_2$ spectrum is regarded as a proof of the competition between OH- and π-bonding sites in $t9$ and $t7$, derived from the close binding energies of both types of sites. As evaluated in the **Quantum chemical calculations** section, OH-bonding of Ar to both these monomers is characterized by stabilization energies which are, even after a resonable rescaling, smaller than the typical value of the binding energy of an Ar ligand to the π electron system of an A(H)$^{+}$ (240 cm^{-1} to 470 cm^{-1} versus 550 ± 50 cm^{-1}).

4.4.4. Spectrum of 1-NpH^{+}$\cdots$(N$_2$)$_2$

The spectrum of 1-NpH^{+}$\cdots$(N$_2$)$_2$ (Figure 7b) was recorded in two fragmentation channels: the low energy range (3000 cm^{-1}...3300 cm^{-1}) was obtained by evaporating only one N$_2$ ligand (2 → 1 fragmentation channel), while excitation in the 3400 cm^{-1}...3600 cm^{-1}

range resulted in the evaporation of both ligands (2 $\rightarrow$ 0 fragmentation channel).

Figure 7. *The IR spectra of 1-NpH$^+$$\cdots$(N$_2$)$_n$ (n = 1...3) obtained via the photodissociation process described in (5); n and m are indicated on each spectrum (left hand and center respectively); the vertical bands are underlining related bands, as indicated on top of the figure.*
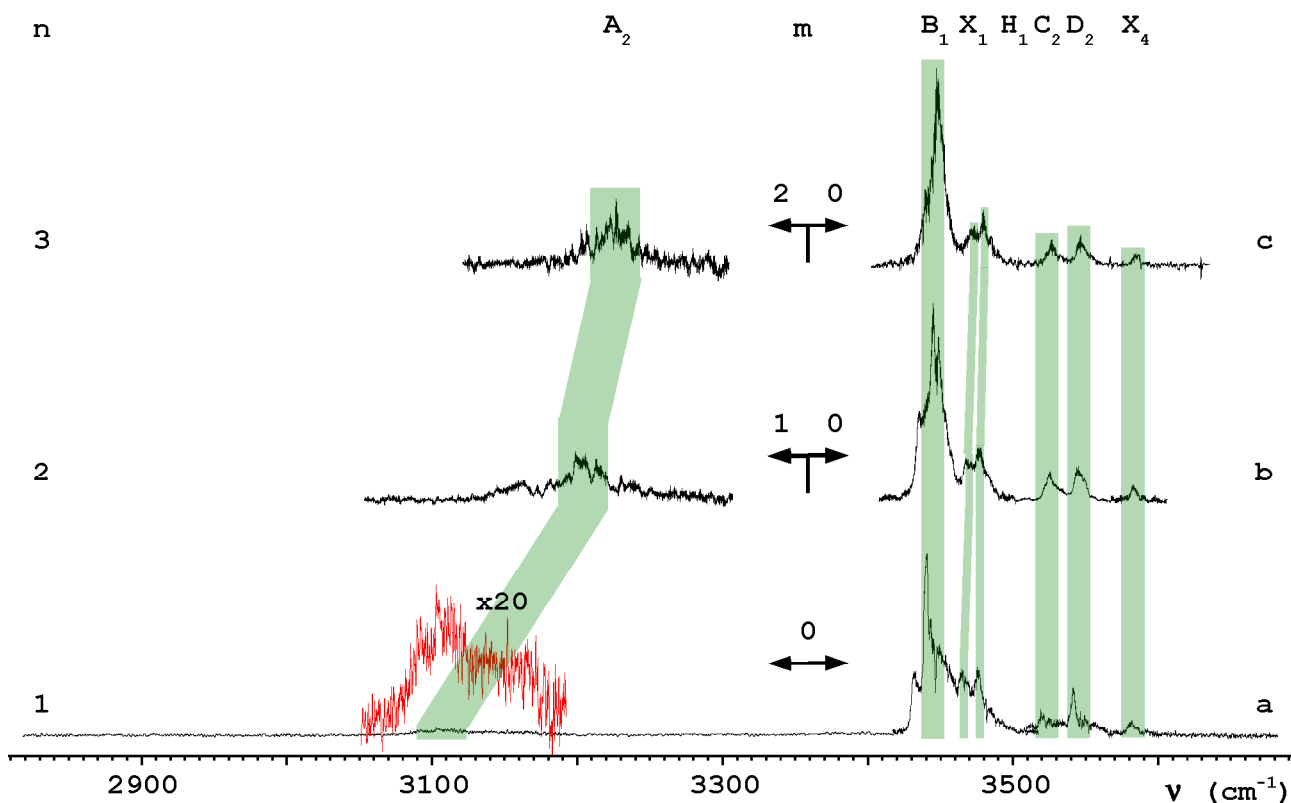
Two bands (A$_2$ at 3162 cm^{-1} and A$_1$ at 3199 cm^{-1}) are observed in the 2 $\rightarrow$ 1 fragmentation channel; based on their positions and shapes they are assigned to the OH-bound $x1\cdots$(N$_2$)$_2$ trimers. The corresponding bands in the PhH$^+$$\cdots$(N$_2$)$_2$ spectrum (also recorded in the 2 $\rightarrow$ 1 fragmentation channel) were also assigned to the equivalent OH-bound $p1\cdots$(N$_2$)$_2$ trimer. Like in the case of 1-NpH$^+$$\cdots$Ar$_2$, the $x1\cdots$(N$_2$)$_2$ trimers are evaluated to have C$_s$ symmetry; the two O-H bonds are equivalent after complexation, so the bands in the spectrum arise from the symmetric and antisymmetric combinations of the two stretch oscillators. Their splitting (37 cm^{-1}) compares very well with the splitting of the two bound O-H vibrations of $p1\cdots$(N$_2$)$_2$ seen in the spectrum of PhH$^+$$\cdots$(N$_2$)$_2$ (38 cm^{-1}). Band A$_2$ is blue-shifted by +66 cm^{-1} with respect to its position in the 1-NpH$^+$$\cdots$N$_2$ spectrum; owing to the greater PA of N$_2$ with respect to the PA of Ar, this shift is much larger than the one identified in the 1-NpH$^+$$\cdots$Ar and 1-NpH$^+$$\cdots$Ar$_2$ spectra (+10 cm^{-1}). At the same time, the blue-shift of band A$_2$ observed here is smaller than the corresponding one seen in the

spectrum of $PhH^+\cdots(N_2)_2$ (+81 cm^{-1}). Such a decrease is somehow suprising, as both **p1** and **t1** have very similar PAs (see below); this difference is also larger than the one expected from the decreased calculated value of the dimer binding energy.

The spectrum recorded in the $2 \rightarrow 0$ fragmentation channel is a replica of the corresponding range from the spectrum of 1-NpH$^+\cdots$N$_2$. Like in the case of the other studied systems, all the bands are found to be slightly blue-shifted. Band B$_1$ (here at 3446 cm^{-1}) is shifted by +6 cm^{-1}, comparable with the shift seen for $PhH^+\cdots(N_2)_n$ (+8 cm^{-1}), while bands C$_2$ and D$_2$ are displaced by +5 cm^{-1}. Also band H$_1$ is clearly present (3468 cm^{-1}), again shifted by just +1 cm^{-1} from the position seen in the 1-Np$^+\cdots(N_2)_2$ spectrum.

One important aspect resulting from the quantum chemical analysis is that all $D_0^{OH, xk\cdots N_2}$ are supposed to be slightly smaller than the corresponding $D_0^{OH, pk\cdots N_2}$. The calculated $D_0^{OH, x1\cdots N_2}$ is close to 2000 cm^{-1} for both dimers, slightly smaller than the ~2150 cm^{-1} evaluated for $D_0^{OH, p1\cdots N_2}$; all other OH-bonded **xk**$\cdots$N$_2$ dimers were calculated to be bound by ~1000 cm^{-1} or less. Driven by the similarity between the **pk** and **xk**, one may evaluate $D_0^{\pi, x1\cdots N_2}$ as smaller than the 950 ± 150 cm^{-1} evaluated for the π-bonded **p1**$\cdots$N$_2$; at the same time, it can be considered that any π-bonded **xk**$\cdots$N$_2$ dimer (k ≥ 2) is characterized by a D$_0$ smaller than the one of the π-bonded **p3**$\cdots$N$_2$ and **p5**$\cdots$N$_2$ (750 ± 150 cm^{-1}). These estimations are supported by the fact that naphthols offer a much larger molecular body than phenol, yielding a reduction in the effective charge of each π electron system and, consequently, a reduction of the intermolecular interaction. Neglecting the three-body interactions, the D$_0$ of the trimers can be estimated as sums of the dimer interactions. Thus, the total D$_0$ of the **x1**$\cdots$(N$_2$)$_2$ trimers having both ligands OH-bound are evaluated to be above the energy of the excitation photon, while the total D$_0$ of any other trimer is expected to be below the energy of the excitation photon. As the complexes are expected to be vibrationally cold, it results the **x1**$\cdots$(N$_2$)$_2$ will lose one N$_2$ ligand upon ν_{OH} excitation, while all the other trimers will lose both ligands. Overall, it can be seen that the separation of the evaporation channels, depending on the total binding energies of N$_2$ ligands to various monomers, occurs as predicted. The FWHM of bands A$_2$ and A$_1$ (38 cm^{-1} and 30 cm^{-1} in the 1-NpH$^+\cdots$(N$_2$)$_2$ spectrum) are much smaller than the one of band A$_2$ in the 1-NpH$^+\cdots$N$_2$ spectrum (66 cm^{-1}), suggesting a vibrational "cooling" of the **x1**$\cdots$(N$_2$)$_2$ trimers with respect to their precursor dimers.

4.4.5. Spectra of 1-NpH$^+$···L$_n$ (L = Ar, N$_2$; n = 3...6)

The spectrum of 1-NpH$^+$···Ar$_3$ develops fairly monotonically, in line with the characteristics exhibited by the dimers and trimers spectra. All bands are continuing their complexation-induced incremental blue-shifts; the FWHMs of bands A$_2$ and A$_1$ decrease with respect to the values seen in the trimer spectrum, signaling a vibrational "cooling" of the $x1$···Ar$_3$ complexes of type 2Hπ. Starting from 1-NpH$^+$···Ar$_4$, the main dissociation channel of the $x1$···Ar$_n$ complexes changes from n → 0 to n → 1, reflecting the fact that the total binding energy of the ligands attached to $x1$ exceeds the energy of the photons exciting the $v^s_{x1···Ar_n}$ or $v^{as}_{x1···Ar_n}$ vibrations. Also from 1-NpH$^+$···Ar$_4$ onwards, one more band (A$_3$) develops in between the two already known A$_2$ and A$_1$; such a feature has been observed also in the spectra of PhH$^+$···Ar$_3$ and PhH$^+$···Ar$_4$. Although the precise assignment of this band is uncertain, its position with respect to the other $v^b_{xk···Ar_n}$ vibrations and its presence in the same fragmentation channel as A$_2$ and A$_1$ suggest that it originates either from a presently unidentified $x1$···Ar$_n$ isomer or is a harmonic (combination band) of some unidentified vibration(s) of the 2H(n-2)π complexes. Simultaneous with the appearance of band A$_3$, both band A$_2$ and A$_1$ are red-shifted with respect to the position seen in the spectrum of the tetramers; further addition of up to two Ar ligands (1-NpH$^+$···Ar$_5$ and 1-NpH$^+$···Ar$_6$) results in all three bands resuming their incremental blue-shifts. Finally, for the $x1$···Ar$_6$ complexes it can be seen that the 6 → 2 dissociation channel becomes the dominant one; the apparent splitting of band A$_1$ (3385 cm^{-1} and 3397 cm^{-1}) has not been analyzed further.

A significant detail of this spectra sequence is the fact that, up to the spectrum of 1-NpH$^+$···Ar$_5$, all complexes except the ones derived from $x1$ are losing all ligands upon vibrational excitation. This has little to do with the modest increase in excitation energy from <3400 cm^{-1} for $x1$···Ar$_n$ to >3500 cm^{-1} for 1-NpH$^+$···Ar$_5$; the parameter driving this change is the total D$_0$ of the complexes. Indeed, the observed fragmentation channel is consistent with the finding that D$_0$ of the tn···Ar (n ≠ 1) dimers is at most half of D$_0$ of the $x1$···Ar dimers; even more, this difference implies that D$_0$ of the $x1$···Ar dimers is close to the D$_0$ of other OH-bound dimers plus D$_0$ of a π-bound Ar ligand.

Also noticeable is the finding that while bands C$_1$, C$_2$, and D$_2$ (assigned as originating from $t9$···Ar$_n$ and $t7$···Ar$_n$ respectively) are the main contributors to the 6 → 0 dissociation channel, band B$_1$ (originating from $t5$···Ar$_n$ and $t3$···Ar$_n$) is the major feature of the 6 → 1 IRPD spectrum. Again, this separation, although incomplete, is in line with the predicted differences in D$_0$ of various dimers.

Band C_1 (assigned to $n\pi$ isomers of $t9\cdots Ar_n$) can be seen in all spectra, while band D_1 (assigned to $n\pi$ isomers of $t7\cdots Ar_n$) disappears starting from n = 4. Consequently, it seems that OH-bonding of Ar to $t9$ is less favourable than OH-bonding to $t7$. This finding is at odds with the calculations, which predict that while $v^f_{t9\cdots Ar} < v^f_{t7\cdots Ar}$, the OH-bound $t9\cdots Ar$ dimer is more stable than $t7\cdots Ar$: $D_0^{OH, t9\cdots Ar} > D_0^{OH, t7\cdots Ar}$. However, the conclusion that OH-bonding of Ar to $t9$ is less favourable than OH-bonding to $t7$ might very well be flawed, as it is based on the assumption that all the intermolecular π bonds are equally strong.

Like in case of $1\text{-NpH}^+\cdots Ar_n$, the spectrum of $1\text{-NpH}^+\cdots(N_2)_3$ reproduces the features of the $1\text{-NpH}^+\cdots(N_2)_2$ spectrum: all bands are modestly blue-shifted, but the general structure of the spectrum is maintained. The bands observed under $3300\ cm^{-1}$ were recorded in the $3 \rightarrow 2$ fragmentation channel, while the ones seen above $3300\ cm^{-1}$ were recorded in the $3 \rightarrow 0$ fragmentation channel. This early separation underlines the strength of the bonds created by N_2 in $x1\cdots(N_2)_3$ with respect to the ones of Ar. It is interesting to note that, like it is seen in the $PhH^+\cdots(N_2)_3$ spectrum, only one band (A_2 at $3224\ cm^{-1}$) can be connected to O-H stretch vibrations of $x1\cdots(N_2)_3$. Two ways of explaining this have been found for $PhH^+\cdots(N_2)_3$: either the splitting of the two expected bands is too small and they are unresolved in the recording, or the two expected bands overlap only in the tetramer spectrum. Based on the ratio between the IR intensities resulting from calculations, the final assignment was to $v^{as}_{p1\cdots(N_2)_n}$. As the relative magnitudes of the shifts and splittings have been found quasi-identical for both systems, it is hard to tip the balance in favor of any of these possible explanations, so a similar assignment ($v^{as}_{t1\cdots(N_2)_3}$) will be given to band A_2. The mirroring between the characteristics exhibited by the bands A_1 and A_2 of $PhH^+\cdots(N_2)_n$ on one hand and by the bands A_1 and A_2 of $1\text{-NpH}^+\cdots(N_2)_n$ (n = 1, 2, 3) on the other hand shows that the microsolvation of both $p1$ and (at least) $t1$ starts in an identical way. The evaporation channels observed for excitation of bands B_1, C_2, and D_2 confirm the assignment of these bands to carbenium isomers.

The bands $3476\ cm^{-1}$ and $3581\ cm^{-1}$ in the $1\text{-NpH}^+\cdots N_2$ spectrum, $3477\ cm^{-1}$ and $3582\ cm^{-1}$ in the $1\text{-NpH}^+\cdots(N_2)_2$ spectrum as well as $3480\ cm^{-1}$ and $3584\ cm^{-1}$ in the $1\text{-NpH}^+\cdots(N_2)_3$ spectrum are presently unidentified. Based on their position, it seems reasonable to group them as X_1 ($3476\ cm^{-1}$, $3477\ cm^{-1}$ and $3480\ cm^{-1}$) and X_4 ($3581\ cm^{-1}$, $3582\ cm^{-1}$ and $3584\ cm^{-1}$). The hypothesis that all three X_1 (X_4) bands have a common origin is supported by the slight blue-shifts seen within each group. Their observed characteristics can be summarized as follows: (a) both X_1 and X_4 are present in all $1\text{-NpH}^+\cdots(N_2)_n$ (n = 1...3) spectra; (b) the magnitude of their complexation-induced blue-

shifts, as seen between the between 1-NpH$^+$···N$_2$ and 1-NpH$^+$···(N$_2$)$_3$ spectra, (+4 cm^{-1} and +3 cm^{-1} respectively) are slightly smaller than the ones of bands C$_2$ (+6 cm^{-1}) and D$_2$ (+5 cm^{-1}); (c) no assigned band has been connected with a purely π-bound isomer. Given the above-listed characteristics, one can make a few educated guesses about them.

First of all, the positions and IR activities of X$_1$ and X$_4$ in the 1-NpH$^+$···N$_2$ spectrum are not compatible with the evaluated characteristics of any $v^f_{tk\cdots N_2}$ derived from π-bound tk···N$_2$ dimers; such an assignment would anyway be doubtful given their presence in all 1-NpH$^+$···(N$_2$)$_n$ (n = 1...3) spectra.

Another possible origin of one such band would be the combination between a $v^b_{tk\cdots N_2}$ and the corresponding intermolecular stretch vibration $v^s_{tk\cdots N_2}$. Considering the IR activities of the bands in the recorded spectrum, the best candidates are the combination bands between the components of band B$_1$ and their corresponding intermolecular stretches: $v^b_{t5\cdots N_2} + v^s_{t5\cdots N_2}$ and $v^b_{t3\cdots N_2} + v^s_{t3\cdots N_2}$. However, these bands are expected to occur close to 3530 cm^{-1}, far away from both X$_1$ and X$_4$.

Considering their positions (close to bands assigned to $v^b_{tk\cdots N_2}$) and their persistence in all 1-NpH$^+$···(N$_2$)$_n$ (n = 1...3) spectra, these two bands might also be assigned to fundamental stretch vibrations of ligand-complexated O-H bonds of so-far unidentified isomers. Thus, the position of band X$_4$, at a higher frequency than the bands originating from $v^b_{tk\cdots N_2}$ (k = 7, 9), could mean that the monomer from which it derives is protonated in such a way that the O-H bound suffers little perturbation. An interesting possibility is that bands X$_1$ originate from some ck···(N$_2$)$_n$ (k ≥ 3) isomers. As the most stable ck monomer is $c5$, the normal modes of the $c5$···N$_2$ complex have been calculated. This calculation predicts the frequency of the $v^b_{c5\cdots N_2}$ vibration as 3498 cm^{-1}, which does not even roughly match any of the unidentified bands. It should be noted that the spectra of 1-Np$^+$···(N$_2$)$_n$ (n = 1...5) exhibit a sequence of bands attributed to $v^b_{c-1-Np^+\cdots(N_2)_n}$; these bands occur ~30 cm^{-1} above the corresponding bands of t-1-Np$^+$···(N$_2$)$_n$. Following this, the assignment of bands X$_1$ will be left open.

4.4.6. Site-dependent proton affinity of x-1-NpH$^+$ rotamers

Proton affinities of naphthols have not been measured experimentally; even information derived frum quantum chemical calculations is rather scarce.[36] In the following, site-specific proton affinities of t-1-Np will be derived from the calculations

presented above, using as reference the data available for Ph. It should be noted that the calculations presented here are not done at the level of theory recommended for quantum chemical evaluations of PA (G2).[37],[38],[39] However, comparisons between the presently calculated and previously reported values for PA of Ph[20],[40] may allow to reevaluate how suitable the B3LYP/6-311++(2df,2pd) level is for determining PA of monohydroxyarenes.

As previous spectroscopic studies have shown, the complexation-induced red-shift in the proton donor stretch vibration of H-bound $XH^+ \cdots L$ dimers (Δv_{XH}) is correlated with the difference in the proton affinities (PAs) of the two bases X and L. More exactly, for a given ligand species L, Δv_{XH} is directly correlated to PA(X): the larger the PA(X), the stronger the intermolecular H-L bond and the larger the Δv_{XH}. The shifts depend also on the PA of the ligand i.e. Δv_{XH} are expected to be larger for $L = N_2$ compared to $L = Ar$, because $PA(N_2) > PA(Ar)$ (494 kJ/mol vs. 369 kJ/mol).[28]

Table 6. *Site-specific PA of Ph and t-1-Np, leading to the formation of the various isomers proposed and identified in the spectra: values derived from the presently done calculations (QC); averages over the groups of spectroscopically indiscernible isomers ($\overline{QC}$); experimental values listed in literature; evaluation of PAs derived by scaling $\overline{QC}$ values to match the experimental values of PA$_{Ph}$ (scaled $\overline{QC}$); values derived from literature data using the independent substituent approximation (ISA).*

site	p1	p3 p5 p7	t1	t3 t5	t7 t9
QC	743.0	804.3 821.5 810.4	752.3	853.5 871.6	836.8 830.0
$\overline{QC}$	743.0	812.0	752.3	862.5	833.4
literature	753.0	817.3			
scaled $\overline{QC}$			762.1	868.1	838.9
ISA				869.8	

Table 6 shows a comparison of the presently evaluated data with other published calculations and with the values previously measured. The calculated values compare well with the general trends underlined above. Even more, it can be seen that the isomer-selective PA of Ph is reproduced within 1.5% accuracy,[20],[40] suggesting that the direct quantum chemical evaluation are yielding meaningful results. Considering that due to the similarity between the two systems the underevaluation is the same, it results that the average affinity for protonation at the *t3* or *t5* sites is 868.1 kJ/mol. For the protonation process leading to oxonium isomers of 1-NpH$^+$, the scaled affinity is 762.1 kJ/mol. Although sites *t7* and *t9* have no equivalent in PhH$^+$, it seems reasonable to rescale them

using the same factor as for *t3* and *t5*, thus obtaining an average PA of 838.9 kJ/mol.

Alternatively, an evaluation of the site-specific PA of the *t3* and *t5* sites can be evaluated using the independent substituent approximation (ISA) developed by Eckert-Maksic.[36],[41] This theory states that the PA of a polysubstituted molecule can be derived from the PA of the nonsubstituted parent, to which increments specific to each substituent (species and position with respect to the protonation site) are added. The theory has previously been used to predict site-specific PAs of phenol and naphthols using only quantum chemical calculations; in the present work it will be applied using experimental results provided in the literature. This is indeed possible if one regards naphthalene ($\equiv$ Na) as a benzene molecule with two substitutions; thus, hydroxynaphthalenes can be treated as triple substituted benzenes. More exactly, x-1-Np can be regarded as a benzene molecule (ring atoms 2, 3, 4, 5, 6, 11 on Figure 1) to which substituting groups are attached to C_6 and C_{11} (the hydrocarbon chain which builds the second ring) and also to C_2 (the hydroxyl group). Thus, the average PA of the *x3* and *x5* sites can be estimated as

$$\overline{PA}_{xk}\big|_{k=3,5} = PA_{Bz} + [PA_{Na} - PA_{Bz}] + [PA_{Ph} - PA_{Bz}] \Rightarrow$$

$$\Rightarrow \overline{PA}_{xk}\big|_{k=3,5} = PA_{Na} + PA_{Ph} - PA_{Bz}$$

(7)

The literature gives the following values for the proton affinities: PA_{Bz} = 750.4 kJ/mol[28], PA_{Na} = 802.9 kJ/mol[28] (site unspecified), and PA_{Ph} = 817.3 kJ/mol (carbenium protonation).[40] It follows that $\overline{PA}_{xk}\big|_{k=3,5}$ = 869.8 kJ/mol, which is in excellent agreement with the calculated value.

The ISA method cannot be applied to study the protonation of x-1-Np at the ring B (sites *x7* and *x9*); also excluded are the two *x1* sites. Indeed, in all these three cases, the protonation does not take place at the benzene ring, but at the substituent. At the present moment, the best evaluations available are the ones resulting from calculations.

4.4.7. Ligand binding energies

The photofragmentation branching ratios (Table 7) have been measured for resonant excitation of a number of v_{OH} bands of 1-NpH$^+\cdots$Ar$_n$ listed in Table 5, namely A_2, B_1, C_2, and D_2, and have been used to roughly estimate the ligand binding energies. For estimating D_0 for the various ligand positions, a simple model is employed. The ligands are classified as OH-bound and others (further denoted π-bound), with $D_0(H) > D_0(\pi)$; all non OH-bound ligands are assumed to have the same binding energy. It is also assumed that the entire absorbed photon energy (v_{OH}) is available for subsequent ligand evaporation, which starts

with the weakest bound ligands.[7],[8],[9],[11],[12],[13],[16]

An overview of the observed photofragmentation patterns is shown in Figure 8. It can be seen that, in general, only one or two major fragment channels (m) are obtained for a given parent cluster size (n); this agrees well with previous studies on related systems.[7],[8],[9],[11],[12],[13],[16] It should also be noted that, in very few cases, the branching spreads over three significant channels; the implications of these special cases will be discussed later. The fragmentation pattern observed while exciting the band assigned to $\nu^{as}_{x1\cdots Ar_n}$ (3374 cm^{-1} for 1-NpH$^+$$\cdots$Ar, then following the maximum) exhibits the earliest branching (n = 4 $\rightarrow$ m = 1). This behaviour is expected, as the calculations show that the two OH-bound Ar ligands of $x1\cdots Ar_n$ (n > 2) posses the strongest OH$\cdots$Ar bonds of all 1-NpH$^+$$\cdots$Ar$_n$. Also the fragmentation pattern driven by $\nu^b_{t3/5\cdots Ar_n}$ (3516 cm^{-1}) suggests that $tk\cdots$Ar (k = 3, 5) are the dimers with the second highest binding energy; again, the prediction based on calculations proved to be correct. Finally, the isomers responsible for the bands C$_2$ and D$_2$ are forming the weakliest bound complexes: the corresponding branching from m = 0 to m = 1 occurs at n = 6 for both of them.

Table 8. *The photofragmentation branching ratios observed at the excitation of O-H stretch vibrations of various isomers of 1-NpH+$\cdots$Arn, expressed as percentage of the total fragment production.*

	m												
	0	1	2	3	0	1	2	0	1	2	0	1	2
n	$\nu^{as}_{x1\cdots Ar_n}$				$\nu^b_{t3/5\cdots Ar_n}$			$\nu^b_{t7\cdots Ar_n}$			$\nu^b_{t9\cdots Ar_n}$		
1	100				100			100			100		
2	100				100			100			100		
3	100				100			96	4		100		
4	21	79			99	1		99	1		100		
5	20	47	27	6	95	5		90	4	6	100		
6	0	8	77	15	25	72	3	74	22	4	63	19	18
7	0	9	56	35	15	45	40	18	70	12	26	53	21

The major branching of the $x1\cdots$Ar$_7$ (7 $\rightarrow$ 2 $\Rightarrow$ 5$\cdot$D$_0^{\pi,\,x1\cdots Ar}$ < 3400 cm^{-1}), implies that D$_0^{\pi,x1\cdots Ar}$ < 680 cm^{-1}. Using this result together with the $x1\cdots$Ar$_4$ branching (4 $\rightarrow$ 1 $\Rightarrow$ 3400 cm^{-1} < 2$\cdot$D$_0^{OH,\,x1\cdots Ar}$+2$\cdot$D$_0^{\pi,x1\cdots Ar}$), it results that 1020 cm^{-1} < D$_0^{OH,x1\cdots Ar}$. At the same time, the major evaporation channel of $x1\cdots$Ar$_6$ (6 $\rightarrow$ 2 $\Rightarrow$

Figure 8. *The photofragmentation branching ratios observed at the excitation of O-H stretch vibrations of various isomers of 1-NpH⁺···Arₙ. The red lines mark the number of ligands in the parent complexes while the black ones represent the resulting fragments (percentage of the total fragment production). The wavelength at which the photofragmentation processes were recorded match the position of the bands maxima.*
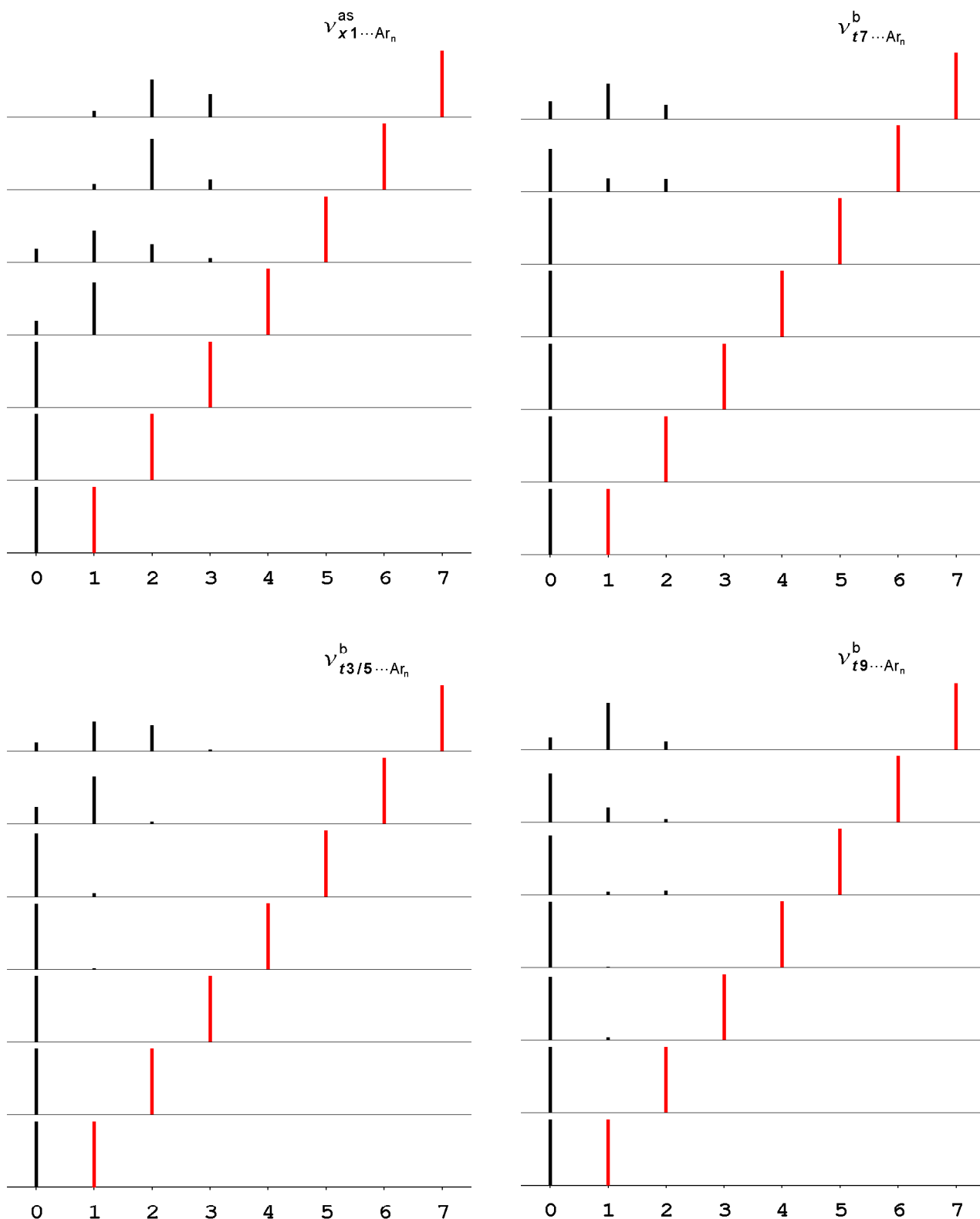
$4 \cdot D_0^{\pi, x1 \cdots Ar} + D_0^{OH, x1 \cdots Ar} < 3400 \text{ cm}^{-1}$), shows that $595 \text{ cm}^{-1} < D_0^{\pi, x1 \cdots Ar}$. This result can be inserted in the inequality resulting from the $3 \rightarrow 0$ branching, yielding $D_0^{OH, x1 \cdots Ar} < 1400 \text{ cm}^{-1}$.

For $tk \cdots Ar_n$ (k = 3, 5), the branching ratios can be expanded by following the trend exhibited by n = 6 and n = 7; it is reasonable to consider that for n = 8 the main fragmentation product has m = 2. Thus, from the $8 \rightarrow 2$ and $6 \rightarrow 1$ branchings, it results that $500 \text{ cm}^{-1} < D_0^{\pi, t3/5 \cdots Ar} < 700 \text{ cm}^{-1}$, while from the $5 \rightarrow 0$ and from the assumption that $D_0^{\pi, t3/5 \cdots Ar} < D_0^{OH, t3/5 \cdots Ar}$ it results that $500 \text{ cm}^{-1} < D_0^{OH, t3/5 \cdots Ar} < 1500 \text{ cm}^{-1}$. It should be noted that this range can be slightly narrowed down remembering that $D_0^{OH, p3/5 \cdots Ar} < D_0^{OH, p1 \cdots Ar}$; thus, it can be said that $500 \text{ cm}^{-1} < D_0^{OH, t3/5 \cdots Ar} < 1400 \text{ cm}^{-1}$.

Finally, the photofragmentation of the $tk \cdots Ar_n$ (k = 7, 9) is unable to provide ranges for the D_0 of both types of ligands. This is the result of the absence of an $n \rightarrow 2$ fragmentation channel, which would have enabled the evaluation of $D_0^{\pi, t7/9 \cdots Ar}$. Thus, the fragmentation channels of the two largest clusters $(6 \rightarrow 0$ and $7 \rightarrow 1)$ implies that $D_0^{OH} + 5 \cdot D_0^{\pi} < 3600 \text{ cm}^{-1} < D_0^{OH} + 6 \cdot D_0^{\pi}$. The two inequalities can be supplemented by two others, one derived from the calculations and the other one derived from previous evaluations done on other $A(H)^+ \cdots Ar_n$ complexes. From the quantum chemical calculations it is known that $tk \cdots Ar_n$ (k = 7, 9) are bound by the smallest D_0^{OH}; this implies that $D_0^{OH, t7/9 \cdots Ar} < 1400 \text{ cm}^{-1}$. Also, investigations of other $A(H)^+ \cdots Ar_n$ complexes are showing that π-bonding of Ar to $A(H)^+$ is rather insensitive to the detailed structure of $A(H)^+$, ranging from 400 cm^{-1} to 700 cm^{-1}; it is thus justified to assume that $400 \text{ cm}^{-1} < D_0^{\pi, t7/9 \cdots Ar}$. Together, these inequalities can be translated into $360 \text{ cm}^{-1} < D_0^{OH, t7/9 \cdots Ar} < 1400 \text{ cm}^{-1}$ and $400 \text{ cm}^{-1} < D_0^{\pi, t7/9 \cdots Ar} < 540 \text{ cm}^{-1}$.

For the $1\text{-NpH}^+ \cdots (N_2)_n$ (n = 1, 2, 3), the only fragmentation information available is the one extracted from the IRPD spectra plotted in Figure 7. Although insufficient for a complete characterization, the fragmentation branching sets certain limits for the binding energies. The $2 \rightarrow 1$ evaporation channel implies $1600 \text{ cm}^{-1} < D_0^{OH, x1 \cdots N_2}$, while the $3 \rightarrow 2$ channel shows that $3200 \text{ cm}^{-1} < D_0^{OH, x1 \cdots N_2} + D_0^{\pi, x1 \cdots N_2}$. As no evaluation can be made for $D_0^{\pi, x1 \cdots N_2}$, one has to turn to the values known for the $PhH^+ \cdots (N_2)_n$ complexes. It results that, if $D_0^{\pi, x1 \cdots N_2} \approx D_0^{\pi, p1 \cdots N_2}$, then $2100 \text{ cm}^{-1} < D_0^{OH, x1 \cdots N_2} < 2400 \text{ cm}^{-1}$. However, the range should

be enlarged, as the relation between $D_0^{\pi, x1\cdots N_2}$ and $D_0^{\pi, p1\cdots N_2}$ is not one of identity. No meaningful information can be extracted for the complexes built around *tk* (k > 2).

Table 8. *Experimental (exp) and calculated (QC) estimates for the site-specific binding energies of Ar toward 1-NpH⁺ and PhH⁺.*[7],[16]

site	D_0 (cm⁻¹) exp	D_0 (cm⁻¹) QC	D_0 (cm⁻¹) QC	D_0 (cm⁻¹) exp	site
$D_0^{OH, x1\cdots Ar}$	1200±200	790	868	1150±300	$D_0^{OH, p1\cdots Ar}$
$D_0^{\pi, x1\cdots Ar}$	640± 40			650±200	$D_0^{\pi, p1\cdots Ar}$
$D_0^{OH, t3/5\cdots Ar}$	950±450	330	371	650±150	$D_0^{OH, p3/5\cdots Ar}$
$D_0^{\pi, t3/5\cdots Ar}$	600±100			600±100	$D_0^{\pi, p3/5\cdots Ar}$
$D_0^{OH, t7/9\cdots Ar}$	850±550	194			
$D_0^{\pi, t7/9\cdots Ar}$	470± 70				

All the values derived here for 1-NpH⁺$\cdots$L$_n$, and previously for PhH⁺$\cdots$L$_n$ are listed in Table 8. It can be seen that for *x1*$\cdots$Ar$_n$ the experimental binding energies are basically identical. The broad range of $D_0^{OH, t3/5\cdots Ar}$ is the result of the incomplete fragmentation scheme. Very important is the fact that the ranges of $D_0^{OH, t7/9\cdots Ar}$ and $D_0^{\pi, t7/9\cdots Ar}$ are overlaping, giving support to the very low estimates resulting from calculations. However, it can be seen that the theoretical estimates are largely underestimating the intermolecular interaction.

4.4.8. Microsolvation model

Typically, the total interaction in ion-ligand complexes with nonpolar ligands is mainly composed of the two-body interaction terms. Indeed, the interaction in neutral Ar$\cdots$Ar and N$_2\cdots$N$_2$ is on the order of $D_0 \approx 100$ cm⁻¹, rendering the "chaining" of ligands energetically inefficient with respect to their direct binding to the cation.[42],[43] As also three-body forces are weak, the 1-NpH⁺$\cdots$L$_n$ cluster growth is mainly driven by the 1-NpH⁺$\cdots$L dimer potential. Thus, the derived solvation sequence for the most stable 1-NpH⁺$\cdots$L$_n$ complexes starts with the formation of a H-bound 1-NpH⁺$\cdots$L dimer core, which is then further solvated by (n-1) π-bound and / or CH-bound ligands. This is especially true for the *x1*$\cdots$Ar$_n$ and *t3/5*$\cdots$Ar$_n$ systems; the sequence is not so clear anymore for the *t7/9* isomers. Here, the apparently weak OH$\cdots$Ar interaction makes π-bonding sites rather attractive, as seen by the persistence of the $v_{t7/9\cdots Ar_n}^f$ bands even in the spectra recorded for n > 3. A cluster growth

process similar to the one proposed for the $x1\cdots Ar_n$ and $t3/5\cdots Ar_n$ systems was also deduced for $Ph(H)^+\cdots L_n$, $1\text{-}Np^+\cdots L_n$, $Im^+\cdots L_n$, and $An^+\cdots L_n$ with either Ar or N_2 ligands: first, the available acidic protons of the of the $OH_{(2)}$ and NH_2 groups are solvated by H-bound ligands, after which further π-bound ligands are attached to the aromatic ring.

The solvation model presented here can be observed for the $x1\cdots Ar_n$ complexes from their IRPD spectra. Indeed, the complexation induced shifts of the $v^s_{x1\cdots Ar_n}$ and $v^{as}_{x1\cdots Ar_n}$ give clues regarding the cation-ligand and ligand-ligand takes place. In Figure 8 are presented the average values of the two O-H stretch vibrations of $x1\cdots Ar_n$ and of $p1\cdots Ar_n$. As the free O-H vibration of $x1\cdots Ar$ could not be localized in the experimental spectrum, the position evaluated from calculations was used. Also the frequencies of the O-H vibrations of the bare 1-NpH$^+$ have been extracted from calculations. The values of v^s_{p1} and v^{as}_{p1} have been taken from literature.[17]

Figure 8. *Experimental $\bar{v}_{OH}$ frequencies of the $x1\cdots Ar_n$ and $p1\cdots Ar_n$ dimers as a function of the cluster size n (Table 5). $\bar{v}_{OH}$ for the bare 1-NpH$^+$ as well as $v^f_{x1\cdots Ar}$ are evaluated from quantum chemical calculations. The values of v^s_{p1} and v^{as}_{p1} have been taken from literature.*
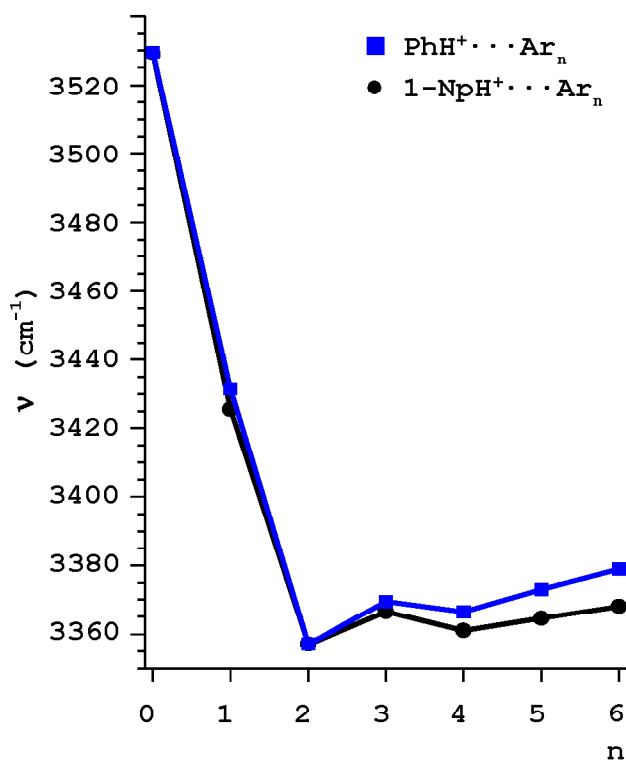
From the plot it can be seen that the microsolvation of $x1$ mirrors closely the one of $p1$. The first two ligands are inducing large red-shifts in $\bar{v}_{OH}$ because of the destabilization of the O-H bond. The magnitude of the red-shift which occurs upon the addition of the second ligand (34 cm^{-1}) is similar to the one produced by the attachement of the first ligand (52 cm^{-1}). The H-bound $x1\cdots Ar_2$ trimer is further solvated by π-bound ligands, which slightly destabilize the intermolecular H-bonds to the first two ligands via noncooperative three-body forces, which in turn stabilize the intramolecular O-H bonds. This results in small

incremental blue-shifts of $\bar{\nu}_{OH}$. At the same time, the noncooperative three-body interactions between the various π-bound ligands result in a decrease in magnitude for the incremental blue-shifts, essentially leading to the convergence of the $\bar{\nu}_{OH}$ to a certain "solvated" value. This limit is not reached within the investigated cluster size, as the first solvent shell around *x*1 is not complete even at n = 6. As there are no Ar matrix isolation studies of 1-NpH⁺, it is not possible to expand the analysis of the band shifts.

4.5. Conclusions

The present study of 1-NpH⁺ was focused on the IR spectroscopy of size-selected 1-NpH⁺···Lₙ complexes (L = Ar, N₂; n = 1...6). IRPD spectra were recorded over the O-H stretch vibration range of these complexes. Quantum chemical calculations were employed to provide a basic description of the monomers and dimers observed. Comparison of the presently recorded IRPD spectra with the ones of PhH⁺···Lₙ complexes (L = Ar, N₂; n = 1...6) was used to assist in the assignment of the observed structures.

The results show that, in the output of the presently used ion source, three classes of 1-NpH⁺ isomers can be identified: oxonium ions (1-Np protonated at the O atom); carbenium ions obtained by protonation in the *para* and *ortho* positions with respect to the OH functional group; carbenium ions obtained by the addition of a proton to well-defined sites on the second naphthalene ring. The spectral identification of these three classes of protonation sites is supported by their different photofragmentation patterns. No spectral signature can be associated with any other carbenium isomers.

As the O-H stretch vibration of the *cis* and *trans* rotamers are largely overlapping, there is no experimental evidence to identify the dominant rotamer in the expansion. The quantum chemical results suggest that: the *cis* rotamers are placed slightly higher on the PES than the *trans* ones; the stability of the *cis*-based dimers is lower; the ν_{OH} stretch oscillators of these dimers are less IR-active. Thus, there is a certain collection of theoretical evidence indicating that *cis* rotamers are - at best - of less significance than the *trans* ones.

The analysis of the photofragmentation branching ratios yields ligand binding energies for the OH- and π-bonds of the solvent molecules. The experimental values show that the chosen computational level (B3LYP/6-311++(2df,2pd)) is able to describe the interaction, albeit only at a qualitative level.

The cluster size-dependent frequency shifts demonstrate that the microsolvation of *x*1, and *t5* / *t3* in an Ar or N₂ environment starts in a very similar fashion: first, the acidic

93

OH bond(s) are complexated, the following ligands probably form π-bonds to the ring system. The ligand binding energies show the same picture, as the OH-bound ligand(s) is(are) far better stabilized than the π-bound ones; this implies that OH-bonding is much more favorable, thus placing it right at the beginning of the microsolvation process. For this energetic reason, the microsolvation model presented above is not applicable for the *t7 / t9* isomers, for which both the average binding energy and the binding energy of the OH-bound ligand are less than 600 cm^{-1}.

Finally, it is important to note that the used experimental setup is a suitable tool for preparing beams of well-specified isomeric ions, because of the double mass selection coupled with the spectral analysis. Even more, the method sets a certain upper limit for the internal energy of the selected species. This means that cations which are fundamentally unstable in condensed phase can be selected and their spectral, thermodynamic, or kinetic properties can be observed.

References

[1] March J., *Advanced Organic Chemistry: Reactions, Mechanisms, and Structure*, Wiley (New York, 1982)

[2] Fialkov A.B., Dennenbaum J., Homann K.H., *Combust. Flame* **125** (2001) 763

[3] Snow T.P., Le Page V., Keheyan Y., Bierbaum M., *Nature* **391** (1998) 259

[4] Reed C.A., Kim K.C., Stoyanov E.S., Stasko D., Tham F.S., Mueller L.J., Boyd P.D.W., *J. Am. Chem. Soc.* **125** (2003) 1796

[5] Perkampus H.H., Baumgarten E., *Angew. Chem. - Int. Ed.* **3** (1964) 776

[6] Olah G.A., White A.M., O'Brien D.H., *Chem. Rev.* **70** (1970) 561

[7] Solca N., Dopfer O., *J. Chem. Phys.* **120** (2004) 10470

[8] Solca N., Dopfer O., *J. Phys. Chem. A* **105** (2001) 5637

[9] Solca N., Dopfer O., *Phys. Chem. Chem. Phys.* **6** (2004) 2732

[10] Dopfer O., Olkhov R.V., Maier J.P., *J. Chem. Phys.* **111** (1999) 10754

[11] Solca N., Dopfer O., *Chem. Eur. J.* **9** (2003) 3154

[12] Solca N., Dopfer O., *Eur. Phys. J. D* **20** (2002) 469

[13] Solca N., Dopfer O., *J. Phys. Chem. A* **106** (2002) 7261

[14] Olah G.A., Mateescu Gh.D., Mo Y.K., *J. Am. Chem. Soc.* **95** (1973) 1865

[15] Olah G.A., Mo Y.K., *J. Org. Chem.* **38** (1973) 353

[16] Solca N., Dopfer O., *Chem. Phys. Lett.* **342** (2001) 191

[17] Solca N., Dopfer O., *J. Am. Chem. Soc.* **126** (2004) 1716

[18] M.J. Frisch, G.W. Trucks, H.B. Schlegel, G.E. Scuseria, M.A. Robb, J.R. Cheeseman, J.A. Montgomery Jr., T. Vreven, K.N. Kudin, J.C. Burant, J.M. Millam, S.S. Iyengar, J. Tomasi, V. Barone, B. Mennucci, M. Cossi, G. Scalmani, N. Rega, G.A. Petersson, H. Nakatsuji, M. Hada, M. Ehara, K. Toyota, R. Fukuda, J. Hasegawa, M. Ishida, T. Nakajima, Y. Honda, O. Kitao, H. Nakai, M. Klene, X. Li, J.E. Knox, H.P. Hratchian, J.B. Cross, V. Bakken, C. Adamo, J. Jaramillo, R. Gomperts, R.E. Stratmann, O. Yazyev, A.J. Austin, R.

Cammi, C. Pomelli, J.W. Ochterski, P.Y. Ayala, K. Morokuma, G.A. Voth, P. Salvador, J.J. Dannenberg, V.G. Zakrzewski, S. Dapprich, A.D. Daniels, M.C. Strain, O. Farkas, D.K. Malick, A.D. Rabuck, K. Raghavachari, J.B. Foresman, J.V. Ortiz, Q. Cui, A.G. Baboul, S. Clifford, J. Cioslowski, B.B. Stefanov, G. Liu, A. Liashenko, P. Piskorz, I. Komaromi, R.L. Martin, D.J. Fox, T. Keith, M.A. Al-Laham, C.Y. Peng, A. Nanayakkara, M. Challacombe, P.M.W. Gill, B. Johnson, W. Chen, M.W. Wong, C. Gonzalez, J.A. Pople, *Gaussian 03, Revision D.01 Gaussian, Inc., Wallingford CT* (2004)

[19] Heidrich D., *Angew. Chem. - Int. Ed.* **41** (2002) 3208

[20] DeFrees D.J., McIver R.T., Hehre W.J., *J. Am. Chem. Soc.* **99** (1977) 3853

[21] Tishchenko O., Pham-Tran N.N., Kryachko E.S., Nguyen M.T., *J. Phys. Chem. A* **105** (2001) 8709

[22] Andrei H.S., Solca N., Dopfer O., *Phys. Chem. Chem. Phys.* **6** (2004) 3801

[23] Boys S.F., Bernardi F., *Mol. Phys.* **19** (1970) 553

[24] Chalasinski G., Szczesniak M.M., *Chem. Rev.* **94** (1994) 1723

[25] Csaszar P., Pulay P., *J. Mol. Struct. (Theochem)* **114** (1984) 31

[26] Farkas Ö., Schlegel H.B., *J. Chem. Phys.* **111** (1999) 10806

[27] Simons J., Jørgensen P., Taylor H., Ozment J., *J. Phys. Chem.* **87** (1983) 2745

[28] Hunter E.P., Lias S.G., *J. Phys. Chem. Ref. Data* **27** (1998) 413

[29] Dopfer O., *Int. Rev. Phys. Chem.* **22** (2003) 437

[30] Solca N., Dopfer O., *J. Am. Chem. Soc.* **125** (2003) 1421

[31] Solca N. and Dopfer O., *Chem. Phys. Lett.* **347** (2001) 59

[32] Camy-Peyret C., Flaud J.M., Guelachvili G. and Amiot C., *Mol. Phys.* **26** (1973) 825

[33] Guelachvili G., Rao K.N., *Handbook of Infrared Standards*, Academic Press (London, 1993)

[34] NIST, *Computational Chemistry Comparison and Benchmark DataBase*, http://srdata.nist.gov/cccbdb/

[35] Solca N., Dopfer O., *J. Mol. Struct.* **563** (2001) 241

[36] Eckert-Maksic M., Antol I., Klessinger M., Maksic Z.B., *J. Phys. Org. Chem.* **12** (1999) 597

[37] Curtiss L.A., Raghavachari K., Trucks G.W., Pople J.A., *J. Chem. Phys.* **94** (1991) 7221

[38] Smith B.J., Radom L., *Chem. Phys. Lett.* **231** (1994) 345

[39] Smith B.J., Radom L., *J. Am. Chem. Soc.* **115** (1993) 4885

[40] Lau Y.K., Kebarle P., *J. Am. Chem. Soc.* **98** (1976) 7452

[41] Eckert-Maksic M., Klessinger M., Maksic Z.B., *Chem. Phys. Lett.* **232** (1995) 472

[42] Hutson J.M., *Annu. Rev. Phys. Chem.* **41** (1990) 123

[43] Aquilanti V., Bartolomei M., Cappelletti D., Carmona-Novillo E., Pirani F., *J. Chem. Phys.* **117** (2002) 615

5. IRPD spectroscopy of $Im^+ \cdots L_n$ complexes (L = Ar, N_2; n = 1 ... 3)

**Abstract** The intermolecular interaction between the imidazole cation ($C_3N_2H_4^+$, henceforth denoted Im^+) and nonpolar ligands is characterized in the ground electronic state by infrared photodissociation (IRPD) spectroscopy of size-selected $Im^+ \cdots L_n$ complexes (L = Ar, N_2, $n \leq 3$) and quantum chemical calculations performed at the UMP2/6-311G(2df,2pd) and UB3LYP/6-311G(2df,2pd) levels of theory. The complexes are created in an electron impact cluster ion source, which predominantly produces the most stable isomers of a given cluster ion. The analysis of the size-dependent frequency shifts of both the N-H and the C-H stretch vibrations and the photofragmentation branching ratios provides valuable information about the stepwise microsolvation of Im^+ in a nonpolar hydrophobic environment, including the formation of structural isomers, the competition between various intermolecular binding motifs (H-bonding and π-bonding) and their interaction energies, and the acidity of both the CH and NH protons. In line with the calculations, the IRPD spectra show that the most stable $Im^+ \cdots L$ dimers feature planar H-bound equilibrium structures with nearly linear H-bonds of L to the acidic NH group of Im^+. Further solvation occurs at the aromatic ring of Im^+ via the formation of intermolecular π-bonds. Comparison with neutral $Im \cdots Ar$ demonstrates the drastic effect of ionization on the topology of the intermolecular potential, in particular in the preferred aromatic substrate-nonpolar recognition motif, which changes from π-bonding to H-bonding.

5.1. Introduction

Imidazole ($C_3N_2H_4$, henceforth denoted Im) is a planar heterocyclic aromatic molecule (Figure 1a) and occurs as an essential constituent in many biomolecular building blocks, such as the DNA bases adenine and guanine, and the histidine residue of proteins.[1] In aqueous biological environments, Im, its charged as well as its protonated analogues are involved in electron transfer in photosynthesis, in many biologically important enzymatic processes, in protein structure determination, and in proton shuttles.[1],[2],[3],[4] The important role of aromatic molecules and their cations for biological and chemical recognition as well

as organic reaction mechanisms has also been emphasized in recent reviews.[5],[6],[7],[8] Fundamental understanding of these phenomena at the molecular level requires the detailed knowledge of the intermolecular potential of Im, Im$^+$ and ImH$^+$ interacting with the surrounding environment. In the following, IR spectra and quantum chemical calculations of Im$^+$ solvated by a well-defined number of nonpolar ligands (L = Ar, N$_2$) are presented, with the aim to elucidate the interaction of the radical cation of this basic biomolecular building block with a hydrophobic environment.

Figure 1. *Structure of the calculated monomers and dimers, as evaluated at the UMP2/6-311G(2df,2pd) level: **a** Im$^{(+)}$; **b** interatomic distances for Im (top) and for Im$^+$ (bottom); **c** atomic charges derived by AIM for Im (top) and for Im$^+$ (bottom); **d** Im$^+\cdots$Ar(H); **e** Im$^+\cdots$N$_2$(H); **f** Im$^+\cdots$Ar(π); **g** Im$^+\cdots$N$_2$(π); **h** the most stable Im$^+\cdots$N$_2$(CH).*
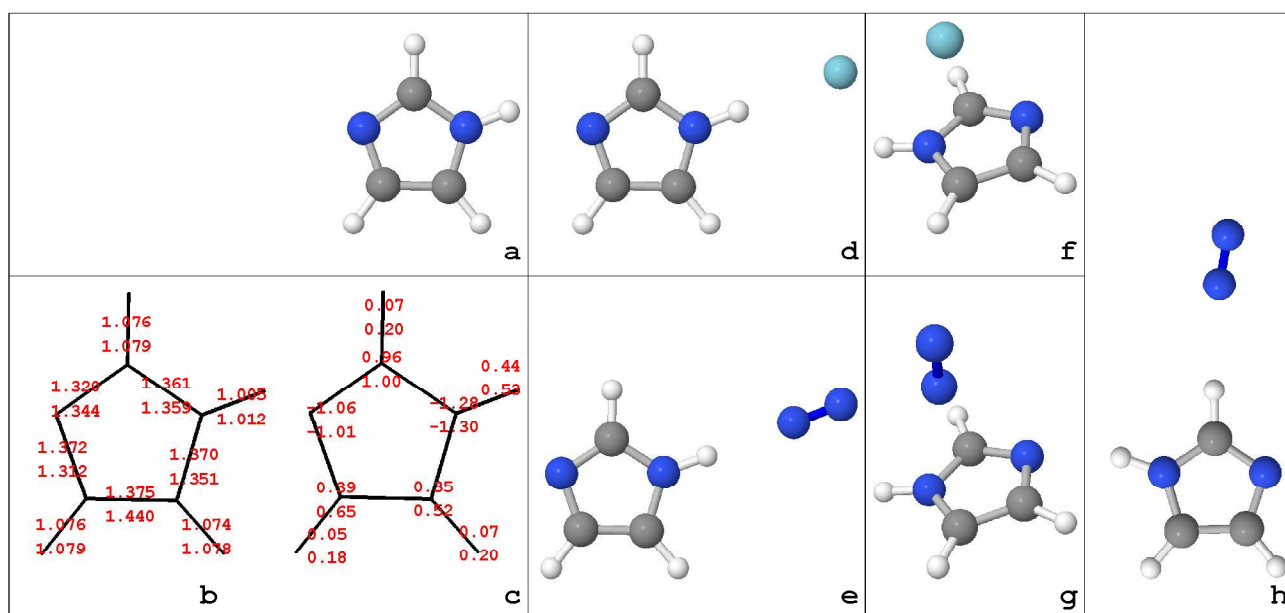
The interaction of the Im$^{(+)}$ with solvent molecules takes place via well-defined families of binding sites: ligand molecules can interact with the π-electron system of the aromatic ring (π-bond), form H-bonds to the acidic protons of Im (N-H$\cdots$L or C-H$\cdots$L), or serve as a proton donor in a H-bond to the basic N atom of Im. The preferred binding motif of the Im$^{(+)}\cdots$L interaction strongly depends on whether Im is in its neutral or cation form as well as on fundamental properties of L, such as its polarity and proton donor and proton acceptor abilities.

While related aromatic complexes have been extensively studied via resonant multiphoton excitation schemes (because of their cluster size, state, and isomer selectivity)[5],[9],[10],[11], relatively few gas-phase spectroscopic data exist for Im$\cdots$L complexes. One reason might be that the high excitation energy of the first excited singlet

state of $Im^{[12]}$ is rather inconvenient for the application of resonant multiphoton excitation schemes. The experimental results from the literature are summarized below.

A rotational millimeter wave spectrum of neutral $Im \cdots Ar$ has been previously recorded in a supersonic jet and is consistent with a π-bound equilibrium structure.[13] The characteristic parameters of this structure are: $Ar \cdots ring$ separation $R \cong 3.48$ Å; intermolecular stretch frequency $v_s = 44\ cm^{-1}$; force constant $k_s = 2.88\ N/m$, and dissociation energy $D_0 \cong 302\ cm^{-1}$. Apparently, Im prefers π-bonding to nonpolar ligands in its singlet electronic ground state (S_0, $^1A'$), because in this configuration the dispersion interaction between L and the π-electron system of Im is maximized. No information appears to be available for the corresponding $Im \cdots N_2$ dimer. The quadrupolar N_2 ligand is known for its ability to form both H-bonds and π-bonds to acidic aromatic molecules. For example, complexes of N_2 with aniline $(An)^{[14]}$ and 1-naphthol $(1\text{-}Np)^{[15]}$ feature π-bound equilibrium structures, whereas that with phenol $(Ph)^{[16],[17]}$ prefers H-bonding. The biologically relevant $Im \cdots H_2O$ interaction has been studied via both quantum chemical calculations and Ar matrix isolation IR spectroscopy[18]. The major competing interaction motifs identified are: $N\text{-}H \cdots O$ H-bonding between the acidic NH group of Im (proton donor) and the O atom of H_2O (proton acceptor) and $O\text{-}H \cdots N$ H-bonding between the acidic OH group of H_2O (proton donor) and the basic N atom of Im (proton acceptor).[18],[19],[20] These H-bonds are mainly stabilized by electrostatic and induction forces. $C\text{-}H \cdots O$ H-bonding of H_2O to the less acidic CH groups of Im and the bonding between Im and H_2O via the π-electron system on one side and a proton of H_2O on the other side are predicted to be less stable than both N-H-O-type contacts.[21]

Experimental and theoretical information about the Im^+ radical cation and its complexes with neutral ligands is rather sparse. Early photoelectron, photoionization, and photofragmentation studies demonstrated that the planar $^2A''$ electronic ground state of Im^+ (D_0) is obtained by removal of one electron from the $3a''$ orbital, which is a bonding π orbital delocalized over the whole aromatic ring.[22],[23],[24] The photoelectron spectrum[23] yielded two ring vibrations, with frequencies of $970\ cm^{-1}$ and $1320\ cm^{-1}$, but no spectroscopic information is available for the N-H and C-H stretch vibrations of Im^+. Recent low-level and rather simplistic calculations have investigated the structures, vibrational frequencies, IR intensities, and charge distributions of Im and its radical cation, as well as various intermolecular binding motifs of the $[Im \cdots Im]^+$ dimer.[25] Neither mass spectrometric nor spectroscopic data seem to be available for any $Im^+ \cdots L_n$ complex. Hence, the present spectra of $Im^+ \cdots Ar$ and $Im^+ \cdots (N_2)_n$ (n = 1...3) provide the first spectroscopic information

about the structure and stability of $Im^+\cdots L_n$ clusters.

Ionization of Im is expected to have a large impact on the topology of the intermolecular interaction with both polar and nonpolar ligands, because the excess charge provides additional electrostatic and inductive contributions to the intermolecular attraction.[9],[26],[27] The large difference between the ionization energy (IE) of Im (9.91 eV)[28] and the IE of Ar (15.76 eV)[28] or N_2 (15.58 eV)[28] implies that the positive charge in $[Im\cdots Ar_n]^+$ and $[Im\cdots(N_2)_n]^+$ will be strongly localized on Im. Thus, the complexes are properly described as weakly bound noncovalent complexes - $Im^+\cdots L_n$ (L = Ar, N_2). Given the charge localization, these complexes are mainly stabilized by induction and electrostatic forces, whereas contributions from charge transfer to the interaction are negligible.

It is known that acidic aromatic molecules A are interacting with rare gas (Rg) atoms and with nonpolar molecules (e.g., CH_4 and N_2) mainly via the π-electron system. It is remarkable that often the interaction motif switches to H-bonding upon ionization.[27] This $\pi \rightarrow$ H switch was only recently observed for a variety of A$\cdots$L dimers, including Ph$\cdots$L (L = Rg, CH_4), An$\cdots$L (L = Ar, N_2), 1-Np$\cdots$Ar, and In$\cdots$Ar, suggesting that is a general phenomenon for this type of complexes.[27] The explanation of this ionization-induced π-bonding $\rightarrow$ H-bonding switch relies on the fact that while in the neutral A$\cdots$L dimers the attraction is dominated by dispersion forces (which favor π-bonding), in the cation $A^+\cdots$L dimers the major contribution to the attraction is provided by induction forces, leading to a strong affinity for H-bonding.[27] On the other hand, dimers of nonacidic aromatic molecules with nonpolar L (such as Bz$\cdots$L) feature π-bound equilibrium structures in both the neutral and the cation ground electronic states, because the aromatic CH groups are not sufficiently acidic to make H-bonding more stable than π-bonding. On the basis of these considerations, both $Im^+\cdots$L dimers investigated in the present work (L = Ar, N_2) are expected to exhibit H-bound global minima, in which L binds to the acidic NH group, and π-bound local minima.

As Im represents a well-defined building block of various biologically relevant molecules, the present IR spectroscopic and theoretical study on size-selected $Im^+\cdots L_n$ complexes (L = Ar, N_2, $n \leq 3$) offers the chance of developing a model for the solvation of biomolecules by nonpolar, and later on, polar environments. It is expected that the microsolvation of the highly acidic Im^+ cation in a nonpolar solvent will underline the way the competition between H-bonding and π-bonding drives the complexation sequence. As the ability of the NH group to form H-bonds to a ligand is correlated with its acidity, the IR

spectra of H-bound $Im^+\cdots L$ dimers directly probe the acidity of Im^+ and eventually enable a first estimate of the unknown proton affinity of the imidazyl radical. Similarly, the IR spectra of $Im^+\cdots L_n$ provided the first experimental information about the strength of the CH groups in Im^+. Comparison of $Im\cdots L$ with $Im^+\cdots L$ and $ImH^+\cdots L$ will reveal the effects of both ionization and protonation of Im on the acidity of the NH protons and the interaction with a nonpolar environment.

5.2. Quantum chemical calculations

Although calculations for Im have been reported, the literature seems to lack information regarding $Im^+\cdots L$ (L = Ar, N_2) dimers, which are of paramount importance for explaining the properties of the Im cation. This fact has prompted the rather extensive study reported here.

Ab initio methods are known to reliably describe the properties of both the π-bonds and the H-bonds between small aromatic molecules and nonpolar or polar ligands $(A^+\cdots L)$.[29] For this reason, the level of theory chosen here for characterizing the effects of both ionization and complexation on the properties of Im is UMP2. In order to facilitate comparisons between the present study and previously investigated systems $(Ph^+\cdots L,$[29] $In^+\cdots L,$[30] $An^+\cdots L,$[31],[32] and $1\text{-}Np^+\cdots L),$[33] the same set of calculations were carried out using UB3LYP. Density functional theory (UB3LYP) is far less computationally expensive than the ab initio approach, but it is able to properly describe only the H-bonded systems. It fails to properly account for the dispersion interactions, which are significant for π-bonding in $A^+\cdots L$ dimers. Thus, calculations for Im, Im^+, and several $Im^+\cdots L$ dimers (L = Ar, N_2) have been carried out at both UMP2/6-311G(2df,2pd) and UB3LYP/6-311G(2df,2pd) levels of theory using the Gaussian 03 quantum chemistry package[34]; unless specified, all the calculated numbers presented below are the ones derived at the UMP2 level.

The stationary points were identified via fully relaxed scans; the intermolecular interactions were counterpoise corrected for basis set superposition error (BSSE);[35],[36] the intermolecular interaction energies were also adjusted to properly account for zero-point vibrational energy. The equilibrium geometries are depicted in Figure 1; all the geometrical and energetical parameters relevant for the present work are summarized in Table 1, which contains:

* intramolecular N-H and C-H bond lengths (r_{NH}, r_{CH}), the corresponding stretch frequencies (v_{NH}, v_{CH}), and their IR intensities (I_{NH}, I_{CH})

* intermolecular bond length (r_{HL} or r_{ring-L}), stretch frequency (v_s) and its IR intensity (I_s), and

Table 1. *Properties of the intramolecular N-H and C-H bonds (r_{HL}, r_{CH}, v_{NH}, v_{CH}, I_{NH}, I_{CH}) and the intermolecular bonds (r_{HL}, r_{ring-L}, D_0, v_s) for the equilibrium structures of Im, Im⁺, and several Im⁺···L isomers calculated at the UMP2/6-311G(2df,2pd) and UB3LYP/6-311G(2df,2pd) levels. Harmonic frequencies were scaled down by 0.9466 (UMP2) and 0.9600 (UB3LYP).*

complex	r_{NH} (Å)	r_{CH} (Å) 6	7	9	v_{NH} cm⁻¹ (I_{NH}) (km/mol)	v_{CH6} cm⁻¹ (I_{CH6}) (km/mol)	v_{CH7} cm⁻¹ (I_{CH7}) (km/mol)	v_{CH9} cm⁻¹ (I_{CH9}) (km/mol)	r_{HL} r_{ring-L} (Å)	D_0 (cm⁻¹)	v_s cm⁻¹ (I_s) (km/mol)
					MP2/6-311G(2df,2pd)						
Im	1.0045	1.0742	1.0758	1.0755	3505 (74)	3120 (3)	3147 (1)	3126 (0)			
Im⁺	1.0118	1.0775	1.0793	1.0787	3431 (231)	3119 (25)	3136 (16)	3125 (36)			
Im⁺···Ar (H)	1.0147	1.0774	1.0793	1.0786	**3374 (561)**	3119 (23)	3136 (14)	3126 (34)	2.41	554	66 (11)
Im⁺···N₂ (H)	1.0191	1.0774	1.0792	1.0786	**3302 (818)**	3119 (21)	3136 (12)	3126 (35)	2.05	1562	106 (14)
Im⁺···Ar (π)	1.0117	1.0774	1.0793	1.0786	3433 (227)	3119 (24)	3136 (16)	3126 (35)	3.42	388	53 (14)
Im⁺···N₂ (π)	1.0114	1.0773	1.0792	1.0786	3436 (224)	3119 (22)	3137 (16)	3127 (33)	3.12	888	75 (12)
Im⁺···N₂ (CH6)	1.0799	**1.0799**	1.0774	1.0793	3433 (232)	**3108 (93)**	3135 (21)	3125 (29)	2.42	701	66 (9)
Im⁺···N₂ (CH7)	1.0795	1.0786	**1.0786**	1.0792	3434 (223)	3121 (40)	**3105 (142)**	3129 (1)	2.37	858	73 (9)
Im⁺···N₂ (CH9)	1.0811	1.0786	1.0786	**1.0811**	3434 (223)	3121 (21)	3136 (20)	**3102 (126)**	2.35	872	73 (10)
					B3LYP/6-311G(2df,2pd)						
Im	1.0046	1.0749	1.0775	1.0767	3515 (50)	3111 (7)	3142 (2)	3114 (0)			
Im⁺	1.0131	1.0792	1.0799	1.0797	3431 (209)	3110 (21)	3124 (7)	3117 (45)			
Im⁺···Ar (H)	1.0166	1.0791	1.0797	1.0796	**3363 (547)**	3111 (21)	3125 (3)	3119 (45)	2.47	454	58 (11)
Im⁺···N₂ (H)	1.0212	1.0790	1.0796	1.0796	**3288 (833)**	3111 (20)	3125 (4)	3119 (40)	2.08	1362	102 (14)
Im⁺···N₂ (CH6)	1.0129	**1.0811**	1.0791	1.0798	3433 (210)	**3095 (92)**	3124 (9)	3118 (43)	2.46	531	62 (9)
Im⁺···N₂ (CH7)	1.0128	1.0796	**1.0815**	1.0798	3434 (199)	3113 (26)	**3088 (157)**	3121 (8)	2.39	706	70 (9)
Im⁺···N₂ (CH9)	1.0128	1.0796	1.0791	**1.0819**	3434 (201)	3110 (20)	3124 (17)	**3093 (137)**	2.39	656	69 (10)

102

dimer dissociation energy (D_0, ZPE-corrected).

The values marked with bold characters correspond to the intramolecular bonds affected by ligand binding. Harmonic vibrational frequencies were scaled down by 0.9466 (0.9600 for UB3LYP) to match the calculated N-H stretch frequencies of Im^+ with the experimental one estimated from the IRPD spectrum of $Im^+\cdots Ar$ (vide infra, $\nu_{NH} = 3431$ cm^{-1}). For the monomers and H-bound dimers, the UMP2 and UB3LYP calculations yield similar energetic, structural, and vibrational data; for the π-bound dimers only the UMP2 data are considered.

5.2.1. Monomers

Geometry optimization in the ground electronic state of both Im ($^1A''$, S_0) and Im^+ ($^2A''$, D_0) results in planar equilibrium structures with C_s symmetry. The effect of the ionization can be seen in Figure 1b, which compares the intramolecular bonds of the S_0 and D_0 states. Previous experiments are showing that the ionization of Im removes an electron from the bonding 3a'' molecular orbital, which is delocalized over the aromatic ring.[23] As a consequence, the ring shrinks slightly up upon ionization (see Figure 1b), giving rise to Franck-Condon activity in the two symmetric ring stretch modes observed in the He(I) photoelectron spectra.[23] Simultaneously, the N-H and all three C-H bonds become weaker and longer, inducing shifts in the corresponding stretch frequencies of -1 cm^{-1} > $\Delta\nu_{CH}$ > -12 cm^{-1} and $\Delta\nu_{NH} = -74$ cm^{-1}, respectively. The N-H stretch normal mode is essentially localized on the N-H bond, whereas the C-H stretch normal modes are largely delocalized over all three C-H bonds, resulting in similar C-H stretch frequencies. The scaled ν_{NH} and ν_{CH} frequencies calculated for neutral Im show deviations of less than 15 cm^{-1} (26 cm^{-1} for UB3LYP) from the measured values ($\nu_{NH} = 3518$ cm^{-1}, $\nu_{CH} = 3160$ cm^{-1}, 3135 cm^{-1}, and 3135 cm^{-1}),[37] demonstrating that the chosen theoretical levels appropriately describe the monomer properties. Atoms-in-molecules (AIM) analyses have been performed for both Im and Im^+ in order to get a glimpse of the charge distribution around the molecule (Figure 1c). In general, the AIM analyses yielded charge distributions which are very different from those obtained via Mulliken population analysis. The Mulliken approach is, however, known to be very sensitive to the theoretical level, whereas the AIM method provides reliable and level-independent charge distributions.[38] Hence, the Mulliken charges are not considered further. Comparison of the AIM population analyses reveals that the additional positive charge is mainly distributed over the two neighboring ring C atoms and the four protons. This increase of the positive charge around the protons strongly enhances the IR activities of all ν_{CH} and ν_{NH} fundamentals.

5.2.2. NH-bound dimers

The intermolecular $Im^{+}\cdots L$ H-bound dimers (which will further be denoted $Im^{+}\cdots L(H)$) feature planar - C_s symmetry - optimum geometries. The intermolecular $H\cdots L$ bonds are nearly aligned with the N-H bonds, the deviation of $\theta_{N-H\cdots L}$ from linearity being in each case smaller than 0.5° (see Figure 1d and Figure 1e). In the case of the $Im^{+}\cdots N_2(H)$ dimer this nearly linear configuration extends also for $\theta_{H\cdots N\equiv N}$; responsible for this is the anisotropy of the long-range charge-quadrupole and charge-induced dipole interactions which are maximized when the N_2 ligand aligns in such a way that the diatomic axis points toward the positive charge. The intermolecular bond is shorter for $Im^{+}\cdots N_2$ than for $Im^{+}\cdots Ar$ (r_{HAr} = 2.41 Å and r_{HN2} = 2.05 Å) because of the larger parallel polarizability of N_2 versus Ar (2.38 $Å^3$ versus 1.64 $Å^3$) and its additional quadrupole moment (-5.00 $C\cdot m^2$)[39],[40],[41] which lead to a stronger induction and electrostatic attraction in the complexes having N_2 as ligand. Not only r_{HL} is affected, but also the intermolecular stretch frequency goes up from v_s = 66 cm^{-1} for $Im^{+}\cdots Ar$ to v_s = 106 cm^{-1} for $Im^{+}\cdots N_2$. Of course, the dissociation energy is affected in a similar fashion: D_0 = 554 cm^{-1} for $Im^{+}\cdots Ar(H)$ to D_0 = 1561 cm^{-1} for $Im^{+}\cdots N_2(H)$. The ligands are pulling the proton to which they bind away from the molecular body; in the present case the N-H intramolecular bond expands by Δr_{NH} = 0.0029 Å for $Im^{+}\cdots Ar(H)$ and Δr_{NH} = 0.0073 Å for $Im^{+}\cdots N_2(H)$. This bond elongation implies a weakening of the potential "seen" by the proton, red-shifting the stretch vibration and, at the same time, greatly enhancing the corresponding IR oscillator strength: Δv_{NH} = -57 cm^{-1} & $\Delta I_{NH} \cong 140\%$ for $Im^{+}\cdots Ar(H)$ and Δv_{NH} = -129 cm^{-1} & $\Delta I_{NH} \cong 250\%$ for $Im^{+}\cdots N_2(H)$. As all these parameters are correlated with the strength of the intermolecular H-bond it results that IR spectroscopy in the N-H stretch range may be a suitable tool to probe the acidity of the NH group in Im^{+} and its ability to form H-bonds.

5.2.3. π-bound dimers

In addition to the H-bound global minima, the intermolecular $Im^{+}\cdots L$ potential energy surfaces possess less stable minima located roughly above the center of the ring. The configurations resulting from the attachement of the ligand to these sites are shown in Figure 1f and Figure 1g and will be denoted $Im^{+}\cdots L(\pi)$. The N_2 ligand in $Im^{+}\cdots N_2(\pi)$ is sitting nearly perpendicular to the ring plane, slightly pointing toward the atom known to hold the maximum partial positive charge. Similar to the H-bond in $Im^{+}\cdots L(H)$, the intermolecular π-bonding of N_2 to Im^{+} yields a complex which is more stable than the corresponding

$Im^+ \cdots Ar(\pi)$, as demonstrated by the ring$\cdots$ligand separation ($r_{ring-N2}$ = 3.15 Å < $r_{ring-Ar}$ = 3.43 Å), the larger intermolecular stretch frequency (v_s = 75 cm^{-1} for $Im^+ \cdots N_2(\pi)$ > v_s = 53 cm^{-1} for $Im^+ \cdots Ar(\pi)$), and the higher dissociation energy (D_0 = 888 cm^{-1} for $Im^+ \cdots N_2(\pi)$ > D_0 = 388 cm^{-1} for $Im^+ \cdots Ar(\pi)$). Intermolecular π-bonding has only modest effects on the properties of the N-H and the C-H bonds of Im^+, with $|\Delta r_{NH}|$ < 0.0004 Å, $|\Delta r_{CH}|$ < 0.0002 Å, $\Delta v_{NH} \leq$ 5 cm^{-1}, $\Delta v_{CH} \leq$ 2 cm^{-1}, ΔI_{NH} < 5%, and ΔI_{CH} < 17%. As expected, the UB3LYP calculations fail to reliably describe the π-bonds in $Im^+ \cdots L(\pi)$. They yield equilibrium structures in which the ligands are largely displaced from the center of the aromatic ring toward the C-C bond. Moreover, the dissociation energies are much lower than those obtained at the UMP2 level.
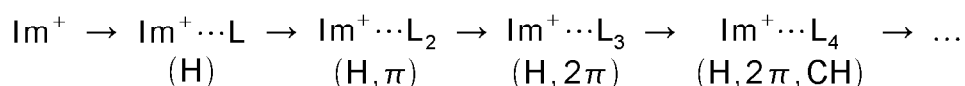
5.2.4. CH-bound dimers

H-bonding of L to the aromatic CH groups yields further local minima on the $Im^+ \cdots L$ potentials, denoted $Im^+ \cdots L(CH)$ (see Table 1). For the present work only the $Im^+ \cdots N_2(CH)$ dimers have been optimized; out of the three computed dimers, only one (Figure 1h) will be discussed in detail. The criterion for selecting this specific isomer is its stability (D_0 = 872 cm^{-1} > 858 cm^{-1} > 701 cm^{-1}) which is correlated with the highest positive partial charge on the corresponding CH proton (q_H = 0.21e > 0.20e > 0.18e). An important detail which results from this evaluation of the binding energies is that this most stable $Im^+ \cdots N_2(CH)$ dimer is marginally less stable than $Im^+ \cdots N_2(\pi)$. Consequently, the H-bonds to the CH groups are significantly less stable than the H-bond to the NH group. This result is consistent with the larger acidity of the NH group and the larger positive partial charge on the corresponding proton (q_H = 0.53 e). Significantly, the unambiguous spectroscopic signature of the $Im^+ \cdots N_2(CH)$ isomers is the small but noticeable red-shift in the frequency ($\leq$ -23 cm^{-1}) and the strong enhancement in the IR intensity (by a factor of 3.5) of the stretch vibration of the CH group acting as the proton donor (Table 1).

The large negative partial charge at the nonprotonated N atom of Im^+, q_N = -1.01 e, suggests that this binding site may also be attractive for neutral ligands. Two test calculations have been carried out at the UB3LYP level, with starting geometries placing the N_2 ligand with the center of the N≡N bond in front of the nonprotonated N atom of Im^+. In the first case the geometry of the complex was selected planar and the optimized structure was a $Im^+ \cdots N_2(CH)$ dimer. In the second attempt the ligand was placed perpendicular to the Im^+ plane; the optimization stopped in a saddle point of fourth order. The explanation is that there is a significant Pauli repulsion resulting from the lone pair at the nonprotonated N atom which prevents this position from being a favorable binding site

in $Im^+\cdots L$ dimers. In contrast, H-bonds to the acidic protons of Im^+ are advantageous binding motifs, because of the significant positive partial charges on these protons and the resulting reduced Pauli repulsion, which allows for a closer approach of L.

Thus, according to the calculations, the H-bonds to the NH group in $Im^+\cdots L$ are more stable than the π-bonds, which in turn are (slightly) more stable than the H-bonds to the CH groups. Assuming that each only π-binding site can accomodate only one ligand and considering the dimer stability order mentioned above, one can predict that the strongest bound $Im^+\cdots L_n$ clusters are the ones growing sequentially along the line:

$$Im^+ \rightarrow \underset{(H)}{Im^+\cdots L} \rightarrow \underset{(H,\pi)}{Im^+\cdots L_2} \rightarrow \underset{(H,2\pi)}{Im^+\cdots L_3} \rightarrow \underset{(H,2\pi,CH)}{Im^+\cdots L_4} \rightarrow \ldots$$

5.3. Experimetal details

IRPD spectra of mass-selected $Im^+\cdots L_n$ complexes (L = Ar, N_2, n ≤ 3) were recorded over the N-H and C-H stretch ranges using the QOQ tandem mass spectrometer coupled to the electron impact ion source (EI + QMF1 + OP + QMF2) described in the experimental section of this work. Only the details specific to the $Im^+\cdots L_n$ experiment are presented here. The expanding gas mixture was produced by seeding Im vapor (T ≅ 370 K) in the flow of the ligand / buffer gas (Ar or N_2 at static pressures of 4...5 bar). $Im^+\cdots L_n$ clusters were produced by EI of Im and subsequent three-body association reactions in the high pressure region of the expansion:[29],[30],[31],[32],[42]

$$Im + e^- \rightarrow Im^+ + 2\cdot e^- \tag{1}$$

$$Im^+\cdots L_{n-1} + L + M \rightarrow Im^+\cdots L_n + M \qquad M = L, Im \tag{2}$$

Previous experiments of small (substituted and / or protonated) arenes are showing that this reaction sequence produces the most stable $A(H)^+\cdots L_n$ complexes and to smaller extent less stable isomers.[27] Alternative mechanisms involve the formation of neutral $Im\cdots L_n$ complexes and their subsequent electron impact ionization or the formation of a neutral L_n cluster followed by its attachment to a Im^+ cation. These mechanisms are known to play only a minor role in the formation of complexes in the ion source used here.[42]

Figure 2 shows a mass spectrum of the ion source recorded after optimization for $Im^+\cdots(N_2)_n$ generation. The spectrum is dominated by N_n^+ and $X^+\cdots(N_2)_n$ cluster ions, with X^+ being either Im^+, ImH^+, or H_2O^+; here H_2O is a contaminant coming from the gas lines or the gas bottle. Im can fragment upon EI, resulting in a sequence of fragments out of which
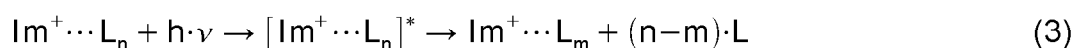
the strongest visible in the recorded mass spectrum corresponds to HCN loss,[43] leading to CH_2CNH^+ (41 u); a somewhat weaker fragment channel produces $HCNH^+$ (28 u), but the corresponding signal is masked by the very intense N_2^+ peak. The intensity ratios of $Im^+\cdots(N_2)_n$ are on the order of $50:2.5:2:1$ for $n = 0...3$, confirming the formation of weakly bound noncovalent complexes.

Figure 2. *Mass spectrum of the EI ion source output, obtained after optimization for $Im^+\cdots(N_2)_n$ generation; carrier gas was N_2 at 4 bar stagnation pressure; the Im sample was heated at $\cong 370$ K.* ▼ *marks the sequence of $Im^+\cdots(N_2)_n$ (68 + n·28 u) as well as the neighbouring $ImH^+\cdots(N_2)_n$ (69 + n·28 u). Other easily identifiable sequences are N_n^+ (▼) and $H_2O^+\cdots(N_2)_n$ (▼), H_2O being a contaminant coming from the gas system. The peaks marked* ▼ *show the presence of $Im_2H^+(\cdots N_2)$. The inset shows a vertically expanded version of the spectrum (X25) to ease the identification of weak peaks.*
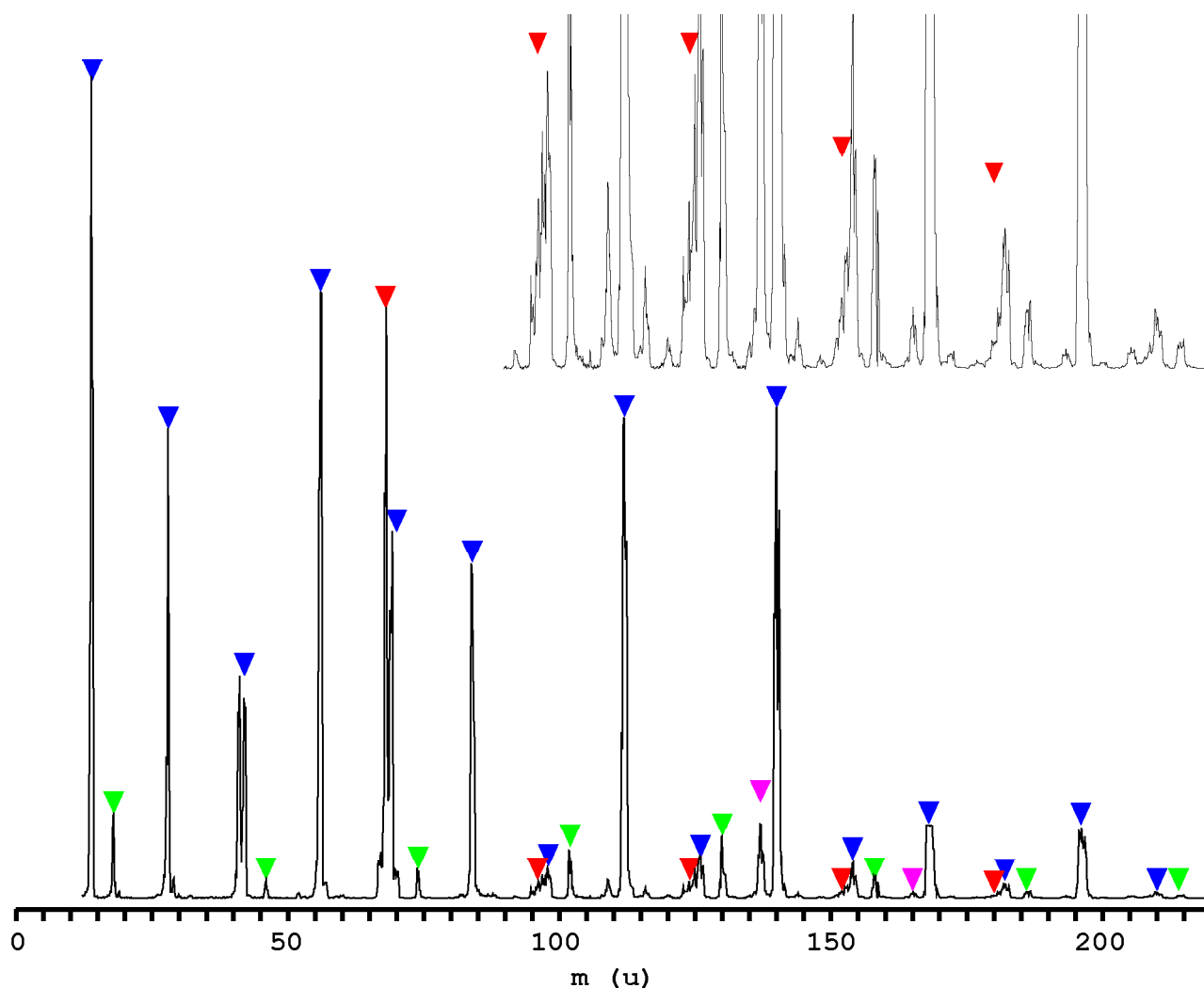
The IR spectra of $Im^+\cdots L_n$ are obtained by monitoring the amount of $Im^+\cdots L_m$ fragments generated in the octopole by the absorption of the IR laser beam by $Im^+\cdots L_n$ as

a function of the wavelength of the excitation IR laser:

$$\mathrm{Im}^+ \cdots \mathrm{L}_n + h \cdot v \rightarrow [\mathrm{Im}^+ \cdots \mathrm{L}_n]^* \rightarrow \mathrm{Im}^+ \cdots \mathrm{L}_m + (n-m) \cdot \mathrm{L} \qquad (3)$$

As the energy density of the excitation laser beam was too low ($I < 200$ kW/cm^2) for multiple photon absorption to occur, no other photodissociation channels were observed. For $\mathrm{Im}^+ \cdots (\mathrm{N}_2)_n$ parent complexes with $n > 1$, several fragment channels m were observed.

As an example, Figure 3 compares the mass spectra obtained for mass selecting $\mathrm{Im}^+ \cdots (\mathrm{N}_2)_2$ with QMF1 and scanning QMF2 without laser operation (lower part) and with resonant laser excitation (upper part). With the laser switched off, the mass spectrum displays $m = 0$ and 1 fragment ions arising from metastable decay (MD) of hot parent clusters and / or collision-induced dissociation (CID) with background gas in the octopole region. The small fraction of MD demonstrates that the $\mathrm{Im}^+ \cdots (\mathrm{N}_2)_2$ complexes reaching the octopole region have, in average, little internal energy. When the laser beam is resonantly exciting a vibration of the $\mathrm{Im}^+ \cdots (\mathrm{N}_2)_2$ complex, the mass spectrum reveals additional fragmentation into both the $m = 0$ (83%) and $m = 1$ (17%) fragment channels caused by resonant laser-induced dissociation (LID). Previous studies on related complexes demonstrated that the IR spectra recorded in the major fragment channels are similar.[30],[31],[33],[42] Consequently, IRPD spectra of $\mathrm{Im}^+ \cdots \mathrm{L}_n$ were recorded only in the dominant fragment channel.

Figure 3. *Mass spectra obtained by mass-selecting Im$^+$···(N$_2$)$_2$ with QMF1 and scanning QMF2. The lower trace was recorded without laser operation and the observed Im$^+$···(N$_2$)$_m$ fragment ions arise from metastable decay and / or collision-induced dissociation with background gas. The upper trace was recorded during excitation of the v_{NH} stretch vibration of Im$^+$···(N$_2$)$_2$ (3313 cm^{-1}) which induces additional fragmentation into both fragment channels.*
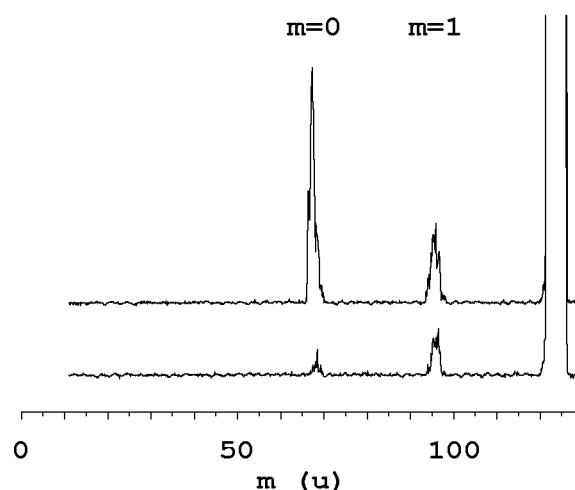

Calibration of the laser frequency to an accuracy of better than 1 cm^{-1} was accomplished by comparison of the optoacoustic spectra of NH_3 recorded simultaneously with the IRPD spectra with literature tables and by analyzing the atmospheric water

absorptions along the IR laser path.[44],[45]

5.4. Results and discussion

The IRPD spectra of $Im^+\cdots Ar$ and $Im^+\cdots(N_2)_n$ (n = 1...3) recorded over the C-H and N-H stretch ranges are shown in Figure 4. A list of band origins, their full width half maxima (FWHM) as well as their vibrational and isomeric assignments is presented in Table 2. The assigned ν_{NH} frequencies of the most stable isomers of all $Im^+\cdots L_n$ clusters investigated are plotted in Figure 6 as a function of the cluster size n.

Figure 4. *IRPD spectra of $Im^+\cdots Ar$ and $Im^+\cdots(N_2)_n$ (n = 1...3) recorded over the N-H and C-H stretch ranges in the Im^+ fragment channel. The vibrational and isomer assignments of the transition observed (A, B, C) are listed in Table 2.*
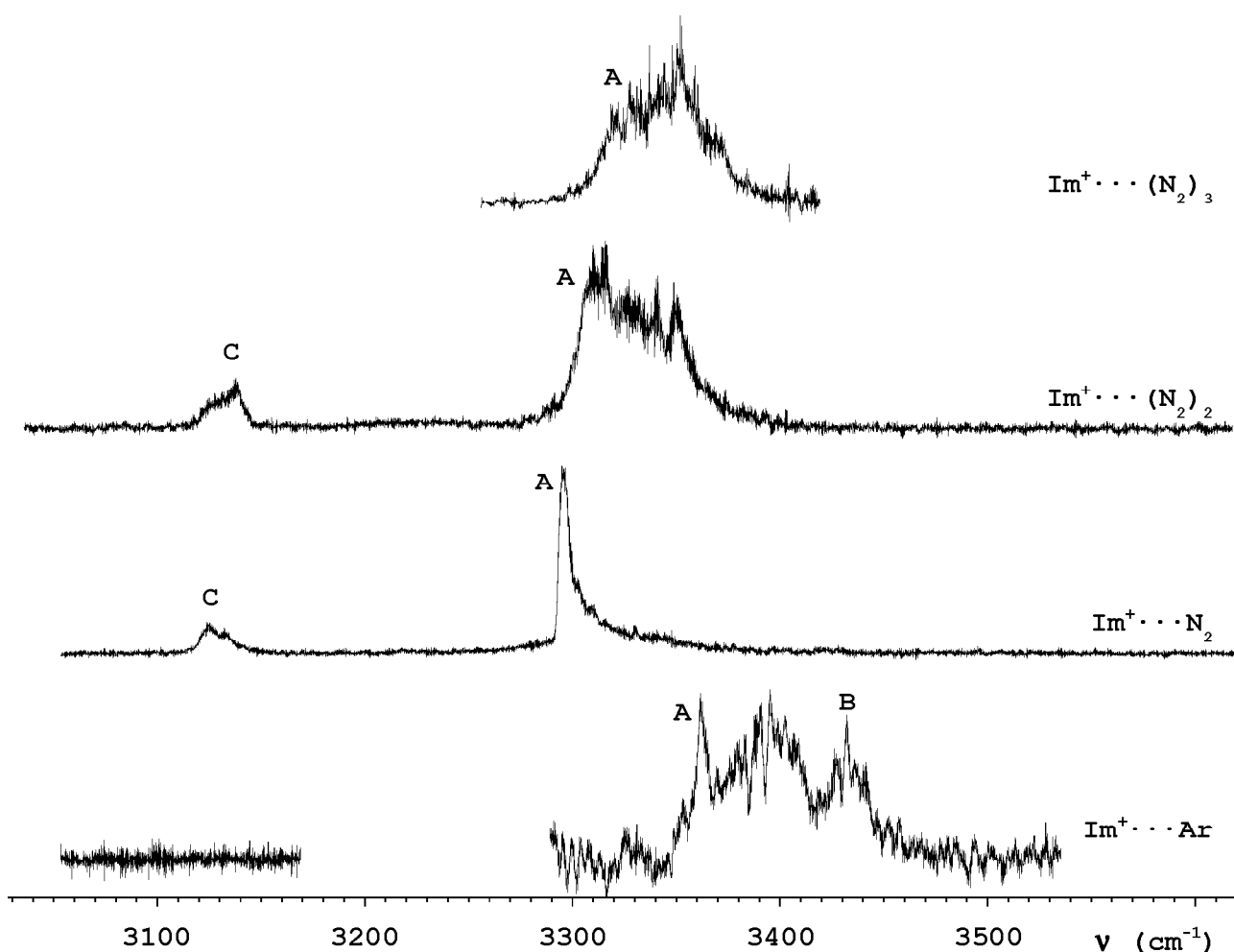
To assign the vibrational bands observed in the IRPD spectra of the $Im^+\cdots L_n$ clusters, it is instructive to consider the frequencies of the N-H and C-H stretch fundamentals of the

isolated Im^+ chromophore. As ν_{NH} and ν_{CH} of bare Im^+ have not been measured yet, one has to rely on approximations based on the calculations. One such way for obtaining an estimation of ν_{NH} and ν_{CH} relies on the experimental frequencies of neutral Im (ν_{NH} = 3518 cm^{-1} and ν_{CH} = 3160 cm^{-1}, 3135 cm^{-1}, and 3135 cm^{-1})[37] and on the calculations done for Im and for Im^+. The calculated harmonic vibrations of Im^+ are to be scaled using the average correction factor resulting from the calculations on Im. At the UMP2 level, this factor is found to be 0.9503 and the estimated frequencies of Im^+ are: ν_{NH} = 3444 cm^{-1} and ν_{CH} = 3149 cm^{-1}, 3134 cm^{-1}, and 3134 cm^{-1}. At the UB3LYP level the scaling factor is 0.9651, yielding for Im^+ the following estimated frequencies: ν_{NH} = 3449 cm^{-1} and ν_{CH} = 3141 cm^{-1}, 3134 cm^{-1}, and 3127 cm^{-1}. Another approach, this time useful only for estimating ν_{NH} of Im^+, employs the measured frequency of the related heterocyclic In^+ cation (ν_{NH} = 3454 cm^{-1})[46] and the ratio of the harmonic frequencies of In^+ and Im^+ (ω_{NH} =3609 cm^{-1} and 3574 cm^{-1}) evaluated at the UB3LYP level; this route yields ν_{NH} = 3421 cm^{-1} for Im^+, in good agreement with the values estimated from the first approach. As both methods can be considered equally reliable, one can use the average of these three evaluation: $\bar{\nu}_{NH}$ = 3438 cm^{-1}.

Table 2. *Band origins and widths (FWHM, in parentheses) of the transitions observed in the IRPD spectra of $Im^+ \cdots L_n$, along with their vibrational and isomer assignments. For the strongly asymmetric ν_{NH} band of the H-bound isomers (band A), the given position corresponds to the maximum of the P branch head which occurs close to the band origin. For the symmetric bands B and C, the band centers are listed. (H/xπ) denotes an isomer with one H-bound and x π-bound ligands (1 + x = n).*

ν (cm^{-1})	band	vibration	isomer
3361 (52)	A	ν_{NH}	$Im^+ \cdots Ar$ (H)
3433 (16)	B	ν_{NH}	$Im^+ \cdots Ar$ (π)
3295 (6)	A	ν_{NH}	$Im^+ \cdots N_2$ (H)
3128 (16)	C	ν_{CH}	$Im^+ \cdots N_2$ (H)
3313 (54)	A	ν_{NH}	$Im^+ \cdots (N_2)_2$ (H/π)
3132 (20)	C	ν_{CH}	$Im^+ \cdots (N_2)_2$ (H/π)
3323 (60)	A	ν_{NH}	$Im^+ \cdots (N_2)_3$ (H/2π)

5.4.1. The $Im^+ \cdots Ar$ dimer

The IRPD spectrum of $Im^+ \cdots Ar$ in Figure 4 displays a rather broad but structured absorption in the N-H stretch range. Two transitions are identified and assigned to the ν_{NH} fundamentals of the H-bound and π-bound isomers of $Im^+ \cdots Ar$. Their assignments are based on the band positions, relative IR intensities, and band profiles, as well as the comparison with the calculations.

It is known that intermolecular π-bonding has essentially no influence on the properties of the N-H bond, and vice versa - N-H stretch excitation does not affect the properties of the π-bond. This means that the stretch vibration of a π-bound isomer is expected to occur close to the ν_{NH} frequency predicted for bare Im^+. Band B, centered at 3433 cm^{-1}, is only 5 cm^{-1} away from the $\bar{\nu}_{NH}$ estimated above and exhibits a symmetric band profile. Based on its position and profile,[29] it is assigned to ν_{NH} of the π-bound $Im^+ \cdots Ar$ dimer (Figure 1f). The ratio between the position of band B and the harmonic frequency of the N-H stretch vibration of $Im^+ \cdots Ar(\pi)$ - ω_{NH} - is used as scaling factor (0.9466) for determining the band positions for all studied systems (Table 1). As the harmonic calculations are predicting for ω_{NH} a blue shift of +2 cm^{-1} upon π-bonding with Ar, one can get 3431 cm^{-1} as best estimate for the ν_{NH} of bare Im^+. The advantage of this estimation is that it relies only on the experimental value of ν_{NH} obtained for a closely related system and on calculations done at a level proven to yield meaningful results. This value will further be used for evaluating the experimental complexation-induced frequency shifts, $\Delta\nu_{NH}$, as well as for providing the scaling factor of the UB3LYP calculations (0.9600). It should be noted that, although band B was unequivocally assigned to $Im^+ \cdots Ar(\pi)$, there are several other binding sites from which the ligand has also little impact on the N-H bond. One such category of dimers is $Im^+ \cdots Ar(CH)$. Fortunately however, the calculations described in the previous section suggest that these CH-bonded complexes are less stable than $Im^+ \cdots Ar(\pi)$. This conclusion is further supported by theoretical and spectroscopic data obtained for $BzH^+ \cdots Ar$,[47] $Bz^+ \cdots Ar$,[48] and $PhH^+ \cdots Ar$,[49] which also demonstrated that the intermolecular $CH \cdots Ar$ bonds in $A(H)^+ \cdots Ar$ dimers are less stable than the corresponding $\pi \cdots Ar$ bonds. The width and shape of band B (~16 cm^{-1}) could be reproduced by band contour simulations, using an effective rotational temperature of around 150 K and some realistic approximations. More precisely, it was considered that the transition dipole lies along the N-H bond; the rotational constants (A = 0.160282 cm^{-1}, B = 0.048490 cm^{-1}, C = 0.047647 cm^{-1}) are taken from the UMP2 calculations for $Im^+ \cdots Ar(\pi)$ and are assumed to be the same in both vibrational states.

In addition to the ν_{NH} band of the π-bound dimer (B), the $Im^+\cdots Ar$ spectrum reveals a blue shaded band (A) displaying a sharp head near 3361 cm^{-1} and a rather broad feature around 3400 cm^{-1}. This transition is attributed to ν_{NH} of the H-bound $Im^+\cdots Ar$ isomer shown in Figure 1d. The blue shaded band contour is characteristic for the excitation of a proton donor stretch vibration, because the intermolecular H-bond becomes stronger and shorter in the excited vibrational state, resulting in larger rotational constants.[26] The sharp head of the band is attributed to the P branch, while the "hump" is considered to be part of the R branch. The vibrational band origin of such transitions is placed close to the maximum of the P branch, hence the latter is taken in the present work as an approximate value for the band origin. The red-shift upon complexation amounts to $\Delta\nu_{NH}$ = -69 cm^{-1}, as derived from the evaluated position of ν_{NH} for the bare imidazole cation. The calculation slightly underestimates this red-shift ($\Delta\nu_{NH}$ = -56 cm^{-1}); similarly, previous calculations for the O-H stretch fundamental of the related $Ph^+\cdots Ar(H)$ dimer, conducted at the same level, are yielding a underestimated red-shift ($\Delta\nu_{OH}^{calc}$ = -56 cm^{-1}, $\Delta\nu_{OH}^{exp}$ = -70 cm^{-1}).[50] The UB3LYP level yields a value ($\Delta\nu_{NH}$ = -62 cm^{-1}) in better agreement with the experiment.

The scan over the expected range of the C-H stretch vibrations (3050 cm^{-1} to 3170 cm^{-1}) reveals no detectable absorption. This is probably the result of the rather low signal-to-noise level achived in this spectrum, as the calculations are predicting the IR intensities of all ν_{CH} fundamentals of both $Im^+\cdots Ar(H)$ and $Im^+\cdots Ar(\pi)$ to be roughly one order of magnitude smaller than the IR intensities of the ν_{NH} fundamentals. One of the reasons for the relatively low signal levels in the $Im^+\cdots Ar$ spectrum results from the rather large amounts of $[N_2\cdots Ar_2]^+$ which were produced from the remaining N_2 impurities in the gas inlet system. As this complex has the same mass as the targeted $Im^+\cdots Ar$ (m = 108 u), its MD process ($[N_2\cdots Ar_2]^+ \rightarrow [N_2\cdots Ar]^+ + Ar$) is "swamping" the background of the targeted LID process ($Im^+\cdots Ar \rightarrow Im^+ + Ar$).

The millimeter wave spectrum of neutral $Im\cdots Ar$ has been unequivocally connected to a π-bound structure; as no experimental evidence for the H-bound isomer has been reported so far, this π-bound structure is considered to be the global minimum. By far, in the fundamental electronic state of Im (S_0), the largest part of the attractive intermolecular interaction is the dispersion interaction between Ar and the π-electron system of the aromatic ring. Ionization of $Im\cdots Ar(\pi)$ enhances the attraction by introducing charge-induced dipole forces, which lead to a contraction of the intermolecular bond. This contraction can be checked via a comparison of the potential parameters derived from the millimeter wave spectrum of $Im\cdots Ar$ ($D_0 \cong 302$ cm^{-1}, ν_s = 44 cm^{-1}, $r_{ring-Ar}$ = 3.48 Å) with the

values calculated at UMP2/6-311G(2df,2pd) level for Im···Ar ($D_0 \cong 205$ cm^{-1}, $v_s = 43$ cm^{-1}, $r_{ring-Ar} = 3.54$ Å) and for Im$^+$···Ar ($D_0 = 388$ cm^{-1}, $v_s = 53$ cm^{-1}, $r_{ring-Ar} \cong 3.42$ Å). A similar contraction ($\Delta r_{ring-Ar} = -0.07$ Å) upon ionization has also been derived from the analysis of rotationally resolved spectra of Bz$^{(+)}$···Ar(π). As seen, the IRPD spectrum and the calculated dimers of Im$^+$···Ar clearly demonstrate that the H-bond is the preferred intermolecular recognition site in D_0, because of the induction interaction between the Im$^+$ charge distribution and the polarizability of Ar which is by far stronger than the interaction between Ar and the π-electron system of the cation. Judging by the results of the calculations, it seems that the large positive partial charge on the acidic NH proton is responsible with the stabilization of the H-bond on ionization.

The apparent ionization-induced switch in the preferred recognition motif from π-bonding to H-bonding has recently been demonstrated for several A$^{(+)}$···Ar and A$^{(+)}$···CH$_4$ dimers involving aromatic molecules A$^{(+)}$ with acidic functional YH$_k$ groups (Y = O, N) and appears to be a general phenomenon. The molecules investigated so far are: (para-halogenated) Ph, An, In, 1-Np, and Im. H-bonds to Ar are also the most stable binding pattern for protonated aromatic molecules (AH$^+$) featuring acidic functional groups, such as PhH$^+$, 1-NpH$^+$, and ImH$^+$. The significance of the YH$_k$ groups acidity is underlined by the preference of Ar and CH$_4$ for π-bonding to A(H)$^+$ without acidic substituents, such as Bz(H)$^+$: both the aromatic and aliphatic C-H bonds in A(H)$^+$ are only little acidic, so that dispersion forces favoring π-bonds override the induction forces favoring H-bonds.

5.4.2. The Im$^+$···N$_2$ dimer

The Im$^+$···N$_2$ spectrum displays a single blue shaded band in the N-H stretch range at around 3295 cm^{-1} (A), which can readily be assigned to v_{NH} of the H-bound isomer shown in Figure 1e. The calculations yield a red-shift of $\Delta v_{NH} = -129$ cm^{-1}, which is comparable, albeit still slightly underestimating, with the experimental value ($\Delta v_{NH} = -135$ cm^{-1}). The red-shift resulting from the UB3LYP calculations ($\Delta v_{NH} = -143$ cm^{-1}) is also in good agreement with the experiment. A higher resolution scan over the range of this v_{NH} band can be seen in Figure 5; the smooth line is a contour of the band, resulted from a simulation of the corresponding fundamental transition.[51] The effective rotational temperature was considered to be T = 100 K and the band origin was taken as $v_0 = 3296.2$ cm^{-1}. While the ground-state rotational constants were taken from the UMP2 calculation (A = 0.337307 cm^{-1}, B = 0.032662 cm^{-1}, and C = 0.029779 cm^{-1}), the upper-state constants (A = 0.337318 cm^{-1}, B = 0.033268 cm^{-1}, and C = 0.030282 cm^{-1}) were obtained by

assuming that, upon v_{NH} excitation, the intermolecular bond shrinks by Δr_{HN2} = -0.05 Å. A contraction of this magnitude is typical for excitation of proton donor stretch vibrations in proton-bound dimers with this type of interaction energy.[52] The transition dipole is assumed to lie along the N-H bond. Finally, the FWHM of the ro-vibrational lines used in the convolution was considered to be 0.3 cm^{-1}. Even a superficial comparison of the experimental and simulated spectra reveals additional signal in the blue wing of the measured transition (indicated by asterisks in Figure 5), which cannot be reproduced by simulations even under significant variations of both T and ΔR within the physically meaningful parameter space. This additional signal is attributed to sequence transitions of the type $v_{NH} + v_x \leftarrow v_x$, where v_x are intermolecular vibrations. Such transitions were previously observed in related H-bound dimers. They occur at higher frequency than the v_{NH} fundamental, because the frequencies of the intermolecular stretch and bend modes increase upon v_{NH} excitation due to the stronger and more rigid intermolecular bond.[26]

Figure 5. *Experimental and simulated IR spectrum of the v_{NH} band of Im$^+$···N$_2$(H). The additional signal in the blue wing of the experimental transition (indicated by asterisks) arises from sequence hot bands which have not been included in the simulation.*
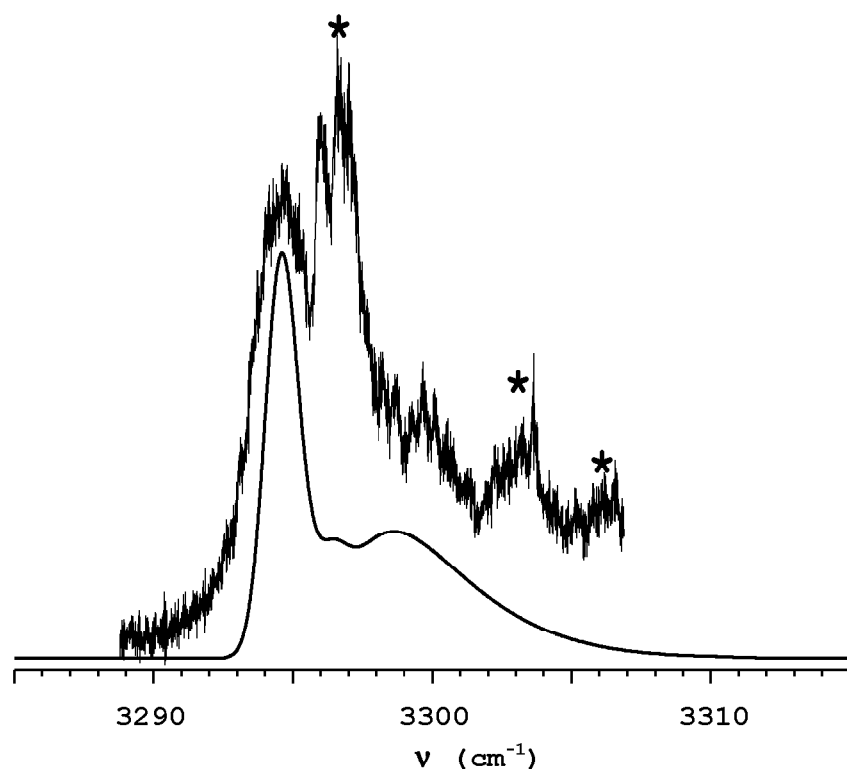
No absorption is detected in the Im'···N$_2$ spectrum in Figure 4 near the position of the free v_{NH} (3430 cm^{-1}). The primary implication is that the abundance of Im$^+$···N$_2$(π) is below the detection limit. Similarly, π-bound isomers were not observed in the IRPD spectra of An$^+$···N$_2$, Ph(H)$^+$···N$_2$, and 1-Np$^+$···N$_2$. The IRPD of closest related system, In$^+$···N$_2$, shows a weak signal corresponding to In$^+$···N$_2$(π). It should be noted that the frequency of the N-H

stretch mode of In^+ is larger than the one of Im^+ (ν_{NH} = 3454 cm^{-1} versus ν_{NH} = 3433 cm^{-1}) implying that In^+ is less acidic than Im^+. Thus, it seems that π-bonding becomes competitive with H-bonding for $A(H)^+ \cdots N_2$ dimers with not very acidic $A(H)^+$. Following this trend, N_2 complexes of $A(H)^+$ without acidic functional groups, such as $Bz(H)^+$, prefer π-bonds with N_2 over H-bonds. As a consequence, the absence of signal in the free ν_{NH} range implies that all $Im^+ \cdots N_2(\pi)$ and $Im^+ \cdots N_2(CH)$ dimers are below the detection limit.

In addition to ν_{NH} of $Im^+ \cdots N_2(H)$, the $Im^+ \cdots N_2$ spectrum features a band (C) near 3128 cm^{-1}, which is attributed to the three overlapping C-H stretch fundamentals, ν_{CH}, of the $Im^+ \cdots N_2(H)$ isomer. On the basis of the arguments detailed above, the three ν_{CH} vibrations of bare Im^+ are expected to occur between 3134 cm^{-1} and 3149 cm^{-1} (or, from the UB3LYP calculations, between 3135 cm^{-1} and 3141 cm^{-1}), in acceptable agreement with the observed band. H-bonding at the NH group induces essentially no frequency shifts for ν_{CH} (Table 1), implying that the 3128 cm^{-1} band in the $Im^{\cdot} \cdots N_2$ spectrum provides a very good approximation to the bare Im^+ transitions (messenger technique). The ratio of the integrated intensities of the ν_{NH} and ν_{CH} bands (6.5), although not in very good agreement with the ratio predicted for $Im^+ \cdots N_2(H)$ (12 for the UMP2 calculation and 13 for the UB3LYP one) is close enough taking into account that experimental intensity ratios of widely separated bands are only accurate to within a factor of 2. The $Im^+ \cdots N_2$ spectrum lacks strong absorptions in the spectral range of the intense ν_{CH} vibrations of the $Im^+ \cdots N_2(CH)$ dimers (3050 cm^{-1}...3100 cm^{-1}), confirming the absence of significant concentrations of these isomers in the molecular beam.

5.4.3. Relative abundance of $Im^+ \cdots L(H)$ versus $Im^+ \cdots L(\pi)$

The ratios of the integrated ν_{NH} band intensities observed in the IRPD spectra of $Im^+ \cdots L$ can be used to estimate the relative abundances of the H-bound and π-bound isomers in the plasma expansion, using the calculated ν_{NH} IR oscillator strengths given in Table 1. For $Im^+ \cdots Ar$, this procedure results in an abundance ratio of $N_H : N_\pi \cong 1.2$, on the basis of the experimental ν_{NH} intensity ratio of ~3 and the theoretical ratio of $I_H : I_\pi \cong 2.5$. For $Im^+ \cdots N_2$, a lower limit for $N_H : N_\pi > 10$ can be estimated from the achieved signal-to-noise ratio (~50) and $I_H : I_\pi \cong 3.7$. The larger abundance of the $Im^+ \cdots L(H)$ isomers suggests that they are more stable than the $Im^+ \cdots L(\pi)$ dimers, because the EI source produces predominantly the most stable isomer of a given complex. Moreover, the energy difference between both isomers appears to be significantly larger for $Im^+ \cdots N_2$ than for $Im^+ \cdots Ar$, resulting in a much less efficient production of the π-bound isomer for the N_2-containing

complex. This observation is in line with the quntum chemical calculations (Table 1).

5.4.4. Larger Im$^+\cdots$(N$_2$)$_n$ complexes

Similar to Im$^+\cdots$N$_2$, the IRPD spectrum of the Im$^+\cdots$(N$_2$)$_2$ trimer in Figure 4 reveals two bands, A and C, at 3313 cm^{-1} and 3132 cm^{-1}, which display only small incremental blue shifts of Δv_{NH} = 18 cm^{-1} and Δv_{CH} = 4 cm^{-1} from the closest dimer transitions. Their positions and shapes drive their assignment to v_{NH} and v_{CH} fundamentals of an Im$^+\cdots$(N$_2$)$_2$ isomer obtained by π-bonding a ligand molecule to Im$^+\cdots$N$_2$(H); this isomer will be denoted Im$^+\cdots$(N$_2$)$_2$(H/π). The calculations for the Im$^+\cdots$N$_2$(π) dimer show that a π-bound ligand slightly strengthens the N-H bond (Δr_{NH} = -0.0004 Å, Δv_{NH} = 5 cm^{-1}). This can be extrapolated to Im$^+\cdots$(N$_2$)$_2$(H/π) in the following way: the addition of a π-bound ligand leads to a N-H bond contraction, which is equivalent with a reduction in acidity for the NH group, resulting in decreased strength of the NH$\cdots$N$_2$ bond. The weakening of the NH$\cdots$N$_2$ bond leads to a slightly smaller red-shift of v_{NH} or, with respect to v_{NH} of Im$^+\cdots$N$_2$, to a small blue-shift. The v_{NH} band is again shaded to the blue, but the head created by the P branch is less prominent, leading to a larger FWHM of the band as compared to that of the dimer. The jagged and rather broad appearance of band A may also indicate the presence of a less stable isomer (denoted Im$^+\cdots$(N$_2$)$_2$(2H)), featuring two ligands directly interacting with the NH group of Im$^+$. Such isomers were previously invoked to explain the large incremental blue shift of Δv_{NH} = 25 cm^{-1} observed in the related In$^+\cdots$(N$_2$)$_2$ cluster upon the addition of a second ligand to In$^+\cdots$N$_2$. Hence, part of the signal in the blue wing of band A may be attributed to Im$^+\cdots$(N$_2$)$_2$(2H) isomers. Much like the spectrum of Im$^+\cdots$N$_2$, the spectrum of the trimer lacks absorptions in the range (3050 cm^{-1}...3100 cm^{-1}) where N$_2$-bound v_{CH} vibrations are expected to occur. This means that the amount of Im$^+\cdots$(N$_2$)$_2$ isomers in which the second ligand forms a H-bond to one of the CH groups is insignificant.

Similar to Im$^+\cdots$(N$_2$)$_2$, the Im$^+\cdots$(N$_2$)$_3$ spectrum displays a broad and blue shaded band (A) in the N-H stretch range. Its blue-shift of Δv_{NH} = 10 cm^{-1} with respect to band A of Im$^+\cdots$(N$_2$)$_2$ suggests the assignment to an isomer with one H-bound and two π-bound ligands, Im$^+\cdots$(N$_2$)$_2$(H/2π).

5.4.5. Ligand binding energies

The IRPD spectra and the calculations of Im$^+\cdots$L as well as previous studies of similar systems suggest that the H-bond of Ar to Im$^+$ is more stable than the π-bond. Recent

116

determinations of accurate binding energies (D_0) of related $A^+\cdots Ar(\pi)$ dimers, such as $Bz^+\cdots Ar$ (512 ± 3 cm^{-1}), para-difluorobenzene$^+\cdots Ar$ (572 ± 6 cm^{-1}), $In^+\cdots Ar$ (537 ± 10 cm^{-1}), and $Ph^+\cdots Ar$ (535 ± 3 cm^{-1}), suggest that the strength of the π-bond of Ar to an aromatic cation A^+ is rather insensitive to the detailed structure of A^+. Hence, $D_0(\pi)$ of $Im^+\cdots Ar$ may be estimated as 550 ± 100 cm^{-1}, larger than $D_0(\pi) = 388$ cm^{-1} resulting from calculations (Table 1). It is interesting to note that a similar value $D_0(\pi) \cong 570$ cm^{-1} can be extrapolated by rescaling the calculated $D_0(\pi)$ of $Im^+\cdots Ar$ with the ratio between the experimental and the calculated D_0 of $Im\cdots Ar$. Assuming that the theoretical level underestimates the strength of the π-bond and H-bonds with similar magnitude, the predicted $D_0(H) = 554$ cm^{-1} results in an estimated $D_0(H) \cong 815$ cm^{-1} for $Im^+\cdots Ar(H)$.

The photofragmentation branching ratios measured for resonant ν_{NH} excitation of the $H/(n-1)\pi$ isomers of $Im^+\cdots(N_2)_n$ provide more information about the ligand binding energies. In agreement with previous studies on related systems, the range of photoinduced fragment channels (m) for a given parent cluster size (n) is narrow: at most two major fragment channels are observed. This information can be used to roughly estimate ligand binding energies within the framework of the simple model which assumes that the absorbed photon energy (ν_{NH}) is available for subsequent ligand evaporation. For this purpose, the ligands are classified as H-bound and π-bound, with dissociation energies of $D_0(H) > D_0(\pi)$. Moreover, all π-bound ligands are assumed to have the same binding energy. The measured branching ratios are: m = 0 (100%) for n = 1; m = 0 (83%) and m = 1 (17%) for n = 2; m = 0 (57%) and m = 1 (43%) for n = 3. From the branching ratio of the tetramer and from its assumed most stable structure - $Im^+\cdots(N_2)_3(H/2\pi)$ - it results that the sum of the binding energies of all three ligands is roughly equal to the energy of the excitation photon ($\nu_{NH} \cong 3300$ cm^{-1}).

Similar to the corresponding Ar complexes, the dissociation energies of $A(H)^+\cdots N_2(\pi)$ are relatively insensitive to the detailed structure of $A(H)^+$:

$Ph^+\cdots N_2$ (π)	$An^+\cdots N_2$ (π)	$BzH^+\cdots N_2$ (π)	$1-Np^+\cdots N_2$ (π)	$PhH^+\cdots N_2$ (π) (carbenium)
750 ± 150 cm^{-1}	700 ± 200 cm^{-1}	~ 800 cm^{-1}	650 ± 150 cm^{-1}	750 ± 150 cm^{-1}

Hence, it may be considered that for the $Im^+\cdots N_2(\pi)$ dimer 600 cm$^{-1} < D_0 < 900$ cm^{-1}, in good agreement with the UMP2 calculations ($D_0(\pi) = 888$ cm^{-1}, Table 1). In contrast to π-bonding, the strength of the H-bonds in $A(H)^+\cdots N_2$ depends sensitively on the acidity of the proton donor group of $A(H)^+$; the calculations yield $D_0(H) = 1561$ cm^{-1} (Table 1) for

$Im^+{\cdots}N_2(H)$. Comparison of the photofragmentation data which shows that $2{\cdot}D_0$ (π) + $D_0(H)$ ≤ 3300 cm^{-1} with the quantum chemical well depths of $D_0(\pi)$ = 888 cm^{-1} and $D_0(H)$ = 1561 cm^{-1} for the $Im^+{\cdots}N_2$ dimer results in excellent agreement.

The total interaction in ion-ligand complexes with nonpolar ligands is mainly composed of the two-body interaction terms. The interaction in neutral Ar_2 and $(N_2)_2$ is on the order of D_0 ≈ 100 cm^{-1}. Consequently, for any angular orientation the optimal $Im^+{\cdots}L$ interaction is significantly stronger than the $L{\cdots}L$ attraction. Hence, the $Im^+{\cdots}L_n$ cluster growth is mainly driven by the $Im^+{\cdots}L$ dimer potential, because three-body forces are weak. The derived solvation sequence for the most stable $Im^+{\cdots}L_n$ complexes starts with the formation of a H-bound $Im^+{\cdots}L$ dimer core, which is then further solvated by (n-1) π-bound and / or CH-bound ligands. A similar cluster growth process was also deduced for $Ph(H)^+{\cdots}L_n$, $1{\text -}Np^+{\cdots}L_n$, and $An^+{\cdots}L_n$ with either Ar or N_2 ligands: first, the available acidic protons of the of the $OH_{(2)}$ and NH_2 groups are solvated by H-bound ligands, after which further π-bound ligands are attached to the aromatic ring.
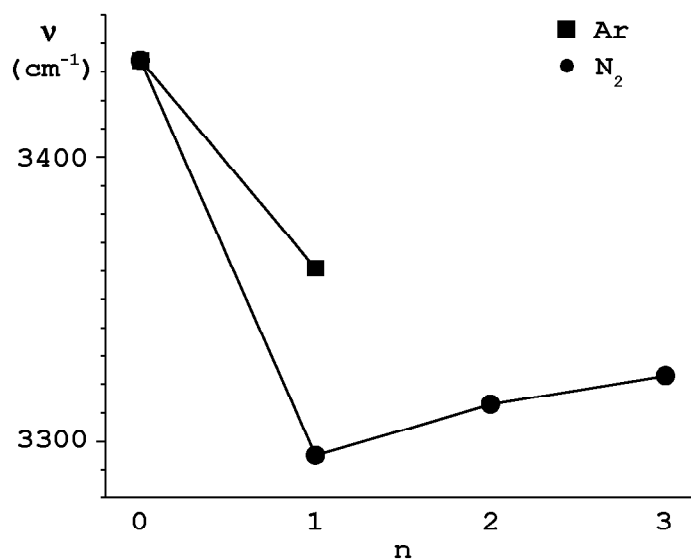
Figure 6. *Plot of the positions of the observed bands assigned to v_{NH} as a function of the cluster size n (Table 2). The frequency of the v_{NH} vibration of bare Im^+ is evaluated as 3431 cm^{-1}.*

The plots of v_{NH} of the most stable $Im^+{\cdots}L_n$ isomers as a function of the cluster size n in Figure 6 mirror the preferred evolution of the solvation (sub)shells. The first H-bound ligand induces a large red-shift in v_{NH} because of the destabilization of the N-H bond upon intermolecular H-bonding. The magnitude of Δv_{NH} is correlated with the strength of the intermolecular interaction, leading to a larger shift for L = N_2 than for L = Ar. The H-bound $Im^+{\cdots}N_2$ dimer is further solvated by π-bound ligands, which induce small incremental blue-shifts of v_{NH}. Thus, π-bound ligands slightly destabilize the intermolecular H-bond to the first ligand via noncooperative three-body forces, which in turn stabilize the intramolecular N-H bond. Because of noncooperative three-body interactions, the magnitude of the

incremental blue-shift decreases with the number of π-bound ligands in the complex. The ν_{NH} frequencies are not converged at the largest cluster size investigated, because the first solvent shell around Im^+ is not complete at $n = 3$. Unfortunately, neither Ar nor N_2 matrix isolation studies are available for Im^+, preventing a quantitative comparison of the $Im^+\cdots L_n$ cluster band shifts with the bulk limit ($n \to \infty$) at the present stage.

5.4.6. Proton affinity of the imidazyl radical

Previous spectroscopic studies have shown that $\Delta\nu_{XH}$, the complexation-induced red-shift in the proton donor stretch vibration of H-bound $XH^+\cdots L$ dimers, is correlated with the difference in the proton affinities (PAs) of the two bases X and L. Thus, for a given ligand species L, $\Delta\nu_{XH}$ is directly correlated to PA(X): the larger the PA(X), the stronger the intermolecular H-L bond and the larger the $\Delta\nu_{XH}$. This trend can be used to derive unknown PA values of bases X from IR spectra of their $XH^+\cdots L$ dimers. This procedure was already applied to $XH^+ = In^+$ and $1-Np^+$ to obtain the first experimental estimates for the PA of the indolyl and 1-naphthoxy radicals. The relative red shifts measured for a series of H-bound N_2-based dimers show a decrease correlated with the increase in PAs. The $\Delta\nu_{XH}/\nu_{XH}$ ratio for $Im^+\cdots N_2(H)$ of 3.96% determined in the present work is significantly larger than that of $In^+\cdots N_2(H)$, implying that the NH group in Im^+ is considerably more acidic than that in In^+. This trend is also seen in the smaller ν_{NH} frequency of Im^+ compared to that of In^+ (3430 cm^{-1} and 3454 cm^{-1}). Linear interpolation of the known values for Ph^+ and An^+ (Table 3) yields for the imidazyl radical PA $\cong$ 890 kJ/mol. Like in the case of t-1-Np$^+$, the error bars should be conservatively considered as ± 30 kJ/mol.

Table 3. *PAs of various radicals as function of the relative complexation-induced red-shifts. Bold symbols mark known PAs which were used to linearly interpolate all the other values.*

$XH^+\cdots N_2$	SiOH$^+$	Ph$^+$	Im$^+$	t-1-Np$^+$	In$^+$	An$^+$
$\dfrac{\Delta\nu_{XH}}{\nu_{XH}}$	14.1%	**4.8%**	~3.96%	3.13%	2.2%	0.57%
PA (kJ/mol)	778	**873**	~890	908	923	950

Similar to ν_{NH}, the ν_{CH} frequencies are a measure of the strength and acidity of the C-H bonds. The calculations demonstrate that all three CH groups in Im^+ feature similar bond lengths and stretch frequencies, implying that they are of comparable acidity. Comparison of the experimental ν_{CH} values of Im (3135 cm^{-1} ... 3160 cm^{-1}) and Im^+

($\cong 3128$ cm^{-1}) confirms the theoretical prediction of a slight decrease in the C-H bond strength upon ionization. The fact that v_{CH} appears to slightly increase upon sequential N_2 complexation (Table 2) suggests that the C-H bond strength increases again by π-bound solvation. Comparison of v_{CH} of Im$^+$ ($\sim$3128 cm^{-1}) with those of aromatic C-H stretch modes (sp^2 hybridization of C) of related aromatic molecules illustrates the dependence of the C-H bond strengths upon variation of the details of the molecular structure and composition. For example, the average v_{CH} value of the smallest aromatic hydrocarbon ion, c-C$_3$H$_3^+$ (3144 cm^{-1}), is slightly larger than that of Im$^+$ while the measured v_{CH} values of Bz$^+$ (3093 $\pm$ 15 cm^{-1}) are somewhat smaller. The closest related cation which was previously investigated - In$^+$ - also exhibits somewhat less acidic C-H bonds than those of Im$^+$, as demonstrated by its v_{CH} values (3071 cm^{-1} and 3100 cm^{-1}).

5.5. Conclusions

The stepwise microsolvation of the Im$^+$ cation in the nonpolar solvents Ar and N_2 has been investigated experimentally by IRPD and theoretically via quantum chemical calculations of size-selected Im$^+$$\cdots$L$_n$ complexes (L = Ar, N_2). Analysis of the n- and L-dependent complexation-induced frequency shifts of the N-H stretch vibrations demonstrates that the preferred ion-ligand binding motif between Im$^+$ and L is H-bonding to the acidic NH group, whereas π-bonding to the aromatic ring and H-bonding to the CH groups are less favorable. Thus, the most stable Im$^+$$\cdots$Ar structure (H-bound isomer) differs qualitatively from that of the neutral dimer (π-bound structure), emphasizing the large impact of ionization on the interaction potential and the preferred recognition motif between acidic aromatic molecules (A) and nonpolar ligands. The ionization induced $\pi \rightarrow$ H switch in the preferred binding type in A$^{(+)}$$\cdots$Ar complexes has now been established for a large variety of A$^{(+)}$ molecules with acidic functional YH$_k$ groups (Y = O, N) and seems to be a general phenomenon. Consequently, the preferred Im$^+$$\cdots$L$_n$ cluster growth begins with the formation of H-bound Im$^+$$\cdots$L dimers, which are further solvated by (n-1) π-bound ligands. The Δv_{NH} shift of Im$^+$$\cdots$$N_2$(H) yields a first experimental estimate for the PA of the imidazyl radical of $\cong$ 890 $\pm$ 30 kJ/mol, demonstrating that IR spectroscopy of cluster ions can be used to probe thermochemical properties of transient radicals. Significantly, the IRPD spectra of Im$^+$$\cdots$L$_n$ yield the first spectroscopic information about the v_{CH} and v_{NH} vibrations of bare Im$^+$, demonstrating that IR spectroscopy of cluster ions can also be used to probe fundamental properties of isolated ions (messenger technique). Comparison

between ν_{CH} and ν_{NH} of Im and Im$^+$ suggests that ionization enhances the acidity of both the C-H and N-H bonds of this fundamental biomolecular building block.

References

[1] Stryer I., *Biochemistry*, Freeman (New York, 1996)

[2] Noguchi T., Inoue Y., Tang X., *Biochemistry* **38** (1999) 399

[3] Kyte J., *Mechanisms in Protein Chemistry* , Garland (New York, 1995)

[4] Bachovchin W.W., *Biochemistry* **25** (1986) 7751

[5] Brutschy B., *Chem. Rev.* **100** (2000) 3891

[6] Brutschy B., *Chem. Rev.* **92** (1992) 1567

[7] Kim K.S., Tarakeshwar P., Lee, J.Y., *Chem. Rev.* **100** (2000) 4145

[8] Meyer E.A., Castellano R.K., Diederich F., *Angew. Chem. - Int. Ed.* **42** (2003) 1210

[9] Muller-Dethlefs K., Dopfer O., Wright T.G., *Chem. Rev.* **94** (1994) 1845

[10] Kleinermanns K., Gerhards M., Schmitt M., *Ber. Bunsen-Ges. Phys. Chem.* **101** (1997) 1785

[11] Neusser H.J., Krause H., *Chem. Rev.* **94** (1994) 1829

[12] Serrano-Andres L., Fulscher M.P., Roos B.O., Merchan M., *J. Phys. Chem.* **100** (1996) 6484

[13] Caminati W., Melandri S., Millemaggi A., Favero P.G., *Chem. Phys. Lett.* **294** (1998) 377

[14] Schafer M., Pratt D.W., *J. Chem. Phys.* **115** (2001) 11147

[15] Zierhut M., Roth W., Dummler S., Fischer I., *Chem. Phys.* **305** (2004) 123

[16] Fujii A., Miyazaki M., Ebata T., Mikami N., *J. Chem. Phys.* **110** (1999) 11125

[17] Schmitt M., Ratzer C., Meerts L., *J. Chem. Phys.* **120** (2004) 2752

[18] Van Bael M.K., Smets J., Schoone K., Houben L., McCarthy W., Adamowicz L., Nowak M.J., Maes G., *J. Phys. Chem. A* **101** (1997) 2397

[19] Carles S., Lecomte F., Scherman J.P., Desfrancois C., *J. Phys. Chem. A* **104** (2005) 125

[20] Talbot F.O., Simons J.P., *Eur. Phys. J. D* **20** (2002) 389

[21] Scheiner S., Kar T., Pattanayak J., *J. Am. Chem. Soc.* **124** (2002) 13257

[22] Main-Bobo J., Olesik S., Gase W., Baer T., Mommers A.A., Holmes J.L., *J. Am. Chem. Soc.* **108** (1986) 677

[23] Cradock S., Findlay R.H., Palmer M.H., *Tetrahedron* **29** (1973) 2173

[24] Tamsey B.G., *J. Org. Chem.* **44** (1979) 2093

[25] Yan S., Bu Y., Cao Z., Li P., *J. Phys. Chem. A* **108** (2004) 7038

[26] Bieske E.J., Dopfer O., *Chem. Rev.* **100** (2000) 3963

[27] Dopfer O., *Z. Phys. Chem.* **219** (2005) 125

[28] Lias S.G., Liebman J.F., Levin R.D., *J. Phys. Chem. Ref. Data* **13** (1984) 695

[29] Solca N., Dopfer O., *Chem. Phys. Lett.* **325** (2000) 354

[30] Solca N., Dopfer O., *Phys. Chem. Chem. Phys.* **6** (2004) 2732

[31] Solca N., Dopfer O., *J. Phys. Chem. A* **106** (2002) 7261

[32] Solca N., Dopfer O., *Eur. Phys. J. D* **20** (2002) 469

[33] Andrei H.S., Solca N., Dopfer O., *Phys. Chem. Chem. Phys.* **6** (2004) 3801

[34] M.J. Frisch, G.W. Trucks, H.B. Schlegel, G.E. Scuseria, M.A. Robb, J.R. Cheeseman, J.A. Montgomery Jr., T. Vreven, K.N. Kudin, J.C. Burant, J.M. Millam, S.S. Iyengar, J. Tomasi, V. Barone, B. Mennucci, M. Cossi, G. Scalmani, N. Rega, G.A. Petersson, H. Nakatsuji, M. Hada, M. Ehara, K. Toyota, R. Fukuda, J. Hasegawa, M. Ishida, T. Nakajima, Y. Honda, O. Kitao, H. Nakai, M. Klene, X. Li, J.E. Knox, H.P. Hratchian, J.B. Cross, V. Bakken, C. Adamo, J. Jaramillo, R. Gomperts, R.E. Stratmann, O. Yazyev, A.J. Austin, R. Cammi, C. Pomelli, J.W. Ochterski, P.Y. Ayala, K. Morokuma, G.A. Voth, P. Salvador, J.J. Dannenberg, V.G. Zakrzewski, S. Dapprich, A.D. Daniels, M.C. Strain, O. Farkas, D.K. Malick, A.D. Rabuck, K. Raghavachari, J.B. Foresman, J.V. Ortiz, Q. Cui, A.G. Baboul, S. Clifford, J. Cioslowski, B.B. Stefanov, G. Liu, A. Liashenko, P. Piskorz, I. Komaromi, R.L. Martin, D.J. Fox, T. Keith, M.A. Al-Laham, C.Y. Peng, A. Nanayakkara, M. Challacombe, P.M.W. Gill, B. Johnson, W. Chen, M.W. Wong, C. Gonzalez, J.A. Pople, *Gaussian 03, Revision D.01 Gaussian, Inc., Wallingford CT* (2004)

[35] Boys S.F., Bernardi F., *Mol. Phys.* **19** (1970) 553

[36] Chalasinski G., Szczesniak M. M., *Chem. Rev.* **94** (1994) 1723

[37] King S.T., *J. Phys. Chem.* **74** (1970) 2133

[38] Cioslowski J., Hay P.J., Ritchie J.P., *J. Phys. Chem.* **94** (1990) 148

[39] Hirschfelder J.O., Curtis C.F., Bird R.B., *Molecular Theory of Gases and Liquids*, John Wiley & Sons (New York, 1954)

[40] Gray C.G., Gubbins K.E., *Theory of molecular fluids*, Clarendon (Oxford, 1984)

[41] Buckingham A.D., *Adv. Chem. Phys.* **12** (1967) 107

[42] Solca N., Dopfer O., *J. Phys. Chem. A* **105** (2001) 5637

[43] Linstrom P.J., Mallard W.G., *NIST Chemistry Webbook*, http://webbook.nist.gov/chemistry/

[44] Camy-Peyret C., Flaud J.M., Guelachvili G., Amiot C., *Mol. Phys.* **26** (1973) 825

[45] Guelachvili G., Rao K. N., *Handbook of Infrared Standards*, Academic Press (London, 1993)

[46] Unterberg C., Jansen A., Gerhards M., *J. Chem. Phys.* **113** (2000) 7945

[47] Solca N., Dopfer O., *Chem. Eur. J.* **9** (2003) 3154

[48] Bakker J.M., Satink R.G., von Helden G., Meijer G., *Phys. Chem. Chem. Phys.* **4** (2002) 24

[49] Solca N., Dopfer O., *J. Chem. Phys.* **120** (2004) 10470

[50] Solca N., Dopfer O., *J. Mol. Struct.* **563** (2001) 241

[51] Luckhaus D., Quack M., *Mol. Phys.* **68** (1989) 745

[52] Dopfer O., Nizkorodov S.A., Olkhov R.V., Maier J.P., Harada K.J., *Phys. Chem. A* **102** (1998) 10017

6. IRPD spectroscopy of (protonated Imidazole)···L_n complexes
(L = Ar, N_2, H_2O; n = 1 ... 8)

Abstract The intermolecular interaction between the protonated imidazole ($C_3N_2H_5^+$, henceforth denoted ImH^+) and selected ligands is characterized in the ground electronic state by infrared photodissociation (IRPD) spectroscopy of size-selected $ImH^+ \cdots L_n (\cdots N_2)$ complexes (L = Ar, N_2, H_2O; n ≤ 8) and quantum chemical calculations performed at the MP2/6-311G(2df,2pd) level of theory. Like in the other presented experiments, the complexes are created in an electron impact cluster ion source, which predominantly produces the most stable isomers of a given cluster ion. The analysis of the size-dependent frequency shifts of the N-H stretch vibrations of the $ImH^+ \cdots L_n$ complexes (L = Ar, N_2; n = 1 ... 8) and their photofragmentation branching ratios provides valuable information about the stepwise microsolvation of ImH^+ in a nonpolar hydrophobic environment, including the formation of structural isomers, the competition between various intermolecular binding motifs (H-bonding and π-bonding) as well as their interaction energies, and the acidity of the NH protons. The analysis of the IRPD spectra of the $ImH^+ \cdots (H_2O)_n (\cdots N_2)$ complexes (n = 1, 2) reveals the influence of the proton affinities of Im and H_2O on the preferred pattern for the microsolvation of ImH^+ in H_2O.

6.1. Introduction

Processes like protonation and microhydration are relevant for a variety of fundamental phenomena in biophysical chemistry, such as molecular recognition,[1],[2],[3],[4] enzyme catalysis,[5],[6],[7] and proton transport.[8],[9],[10] Detailed understanding of these phenomena at the molecular level requires the characterization of the interactions between protonated biomolecules and H_2O. The spectroscopic characterization of isolated clusters in molecular beams provides currently the most direct and most detailed experimental access to such interaction potentials.

There is, however, a general lack of spectroscopic information on the microhydration of even simple protonated amino acids and DNA bases owing to difficulties in the

production of sufficient cluster-ion concentrations. Recently however, experiments on gas-phase microhydration of protonated amino acids have been reported, revealing information about vibrational properties of such complexes.[11],[12],[13] The lack of spectroscopic investigations on biologically relevant systems is quite the norm, as their physical properties (for example H-bonding in their solid-state form) are making difficult the production of large enough densities of such molecules in the gas phase. In this case, simpler molecules are used for modeling and studying the properties of some functional elements of a biomolecule. Following this approach, the present chapter presents an IRPD spectroscopic and quantum chemical study of protonated imidazole under controlled solvation conditions.

Figure 1. *Atom identification for the most stable isomer of ImH⁺ (a); selected isomers of protonated histidine (b), protonated histamine (c), protonated adenine (d), and protonated guanine (e).*
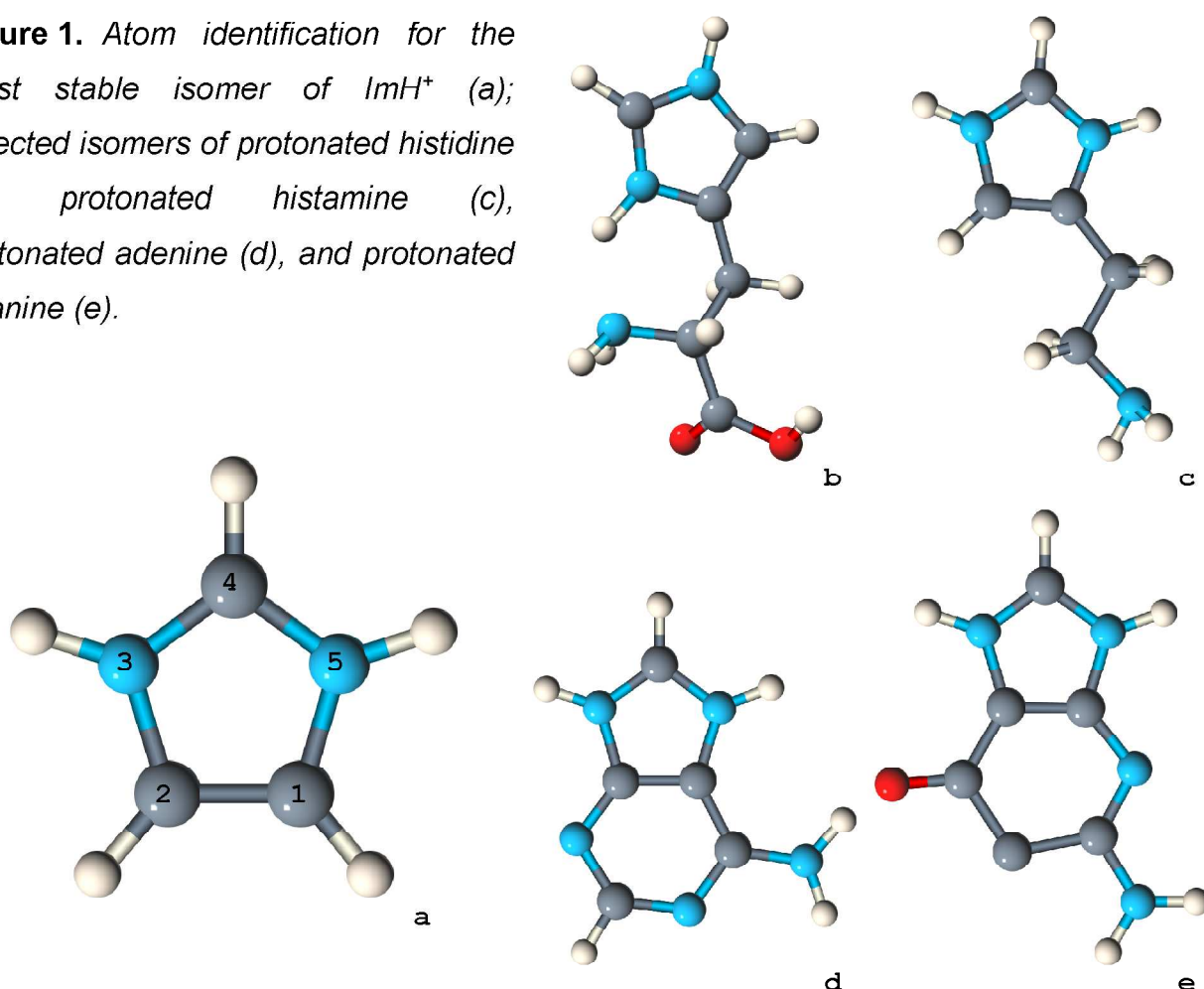
Imidazole ($C_3N_2H_4$, henceforth denoted Im) and its protonated form (Figure 1) are basic chemical units in a variety of important biomolecular building blocks, including the amino acid histidine (His) and the DNA bases adenine and guanine. The combined presence of an acidic N-H bond and a basic N atom on the molecular ring offers the ability to both protonate (resulting imidazolium)[14] and deprotonate (forming imidazolate). This

ability makes aqueous solutions of Im good basic pH buffers for pH values around 9 ... 10. A tautomeric ylide form of neutral imidazole (ImY, 124.8 kJ/mol less stable than Im - ZPE-corrected value) is also known to exist and has been found as a reactive species in exchange processes.[14] The ability of His to both accept and donate a proton at physiological pH values is used in a plethora of biochemical processes to shuttle protons, for example, in active centers of proteins such as the catalytic triad in serine proteases.[7],[8] The ability of all molecules that contain an Im fragment to shuttle protons is explained by the above-mentioned structure of the Im ring: while the basic N atom picks a H^+, the acidic N-H group releases its H^+. This mechanism was previously investigated in solid-state experiments.[8],[15],[16] Quantum chemical calculations demonstrate that the structural and vibrational properties of the acidic NH groups in ImH^+ are similar to those in $HisH^+$ and in some isomers of protonated adenine or guanine. Consequently, isolated $ImH^+\cdots(H_2O)_n$ complexes are valuable model systems to characterize the sequential hydration of these protonated biomolecular building blocks and to unravel the mechanistic details of the solvent and charge-assisted proton-shuttle properties of the His residue in enzymatic proteins.

In recent years, a number of theoretical papers have attempted to model Im or ImH^+ either directly,[17],[18],[19] or as a building block of other molecules.[20],[21],[22] The interaction of such species with various molecules with biological relevance has also been studied.[23] However, while such studies obtain properties of $Im(H)^{(+)}$ either isolated or interacting with a finite number of surrounding molecules, they lack direct experimental support. The available spectroscopic information was obtained mainly via Raman spectra of acidified solutions of Im.[24],[25],[26] Limited gas-phase information is available via MALDI-IRMPD of protonated N-acetyl-alanine and alanyl-histidine,[27] H/D exchange on protonated histidine and histidine methyl ester,[28] or via neutralization-reionization mass spectrometry of Im.[29] All these experiments concluded that the preferred protonation site of the Im moiety is the basic N atom.

Despite the large interest in the ImH^+ interaction with H_2O, previous studies on isolated $ImH^+\cdots(H_2O)_n$ clusters are rather limited. Available experimental information relies exclusively on mass spectrometry, yielding incremental hydration enthalpies of 62.0 kJ/mol, 52.7 kJ/mol, and 51.1 kJ/mol for n= 1, 2, 3, respectively.[30] Quantum chemical calculations reveal that the H bonds of H_2O to the NH groups are significantly more stable than the H bonds of H_2O to the CH donors and the π bonds of H_2O to the aromatic ring. In addition, the acidity of the NH bonds, and thus their catalytic effect for proton transfer, was predicted to depend strongly on the degree of hydration.

125

An effective way of probing the properties of ImH^+ is to analyze the spectroscopic and energetic properties of weakly bound complexes between ImH^+ and nonpolar ligands: $ImH^+\cdots L_n$ (L = Ar, N_2). The size-dependent frequency shifts of the stretch vibrations and the photofragmentation branching ratios provide valuable information about the stepwise microsolvation of ImH^+ in the nonpolar environment of the ligands, including the formation of structural isomers as well as their interaction energies.

In general, the interaction between Ar and neutral aromatic molecules (A) is best described as dispersion interaction between Ar and the π electron system of A. Such π-bound structures have also been derived from spectroscopic investigations of complexes between Ar and ionized arenes (A^+): phenol$^+\cdots$Ar,[31] indole$^+\cdots$Ar,[32] aniline$^+\cdots$Ar,[33] benzene$'\cdots$Ar,[34] 1-naphthalenole$'\cdots$Ar,[35] and imidazole$'\cdots$Ar.[36] However, in the case of $A^+\cdots$Ar, as well as in the case of the protonated dimer $AH^+\cdots$Ar, a significant role is played by the acidic groups YH_k of the aromatic cation (if present). It has been demonstrated that, when present, such YH_k groups are changing the dominant component of the dimer interaction from the dispersion interaction between Ar and the π electron system of $A(H)^{+[34]}$ to the charge - induced dipole interaction between a proton of a YH_k acidic group and Ar.[31], [32],[33],[35],[36] Given the presence of two such acidic groups (NH), it is expected that the dominant binding motif of $ImH^+\cdots$Ar is H-bonding to one of these groups.

In the present work, the IRPD spectra of $ImH^+\cdots L_n$ (L = Ar, N_2, H_2O) were obtained in a molecular beam expansion, using techniques which have recently been applied for the first time to isolated and microsolvated protonated aromatic molecules, protonated peptides, and proton-bound dimers of amino acids. These studies mainly addressed the question of the preferred protonation site, the dissociation behavior, and the influence of microsolvation in a nonpolar environment. The IRPD spectra recorded in the NH and OH stretch ranges provide invaluable direct spectroscopic information on the acidity of these bonds as well as on the structure and energy of the preferred microsolvation motif. They show the competition between various intermolecular binding motifs (H-bonding and π-bonding) and the influence of the acidity of the NH protons over the microsolvation process. The analysis of the IRPD spectra of the $ImH^+\cdots(H_2O)_n(\cdots N_2)$ complexes (n = 1, 2) reveals the influence of the proton affinities (PA) of Im and H_2O on the preferred pattern for the microsolvation of ImH^+ in H_2O.

6.2. Quantum chemical calculations

The level of theory used for characterizing the effects of complexation on the

properties of ImH$^+$ is MP2. *Ab initio* methods are known to reliably describe the properties of both the π-bonds and the H-bonds between small aromatic molecules and nonpolar or polar ligands (A$^+$···L).[37] Density functional theory (B3LYP) is used only for probing the proton transfer between ImH$^+$ and (H$_2$O)$_n$ (n = 1, 2) as it describes well the interaction between charged systems and the electrical dipole of H$_2$O and is far less computationally expensive than the *ab initio* approach. All calculations have been carried out using the Gaussian 03 quantum chemistry package;[38] unless specified, all the results presented below are the ones derived at the MP2 level. All energetical parameters are corrected for the zero-point energy (ZPE) error using the harmonic frequencies (without any anharmonicity correction). The intermolecular interactions were counterpoise corrected for basis set superposition error (BSSE).[39],[40]

In order to characterize the intramolecular N-H and the intermolecular H···L bonds, *ab initio* quantum chemical calculations were carried out for the relevant monomers (Im, Im$^+$, and ImH$^+$) and for a variety of complexes of ImH$^+$ with nonpolar ligands (Ar and N$_2$). Also the microsolvation of ImH$^+$ in H$_2$O was investigated theoretically by performing quantum chemical calculations on certain isomers of ImH$^+$···(H$_2$O)$_n$(···N$_2$) (n = 0 ... 2). These results are relevant for the assignment of the IRPD spectra of ImH$^+$···(H$_2$O)$_n$(···N$_2$) (n = 0 ... 2) complexes.

6.2.1. Monomers

Theoretical studies of AH$^+$ (A = Bz, Ph, etc.) are showing that the isomers where the proton is bound on the π electron system are actually saddle points on the potential energy

Figure 2. *The PES of Im, evaluated at the MP2/6-311G(2df,2pd) level. The minima correspond to protonation at atoms of the aromatic ring (see Figure 1 for an identification of the atoms), while the maxima are transition states describing the movement of the proton between neighboring atoms of the ring.*
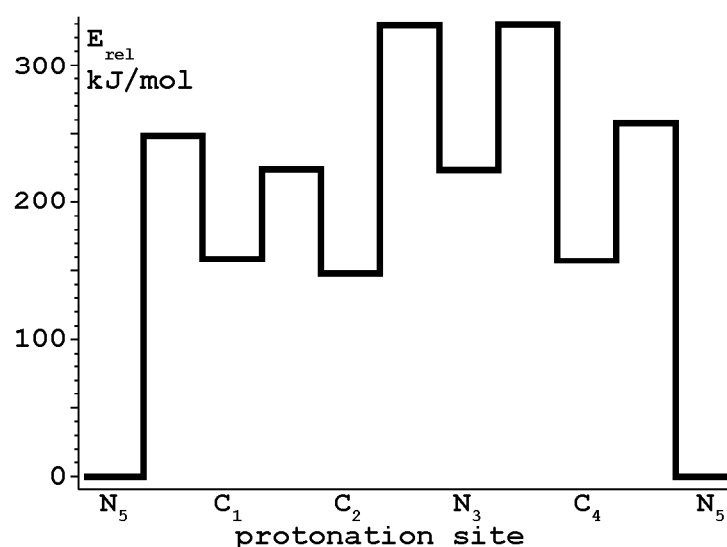
surface (PES).[41] This restricts the range of possible ImH$^+$ isomers to just the five σ

isomers resulting from protonation of the atoms of the ring. The present analysis of the PES of Im (Figure 2 and Table 1) reveals that protonation on any of these five sites yields stable geometries, with the isomer protonated at the N_5 atom lying exceptionally low in terms of stabilization energy (148 ... 223 kJ/mol lower than any other investigated site).

Table 1. *Relative stabilization energies (in kJ/mol) for protonation sites around the ring of Im and for the transition states (TS) connecting these sites, as evaluated at the MP2/6-311G(2df,2pd) level.*

site	N5	TS_{N5-C1}	C1	TS_{C1-C2}	C2	TS_{C2-N3}	N3	TS_{N3-C4}	C4	TS_{C4-N5}
E_{rel} (kJ/mol)	0	248	159	224	148	329	223	330	157	257

Moreover, the PA of Im presently computed for the site of the basic N atom (N_5), 944 kJ/mol, is in good agreement with the experimentally measured value - 936 kJ/mol,[42] demonstrating that the chosen theoretical level is appropriate to accurately describe the properties of ImH^+. This implies that the only experimentally attainable isomer of ImH^+ is the one protonated at N_5; unless specifically noted, ImH^+ will be used to denote the N_5-protonated isomer.

Figure 3. *Structure of the Im (a), Im$^+$ (b), and the most stable (see below) isomer of ImH$^+$ (c), as evaluated at the MP2/6-311G(2df,2pd) level. Interatomic distances (in Å) are indicated for each monomer.*
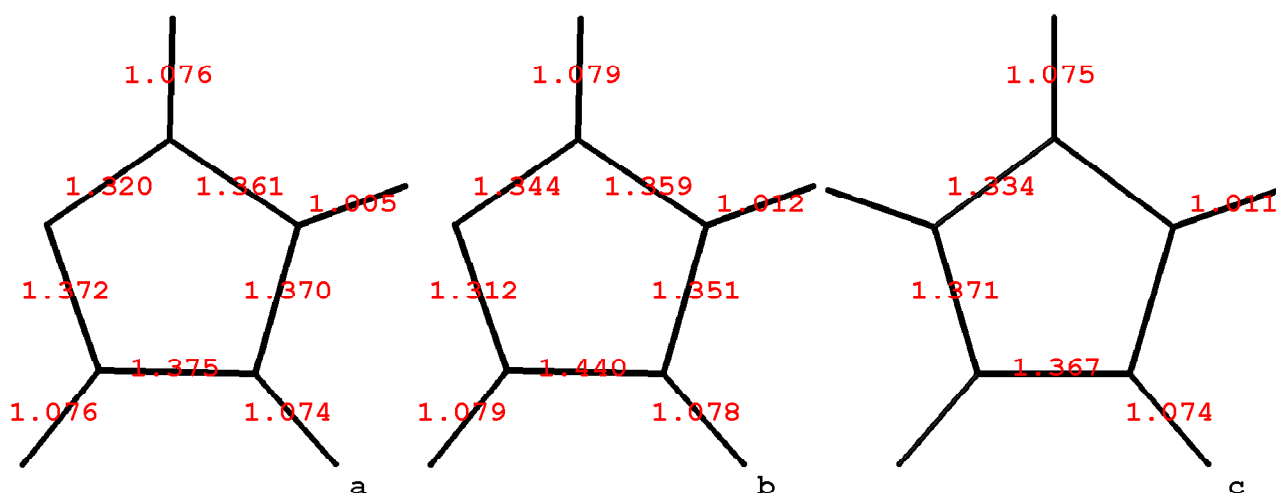
The geometrical properties of $Im^{(+)}$ and ImH^+ which are relevant for the present study are indicated in Figure 3, while the frequencies of the proton stretch vibrations are indicated in Table 2. It can be seen that the transition from neutral to cation is accompanied by rather significant modifications in the geometry of the molecule: with the

notable exception of the C=C bond, all other ring bonds shrink, while the bonds connecting the protons expand. The changes are reflected by the spectra of the monomers. The frequencies of the ω_{CH} stretch vibrations are slightly red-shifted (at most by -12 cm^{-1}), while their IR intensities increase. At the same time, the ω_{NH} stretch vibration is red-shifting by -79 cm^{-1} (more than 2%) while its IR intensity is increasing more than 3 times, from 74 km/mol to 231 km/mol. The most significant implication of these changes is that the acidity of the cation is by far larger than the one of the neutral precursor. In the case of the protonated species, it can be seen that the ring is largely unaffected by the addition of a proton. Given the C_{2v} symmetry of ImH$^+$, some vibrational modes will be coupled. This is the case for two of the C-H stretch vibrations and for the two N-H stretch vibrations; in each case a pair of symmetric and antisymmetric normal modes will replace the individual stretch modes. All three ω_{CH} stretch vibrations are slightly blue-shifted (by ~+34 cm^{-1}), while their IR intensities increase to a level similar with the one seen for the cation. The coupling

Table 2. *Harmonic frequencies (in cm^{-1}) of the proton stretch vibrations of Im, Im$^+$, and ImH$^+$, evaluated at the MP2/6-311G(2df,2pd) level. The IR intensities (in km/mol) are indicated in parentheses.*

vibrational mode	harmonic frequency / cm^{-1} (IR intensity / km/mol)		
	Im	Im$^+$	ImH$^+$
ω_{CH} / ω_{CH}^{as}	3296 (3)	3295 (25)	3329 (27)
ω_{CH}	3302 (0)	3302 (36)	3334 (69)
ω_{CH} / ω_{CH}^{s}	3325 (1)	3313 (16)	3347 (18)
ω_{NH} / ω_{NH}^{as}	3703 (74)	3624 (231)	3638 (397)
ω_{NH} / ω_{NH}^{s}			3645 (33)

between the two degenerate N-H stretching local modes is relatively weak and causes only a small splitting between the corresponding frequencies: $\omega_{NH}^{s} - \omega_{NH}^{as} = 7$ cm^{-1}. The average position of the ω_{NH} stretch vibration is red-shifted by -61 cm^{-1} with respect to the neutral species, less than the red-shift seen in the case of the cation while the average IR intensity of these modes is similar with the one calculated for the cation.

In order to better understand binding motifs and the enhancement of IR activities, the charge distribution of Im, Im$^+$, and ImH$^+$ must be analyzed. The preferred method is atoms-in-molecules (AIM), which, in general, provides level-independent charge distributions.[43] The charge distributions can also be extracted via Mulliken population analysis; however, this approach is known to be very sensitive to the theoretical level. As

the results of the Mulliken analyses are largely different from the ones provided by AIM, they will not be discussed further. Table 3 compares the charge distributions of the three considered species. It can be seen that both the removal of an electron from Im and the addition of a proton to Im result in the augmentation of the positive partial charges, with amounts related to the corresponding partial charge calculated for Im. The increase of the

Table 3. *Charge distributions around Im, Im$^+$, and ImH$^+$, evaluated via AIM at the MP2/6-311G(2df,2pd) level.*

atom	Im	Im$^+$	ImH$^+$
C1	0.395	0.649	0.443
C2	0.352	0.517	0.443
N3	-1.282	-1.296	-1.268
C4	0.955	1.004	1.069
N5	-1.061	-1.013	-1.268
H$_{C1}$	0.051	0.182	0.169
H$_{C2}$	0.067	0.204	0.169
H$_{N3}$	0.444	0.534	0.520
H$_{C4}$	0.068	0.210	0.194
H$_{N5}$			0.520

positive charge around the protons strongly enhances the IR activities of all ν_{CH} and ν_{NH} fundamentals.

Following the analysis of Im(H)$^{(+)}$, a number of complexes have been investigated via quantum chemical calculations performed at the MP2/6-311(2df,2pd) level of theory. The parameters of these structures relevant for the present work are summarized in Table 4 (ImH$^+$···Ar), Table 5 (ImH$^+$···(N$_2$)$_n$), and Table 6 (ImH$^+$···(H$_2$O)$_n$(···N$_2$)) which contain:
* intramolecular N-H, C-H, and O-H bond lengths (r_{NH}, r_{CH}, r_{OH}), the corresponding harmonic stretch frequencies (ω_{NH}, ω_{CH}, ω_{OH}), and their IR intensities (I_{NH}, I_{CH}, I_{OH})
* intermolecular bond length (r_{HL} or r_{ring-L}), harmonic stretch frequency (ω_s) and IR intensity (I_s), as well as the dimer dissociation energy (D_0, ZPE-corrected).

6.2.2. ImH$^+$···Ar

The interaction between ImH$^+$ and Ar has been investigated by considering a number of dimer geometries. The structures corresponding to the equilibrium points identified via calculations are presented in Figure 4.

130

As discussed in **Chapters 3**, **4**, and **5**, the competition between π- and H- binding sites for Ar to an A(H)$^+$ cation is tipped in favor of the latter scheme by the presence of acidic YH_k groups. Such acidic groups are known to interact with ligands via charge - induced dipole.[31],[32],[33],[35],[36] This interaction scheme is expected to occur also in the case of ImH$^+$···Ar. Analyzing the results presented in Table 4, it can easily be seen that, indeed, the strongest intermolecular interaction occurs in the case of the dimer bound via one of the acidic NH protons. This ImH$^+$···Ar H-bound dimer (Figure 4a, further denoted ImH$^+$···Ar(NH)) features a planar optimum geometry. The intermolecular N-H···Ar bond and the corresponding intramolecular N-H bond are nearly collinear (the deviation of $\theta_{N-H\cdots Ar}$ from linearity being smaller than 0.2°). The length of the intermolecular bond (r_{HAr} = 2.46 Å) is compatible with the ones calculated for similar systems.[33] It is remarkable that this bond is slightly longer than the intermolecular separation calculated for Im$^+$···Ar(H) (2.41 Å) as the electrical charge of the ImH$^+$ is shared by the two acidic protons. The effects of this subtle alteration can be found in all monitored parameters; for example, the binding energy (D_0) of this dimer (462 cm^{-1}) is 17% smaller than the one calculated for for Im$^+$···Ar(H) at the same level of theory (D_0 = 554 cm^{-1}).

Figure 4. *Geometries of the equilibrium structures identified for ImH$^+$···Ar: (a) NH-bound; (b) C_1H-bound (TS); (c) C_4H-bound (TS); (d) C_1C_2-bound; (e) π-bound.*
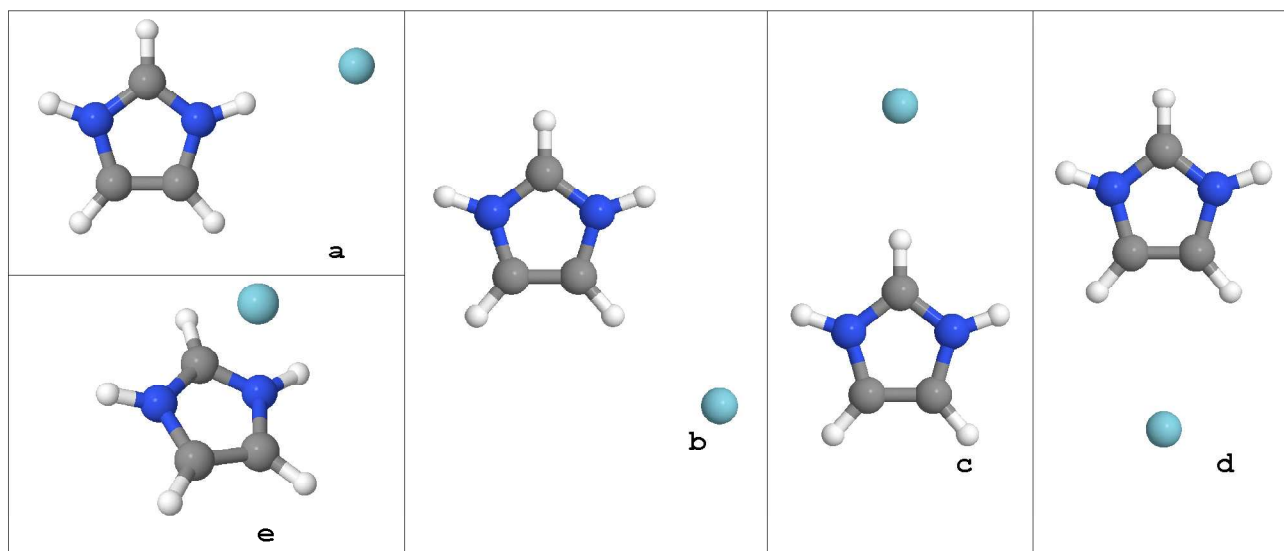
The ligand is pulling the proton to which it binds away from the molecular body; in the present case the N-H intramolecular bond expands by Δr_{NH} = 0.0022 Å while for Im$^+$···Ar(H) the expansion was calculated as Δr_{NH} = 0.0029 Å. The elongation of this intramolecular bond implies a weakening of the potential "seen" by the proton, red-shifting the stretch vibration and, at the same time, greatly enhancing the corresponding IR oscillator strength.

Analysis of the normal modes shows that the bound N-H vibration is derived from the antisymmetric mode of the isolated ImH^+; this allows to properly calculate the red-shift and the IR intensity enhancement. It follows that $\Delta\omega_{NH}$ = -44 cm^{-1} (1.2%) while the IR intensity grows by 1.34; it is instructive to compare these values with the ones calculated for the $Im^+{\cdots}Ar(H)$ complex: $\Delta\omega_{NH}$ = -57 cm^{-1} (1.6%) while the IR intensity enhancement amounts to 1.40. The smaller relative values calculated for the $ImH^+{\cdots}Ar(NH)$ complex with respect to the $Im^+{\cdots}Ar(H)$ complex are consistent with a reduction of the effective partial charge on the NH proton of the binding site. This is not unexpected, as now there are two such protons sharing the same overall charge of the ImH^+ moiety.

Table 4. *Properties of the intramolecular N-H and C-H bonds (r_{NH}, r_{CH}, ω_{NH}, ω_{CH}, I_{NH}, I_{CH}) and of the intermolecular bonds (r_{H-Ar}, $r_{ring-Ar}$, D_0, ω_s) for several $ImH^+{\cdots}Ar$ isomers calculated at the MP2/6-311G(2df,2pd) level. The parameters of the bonds directly affected by complexation are indicated with **bold** numbers.*

complex	ImH$^+$	ImH$^+\cdots$Ar				
		NH	C$_1$H / C$_2$H	C$_4$H	C$_1$=C$_2$	π
r_{C1H} (Å)	1.0739	1.0739	**1.0740**	1.0739	1.0737	1.0739
r_{C2H} (Å)	1.0739	1.0739	1.0739	1.0739	1.0737	1.0739
r_{C4H} (Å)	1.0745	1.0745	1.0745	**1.0748**	1.0745	1.0745
r_{N3H} (Å)	1.0106	**1.0128**	1.0106	1.0105	1.0105	1.0105
r_{N5H} (Å)	1.0106	1.0104	1.0105	1.0105	1.0105	1.0105
ω_{CH} (cm^{-1}) I_{CH} (km/mol)	3329 (27)	3329 (26)	**3329 (43)**	3329 (27)	3332 (24)	3329 (27)
ω_{CH} (cm^{-1}) I_{CH} (km/mol)	3334 (69)	3334 (65)	3334 (73)	**3329 (119)**	3334 (68)	3335 (68)
ω_{CH} (cm^{-1}) I_{CH} (km/mol)	3347 (18)	3346 (17)	3346 (25)	3346 (17)	3349 (20)	3346 (17)
ω_{NH} (cm^{-1}) I_{NH} (km/mol)	3638 (397)	**3596 (531)**	3638 (395)	3639 (390)	3638 (394)	3639 (391)
ω_{NH} (cm^{-1}) I_{NH} (km/mol)	3645 (33)	3643 (172)	3645 (33)	3645 (31)	3645 (35)	3646 (33)
r_{HAr} / $r_{ring-Ar}$ (Å)		2.46	2.86	2.78	3.66	3.43
ω_s (cm^{-1}) I_s (km/mol)		63 (10)	36 (6)	40 (7)	41 (6)	54 (8)
D_0 (cm^{-1})		462	205	252	244	350

The two unique dimers having the fragments bonded along a C-H intramolecular bond (C$_1$-H / C$_2$-H in Figure 4b and C$_4$-H in Figure 4c) have also been investigated, starting

from planar geometries with the Ar atom placed along the investigated C-H bond. Stationary points have been identified during geometry optimization in both cases but subsequent analysis of the vibrational modes has revealed that they are transition states (TS). In the case of the $ImH^+\cdots Ar(C_1H)$, the ligand is not anymore placed along the C_1-H bond axis: $\theta_{C1-H\cdots Ar} = 171.6°$; in the case of the $ImH^+\cdots Ar(C_4H)$, the movement of the ligand is restricted by symmetry along the axis of the C_4-H bond (the complex has the same C_{2v} symmetry as ImH^+). For both these TSs, the normal mode having an imaginary frequency is characterized by in-plane movement of the Ar ligand, around the ImH^+. It results that at least one more minimum must exist in the molecular plane. Indeed, an equilibrium structure with the Ar attaching to the C=C bond has been identified (Figure 4d, further denoted $ImH^+\cdots Ar(CC)$); also in this case the Ar atom is placed along the C_5-H bond axis, resulting a C_{2v} symmetric complex. Analysis of the vibrational modes has shown that this is indeed a minimum on the PES. It is interesting that the dimer binding energies listed in Table 4 imply that the component of the $ImH^+\cdots Ar(C_4H)$ intermolecular interaction which is responsible with stabilizing the system is stronger than the intermolecular interaction of $ImH^+\cdots Ar(CC)$. As it will be shown later on, knowledge about isomers like $ImH^+\cdots Ar(CC)$ is not required for modeling the $ImH^+\cdots Ar$ dimer spectrum or the very beginning of the microsolvation. This approach is supported by theoretical and spectroscopic data obtained for $BzH^+\cdots Ar$,[44] $Bz^+\cdots Ar$,[45] and $PhH^+\cdots Ar$,[46] which have demonstrated that the intermolecular $CH\cdots Ar$ bonds in $A(H)^+\cdots Ar$ dimers are less stable than the corresponding $\pi\cdots Ar$ bonds. Thus, $ImH^+\cdots Ar(C_1H)$, $ImH^+\cdots Ar(C_4H)$, and $ImH^+\cdots Ar(CC)$ will not be further investigated.

In addition to the NH-bound global minima, the interaction between the π electron system of ImH^+ and Ar is creating less stable minima located roughly above the center of the ring. The configuration resulting from the attachment of Ar to one of these sites is shown in Figure 4e and will be denoted $ImH^+\cdots Ar(\pi)$. Analysis of the vibrational modes shows that, much like in the case of Im^+,[36] Ph^+,[31],[37],[47] PhH^+,[48],[49] and other ionic species, such a π-bound structure is a local minimum of the intermolecular PES. From Table 4 it can be seen that the ligand is not affecting the properties of the ImH^+ fragment.

It is instructive to compare the parameters derived here for $ImH^+\cdots Ar(\pi)$ with the ones derived for $Im\cdots Ar(\pi)$ at the same theoretical level and via a rotational millimeter wave spectrum of neutral $Im\cdots Ar$. The latter has been previously recorded in a supersonic jet[50] and is consistent with a π-bound equilibrium structure. The preference of Im for π-bonding toward Ar in its singlet electronic ground state results from the fact that the dispersion

interaction between Ar and Im is maximal, when Ar interacts with the π-electron system of Im. The experimental separation between the Im ring and Ar is $r_{Im-Ar} \cong 3.48$ Å,[50] while the calculated value is $r^{calc}_{Im-Ar} \cong 3.49$ Å, once more demonstrating that the chosen theoretical level is properly describing the intermolecular interaction. Owing to the supplemental charge, the calculated ring - Ar separation of $ImH^+\cdots Ar(\pi)$ shrinks to $r^{calc}_{ImH+-Ar} \cong 3.43$ Å. The same supplemental interaction is driving the harmonic intermolecular stretch frequency ($\omega^s_{ImH+-Ar} = 54$ cm^{-1}) higher than the corresponding value calculated for $Im\cdots Ar(\pi)$ ($\omega^s_{Im-Ar} = 41$ cm^{-1}). For comparison, the experimental value of the $Im\cdots Ar(\pi)$ intermolecular stretch frequency is $v^s_{Im-Ar} = 44$ cm^{-1}.[50] The stronger interaction results also in a greater dissociation energy: $D^{calc}_{0,ImH+-Ar} = 350$ cm^{-1} > $D^{calc}_{0,Im-Ar} = 205$ cm^{-1}. If the calculations are equally underestimating the interaction, the experimental value $D_{0,Im-Ar} \cong 302$ cm^{-1} implies that a better approximation of $ImH^+\cdots Ar(\pi)$ D_0 would be $D_{0,ImH+-Ar} \cong 516$ cm^{-1}, which is similar with D_0 of other $A(H)^+\cdots Ar(\pi)$ systems ($D_{0,indole+-Ar} = 537\pm10$ cm^{-1},[51] $D_{0,aniline+-Ar} = 414\pm28$ cm^{-1},[52] etc.).

6.2.3. $ImH^+\cdots(N_2)_n$ (n = 1, 2)

Attachment of N_2 to ImH^+ has also been studied by analyzing the binding of N_2 to all protons (both C-H and N-H) dimers as well as to the π electron system of ImH^+. The structures corresponding to the equilibrium points identified via calculations are presented in Figure 5, while Table 5 summarizes the relevant parameters of these structures.

Figure 5. *Geometries of the equilibrium structures identified for $ImH^+\cdots N_2$: (a) NH-bound; (b) C_1H-bound; (c) C_4H-bound; (d) π-bound.*
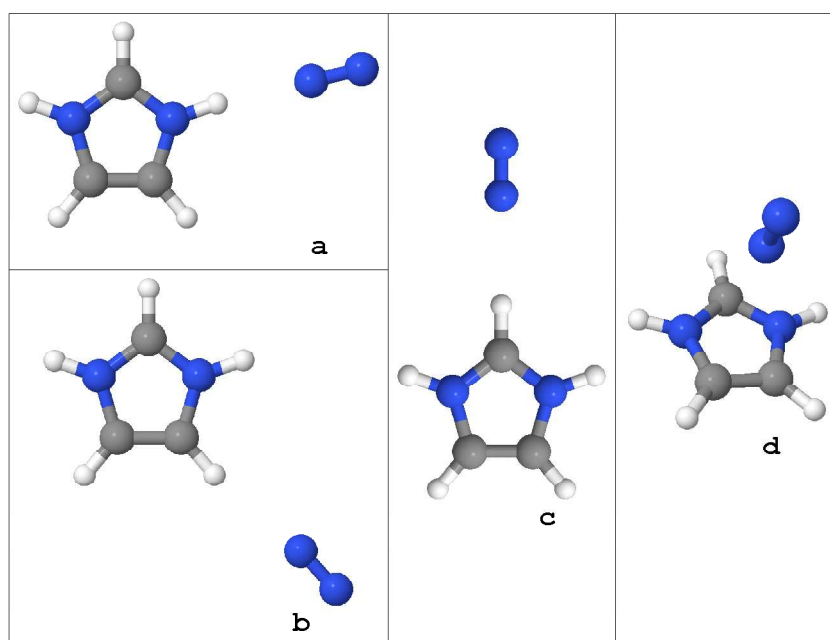
The NH-bound dimer (Figure 5a, further denoted $ImH^+\cdots N_2(NH)$) exhibits a planar structure with the axis of the N≡N bond almost overlapping with the one of the N-H bond

$(\theta_{N-H\cdots N2} = 174.7°$ and $\theta_{H\cdots N\equiv N} = 179.9°)$. It is known that the anisotropy of the long-range charge-quadrupole and charge-induced dipole interactions aligns the N_2 ligand in such a way that the molecular axis points toward the positive charge.[32],[37],[49],[53],[54],[44],[55],[56],[57],[58] The length of the intermolecular bond is smaller than the one calculated for $ImH^+\cdots Ar(NH)$ $(r_{HN2} = 2.10$ Å versus $r_{HAr} = 2.46$ Å) but larger than the one calculated for $Im^+\cdots N_2(H)$ (2.05 Å) because of the slightly different charge distribution. The binding energy of $ImH^+\cdots N_2(H)$, $D_0 = 1344$ cm^{-1}, is ~14% smaller than the one calculated for $Im^+\cdots N_2(H)$ at the same level of theory ($D_0 = 1561$ cm^{-1}). The expansion of the intramolecular N-H bond is $\Delta r_{NH} = 0.0058$ Å, much less than the one of $Im^+\cdots N_2(H)$: $\Delta r_{NH} = 0.0073$ Å. At the same time,

Table 5. *Properties of the intramolecular N-H and C-H bonds (r_{NH}, r_{CH}, ω_{NH}, ω_{CH}, I_{NH}, I_{CH}) and of the intermolecular bonds (r_{H-N2}, $r_{ring-N2}$, D_0, ω_s) for several $ImH^+\cdots(N_2)_n$ (n = 1, 2) isomers calculated at the MP2/6-311G(2df,2pd) level. The parameters of the bonds directly affected by complexation are indicated with* **bold** *numbers.*

complex	ImH$^+$	ImH$^+\cdots N_2$				ImH$^+\cdots (N_2)_2$
		NH	C$_1$H / C$_2$H	C$_4$H	π	NH & NH
r$_{C1H}$ (Å)	1.0739	1.0738	**1.075**	1.0738	1.0738	1.0737
r$_{C2H}$ (Å)	1.0739	1.0738	1.0738	1.0738	1.0738	1.0737
r$_{C4H}$ (Å)	1.0745	1.0744	1.0744	**1.0763**	1.0743	1.0742
r$_{N3H}$ (Å)	1.0106	**1.0164**	1.0104	1.0103	1.0102	**1.0157**
r$_{N5H}$ (Å)	1.0106	1.0102	1.0104	1.0103	1.0102	**1.0157**
ω_{CH} (cm^{-1}) I$_{CH}$ (km/mol)	3329 (27)	3330 (24)	**3321 (92)**	3330 (26)	3330 (25)	3329 (21)
ω_{CH} (cm^{-1}) I$_{CH}$ (km/mol)	3334 (69)	3335 (61)	3334 (74)	**3311 (180)**	3336 (66)	3336 (54)
ω_{CH} (cm^{-1}) I$_{CH}$ (km/mol)	3347 (18)	3347 (16)	3343 (18)	3347 (22)	3347 (15)	3347 (15)
ω_{NH} (cm^{-1}) I$_{NH}$ (km/mol)	3638 (397)	**3534 (732)**	3640 (392)	3641 (383)	3642 (385)	**3536 (1304)**
ω_{NH} (cm^{-1}) I$_{NH}$ (km/mol)	3645 (33)	3646 (189)	3647 (33)	3648 (31)	3649 (32)	**3551 (110)**
r$_{HN2}$ / r$_{ring-N2}$ (Å)		2.10	2.47	2.40	3.04	2.11
ω_s (cm^{-1}) I$_s$ (km/mol)		104 (12)	66 (6)	73 (8)	74 (5)	89 (2) 112 (15)
D$_0$ (cm^{-1})		1344	634	781	718	1327

the frequency of the corresponding stretch vibration shifts by $\Delta\omega_{NH} = -104$ cm^{-1} (2.9%) and its IR intensity grows 1.8 times; the red-shift calculated for $Im^+\cdots N_2(NH)$ was $\Delta\omega_{NH} = -129$ cm^{-1} (3.6%) and the IR intensity increased to 2.5 times the one of the bare

Im$^+$. The unchanged free N-H stretch vibration supports the assertion that the two N-H oscillators are only weakly coupled.

Subsequent attachment of another N_2 ligand to the free N-H group restores the C_{2v} symmetry of the complex (ImH$^+$···$(N_2)_2$(2NH)). With respect to ImH$^+$···N_2(NH), the intermolecular separation is only marginally increasing, r_{NH} becomes shorter, and the average D_0 is marginally decreasing. Also the red-shifts of the ω_{NH} stretch vibrations are smaller than the one of ImH$^+$···N_2(NH): $\Delta\omega_{NH}^s$ = -102 cm^{-1} and $\Delta\omega_{NH}^{as}$ = -95 cm^{-1}. All these changes signal the presence of non-cooperative three-body interactions. Probably the most important aspect is that the total IR activity of the ω_{NH} stretch vibrations increases to almost 3.3 times the one of the bare ImH$^+$.

Both CH-bound dimers (Figure 5b and Figure 5c) investigated were found to be stable. Their stabilization energies are much lower than the one seen for ImH$^+$···N_2(NH), in line with the lower acidity of the C-H bonds. The red-shifts of the bound C-H vibrations are modest (not more than -23 cm^{-1}); however, their IR intensities are greatly enhanced. At the same time, the frequencies of the two ω_{NH} are blue-shifting by 2 ... 3 cm^{-1}, signaling a minor reduction in acidity. Given the low values of D_0 for these systems, it is very probable that ImH$^+$···N_2(CH) dimers will not be produced in detectable amounts in the ion source.

The intermolecular PES of ImH$^+$···N_2 has, like the one of ImH$^+$···Ar, less stable minima located above the center of the ring (Figure 5d). The ligand is nearly perpendicular to the ring plane, slightly pointing toward C_5, which was found (via calculations) to hold the maximum partial positive charge. Intermolecular π-bonding is barely changing the properties of the N-H and the C-H bonds of ImH$^+$, with $|\Delta r_{NH}|$ < 0.0004 Å, $|\Delta r_{CH}|$ < 0.0002 Å, $\Delta\omega_{NH}$ ≤ 5 cm^{-1}, $\Delta\omega_{CH}$ ≤ 2 cm^{-1}, ΔI_{NH} < 5%, and ΔI_{CH} < 17%. The more compact structure of the π-bound system suggests an intermolecular interaction slightly stronger that the one of Im$^+$···N_2(π) ($r_{ring-N2}$ = 3.04 Å versus $r_{ring-N2}$ = 3.15 Å). This is however contradicted by the finding that the stabilization energy of the ImH$^+$···N_2(π) complex is much smaller (718 cm^{-1} versus 888 cm^{-1}). Considering that the spectrum of Im$^+$···N_2[36] had no feature corresponding to a π-bound isomer, it follows that π-bonding will probably be significant only for the late stages of the microsolvation of ImH$^+$.

6.2.4. ImH$^+$···$(H_2O)_n$(···N_2) (n = 0 ... 2)

Following the quantum chemical calculations done for ImH$^+$ complexated with one nonpolar ligand (Ar, N_2), the mono- and di-hydration of ImH$^+$ have been investigated. Also few complexes sharing the formula ImH$^+$···$(H_2O)_n$···N_2 (n = 0 ... 2) have been identified. The

Table 6. *Properties of the intramolecular N-H, C-H, and O-H bonds (r_{XH}, ω_{XH}, I_{XH}, X = N, C, O) and of the intermolecular bonds (r_{H-Ln}, r_{L-L}, D_0, ω_s, I_s) for the studied isomers of ImH⁺···(H₂O)ₙ(···N₂) (n = 1, 2), calculated at the MP2/6-311G(2df,2pd) level. Interatomic distances are given in Å, harmonic frequencies in cm⁻¹, IR intensities in km/mol, and binding energies in cm⁻¹. The parameters of the bonds directly affected by complexation are marked red. Oₙ refers to the water ligand Lₙ (see Figure 6).*

complex	ImH⁺	n	w1	w1n	w2a	w2an	w2b	w2bn
r_{C1H}	1.0739	1.0738	1.0736	1.0736	1.0735	1.0735	1.0735	1.0734
r_{C2H}	1.0739	1.0738	1.0736	1.0736	1.0735	1.0735	1.0735	1.0734
r_{C4H}	1.0745	1.0744	1.0741	1.0741	1.0740	1.0739	1.0739	1.0738
r_{N3H}	1.0106	1.0164	1.0353	1.0339	1.0505	1.0482	1.0306	1.0343
r_{N5H}	1.0106	1.0102	1.0095	1.0144	1.0090	1.0134	1.0306	1.0304
r_{O1H}			0.9589	0.9588	0.9734	0.9730	0.9585	0.9613
r_{O1H}			0.9589	0.9588	0.9572	0.9571	0.9585	0.9581
r_{O2H}					0.9581	0.9580	0.9585	0.9587
r_{O2H}					0.9581	0.9580	0.9585	0.9587
ω_{CH} (I_{CH})	3329 (27)	3330 (24)	3330 (22)	3330 (20)	3331 (18)	3331 (16)	3331 (20)	3331 (19)
ω_{CH} (I_{CH})	3334 (69)	3335 (61)	3337 (60)	3337 (55)	3338 (50)	3338 (45)	3339 (61)	3339 (55)
ω_{CH} (I_{CH})	3347 (18)	3347 (16)	3348 (10)	3348 (10)	3348 (8)	3348 (8)	3349 (2)	3349 (3)
ω_{NH} (I_{NH})	3638 (397)	3534 (732)	3190 (1609)	3212 (1641)	2926 (2467)	2962 (2479)	3249 (2669)	3197 (2282)
ω_{NH} (I_{NH})	3645 (33)	3646 (189)	3654 (190)	3564 (596)	3660 (175)	3578 (593)	3281 (249)	3274 (884)
ω_{OH} (I_{OH})			3871 (48)	3872 (47)	3620 (727)	3629 (680)	3875 (80)	3847 (180)
ω_{OH} (I_{OH})			3971 (123)	3973 (120)	3948 (106)	3949 (105)	3875 (6)	3958 (181)
ω_{OH} (I_{OH})					3882 (25)	3882 (25)	3977 (0)	3874 (42)
ω_{OH} (I_{OH})					3985 (100)	3986 (99)	3977 (232)	3976 (116)
r_{H-L1}		2.10	1.70	1.71	1.60	1.61	1.73	1.70

r_{H-L2}			2.13		2.15	1.73	1.74
r_{L-L}				1.78	1.79		2.21
ω_s^{H-L1} (I_s)	104 (12)	213 (29)	211 (33)	298 (26)	293 (27)	216 (35)	230 (39)
ω_s^{H-L2} (I_s)			97 (9)		93 (5)	189 (0)	196 (10)
ω_s^{L-L} (I_s)				185 (42)	184 (42)		96 (4)
D_0^{total}	1344	5348	6543	8835	9959	10207	10846

Figure 6. Geometries of the studied $ImH^+\cdots(H_2O)_n(\cdots N_2)$ ($n = 0 \ldots 2$) systems:

$n = ImH^+\cdots N_2$; $w1 = ImH^+\cdots H_2O$; $w1n = N_2\cdots ImH^+\cdots H_2O$;

$w2a = ImH^+\cdots H_2O\cdots H_2O$; $w2an = N_2\cdots ImH^+\cdots H_2O\cdots H_2O$;

$w2b = H_2O\cdots ImH^+\cdots H_2O$; $w2bn = N_2\cdots H_2O\cdots ImH^+\cdots H_2O$
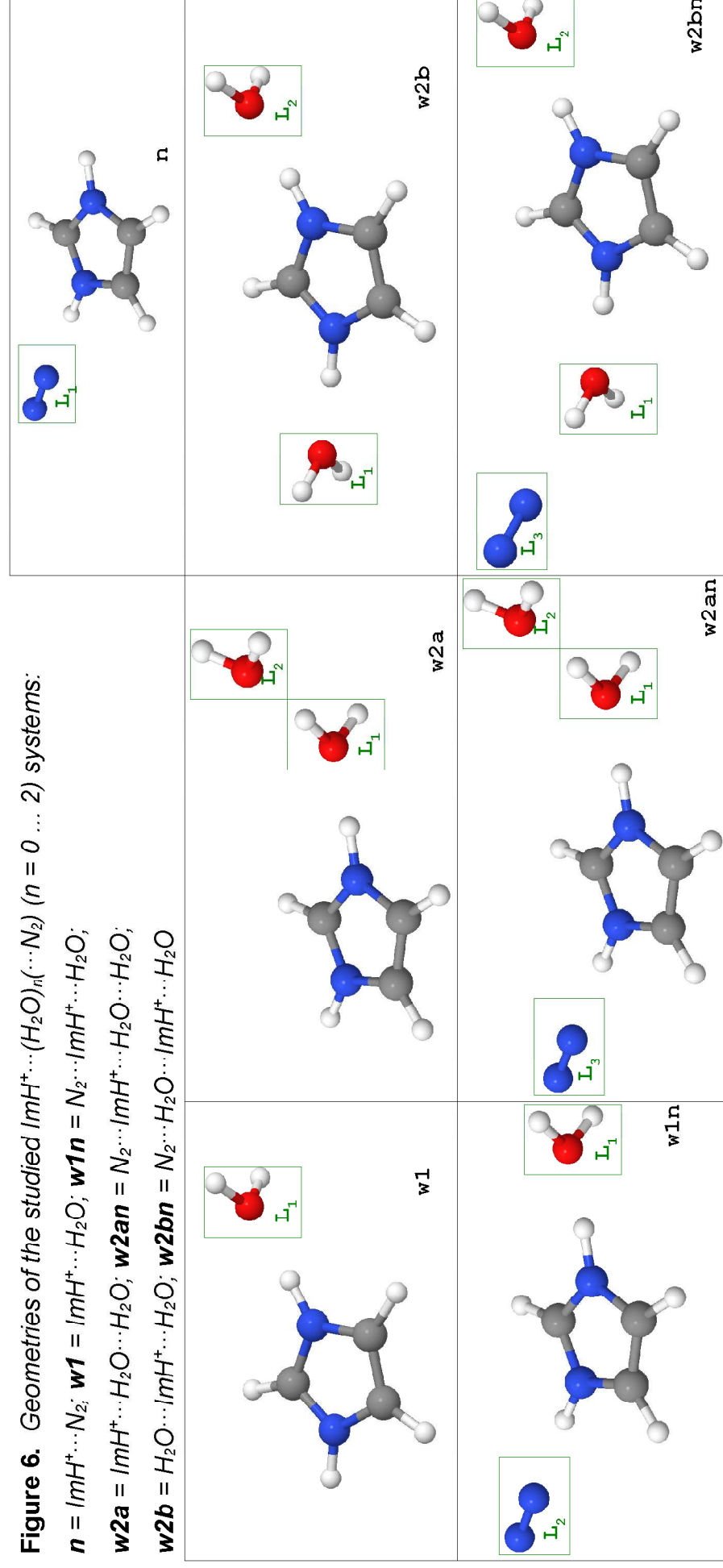
N_2 was attached to the $ImH^+\cdots(H_2O)_n$ ($n = 0 \ldots 2$) moiety via H-bonding to the most acidic proton (NH or OH, depending on availability). The equilibrium structures identified via calculations are presented in Figure 6, while Table 6 summarizes their relevant parameters. The total binding energies listed in Table 6 are the cumulative stabilization energies of the complexes calculated with respect to the involved monomers: ImH^+, H_2O, and N_2.

In line with previous calculations, the $N\text{-}H\cdots OH$ bonds of H_2O to the acidic NH groups of ImH^+ correspond to the most stable binding motif on the intermolecular potential of these ion-dipole complexes (**w1** in Figure 6). Like for all other NH-bound dimers, the three atoms involved in the bonding are almost collinear ($\theta_{N\text{-}H\cdots N2} = 177.7°$). This observation, together with the intermolecular distance ($r_{N\text{-}H\cdots N2} = 1.7$ Å), signals the formation of a weakly bound complex. Owing to the dipole moment of H_2O, the $N\text{-}H\cdots O$ bond is much stronger than the ones of the other investigated systems, resulting in $D_0 = 5348$ cm^{-1}, comparable with the experimental hydration enthalpy (5183 cm$^{-1[30]}$). Even so, the excess proton in **w1** is strongly localized on ImH^+, because the PA of Im exceeds by far that of H_2O (943 kJ/mol versus 691 kJ/mol). The effects of monohydration of ImH^+ via NH-bonding of the ligand are typical for H-bonding, resulting in a significant destabilization of the N-H bond, as indicated by the large bond elongation ($\Delta r_{NH}^h = 0.0247$ Å) and the reduction in the frequency of the corresponding proton stretching mode ($\Delta\omega_{NH}^b = -448$ cm^{-1}) coupled with the increase of its IR intensity (up by a factor 4). In contrast, the free N-H bond and the C-H bonds are nearly unaffected ($\Delta r_{NH}^f = -0.0011$ Å, $\Delta\omega_{NH}^b = 9$ cm^{-1}, $|\Delta r_{CH}| < 0.0004$ Å, $|\Delta\omega_{CH}| < 3$ cm^{-1}). On the other hand, the strong intermolecular interaction increases the acidity of the intramolecular O-H bonds of H_2O: $\Delta r_{OH} = 0.0020$ Å, $\Delta\omega_{OH}^s = -19$ cm^{-1}, $\Delta\omega_{OH}^a = -33$ cm^{-1}.

A consequence of the high D_0 of this dimer is that dissociation might occur only by multiphoton absorption or from already vibrationally excited states. As the energy density of the excitation laser beam used in the experiment is too low ($I < 200$ kW/cm^2) for multiple photon absorption to occur, it follows that all features observed in the dissociation channel $ImH^+\cdots H_2O + h\cdot\nu \rightarrow ImH^+ + H_2O$ are hot bands, resulting from the dissociation of already vibrationally excited $ImH^+\cdots H_2O$. Attachment of a NH-bound N_2 to this system (**w1n** in Figure 6) eliminates this problem, as D_0 of $ImH^+\cdots N_2(NH)$ is much lower than D_0 of $ImH^+\cdots H_2O(NH)$: 1344 cm^{-1} versus 5348 cm^{-1}. In general, the effects of the complexation of **w1** with a NH-bound N_2 are qualitatively similar to those observed in $ImH^+\cdots N_2(NH)$ but somewhat smaller in magnitude, as seen in Table 6 (columns **n**, **w1**, and **w1n**). For example, the total binding energy of this complex (6548 cm^{-1}) is slightly smaller than the

sum of the dimer binding energies (6692 cm^{-1}), signaling typical non-cooperative three-body interactions acting in ion solvation.

Figure 7. *PES of the proton transfer reactions between Im and H$_2$O (♦) and between Im and (H$_2$O)$_2$ (■). For each PES, the origin of the X axis is set on the donor N atom, while the origin of the Y axis is set on the stabilization energy of the corresponding equilibrium geometry. For each step of the PES scan the position of the acceptor O atom is indicated with ♦ for [Im-H-OH$_2$]$^+$ and with ■ for [Im-H-OH$_2$-OH$_2$]$^+$.*
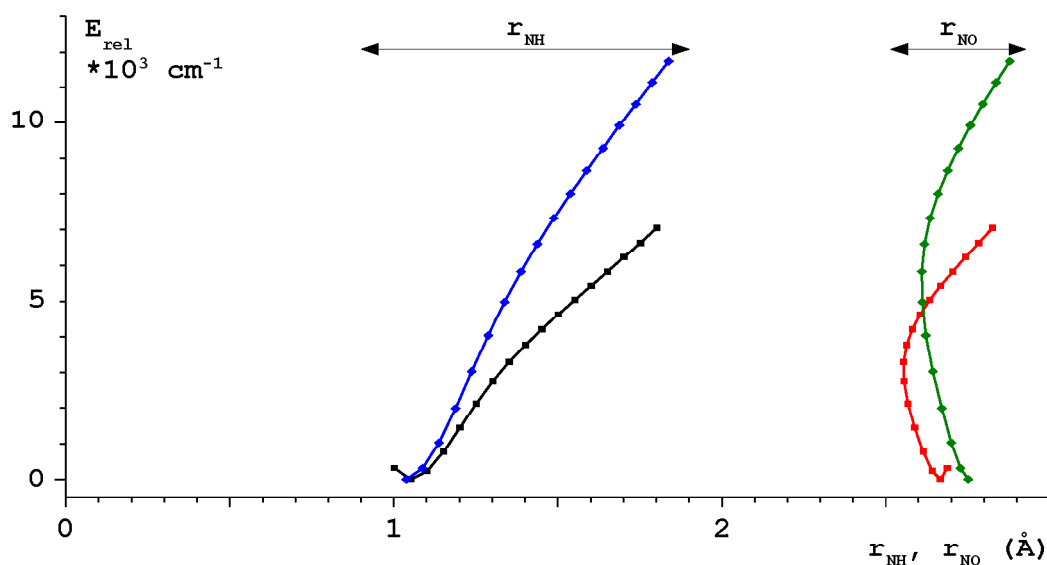
The microhydration of ImH$^+$ was followed by investigating the two most stable isomers of ImH$^+\cdots$(H$_2$O)$_2$, namely ImH$^+\cdots$H$_2$O$\cdots$H$_2$O (water chain solvating one NH proton of ImH$^+$, **w2a** in Figure 6) and H$_2$O$\cdots$ImH$^+\cdots$H$_2$O (water solvating both NH protons of ImH$^+$, **w2b** in Figure 6). The effects of the water chain on the N-H bonds are rather dramatic. The bound proton is pulled away from its normal position by Δr_{NH}^{b} = 0.0399 Å, the frequency of the corresponding stretch vibration decreases ($\Delta\omega_{NH}^{b}$ = -676 cm^{-1}) while its IR intensity increases more than 6 times. At the same time, the acidity of the free N-H bond drops: Δr_{NH}^{f} = -0.0016 Å, $\Delta\omega_{NH}^{b}$ = 15 cm^{-1}. The total binding energy of this complex, involving one intermolecular N-H$\cdots$O bond and one intermolecular O-H$\cdots$O bond amounts to 8835 cm^{-1}. It follows that, at this level of theory, the binding energy of the water dimer to ImH$^+$ is 8007 cm^{-1} (D$_0^{(H2O)2}$ = 828 cm^{-1}, quite far from the experimental ΔH_{375}^{0} = 1255 ± 175 cm^{-1} quoted by [59]). While in the case of **w2a** the two water molecules act together and weaken the N-H bond, in the case of **w2b**, due to non-cooperative three-body interactions, the two N-H bonds are less affected. This can be seen in the smaller elongation of the N-H bonds (Δr_{NH}^{b} = 0.0200 Å) and the blue-shifting of ω_{NH} with respect to **w1**. Also the total binding energy of the complex (10207 cm^{-1}) implies that D$_0$ of each ligand is just 5104 cm^{-1},

less than 80% of the dimer D_0, in good agreement with the decrease of the incremental hydration enthalpies measured for $ImH^+\cdots(H_2O)_n$.[30]

The possible proton transfer processes from ImH^+ to H_2O for the **w1** dimer and from ImH^+ to $(H_2O)_2$ for the **w2b** complex have been investiga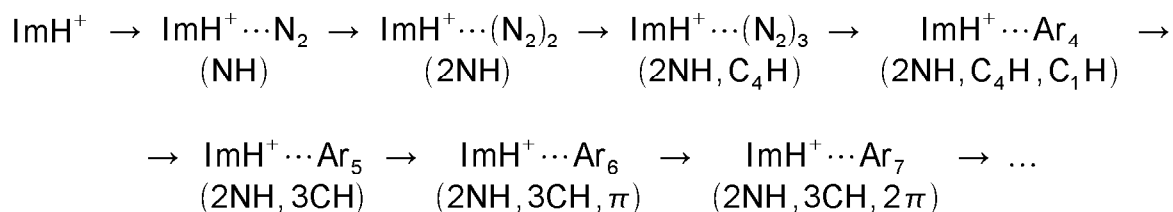ted by monitoring the total stabilization energy of the $[Im-H-OH_2]^+$ and $[Im-H-OH_2-OH_2]^+$, respectively, as a function of the N-H separation. The calculations have been done at the B3LYP/6-311(2df,2pd) level of theory, without BSSE corrections. The resulting PES are depicted in Figure 7 and demonstrate that, although the separation between Im and H_2O (Im and $(H_2O)_2$) initially decreases as the N-H separation increases, the PES is still characterized by one equilibrium position, corresponding to ImH^+. This is not unexpected, as the PA of both H_2O and $(H_2O)_2$ are smaller than the PA of Im (PA_{H2O} = 691 kJ/mol,[42] $PA_{(H2O)2}$ = 808 ± 6 kJ/mol,[60] PA_{Im} = 942.8 kJ/mol).[42]

6.2.5. Model for the microsolvation of ImH^+

According to the calculations, the H-bonds to the NH group in $ImH^+\cdots Ar$ are much more stable than the π-bonds; other binding sites (CH- or CC-) will not be discussed here because of the very low binding energies obtained. Knowing this order in dimer stability, one can predict that the strongest bound $ImH^+\cdots Ar_n$ clusters are the ones growing sequentially along the line:

$$ImH^+ \rightarrow ImH^+\cdots Ar \rightarrow ImH^+\cdots Ar_2 \rightarrow ImH^+\cdots Ar_3 \rightarrow ImH^+\cdots Ar_4 \rightarrow \ldots$$
$$(NH) \qquad (2NH) \qquad (2NH,\pi) \qquad (2NH,2\pi)$$
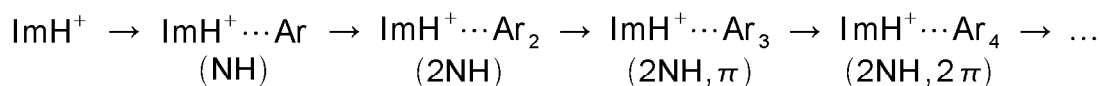
The picture of the microsolvation of ImH^+ in N_2 and the growth of the $ImH^+\cdots(N_2)_n$ complexes is by far more complicated. Within the limits of a simple model, which neglects the contributions of the non-cooperative three body interactions, one might try to extract a sequence of the microsolvation from the available calculations. Thus, based exclusively on the calculated stability of various dimer structures, the most energetically favorable microsolvation scheme is evaluated as:

$$ImH^+ \rightarrow ImH^+\cdots N_2 \rightarrow ImH^+\cdots(N_2)_2 \rightarrow ImH^+\cdots(N_2)_3 \rightarrow \quad ImH^+\cdots Ar_4 \quad \rightarrow$$
$$(NH) \qquad (2NH) \qquad (2NH,C_4H) \qquad (2NH,C_4H,C_1H)$$

$$\rightarrow ImH^+\cdots Ar_5 \rightarrow \quad ImH^+\cdots Ar_6 \quad \rightarrow \quad ImH^+\cdots Ar_7 \quad \rightarrow \ldots$$
$$(2NH,3CH) \qquad (2NH,3CH,\pi) \qquad (2NH,3CH,2\pi)$$

Because of the strong competition between the NH-, π-, and OH- binding sites, no model for microsolvation of ImH^+ in H_2O can be based exclusively on calculations. Thus,

no other estimation for the microhydration onset will be given except that, the first water ligand will probably be NH-bound.

6.3. Experimental details

IRPD spectra of mass-selected $ImH^+\cdots L_n$ complexes (L = Ar, N_2, H_2O, n ≤ 8) were recorded over the C-H, N-H, and O-H stretch ranges using the quadrupole - octopole - quadrupole tandem mass spectrometer coupled to the electron impact ion source (EI + QMF1 + OP + QMF2) described in the **Experimental setup** chapter and previously reported in literature.[61] Only the details specific to the $ImH^+\cdots L_n$ experiment will be presented in the following section. The expanding gas mixture was produced by seeding Im vapor (T ≅ 370 K) in the flow of the carrier / ligand gas (L = Ar, N_2 at static pressures of 4 ... 10 bar) mixed with a protonating agent (H_2, typical L:H_2 mixing ratio is 20:1). In the case of the $ImH^+\cdots(H_2O)_n(\cdots N_2)$ complexes, H_2O was supplied by flowing the N_2 carrier above a small vessel containing water. The pressure of the water vapor proved to be a critical parameter in these experiments; control over it was exerted by cooling the vessel close to the freezing point.

The ions produced via electronic bombardment of this gas mixture are involved in chemical and physical processes leading to the formation of ionic clusters. One of the paths toward these ionic clusters, having high production rate, is described in the following. Brønsted acids[62] XH^+ (X = H_2, Ar, N_2) are formed in the high pressure range of the supersonic expansion via ion-molecule reactions **(1)** & **(2)**:

$$H_2 + e^- \rightarrow H_2^+ + 2e^- \tag{1}$$

$$H_2^+ + X \rightarrow XH^+ + H \qquad (X = H_2, Ar, N_2) \tag{2}$$
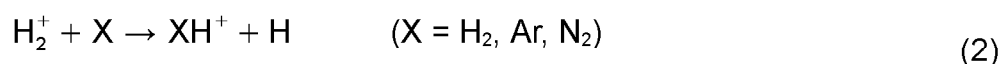
The proton is afterwards transferred to the Im molecule:[62]

$$Im + XH^+ \rightarrow ImH^+ + X \tag{3}$$

The $ImH^+\cdots L_n$ complexes are produced in the supersonic expansion via three-body collisions as shown in **(4)**[47]

$$ImH^+ \cdots L_n + L + M \rightarrow ImH^+ \cdots L_{n+1} + M \qquad M = Im, L; L = Ar, N_2 \tag{4}$$

Previous experiments of small (substituted and / or protonated) arenes are showing that reaction sequence (4) produces the most stable $A(H)^+\cdots L_n$ complexes and to smaller extent less stable isomers.[63] Figure 8 shows a mass spectrum of the ion source recorded

after optimization for $ImH^+\cdots(N_2)_n$ generation. The spectrum is dominated by $(N_2)_nH^+$ and $ImH^+\cdots(N_2)_n$ cluster ions. Im can fragment upon EI, resulting in a sequence of fragments out of which the strongest visible in the recorded mass spectrum corresponds to HCN loss,[64] leading to CH_2CNH^+ (41 u); a somewhat weaker fragment channel produces $HCNH^+$ (28 u), but the corresponding signal is masked by the very intense N_2H^+ peak. The intensity ratios of $ImH^+\cdots(N_2)_n$ are on the order of 40 : 3 : 1 for n = 0...2, confirming the formation of weakly bound noncovalent complexes, as described in (4).

Figure 8. *Mass spectrum of the EI ion source output, obtained after optimization for $ImH^+\cdots(N_2)_n$ generation; carrier gas was a 10:1 mixture of N_2 and H_2 at 6 bar stagnation pressure; the Im sample was heated at ~ 390 K. The major mass sequences are $(N_2)_nH^+$ (1 + n·28 u, labeled with ▲) and $ImH^+\cdots(N_2)_n$ (69 + n·28 u, labeled with ▲). In the low-mass range, peaks corresponding to NH_3^+ and H_3O^+ can easily be identified. The inset shows a vertically expanded version of the spectrum (X40) to ease the identification of weak signals.*
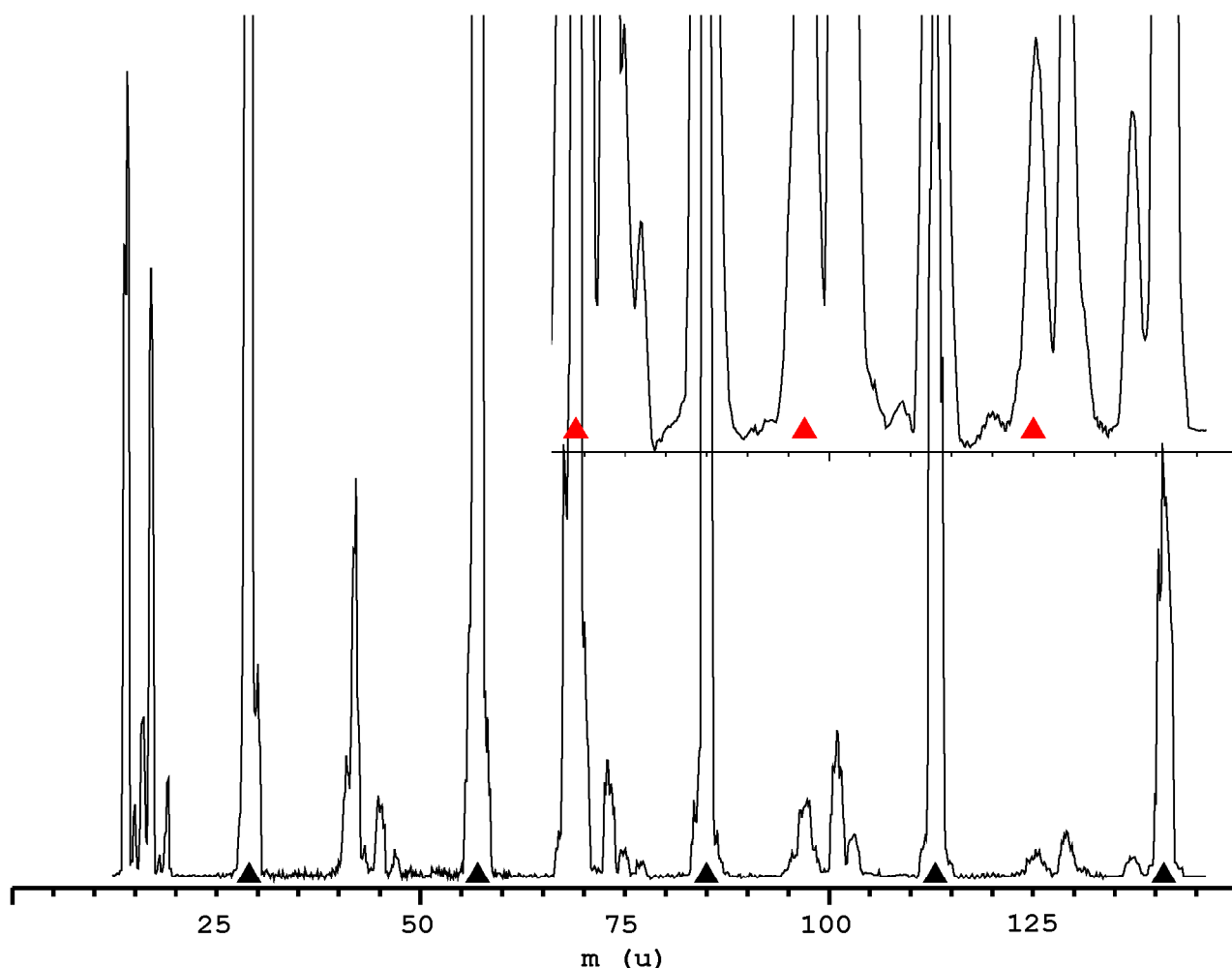
An important aspect of the mechanism described above is that the molecular ions

143

from **(3)** are "hot" (vibrationally excited). The energy from the excitation of one normal mode can "leak" into other normal modes via internal vibrational energy redistribution (IVR). This leads to the excitation of the intermolecular modes above the dissociation level, evaporating some of the ligands. This process occurs simultaneously with the three-body associations **(4)** and effectively drains the internal energy of the complex to a level lower than the binding energy of the weakest bound ligand.

The IR spectra of $ImH^+\cdots L_n$ are obtained by monitoring the amount of $ImH^+\cdots L_m$ fragments generated in the octopole by the absorption of the IR laser beam by $ImH^+\cdots L_n$ as a function of the wavelength of the excitation IR laser:

$$ImH^+\cdots L_n + h\cdot\nu \rightarrow [ImH^+\cdots L_n]^* \rightarrow ImH^+\cdots L_m + (n-m)\cdot L \qquad (5)$$

As the energy density of the excitation laser beam was too low ($I < 200$ kW/cm^2) for multiple photon absorption to occur, no other photodissociation channels were observed. Dissociation of $ImH^+\cdots(H_2O)_n$ complexes was observed exclusively as hot bands. For $ImH^+\cdots L_n$ parent complexes ($L = Ar, N_2$, $n > 1$), several fragment channels m were observed. Previous studies on related complexes demonstrated that the IR spectra recorded in the major fragment channels are similar.[32],[35],[47],[54] Consequently, IRPD spectra of $ImH^+\cdots L_n$ were recorded only in the dominant fragment channel.

Figure 9. *Mass spectra obtained by mass-selecting $ImH^+\cdots(N_2)_3$ with QMF1 and scanning QMF2. The lower trace was recorded without laser operation and the observed $ImH^+\cdots(N_2)_m$ fragment ions arise from metastable decay and / or collision induced dissociation with background gas. The upper trace was recorded while exciting the ν_{NH} stretch vibration of $ImH^+\cdots(N_2)_3$ (3396 cm^{-1}) which induces additional fragmentation into m = 0 (95%) and m = 1 (5%).*
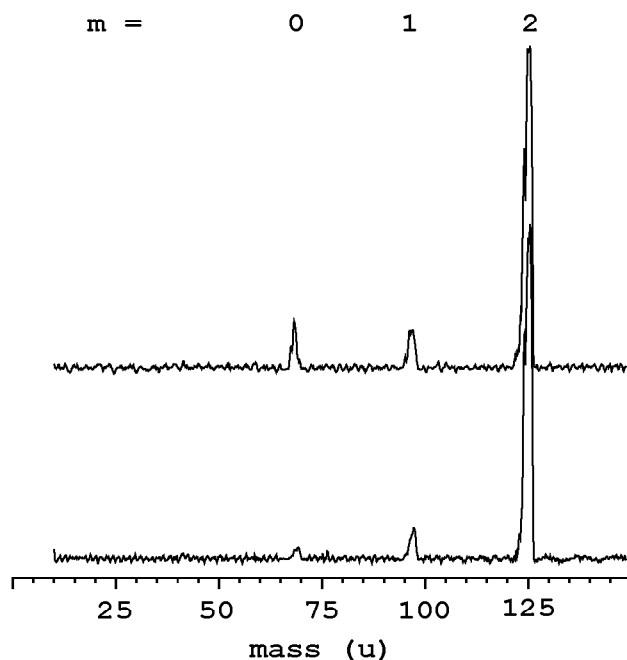
As an example, Figure 9 compares the mass spectra obtained for mass selecting $ImH^+\cdots(N_2)_3$ with QMF1 and scanning QMF2 without laser operation (lower part) and with resonant laser excitation (upper part). Without laser operation, the mass spectrum reveals

144

fragment ions arising from metastable decay (MD) of hot parent clusters and / or collision-induced dissociation (CID) with background gas in the octopole region for all three possible complex dissociation channels. The strength of these signals decreases as the number of lost ligands increases. The small fraction of MD demonstrates that the $ImH^+\cdots(N_2)_3$ complexes reaching the octopole region have, in average, little internal energy. When the laser beam is resonantly exciting a vibration of the $ImH^+\cdots(N_2)_3$ complex, the mass spectrum reveals additional fragmentation into both the m = 0 (95%) and m = 1 (5%) fragment channels caused by resonant laser-induced dissociation (LID).

A recording of the laser power (done using an InSb IR detector) is used to eliminate the ion signal fluctuations caused by variable laser power; this is done by linearly normalizing the ion signal on the laser power. Calibration of the laser frequency to an accuracy of better than 1 cm^{-1} was accomplished by comparing the optoacoustic spectrum of a reference substance (recorded simultaneously with the IRPD spectra) with literature tables. Depending on the investigated range, HDO, NH_3, and H_2O were used as reference substances.[65],[66]

6.4. Results and discussion

The IRPD spectra of $ImH^+\cdots Ar$ and $ImH^+\cdots N_2$, recorded over the C-H and N-H stretch ranges, are shown in Figure 10. The spectra of $ImH^+\cdots Ar_n$ (n = 1 ... 6) and the spectra of $ImH^+\cdots(N_2)_n$ (n = 1 ... 8) are presented in Figure 11. For all $ImH^+\cdots Ar_n$ and $ImH^+\cdots(N_2)_n$ systems, a list of band origins, their full width half maxima (FWHM) as well as their vibrational and isomeric assignments is presented in Table 7. Finally, the spectra of $ImH^+\cdots(H_2O)_n(\cdots N_2)$ (n = 0 ... 2) are displayed in Figure 12, while Table 8 presents a list of observed bands and their proposed assignments.

To support the assignment of the vibrational bands observed in the IRPD spectra of the $ImH^+\cdots L_n$ clusters, it is instructive to consider the frequencies of the N-H and C-H stretch fundamentals of the ImH^+ chromophore. No values have been found in literature for the v_{CH} and v_{NH} of the isolated (gas-phase) ImH^+. However, the frequencies of the C-H stretch vibrations (v_{CH}) have been observed via aqueous Raman spectra of imidazolium salts:[25] 3147 cm^{-1}, 3153 cm^{-1}, and 3180 cm^{-1}. No values have been reported for the frequencies of the N-H stretch modes. Also a solid-state IR spectrum of ImH^+Cl^- salt has revealed a massive absorption band spreading between 2000 cm^{-1} and 3300 cm^{-1}.[25] A number of structures have been identified inside this band and have been assigned to combination bands or harmonics of unspecified vibrational modes from below 2000 cm^{-1}

enhanced via Fermi resonance by a very broad ν_{NH}.[24],[25],[26] The values known for ν_{CH} are useful for generating scaling factors to be applied to the harmonic quantum chemical calculations. It must be stressed that the average scaling factor of 0.9470 found this way contains both the anharmonicity correction and solvation effects, so it is not very reliable.

Table 7. *Band maxima (in cm^{-1}), FWHM (in parentheses, in cm^{-1}), and proposed assignment for ImH^{+}···Ar$_n$ and ImH^{+}···(N$_2$)$_n$.*

n	m	Band	Position (FWHM) (cm^{-1})	Assignment	n	m	Band	Position (FWHM) (cm^{-1})	Assignment
			ImH^{+}···Ar$_n$					ImH^{+}···(N$_2$)$_n$	
1	0	A	3470 (10)	ν^f_{NH} (NH)	1	0	A	3473 (11)	ν^f_{NH} (NH)
		B	3425 (6)	ν^b_{NH} (NH)			B	3376 (10)	ν^b_{NH} (NH)
		C	3170 (14)	ν_{CH} (all)			C	3170 (16)	ν_{CH} (all)
2	0	A	3471 (8)	ν^f_{NH} (NH,π)	2	0	B	3381 (27)	ν^b_{NH} (2NH)
		B	3436 (16)	ν^b_{NH} (NH,?)			C	3172 (15)	ν_{CH} (all)
		C	3168 (12)	ν_{CH} (all)	3	0	B$_{31}$	3396 (17)	ν^b_{NH} (2NH,C$_4$H)
3	0	A	3472 (8)	ν^f_{NH} (NH,2π)			B$_{32}$	3417 (10)	ν^b_{NH} (2NH,π)
		B	3436 (12)	ν^b_{NH} (NH,2?)			B$_{41}$	3400 (11)	ν^b_{NH} (2NH,C$_4$H,C$_1$H)
4	0	B	3437 (5)	ν^b_{NH} (2NH,2?)	4	1	B$_{42}$	3414 (10)	ν^b_{NH} (2NH,C$_4$H,π)
5	0	B	3437 (5)	ν^b_{NH} (2NH,3?)			B$_{43}$	3425 (3)	ν^b_{NH} (2NH,2π)
6	1	B	3438 (4)	ν^b_{NH} (2NH,4?)	5	2	B$_{52}$	3421 (9)	ν^b_{NH} (2NH,C$_4$H,2π)
							B$_{54}$	3433 (5)	ν^b_{NH} (2NH,2π,X)
					6	2	B$_{62}$	3423 (7)	ν^b_{NH} (2NH,C$_4$H,2π,X)
					7	3	B$_{72}$	3424 (6)	ν^b_{NH} (2NH,C$_4$H,2π,2X)
					8	4	B$_{02}$	3428 (9)	ν^b_{NH} (2NH,C$_4$H,2π,3X)

Another approximation of this scaling factor can be obtained starting from the frequencies of the X-H stretch vibrations of neutral Im. The value of these frequencies are available from a gas-phase experiment:[67] ν_{NH} = 3518 cm^{-1} and ν_{CH} = 3160 cm^{-1}, 3135 cm^{-1}, and 3135 cm^{-1}. The scaling factor thus found (0.9503) will be used for an initial guess for the

assignment.

6.4.1. Spectra of ImH$^+$···L (L = Ar, N$_2$)

The spectra of ImH$^+$···L (L = Ar, N$_2$), together the with stick spectra of the calculated NH-bound dimers are presented in Figure 10. The calculated frequencies have been scaled by a factor (0.9525) whose inferring will be detailed in the following.

Figure 10. *IRPD spectra of ImH$^+$···Ar and ImH$^+$···N$_2$ recorded over the N-H and C-H stretch ranges in the ImH$^+$ fragment channel, together with the stick spectra of the calculated NH-bound dimers. The vibrational and isomer assignments of the transition observed (A, B, C) are listed in Table 7.*
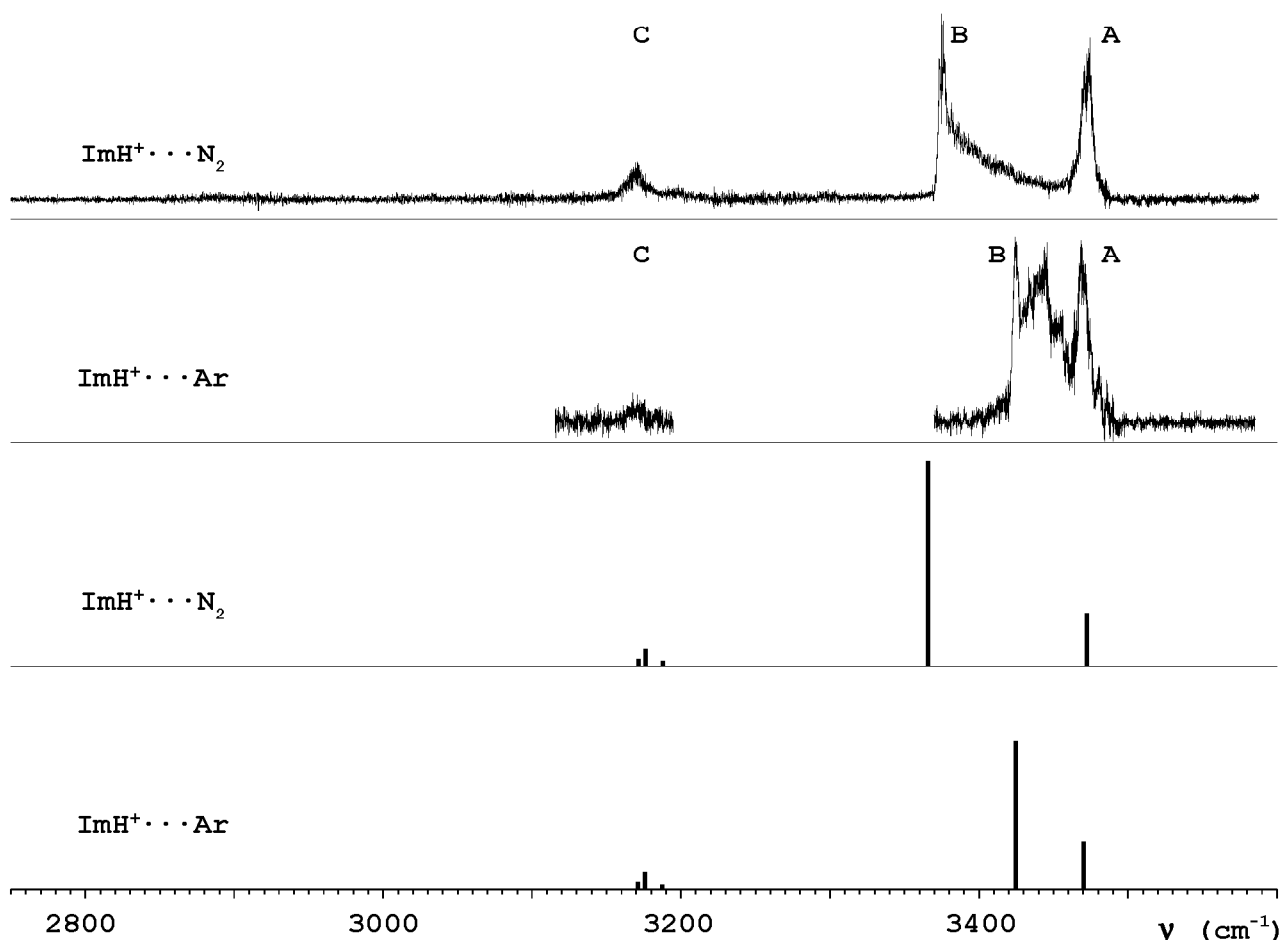
Similar with the spectrum of Im$^+$···Ar,[36] the spectrum of ImH$^+$···Ar exhibits a broad absorption in the N-H stretch range. Two bands can be identified within the observed structure. Given the position and the asymmetric, blue-shaded shape of band B (3425 cm^{-1}), it will be assigned to the Ar-bound ν_{NH} stretch vibration of Im$^+$···Ar(NH). As discussed in previous chapters, such a band contour is characteristic for the excitation of a proton donor stretch vibration, because the intermolecular H-bond becomes stronger and

147

shorter in the excited vibrational state, resulting in larger rotational constants.[53] The origin of the vibrational band is placed close to the sharp head of the band, hence the latter is taken in the present work as an approximate value for the band origin. This assignment for band B implies that at least part of the absorption exhibited in band A (3470 cm^{-1}) is the result of the IR activity of the free ν_{NH} fundamental of ImH$^+\cdots$Ar(NH). The rather symmetric shape of the band supports the assignment. Using this assignment for band A, the factor correcting the calculated harmonic frequencies results as 0.9525. The advantage of this scaling factor is that is based on experimental data directly connected with ImH$^+$; thus, this value will further be used to correct the harmonic calculations. Based on this scaling factor, the frequencies of the stretch vibrations of the bare ImH$^+$ are estimated as ν_{NH}^{as} = 3465 cm^{-1} and ν_{NH}^s = 3472 cm^{-1}. Knowing that the Ar-bound N-H stretch vibration is derived from antisymmetric mode of the bare ImH$^+$, it results that the complexation-induced red-shift of ν_{NH}^b amounts to -40 cm^{-1}.

It is remarkable that this assignment does not imply that ImH$^+\cdots$Ar(π) systems are not present in the ion beam. Even more, as such π-bound isomers have been observed in the ion beam of Im$^+\cdots$Ar, their presence here must be further investigated. Comparing the calculated binding energies of Im$^+\cdots$Ar(π) (388 cm^{-1}) and Im$^+\cdots$Ar(NH) (554 cm^{-1}) on one hand and of ImH$^+\cdots$Ar(π) (350 cm^{-1}) and ImH$^+\cdots$Ar(NH) (462 cm^{-1}) on the other hand, it results that the relative abundance of ImH$^+\cdots$Ar(π) should be even greater than the one of Im$^+\cdots$Ar(π). It is known that intermolecular π-bonding has essentially no influence on the properties of the N-H bond. This corresponds with the results of the quantum chemical calculations which suggest that both the N-H vibrations of ImH$^+\cdots$Ar(π) will be blue-shifted by a π-bound Ar ligand by a modest +1 cm^{-1} with respect to the bare ImH$^+$. At the same time, as the H-binding of Ar breaks the C$_{2v}$ symmetry of the ImH$^+\cdots$Ar(NH) and as Ar is a weak ligand, it results that the free stretch mode of the ImH$^+\cdots$Ar(NH) complex will be slightly red-shifted toward the average frequency of the two stretch modes of the bare ImH$^+$. Given also the 12:1 ratio between the IR intensities of the symmetric and the antisymmetric vibrations of ImH$^+\cdots$Ar(π) and the calculated positions of the bands involved, it results that the two most significant bands around 3440 cm^{-1} (band ν_{NH}^{as} of ImH$^+\cdots$Ar(π) and band ν_{NH}^f of ImH$^+\cdots$Ar(NH)) will probably be separated by just 4 cm^{-1}, less than the FWHM of the band A (8 cm^{-1}). The implication is that the positions of these bands cannot be further refined.

The C-H stretch range of the ImH$^+\cdots$Ar spectrum exhibits one weak absorption band centerer at 3170 cm^{-1}. A cursory investigation of Table 4 shows that the frequencies of the

C-H stretch vibrations (approximated as $0.9525 \cdot \omega_{CH}$) are spread over a maximum of 20 cm^{-1} around 3176 cm^{-1}. Both the position and the FWHM (14 cm^{-1}) of band C are consistent with these parameters.

The spectrum of ImH$^+$$\cdots$N$_2$ is characterized by bands similar as profile with the ones seen in the spectrum of ImH$^+$$\cdots$Ar. The major difference is that band B is now shifted at 3376 cm^{-1}. Assuming an assignment similar with the one of the ImH$^+$$\cdots$Ar spectrum, it follows that band B is red-shifted by -89 cm^{-1} with respect to $\nu_{NH}{}^s$ of ImH$^+$. This shift is more than double the one seen for ImH$^+$$\cdots$Ar, in line with the higher PA of N$_2$ (493.8 kJ/mol) with respect to the PA of Ar (369.2 kJ/mol).[42] The calculated position of this band is 3365 cm^{-1}, resulting in a slightly larger estimated red-shift, probably caused by an overestimation of the intermolecular interaction.

The free N-H vibration is estimated to be blue-shifted by +1 cm^{-1} with respect to the position of $\nu_{NH}{}^{as}$ in the bare ImH$^+$. This is consistent with the experimental observation: band A of ImH$^+$$\cdots$N$_2$ (3473 cm^{-1}) is +3 cm^{-1} blue-shifted with respect to band A of ImH$^+$$\cdots$Ar, which translates into a +2 cm^{-1} blue-shift with respect to the evaluated position of $\nu_{NH}{}^{as}$ of the bare ImH$^+$. It is remarkable that all other calculated dimer structures result in slightly larger blue-shifts of their $\nu_{NH}{}^{as}$ with respect to the bare ImH$^+$: for the second most stable investigated dimer (ImH$^+$$\cdots$N$_2$(C$_4$H)) this blue-shift amounts to +3 cm^{-1}, for ImH$^+$$\cdots$N$_2$($\pi$) it is +4 cm^{-1}, and for ImH$^+$$\cdots$N$_2$(C$_1$H) it drops to +2 cm^{-1}. Also the $\nu_{NH}{}^s$ of these dimers blue-shifts by +3 cm^{-1}, +4 cm^{-1}, and +2 cm^{-1}, respectively. It results that all the ν_{NH}-derived IR activity of the less stable dimers concentrates in a ~9 cm^{-1} range centered on the evaluated position of $\nu_{NH}{}^f$ of ImH$^+$$\cdots$N$_2$(NH). As the FWHM of band A (11 cm^{-1}) is larger than this range, it results that, like in the case of ImH$^+$$\cdots$Ar, the presence in the ion beam of isomers other than the NH-bound one cannot be neither directly confirmed nor infirmed. However, unlike the spectrum of ImH$^+$$\cdots$Ar, the spectrum of ImH$^+$$\cdots$N$_2$ is characterized by almost complete separation of bands A and B. This allows for an indirect estimation of the abundance of ImH$^+$$\cdots$N$_2$(NH) with respect to other species. Indeed, this is possible assuming that the observed IR activity around bands A and B is not distorted by laser power fluctuations and that the quantum chemical calculations accurately depict the ratio between the IR intensities of $\nu_{NH}{}^f$ and $\nu_{NH}{}^b$ of ImH$^+$$\cdots$N$_2$(NH). The calculated 3.9:1 IR intensity ratio (Table 5) results in the assignment to $\nu_{NH}{}^b$ of ImH$^+$$\cdots$N$_2$(NH) of only ~65% from the IR activity around 3473 cm^{-1}.

The C-H stretch range of the ImH$^+$$\cdots$N$_2$ spectrum exhibits, like the one of ImH$^+$$\cdots$Ar, just one absorption band (C) centered on 3170 cm^{-1}, with a FWHM of 16 cm^{-1}. Given that

the abundance of $ImH^+ \cdots N_2(NH)$ greatly exceeds the abundance of any other isomer, it is quite probable that the absorption in the C-H range will be dominated by IR activity of $ImH^+ \cdots N_2(NH)$ dimers. At the same time, a cursory investigation of Table 5 shows that the frequencies of all the free C-H stretch vibrations (approximated as $0.9525 \cdot \omega_{CH}$) are spread over a 16 cm^{-1} range around 3177 cm^{-1}, thus being indiscernible in the conditions of the present experiment. On the other hand, the bound C-H stretch vibrations are red-shifted by a maximum of -23 cm^{-1}, thus being well separated from the other vibrations. Given the characteristics of the experimental spectrum, band C will only be generically assigned to $v_{NH}{}^f$ of $ImH^+ \cdots N_2(NH)$ and, possibly, of other unidentified $ImH^+ \cdots N_2$ isomers.

6.4.2. Spectra of $ImH^+ \cdots Ar_n$ (n = 1 ... 6)

The spectra of $ImH^+ \cdots Ar_n$ (n = 1 ... 6) are presented in Figure 11. The spectrum of $ImH^+ \cdots Ar_2$ reveals three bands A, B, and C, at 3471 cm^{-1}, 3425 cm^{-1}, and 3170 cm^{-1}, respectively. Their assignment is similar with the one of the bands seen in the dimer spectrum. It follows that the v_{NH} bands are characterized by small incremental blue shifts of $\Delta v_{NH}{}^f = +1$ cm^{-1} and $\Delta v_{NH}{}^b = +11$ cm^{-1} from the corresponding dimer transitions. The reduced IR activity around band A signals that although the NH- is the favored binding site, other sites (probably π-) are actually competitive and result in a significant population in the ion beam. As a consequence of the different dimer binding energies calculated in the theoretical section, one can assume that the most favored assignment of band A is to a $ImH^+ \cdots Ar(NH,\pi)$ complex. It is remarkable that band C red-shifts by -2 cm^{-1}; it is very probable that this displacement is not the result of red-shifts of any v_{CH}, but of changes in the dominant binding model from the dimer to the trimer. Indeed, if one assumes that the frequencies of v_{CH} of all dimers are slightly different one from the other but do not change upon further complexation, a change in the dominant binding model from the dimer to the trimer will result in an enhancement of the IR activity in a slightly different position inside band C.

Analyzing the $ImH^+ \cdots Ar_3$ spectrum, it can be seen that the incremental blue-shift of band B is +1 cm^{-1}. This is perfectly understandable as it is known from the dimer calculations that a ligand binding to a site other than NH- has little influence on the properties of the N-H bonds. Assuming that NH- is the most favored binding site, it follows that $ImH^+ \cdots Ar_2(2NH)$ is the dominant type of trimer. Assuming now that complexes are produced in an incremental fashion (see Eq. **(4)**), it results that the bulk of the $ImH^+ \cdots Ar_n$ (n >2) will be comprised from complexes of type (2NH,(n-2)X), with the properties of the

Figure 11. *The IRPD spectra of ImH$^+$···Ar$_n$ (n = 1...6) and ones of ImH$^+$···(N$_2$)$_n$ (n = 1...8). The photodissociation channel is indicated as n→m (see Eq. (5)). The vertical bands are underlining related bands, indicated on the figure.*
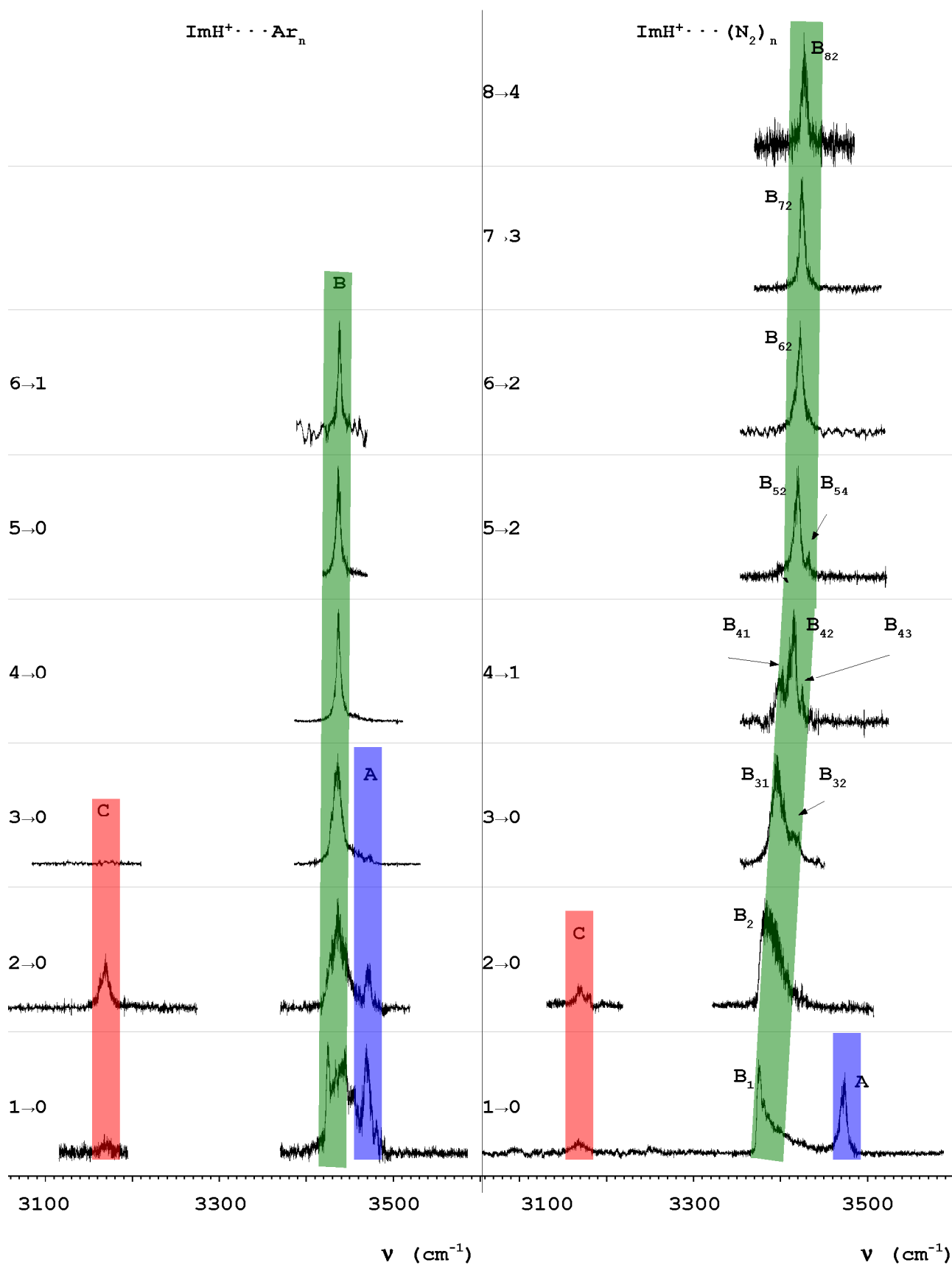
two solvated N-H bonds insensitive to the (n-2) ligands attached to other sites.

The most remarkable feature of the $ImH^+\cdots Ar_3$ spectrum is the presence of band A, slightly blue-shifted (3472 cm^{-1}) with respect to the positions seen in the dimer and trimer spectra. This is another element signaling the competition between NH- and other binding sites. This band (A) is not visible anymore starting from $ImH^+\cdots Ar_4$, meaning that the PES describing interaction between ImH^+ and Ar is characterized by four deep minima and, possibly, by a number of other less favorable binding sites. It must be stressed that this description does not imply equal depth of the PES in all four primary binding sites. Based on these estimations and on the calculations done for various dimers, the simplest solvation model is

$$ImH^I \rightarrow \underset{(NH)}{ImH^I\cdots Ar} \rightarrow \underset{(2NH)}{ImH^+\cdots Ar_2} \rightarrow \underset{(2NH,\pi)}{ImH^+\cdots Ar_3} \rightarrow \underset{(2NH,2\pi)}{ImH^+\cdots Ar_4} \rightarrow \ldots$$
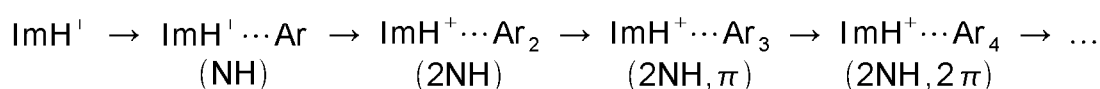
As it can be seen from Figure 11, this model holds true at least up to n = 6. Given the limited photofragmentation information available, binding energy of Ar toward ImH^+ can be given only as an average value: D_0 = 630 ± 55 cm^{-1}.

6.4.3. Spectra of $ImH^+\cdots(N_2)_n$ (n = 1 ... 8)

The spectra of $ImH^+\cdots(N_2)_n$ (n = 1 ... 8) are presented in Figure 11. The microsolvation of ImH^+ in N_2 unfolds in a completely different sequence, as revealed by the trimer spectrum. Here band A is not detectable, implying that, on the PES describing the interaction between ImH^+ and N_2, the NH- sites are much deeper minima than any other sites. Band B, blue-shifted by +5 cm^{-1} with respect to the position seen in the dimer spectrum, is still the dominant feature of the spectrum; its FWHM increases from 10 cm^{-1} (in the dimer spectrum) to 27 cm^{-1}. The incremental blue-shift is larger than the one estimated by the calculations (5 cm^{-1} versus 2 cm^{-1}), probably because band B is actually an envelope covering both ν_{NH}^s and ν_{NH}^{as} of $ImH^+\cdots(N_2)_2(2NH)$. Like in the case of $ImH^+\cdots Ar_2$, the highest IR activity in band C shifts by +2 cm^{-1}.

The $ImH^+\cdots(N_2)_3$ spectrum reveals one interesting feature: aside from the main feature of the spectrum (B_{31}, at 3396 cm^{-1}), one more weak band rises in the same range (B_{32}, at 3417 cm^{-1}). A possible explanation is that, while the first two ligands are clearly NH-bound, the third one can bind in two different sites. It is assumed that these sites are characterized by not-so-different binding energies but largely different impact over the intramolecular N-H bonds. This logical construct seems to be supported by the dimer calculations, which are placing the two π- binding sites slightly higher on the intermolecular

PES than the C_4H- binding site. Even more, while $ImH^+ \cdots N_2(\pi)$ is characterized by a +4 cm^{-1} shift of both ν_{NH} vibrations, it can be seen that this blue-shift decreases to +3 cm^{-1} for $ImH^+ \cdots N_2(C_4H)$. This implies that the dominant feature of the $ImH^+ \cdots (N_2)_3$ spectrum (B_{31}) will be assigned to $ImH^+ \cdots (N_2)_3(2NH,C_4H)$ while the minor feature (B_{32}) will be assigned to $ImH^+ \cdots (N_2)_3(2NH,\pi)$.

Based on the scheme underlined above, the spectrum of $ImH^+ \cdots (N_2)_4$ will be rationalized the following way. Band B_{41} will be assigned to a complex having two NH-bound ligands, one C_4H-bound one, while the remaining ligand is supposed to be bound to some other site than π (most probable C_1H-bound); this assignment fits well with the small incremental blue-shift observed (+4 cm^{-1}). The dominant band (B_{42}) will be assigned to a complex having two NH-bound ligands, one C_4H-bound one, and one π-bound one. It is then obvious that the direct ascendant of this band is B_{32}, which implies that the incremental complexation-induced shift goes toward red (-3 cm^{-1}). It means then that the C_4H-bound and the π-bound ligands are actually hindering one another, thus weakening their influence on the ImH^+ moiety and allowing for a stronger interaction via the acidic N-H protons. The minor band B_{33} is assigned to the $ImH^+ \cdots (N_2)_3(2NH,2\pi)$ isomer.

The spectrum of $ImH^+ \cdots (N_2)_5$ exhibits just two bands. The strongest band, B_{52}, appears blue-shifted with respect to B_{42} but red-shifted with respect to B_{43} (3414 cm^{-1} versus 3421 cm^{-1} versus 3425 cm^{-1}). In line with the previous assignments, it will be associated with an isomer having two NH-bound ligands (large red-shift with respect to A of $ImH^+ \cdots N_2$), two π-bound ones (rather strong complexation-induced blue-shift with respect to B of $ImH^+ \cdots N_2$), and one C_4H-bound one (the complexation-induced blue-shift with respect to B of $ImH^+ \cdots N_2$ is slightly smaller than the one of B_{33}). The minor band B_{54} will be assigned to the $ImH^+ \cdots (N_2)_3(2NH,2\pi,X)$ isomer; the most probable identification of X is C_1H.

The spectra of $ImH^+ \cdots (N_2)_n$ (n = 6, 7, 8) are relatively featureless, as probably all the relevant binding sites are occupied by ligands. Thus, the spectra feature just one band, blue-shifting by circa +3 cm^{-1} per ligand with respect to B_{52}. It results that the most probable assignment of these bands is $ImH^+ \cdots (N_2)_n(2NH,C_4H,2\pi,(n-5)X)$.

Analysis of the photofragmentation data results in estimations for the binding energies. Although not correct, all binding sites bar the NH- ones will be regarded as being characterized by equal binding energies. It results then that the binding energy between ImH^+ and N2 via an NH- binding site must be 1100 ± 250 cm^{-1}. This value does not contain any approximation regarding the solvation model, other than the assumption that the

intermolecular NH-bonds are more stable than any other bonds. Also an average value can be inferred for the stabilization energies of all other binding sites: 770 ± 85 cm^{-1}.

6.4.4. Spectra of ImH^{+}···(H$_2$O)$_n$(···N$_2$) (n = 1, 2)

Both IRPD spectra of ImH^{+}···(H$_2$O)$_n$ (n = 1, 2) shown in Figure 12 were obtained by monitoring the photoinduced loss of a single H$_2$O ligand. The IRPD spectra of ImH^{+}···(H$_2$O)$_n$···N$_2$ (n = 1, 2), also shown in Figure 12, were obtained by monitoring the

Table 8. *The positions of the bands observed in the ImH^{+}···(H$_2$O)$_n$(···N$_2$) (n = 1, 2) spectra and some tentative assignments.*

band	position (cm^{-1})	assignment	band	position (cm^{-1})	assignment
	ImH^{+}···H$_2$O			ImH^{+}···H$_2$O···N$_2$	
X1	2895	?	X1	2897	?
			X3	3000	?
			X4	3079	?
X2	3123	?	X2	3109	?
			C	3170	ν_{CH}
			X5	3215	?
A	3468	ν_{NH}^{f}	B	3405	ν_{NH}^{b}
W1	3630	ν_{OH}^{s}	W1	3640	ν_{OH}^{s}
W2	3710	ν_{OH}^{as}	W2	3725	ν_{OH}^{as}
	ImH^{+}···(H$_2$O)$_2$			ImH^{+}···(H$_2$O)$_2$···N$_2$	
X1	2899	?	X1	2903	?
			X4	3003	?
X2	3031	?	X2	3036	?
			X5	3095	?
			X6	3124	?
			C	3174	ν_{CH}
X3	3150	?	W5	3361	ν_{OH}^{b}
A	3482	ν_{NH}^{f}	B	3427	ν_{NH}^{b}
			W1	3624	ν_{OH}
			W2	3645	ν_{OH}
W1	3634	ν_{OH}	W3	3715	ν_{OH}
W2	3718	ν_{OH}	W4	3731	ν_{OH}

evaporation of the N$_2$ ligand. The positions and tentative assignments for the observed transitions are collected in Table 8. As the dissociation energies (D$_0$ = 5348 cm^{-1} for

Figure 12. *The IRPD spectra of ImH$^+$$\cdots$(H$_2$O)$_n$($\cdots$N$_2$) (n = 1, 2) and the stick spectra of the theoretically investigated complexes. In order to better illustrate the less IR active vibrational modes, all stick spectra are plotted just between 0 km/mol and at 1000 km/mol. The inverted triangles mark the O-H vibrations.*
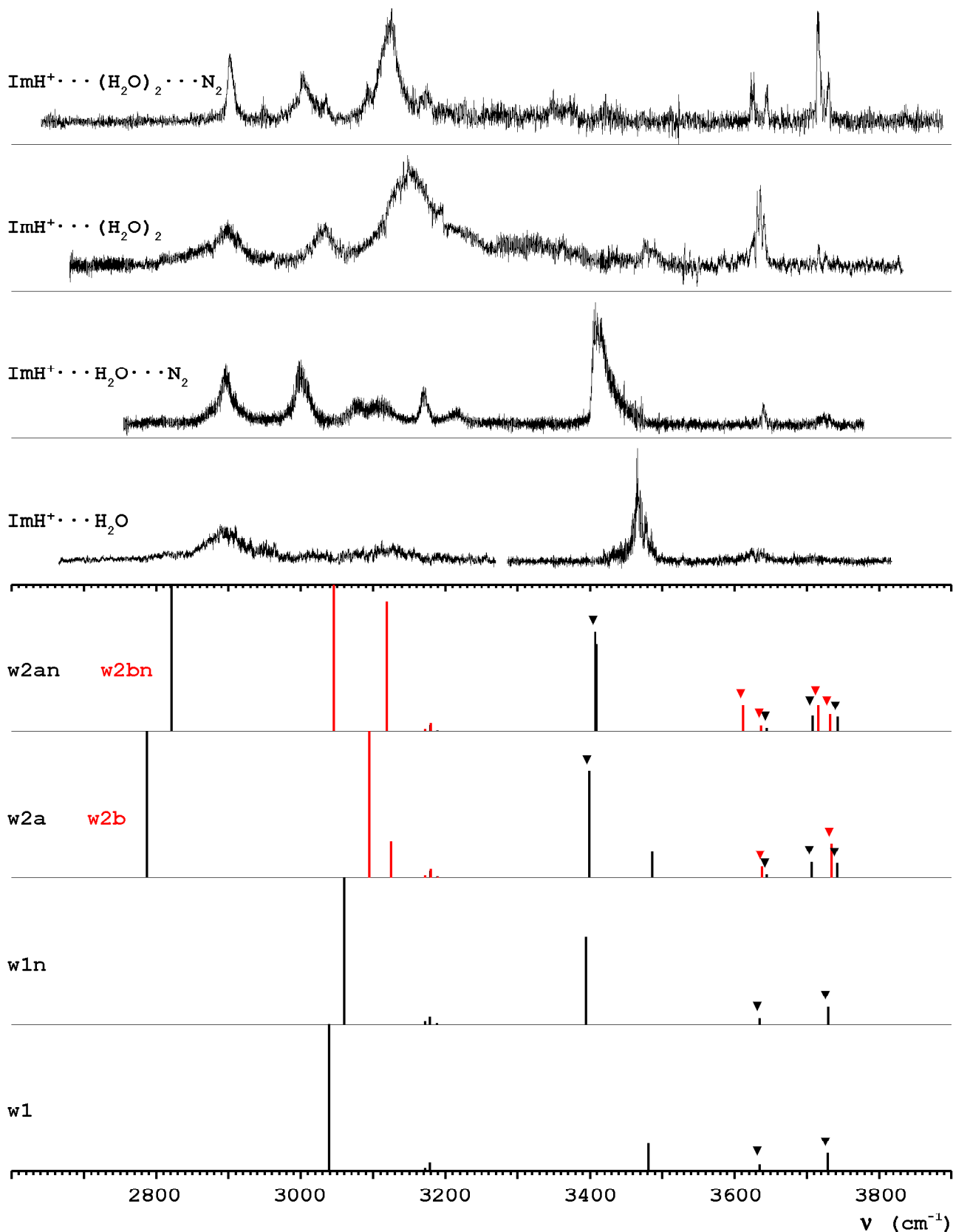
$ImH^+\cdots H_2O$ and $D_0^{total} = 8835\ cm^{-1} / 10207\ cm^{-1}$ for $ImH^+\cdots(H_2O)_2)$ are larger than the frequency of any observed fundamental, only the $ImH^+\cdots(H_2O)_n$ population with internal energy in excess of ~2000 cm^{-1} can be photodissociated under the single-photon absorption conditions. Thus, the observed transitions are, in fact, not fundamental bands but sequence hot bands involving inter- and intramolecular modes (which explains why these bands are relatively broad). Previous experiments with related complexes revealed only minor frequency shifts between the fundamentals and the corresponding sequence transitions.[62],[63],[68]

The predicted harmonic frequencies of the stretch vibrations have been rescaled using the generic factor (0.9525). While this factor is acceptable for the stretch vibrations of ImH^+, it is completely inadequate for the O-H vibrations of H_2O, resulting in 3705 cm^{-1} and 3814 cm^{-1} for the frequencies of the stretch vibrations of H_2O, far from the experimental values (3657 cm^{-1} and 3756 cm^{-1}).[69] In this case, the frequencies of the O-H vibrations will be scaled by 0.9389, which optimizes the match between the evaluated and measured positions of v_{OH}^s and v_{OH}^{as} of H_2O. Scaled stick spectra are presented in Figure 12, together with the corresponding experimental spectra.

Given the complexity of the spectra, they cannot be interpreted independently. Analyzing all experimental spectra, it results that, in general, the IRPD spectra confirm the spectroscopic trends predicted theoretically. As a general trend, it can be seen that the transitions observed in the $ImH^+\cdots(H_2O)_n\cdots N_2$ spectra are narrower than their $ImH^+\cdots(H_2O)_n$ counterparts. It is also relevant to note that the $ImH^+\cdots(H_2O)_n\cdots N_2$ spectra exhibit in the range under 3300 cm^{-1} many more features than the corresponding $ImH^+\cdots(H_2O)_n$.

The O-H stretch range of the $ImH^+\cdots H_2O(\cdots N_2)$ spectra can be completely assigned. The presence in each spectra of only two O-H bands (W1 and W2) suggests that indeed, the H_2O ligand is binding to one of the N-H acidic protons (**w1** on Figure 6). This is confirmed by the presence in the $ImH^+\cdots H_2O$ spectrum of a rather symmetrically shaped band (A) in a position consistent with the v_{NH}^f (here at 3468 cm^{-1}, 3470 cm^{-1} in the $ImH^+\cdots Ar$ spectrum, 3473 cm^{-1} in the $ImH^+\cdots N_2$ spectrum). Even more, analyzing the spectrum of $ImH^+\cdots H_2O\cdots N_2$, it can clearly be seen that, as expected, the v_{NH}^f vibration is replaced by a blue-shaded band (B) red-shifted by -63 cm^{-1} with respect to the position of A from the $ImH^+\cdots H_2O$ spectrum. Owing to the three-body non-cooperative interaction between ImH^+, H_2O, and N_2, the red-shift of band B (with respect to the bare ImH^+) is considerably smaller than the one seen in the $ImH^+\cdots(N_2)_n$ spectra. Thus, band B will be assigned to the N_2-bound v_{NH}^b of a **w1n** complex (see Figure 6). It is significant that while the addition of a N_2 molecule to the $ImH^+\cdots H_2O$ system results in a slight destabilization of the

intramolecular O-H bonds (v_{OH}^s blue-shifts by +10 cm^{-1} while v_{OH}^{as} blue-shifts by +15 cm^{-1}), this effect is completely missing from the calculations. Analysis of the range under 3300 cm^{-1} is considerably more difficult. The only feature which can be positively identified is band C in the spectrum of ImH$^+$···H$_2$O···N$_2$ which can easily be interpreted as derived from the v_{CH} of ImH$^+$. Band X1 cannot be associated with v_{NH}^b (the stretch vibration of the H$_2$O-bound proton) because it appears basically in the same position in all four recorded spectra.

The O-H stretch range of ImH$^+$···(H$_2$O)$_2$ exhibits two bands in the range above 3600 cm^{-1} (W1 and W2), suggesting that the preferred binding model is the one of **w2b** (Figure 6). Analysis of the data from Table 6 shows that this isomer is characterized by the highest total binding energy from the two structures investigated. This finding, combined with the fact that the frequencies of all recorded vibrations are well under the dissociation energy of such a complex, weaken the strength of the assignment. Indeed, if IRPD action is to be observed, the amount of energy which must be stored in the complex before IR excitation grows as the binding energy of the complex increases. Furthermore, the weak band A (3482 cm^{-1}) is readily assigned to the v_{NH}^f vibration of a **w2a** isomer. This means that the ImH$^+$···(H$_2$O)$_2$ parent population must be regarded as consisting of a mixture of **w2a** and **w2b** isomers.

The characteristics of the ImH$^+$···(H$_2$O)$_2$···N$_2$ spectrum are consistent with the ones of the related ImH$^+$···(H$_2$O)$_2$. Here, the addition of the weakly bound N$_2$ has a beneficial effect over the quality of the recording as the binding energy of N$_2$ to the ImH$^+$···(H$_2$O)$_2$ system is considerably smaller than the frequency of any observed vibration. This results on one hand in the reduction of the FWHM of all observed features (as the observed complexes are cooler) and on the other hand in a better signal-to-noise ratio (because the fraction of complexes which will dissociate does not depend anymore on their internal energy). These improvements allow the observation of four bands in the range above 3600 cm^{-1}, possibly originating from O-H stretch vibrations (W1, W2, W3, and W4,). It is relevant to analyze now the calculated positions of the O-H stretch vibrations (Table 6). In each case, due to complexation of one O-H bond, the frequency of the corresponding stretch vibration is red-shifted, well under 3600 cm^{-1} even for **w2bn**. It results then that it is not possible to assign the observed bands to just one isomer, lending support to the assertion that the ImH$^+$···(H$_2$O)$_2$ parent population is comprised of two largely different isomers. Analysis of the range of the ImH$^+$···(H$_2$O)$_2$···N$_2$ spectrum corresponding to band A in the ImH$^+$···(H$_2$O)$_2$ spectrum reveals that this band has vanished, being replaced by two weak features at 3361 cm^{-1} and 3427 cm^{-1}. As suggested by calculations, they will be assigned to the

N_2-bound N-H vibration of the **w2an** isomer (band B at 3427 cm^{-1}) and to the H_2O-bound O-H vibration of the same **w2an** isomer (band W5 at 3361 cm^{-1}). This assignment stems from the observation that the acidity of the free N-H group of **w2a** must be smaller than the acidity of the bare ImH^+ and of **w1**. The lower acidity is the result of the intermolecular interaction between ImH^+ and the water dimer which strongly destabilizes one intramolecular N-H bond while strengthening the other one. Such lowering in the acidity of the N-H proton to which the N_2 ligand is attached implies that the ν_{NH}^{bN2} vibration must occur at higher wavenumber position than the corresponding ones in the $ImH^+ \cdots N_2$ and $ImH^+ \cdots H_2O \cdots N_2$ spectra (3376 cm^{-1} and 3405 cm^{-1}). From all the bands recorded in the range under 3300 cm^{-1}, only band C (3174 cm^{-1}) can be positively identified as being the result of IR absorption in C-H stretch modes.

The assignment of the bands denoted X_n in all $ImH^+ \cdots (H_2O)_2 \cdots N_2$ spectra is unclear. A extensive search of literature databases resulted in a number of papers which discuss the IR spectra of molten, room- and low-temperature Im,[70],[71],[72] of Im salts (ImH^+Cl^-),[25] as well as of an acetonitrile solution of Im[73] and of an aqueous solution of Im-bearing biomolecules.[74] In all these spectra, the range 2000 cm^{-1} ... 3400 cm^{-1} is characterized by very broad and structured absorption bands. Two explanations have been proposed for this. First, it was suggested that these features are the result of Fermi resonances of the stretch vibration of N-H proton(s) complexated by high PA molecules with various combinations and overtones of internal vibrations. Another explanations considers combination bands of the stretch vibration of N-H bound proton(s) with (overtones of) the corresponding intermolecular stretch mode.

Translation of these assignments to the present experiment is not straightforward, as each of these tentative assignments results in certain expected behaviour of the observed spectra features. The former assignment (Fermi resonances of ν_{NH}^{bH2O} with combinations and overtones of internal vibrations) implies that the observed absorption bands will not shift upon complexation. It can be seen that the only band which shifts in small steps is X1. The latter assignment implies that, within each spectrum, the observed bands must be separated by rather equal steps ($\pm n \cdot \nu_s$) and that their strength should rapidly decrease starting from a strong central feature. No spectra exhibits such characteristics. As none of these attempts can be further considered, bands X_n will remain unassigned.

It must be underlined that the assignment of the spectra published in reference [75] is only partially correct. Only the bands above 3300 cm^{-1} have been correctly assigned, as the experimental data available at that time was limited. Recently, spectra of $ImH^+ \cdots (H_2O)_n \cdots Ar$ (n = 1, 2) have been recorded.[76] They are not presented here as they

are rather fragmentary, the signal-to-noise ratio is poor, and there are no quantum chemical calculations done. They reproduce well all the characteristics of the $ImH^+\cdots(H_2O)_n\cdots N_2$ (n = 1, 2) spectra, lending support to the idea that the unassigned X_n bands are derived from ring vibrations.

6.4.5. Binding energy of the $ImH^+\cdots H_2O$ system

The $ImH^+\cdots H_2O$ spectrum provides direct spectroscopic information on the H-bond energy, D_0, and the acidities of both the NH and the OH groups. It is instructive to compare the known properties of the $ImH^+\cdots H_2O$, $indole^+\cdots H_2O$,[51],[77] and $phenol^+\cdots H_2O$[51],[63],[78] systems. It can be seen that ν_{OH}^s red-shifts by -27 cm^{-1}, -21 cm^{-1}, and -38 cm^{-1} respectively, while ν_{OH}^{as} red-shifts by -46 cm^{-1}, -36 cm^{-1}, and -54 cm^{-1} respectively. Also available are accurate D_0 values for $phenol^+\cdots H_2O$ (6520 ± 50 cm^{-1}) and $indole^+\cdots H_2O$ (4790 ± 10 cm^{-1}). Admiting a linear correlation of ν_{OH}^s and ν_{OH}^{as} with the binding energy of the complex, it results that D_0 of $ImH^+\cdots H_2O$ can be approximated as 5600 ± 300 cm^{-1}. This value is compatible with the quantum chemical estimation (5348 cm^{-1}).

6.5. Conclusions

This chapter has presented an experimental IRPD investigation of the stepwise microsolvation of ImH^+ in nonpolar (Ar, N_2) and polar (H_2O) solvents. Quantum chemical calculations of selected cluster geometries have been done at the MP2/6-311G(2df,2pd) level of theory. The IRPD spectra of $ImH^+\cdots L_n$ (L = Ar, N_2) yielded the first spectroscopic information about the ν_{CH} and ν_{NH} vibrations of isolated ImH^+, demonstrating that IR spectroscopy of cluster ions can also be used to probe fundamental properties of isolated ions. The present work has shown that IRPD spectroscopy can provide good estimates of the site-dependent binding energies of cluster cations. In the case of the nonpolar ligands, analysis of the n- and L-dependent complexation-induced frequency shifts of the N-H stretch vibrations show that the way the microsolvation develops depend on the strength of the dimer intermolecular interaction, which, in turn, is a function of the PA of the ligand. Indeed, while the most stable $ImH^+\cdots L_{(2)}$ structure is common for both ligand species (NH-bound isomers), the cluster growth model diverges as $ImH^+\cdots Ar_3$ are probably characterized by one intermolecular π-bond while the N_2-based tetramer population seems to be dominated by complexes having two NH- and one CH-bound ligands.

The application of IRPD to the study of microhydrated protonated imidazole provided for the first time direct spectroscopic information on the properties of the N-H bonds of this

biomolecular building block under isolated and controlled solvation conditions. It was demonstrated that, as protonation enhances the acidity of the N-H groups, the ability for proton conductivity of ImH^+ increases. More work must be done to identify the interactions between the proton stretch vibrations and other vibration modes of $ImH^+(\cdots L)$.

References

[1] Dervan P.B. *Bioorg. & Med. Chem.* **9** (2001) 2215

[2] Lown J.W., Krowicki K., Bhat U.G., Skorobogaty A., Ward B., Dabrowiak J.C. *Biochemistry* **25** (1986) 7408

[3] Kissinger K., Krowicki K., Dabrowiak J.C., Lown J.W. *Biochemistry* **26** (1987) 5590

[4] Dervan P.B., Burli R.W. *Curr. Opin. Chem. Biol.* **3** (1999) 688

[5] Ishida T., Kato S. *J. Am. Chem. Soc.* **125** (2003) 12035

[6] Hu C.H., Brinck T., Hult K. *Int. J. Quant. Chem.* **69** (1998) 89

[7] Overgaard J., Schiott B., Larsen F.K., Iversen B.B. *Chem. Eur. J.* **7** (2001) 3756

[8] Muench W., Kreuer K.-D., Silvestri W., Maier J., Seifert G. *Solid State Ionics* **145** (2001) 437

[9] Kreuer K.D. *Solid State Ionics* **136** (2000) 149

[10] Cheruzel L.E., Pometun M.S., Cecil M.R., Mashuta M.S., Wittebort R.J., Buchanan R.M. *Angew. Chem. Int. Ed.* **42** (2003) 5452

[11] Kamariotis A., Boyarkin O.V., Mercier S.R., Beck R.D., Bush M.F., Williams E.R., Rizzo T.R. *J. Am. Chem. Soc.* **128** (2006) 905

[12] Mercier S.R., Boyarkin O.V., Kamariotis A., Guglielmi M., Tavernelli I., Cascella M., Rothlisberger U., Rizzo T.R. *J. Am. Chem. Soc.* **128** (2006) 16938

[13] Boyarkin O.V., Mercier S.R., Kamariotis A., Rizzo T.R. *J. Am. Chem. Soc.* **128** (2006) 2816

[14] Sundberg R.J., Martin R. B. *Chem. Rev.* **74** (1974) 471

[15] Kawada A., McGhie A.R., Labes M.M. *J. Chem. Phys.* **52** (1970) 3121

[16] Hickman B.S., Mascal M., Titman J.J., Wood I.G. *J. Am. Chem. Soc.* **121** (1999) 11486

[17] El-Azhary A.A. *Spectrochim. Acta A* **59** (2003) 2009

[18] Sadlej J., Edwards W.D. *Int. J. Quant. Chem.* **26** (1992) 409

[19] Magill A.M., Yates B.F. *Aust. J. Chem.* **57** (2004) 1205

[20] Hanus M., Kabelac M., Rejnek J., Ryjacek F., Hobza P. *J. Phys. Chem. B* **108** (2004) 2087

[21] Hasegawa K., Ono T., Noguchi T. *J. Phys. Chem. B* **104** (2000) 4253

[22] Nemukhin A.V., Grigorenko B.L., Topol I.A.,Burt S.K. *J. Phys. Chem. B* **107** (2003) 2958

[23] Cartera M.D., Weaver D.F. *J. Mol. Struct. (Theochem)* **626** (2003) 279

[24] Majoube M., Henry M., ChinskyL., Turpin P.Y. *Chem. Phys.* **169** (1993) 231

[25] Bellocq A.M., Garrigou-Lagrange C. *Spectrochim. Acta* **276** (1971) 1091

[26] Su C.C., Chang H.C., Jiang J.C., Wei P.Y., Lu L.C., Lin S.H. *J. Chem. Phys.* **119** (2003) 10753

[27] Lucas B., Gregoire G., Lemaire J., Maitre P., Glotin F., Schermann J.P., Desfrancois C.

Int. J. Mass. Spectrom. **243** (2005) 105

[28] Kovacevic B., Rozman M., Klasinc L., Srzic D., Maksic Z.B., Yanez M. *J. Phys. Chem. A* **109** (2005) 8329

[29] Nguyen V.Q., Turecek F. *J. Mass. Spectrom.* **31** (1996) 1173

[30] Meot-Ner M. *J. Am. Chem. Soc.* **110** (1988) 3075

[31] Solca N., Dopfer O. *J. Mol. Struct.* **563** (2001) 241

[32] Solca N., Dopfer O. *Phys. Chem. Chem. Phys.* **6** (2004) 2732

[33] Solca N., Dopfer O. *Eur. Phys. J. D* **20** (2002) 469

[34] Dopfer O., Olkhov R.V., Maier J.P. *J. Chem. Phys.* **111** (1999) 10754

[35] Andrei H.S., Solca N, Dopfer O. *Phys. Chem. Chem. Phys.* **6** (2004) 3801

[36] Andrei H.S., Solca N., Dopfer O. *J. Phys. Chem. A* **109** (2005) 3598

[37] Solca N. and Dopfer O. *Chem. Phys. Lett.* **325** (2000) 354

[38] M.J. Frisch, G.W. Trucks, H.B. Schlegel, G.E. Scuseria, M.A. Robb, J.R. Cheeseman, J.A. Montgomery Jr., T. Vreven, K.N. Kudin, J.C. Burant, J.M. Millam, S.S. Iyengar, J. Tomasi, V. Barone, B. Mennucci, M. Cossi, G. Scalmani, N. Rega, G.A. Petersson, H. Nakatsuji, M. Hada, M. Ehara, K. Toyota, R. Fukuda, J. Hasegawa, M. Ishida, T. Nakajima, Y. Honda, O. Kitao, H. Nakai, M. Klene, X. Li, J.E. Knox, H.P. Hratchian, J.B. Cross, V. Bakken, C. Adamo, J. Jaramillo, R. Gomperts, R.E. Stratmann, O. Yazyev, A.J. Austin, R. Cammi, C. Pomelli, J.W. Ochterski, P.Y. Ayala, K. Morokuma, G.A. Voth, P. Salvador, J.J. Dannenberg, V.G. Zakrzewski, S. Dapprich, A.D. Daniels, M.C. Strain, O. Farkas, D.K. Malick, A.D. Rabuck, K. Raghavachari, J.B. Foresman, J.V. Ortiz, Q. Cui, A.G. Baboul, S. Clifford, J. Cioslowski, B.B. Stefanov, G. Liu, A. Liashenko, P. Piskorz, I. Komaromi, R.L. Martin, D.J. Fox, T. Keith, M.A. Al-Laham, C.Y. Peng, A. Nanayakkara, M. Challacombe, P.M.W. Gill, B. Johnson, W. Chen, M.W. Wong, C. Gonzalez, J.A. Pople, *Gaussian 03, Revision D.01 Gaussian, Inc., Wallingford CT* (2004)

[39] Boys S.F., Bernardi F. *Mol. Phys.* **19** (1970) 553

[40] Chalasinski G., Szczesniak M. M. **94** (1994)

[41] Heidrich D. *Angew. Chem. - Intl. Ed.* **41** (2002) 3208

[42] Hunter E. P., Lias S. G. *J. Phys. Chem. Ref. Data* **27** (1998) 413

[43] Cioslowski J., Hay P.J., Ritchie J. P. *J. Phys. Chem.* **94** (1990) 148

[44] Solca N., Dopfer O. *Chem. Eur. J.* **9** (2003) 3154

[45] Bakker J.M., Satink R.G., von Helden G., Meijer G. *Phys. Chem. Chem. Phys.* **4** (2002) 24

[46] Solca N., Dopfer O. *J. Chem. Phys.* **120** (2004) 10470

[47] Solca N., Dopfer O. *J. Phys. Chem. A* **105** (2001) 5637

[48] Solca N., Dopfer O. *Chem. Phys. Lett.* **342** (2001) 191

[49] Solca N., Dopfer O. *J. Am. Chem. Soc.* **126** (2004) 1716

[50] Caminati W., Melandri S., Millemaggi A., Favero P.G. *Chem. Phys. Lett.* **294** (1998) 377

[51] Braun J.E., Mehnert T., Neusser H.J. *Int. J. Mass Spectrom.* **203** (2000) 1

[52] Piest H., von Helden G., Meijer G. *J. Chem. Phys.* **110** (1999) 2010

[53] Bieske E.J., Dopfer O. *Chem. Rev.* **100** (2000) 3963

[54] Solca N., Dopfer O. *J. Phys. Chem. A* **106** (2002) 7261

[55] Dopfer O., Roth D., Maier J.P. *Int. J. Mass Spectrom.* **218** (2002) 281

[56] Roth D., Dopfer O. *Phys. Chem. Chem. Phys.* **4** (2002) 4855

[57] Olkhov R.V., Dopfer O. *Chem. Phys. Lett.* **314** (1999) 215

[58] Dopfer O., Roth D., Maier J.P. *J. Am. Chem. Soc.* **124** (2002) 494

[59] Curtiss L.A., Frurip D.J., Blander M. *J. Chem. Phys.* **71** (1979) 2703

[60] Goebbert D.J., Wenthold P.G. *Eur. J. Mass Spectr.* **10** (2004) 837

[61] Dopfer O. *Int. Rev. Phys. Chem.* **22** (2003) 437

[62] Solca N., Dopfer O. *J. Am. Chem. Soc.* **125** (2003) 1421

[63] Dopfer O. *Z. Phys. Chem.* **219** (2005) 125

[64] Linstrom P.J., Mallard W.G., *NIST Chemistry Webbook*, http://webbook.nist.gov/chemistry/

[65] Camy-Peyret C., Flaud J.M., Guelachvili G., Amiot C. *Mol. Phys.* **26** (1973) 825

[66] Guelachvili G., Rao K.N. *Handbook of Infrared Standards* Academic Press (London, 1993)

[67] King S.T. *J. Phys. Chem.* **74** (1970) 2133

[68] Solca N., Dopfer O. *Chem. Phys. Lett.* **347** (2001) 59

[69] Shimanouchi T. *Tables of Molecular Vibrational Frequencies* National Bureau of Standards (1972)

[70] Belloq A.M., Perchard C., Novak A., Josien M.L. *J. Chim. Phys.* **62** (1965) 1334

[71] Perchard C., Belloq A.M., Novak A. *J. Chim. Phys.* **62** (1965) 1344

[72] Perchard C., Novak A. *J. Chem. Phys.* **48** (1968) 3079

[73] Brzezinski B., Bauer R., Zundel G. *J. Mol. Struct.* **436** (1997) 103

[74] Noguchi T., Inoue Y., Tang X. *Biochemistry* **38** (1999) 399

[75] Andrei H.S., Solca N., Dopfer O. *Chem. Phys. Chem.* **7** (2006) 107

[76] Andrei H.S., Solca N., Dopfer O. *unpublished results*

[77] Unterberg C., Jansen, A., Gerhards, M. *J. Chem. Phys.* **113** (2000) 7945

[78] Dopfer O., Reiser G., Muller-Dethlefs K., Schlag E.W., Colson S.D. *J. Chem. Phys.* **101** (1994) 974

7. IRPD probing of the classical and bridged structures of the ethyl cation

Abstract This chapter presents experimental and quantum chemical investigations of the possible structures of the ethyl cation ($C_2H_5^+$). IRPD spectra of $C_2H_5^+$ complexated with nonpolar ligands (Ar, N_2, CO_2, CH_4) have been recorded over the range of the C-H stretch vibrations, yielding the fingerprint of two different types of structures. The $C_2H_5^+$ and its dimer complexes with the above-mentioned ligands have also been investigated at the MP2/6-311G(2df,2pd) level of theory, yielding a number of stable monomer and dimer structures. This paved the way to rationalize the spectra in terms of weak charge-multipole interaction or very strong bonding of the ligand to $H_3CCH_2^+$ via lone pairs interaction. Thus, for ligands like Ar and CO_2, the spectra exhibit structures assigned to the C-H stretch fundamentals of the bridged (nonclassical) $C_2H_5^+$ moiety, while for N_2 and CH_4, the spectra are shown to be dominated by the fingerprint of the CH_3 and the CH_2 groups. A simulation of the rotational envelopes for the recorded vibrations of $C_2H_5^+\cdots$Ar supports this assignment. The microsolvation of $C_2H_5^+$ in N_2 were also investigated, resulting in an estimate for the average binding energy of the weakly bound complexes $C_2H_5^+\cdots(N_2)_n$ (n > 1).

7.1. Introduction

The ethyl cation ($C_2H_5^+$) is an alkyl cation fundamental for hydrocarbon mass spectrometry[1]. It is a particularly interesting cation as it is the simplest example of protonation of a C=C double bond. It has been recently identified in the mass spectra recorded in the atmosphere of Saturn's moon Titan[2]. It was used as chemical ionization reagent for investigating proton transfer toward a wealth of molecules like monosubstituted benzenes.[3]

Despite its ubiquity, there is still a lack of direct evidence of its structure. Much theoretical and experimental work was aimed at identifying its equilibrium structure by direct observation or by inferring it from the equilibrium structures of its weakly bound complexes. Three geometries[1], have long been considered as candidate structures of

$C_2H_5^+$: two of them are classical acyclic structures ($[H_3CCH_2]^+$ - isomers **a** and **b** in Figure 1) and one is a hydrogen-bridged structure ($C_2H_5^+$ - isomer **c**). Structure **a** was selected as the natural choice: experiments show that this is the equilibrium structure of the ethyl radical (C_2H_5).[4],[5],[6],[7],[8] These experimental evidences are supporting the previously[1],[9] and presently done quantum chemical calculations which show that structure **a** of the ethyl radical is the only minimum on the potential energy surface (PES), while the other two structures probed were found to be 1st order saddle points. The situation proved to be completely different for $C_2H_5^+$, as the sole minimum on the PES is a **c**-type structure (further denoted **c$^+$**). As available computational power increased, **a$^+$** was found to fold into **c$^+$** without any barrier once electron correlation was taken into consideration[1]. Moreover, **b$^+$** was found to be a transition state (TS) for proton scrambling within **c$^+$**. Various calculations cited by Prakash and Schleyer[1] are currently placing **b$^+$** at 19.7 ... 35.1 kJ/mol above **c$^+$**, which was identified as the only stable structure of the ethyl cation. More recently, various papers have dealt with the PES of $C_2H_5^{+[9]}$, $C_2H_7^{+[10],[11],[12]}$, $C_3H_9^{+[13]}$. The common findings of these studies are that the stable structure of $C_2H_5^+$ is **c$^+$** and that dimers of $C_2H_5^+$ can have either classical or nonclassical structures.

Figure 1. *Structures of the three proposed geometries of C_2H_5 and $C_2H_5^+$ together with the atom labeling throughout the text; relevant geometrical parameters, as obtained by optimizing the structures at the MP2/6-311G(2df,2pd) are presented in Table 2.*
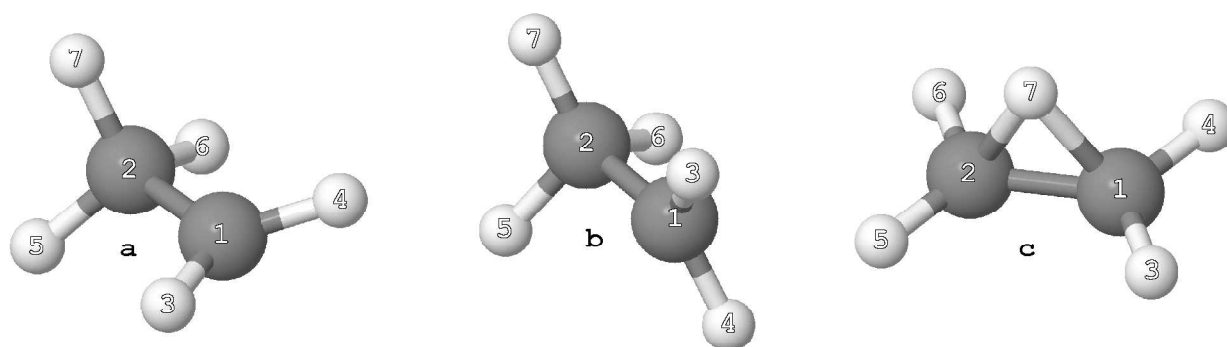
The fact that upon ionization the geometry of the radical changes from **a** to **c** means that there should be a substantial difference between the adiabatic and the vertical ionization potentials of C_2H_5. Photoelectron spectroscopy experiments[14],[15],[16] identified a gradual onset of the photoionization signal, which indicates a significant change in geometry upon ionization. The photoion yield curve exhibits two structures, separated by 19.7 ... 39.7 kJ/mol (depending on the reading position). These structures have been attributed to adiabatic ionization (lower energy) and vertical ionization (higher energy) and their identification is one of the few experimental evidences supporting the hypothesis of

the nonclassical structure of $C_2H_5^+$.

Many other experimental studies focused on high pressure mass spectrometry (HPMS) of weakly bound complexes of $C_2H_5^+$ with a plethora of ligands ($Ar^{[17]}$, $Kr^{[17]}$, $Xe^{[17]}$, $H_2^{[18]}$, $N_2^{[17]}$, $CO_2^{[19]}$, $N_2O^{[19]}$, $CH_4^{[20]}$, $OCS^{[21]}$). The results are the ethyl cation affinities (ECA) listed in Table 1. The small value observed for $C_2H_5^+\cdots Ar$ was justified by considering that Ar interacts only with the bridging H of the nonclassical structure while the somehow large values that dominate the table were explained as the results of rather strong direct interaction between the ligand and one of the C atoms. However, no HPMS experiment can offer direct evidence for the geometry of a molecule or cation.

Table 1. *Proton affinity (PA) and ethyl cation affinity (D_0) for various ligands ($C_2H_5^+ + L \rightarrow C_2H_5^+\cdots L$). The ligands used in the present investigation are marked with* **bold** *symbols.*

Ligand	D_0 (kJ/mol)	PA [22] (kJ/mol)	
Ar [17]	~7.1	369.2	
H_2 [18]	16.7±2.1	422.3	
Kr [17]	13.4±1.3	424.6	
N_2 [17]	15.5±1.3	493.8	
Xe [17]	28.5±1.3	499.6	
CO_2 [19]	27.2±0.8	540.5	
CH_4 [20]	23.0±0.8	543.5	
N_2O [19]	49.0±0.8	549.8	protonation at N
		575.2	protonation at O
OCS [21]	104.2±8.4	628.5	protonation at S

So far, experiments were rather unsuccessful at giving a definitive answer regarding the structures predicted by the calculations. A promising experimental approach is IR spectroscopy, which is sensitive to the molecular structure. However, the simplest experimental implementation - direct IR spectroscopy - has difficulties because it lacks species selection. A mass-selective method, IR photodissociation spectroscopy (IRPD), trades a certain degree of ligand-related perturbation of the investigated ion for species sensitivity (obtained via mass selection)[23].

7.2. Quantum chemical calculations

The theoretical characterization of the ethyl cation and of its complexes has been carried out in form of *ab initio* calculations. These calculations have been done at the

MP2/6-311G(2df,2pd) level, using the Gaussian03[24] quantum chemistry package. In order to obtain a better perspective of the studied systems, calculations have been carried out for isomers of the neutral species C_2H_2, C_2H_4, C_2H_6, and C_2H_5 as well as for the ethyl cation ($C_2H_5^+$). The principal parameters of the resulting equilibrium structures are shown in Table 2. The dimers investigated ($C_2H_5^+\cdots Ar$, $C_2H_5^+\cdots N_2$, $C_2H_5^+\cdots CO_2$, and $C_2H_5^+\cdots CH_4$) are presented in Table 3. All geometrical and energetical parameters of the complexes were obtained accounting for the basis set superposition error (BSSE) on each step of the calculations by requesting counterpoise calculations.[25],[26]

All the energetical parameters in Table 2 and Table 3 are presented with and without including the zero-point energy (ZPE) correction, which is done considering the full (no scaling) harmonic frequencies. There are certain computational artifacts which are affecting the values of both the depth of the intermolecular potential well (D_e) and the binding energy of complexes (D_0). The depth of the intermolecular potential energy well is derived from the total stabilization energy of the complex and from the total stabilization energies of the complex components (monomers):

$$D_e = E_{cpl} - \Sigma(E_{mon})$$ (1)

If the geometry of the $C_2H_5^+$ moiety is strongly affected by complexation, D_e will consist of not only the intermolecular interaction, but will also include the change in energy corresponding to the large geometrical distortion of the $C_2H_5^+$ moiety.

To obtain D_0, one needs to add to each of the terms of (1) the values of the ZPE:

$$D_e = (E_{cpl} - ZPE_{cpl}) - \Sigma(E_{mon} - ZPE_{mon})$$ (2)

This reveals additional problems related to the same complexes for which the ligand is changing the geometry of the $C_2H_5^+$ moiety, as there can be large differences between the frequencies of the normal modes of the complex and the ones of the monomers. These differences originate in the reorganization of the normal modes and not in the simple complexation-induced shifts. For example, the replacement of a methyl C-H stretch vibration with the stretch vibration of the nonclassical proton decreases ZPE by ~500 cm^{-1} while the replacement of the C-C stretch mode of $H_3CCH_2^+$ with the one of the nonclassical $C_2H_5^+$ increases ZPE by ~330 cm^{-1}. As the general trend is rather unpredictible, the true binding energy of a certain complex is considered to lie between the values derived from the corrected and the uncorrected PES ($D_e^{C_2H_5^+\cdots L} > D_{true}^{C_2H_5^+\cdots L} > D_0^{C_2H_5^+\cdots L}$). At the same time, the height of the barriers separating various isomers will be extracted from the uncorrected PES.

Table 2. *Parameters of the investigated structures of C_2H_2, C_2H_4, C_2H_5, C_2H_6, and $C_2H_5^+$, as obtained at the MP2/6-311G(2df,2pd) level: intramolecular distances and angles (r_{xy} and θ_{xyz}); uncorrected (top) and ZPE-corrected (bottom) relative stabilization energies with respect to the most stable isomer of each species (E_{rel}); harmonic frequencies of the C-H stretch vibrations (ω_{CH}) and their IR intensities (I_{IR}, in parentheses). The labeling of atoms can be found in Figure 1; the number of imaginary frequencies are shown in parentheses next to E_{rel}; stick spectra of the vibrations of the $C_2H_5^+$ isomers are presented the experimental results sections.*

isomer	C_2H_2	C_2H_4	C_2H_6
r_{cc} (Å)	1.2093	1.3298	1.5231
r_{cH} (Å)	1.0613	1.0802	1.0880
θ_{HCH} (deg)		117.2	107.7
θ_{HCC} (deg)	180.0	121.4	111.2
ω_{CH} (cm^{-1})	3456 (93)	3186 (10)	3088 (0)
I_{IR} (km/mol)	3544 (0)	3203 (0)	3090 (47)
		3275 (0)	3162 (0)
		3301 (15)	3162 (0)
			3184 (48)
			3184 (48)

isomer	C$_2$H$_5$ a	C$_2$H$_5$ b	C$_2$H$_5$ c	C$_2$H$_5^+$ b$^+$	C$_2$H$_5^+$ c$^+$
r_{12} (Å)	1.4853	1.4851	1.4842	1.4055	1.3784
r_{13} (Å)	1.0770	1.0760	1.0761	1.0861	1.0829
r_{14} (Å)	1.0770	1.0772	1.0761	1.0860	1.0829
r_{25} (Å)	1.0882	1.0923	1.0761	1.1106	1.0829
r_{26} (Å)	1.0882	1.0923	1.0761	1.1106	1.0829
r_{27} (Å)	1.0949	1.0865	1.2763	1.0796	1.3056
θ_{314} (deg)	117.7	117.9	119.4	116.9	119.1
θ_{526} (deg)	108.2	106.2	119.4	96.4	119.1
θ_{527} (deg)	106.7	107.7	113.0	113.8	105.6
E_{rel} (kJ/mol)	0.0 (0) 0.0	0.4 (1) -0.5	186.1 (1) 176.8	34.5 (1) 29.9	0.0 (0) 0.0
ω_{CH} (cm^{-1})	3042 (19)	3055 (19)	2405 (9)	2939 (186)	2228 (54)
I_{IR} (km/mol)	3126 (15)	3110 (14)	3215 (8)	2944 (80)	3181 (34)
	3172 (14)	3177 (15)	3220 (0)	3168 (4)	3184 (0)
	3221 (12)	3225 (11)	3331 (0)	3265 (5)	3292 (0)
	3333 (7)	3338 (6)	3352 (4)	3285 (45)	3309 (70)

7.2.1. Monomers

Experimental evidence and quantum chemical calculations[27],[28],[29],[30],[31],[32],[33] reveal that the molecule is planar in its stable equilibrium geometry. From its structure, three geometries can easily be derived for the ethyl radical (**a**, **b**, and **c** in Figure 1 and Table 2). Analysis of the harmonic frequencies of the optimized geometries reveals that **a** is a minimum on the PES. Structure **b** is a first order saddle point (has one imaginary frequency), more exactly is the TS for the methyl rotation of **a** around the C-C axis. This structure is placed just +0.4 kJ/mol higher in stabilization energy than **a**; such a low value is typical for the process of methyl rotation. Structure **c** is also a first order saddle point, being the TS for the process of switching the methyl group from one carbon atom to the other. It is remakable that, by using the harmonic frequencies, the ZPE correction applied here inverts the positions of points **b** and **c** on the energy scale.

Analysis of the ethyl cation ($C_2H_5^+$) reveals a completely different image. Geometry optimization starting from **a⁺** slides toward **c⁺** without any barrier at the studied level. Indeed, a single point calculation done for **a⁺** on the geometry of **a** reveals the existence of one imaginary frequency, corresponding to the translation of proton 7 (Figure 1) above the C=C bond. Structure **b⁺** is a TS for the scrambling of the protons of **c⁺**; it has one imaginary vibration which describes the path upon which the symmetry-unrestricted optimization of **b⁺** turns into **c⁺**.[9] Structure **c⁺** is the only minimum found on the PES of $C_2H_5^+$.

The equilibrium geometry found for **c⁺** is closely related to the one of C_2H_4: the four aliphatic protons lie in a plane, while the two carbon atoms "float" at just 0.0022 Å above this plane. Even more, the C-H bonds are only slightly expanding upon protonation (+0.0027 Å) while the angle between the two aliphatic protons of each methylene group increases by just 1.8 °. The only major geometry change induced by the protonation is the expansion of the C=C bond ($r_{CC}^{C_2H_4} = 1.3298$ Å and $r_{CC}^{C_2H_5^+} = 1.3784$ Å); however, its length after protonation is still much smaller than the length of the C-C bond calculated for the staggered isomer of C_2H_6 ($r_{CC}^{C_2H_6} = 1.5231$ Å). Also $r_{17} = r_{27} = 1.3056$ Å are considerably longer than any other r_{CH}: $r_{CH}^{C_2H_4} = 1.0802$ Å, $r_{CH}^{C_2H_5^+} = 1.0829$ Å, and $r_{CH}^{C_2H_6} = 1.0880$ Å. It is thus shown that, while affecting the C=C bond, the bridging proton is not breaking it.

Analysis of the C-H stretch vibrations (Table 2) reveals important differences between the two types of isomers: while the C-H stretch vibrations of the acyclic structures (**a**, **b**, **b⁺**) exhibit characteristics typical for methyl groups, the spectrum of the H-bridged isomer

Table 3. Parameters of the investigated dimers $C_2H_5^+\cdots Ar$, $C_2H_5^+\cdots N_2$, $C_2H_5^+\cdots CO_2$, and $C_2H_5^+\cdots CH_4$, as obtained at the $MP2/6\text{-}311G(2df,2pd)$ level: intramolecular distances and angles (r_{xy} and θ_{xyz}); harmonic frequencies of the C–H stretch vibrations (ω_{CH}) and their IR intensities (I_{IR}, in parentheses); intermolecular distances ($r_{X\cdots L}$); binding energies of the complexes (D_0); the harmonic frequency of the intermolecular stretch vibration (ω_s). The labeling of the $C_2H_5^+$ atoms can be found in Figure 1; the number of imaginary frequencies are specified next to D_0; stick spectra of the scaled vibrations (ν_{CH}) are presented in the experimental section.

isomer	$d^+\cdots Ar$	$e^+\cdots Ar$	$b^+\cdots Ar$	$d^+\cdots N_2$	$e^+\cdots N_2$	$a^+\cdots N_2$	$d^+\cdots CO_2$	$e^+\cdots CO_2$
r_{12} (Å)	1.3762	1.3785	1.4047	1.3734	1.3789	1.5160	1.3720	1.3784
r_{13} (Å)	1.0828	1.0827	1.0861	1.0826	1.0821	1.0386	1.0822	1.0817
r_{14} (Å)	1.0828	1.0827	1.0857	1.0826	1.0821	1.0386	1.0822	1.0817
r_{25} (Å)	1.0828	1.0827	1.1106	1.0826	1.0824	1.0355	1.0822	1.0822
r_{26} (Å)	1.0828	1.0827	1.1106	1.0826	1.0824	1.0355	1.0822	1.0822
r_{C7} (Å)	1.3096	1.2931 1.3194	1.0795	1.3163	1.2737 1.3436	1.0378	1.3163	1.2672 1.3529
θ_{314} (deg)	119.0	119.0	117.1	120.5	118.9	110.6	118.9	118.9
θ_{526} (deg)	119.0	119.1	96.1	120.5	119.2	110.4	118.9	119.2
θ_{527} (deg)	105.5	105.6	114.0	105.4	105.6	103.6	105.4	105.6
ω_{CH} (cm⁻¹)	2182 (202)	2230 (50)	2940 (176)	2122 (346)	2245 (51)	3109 (4)	2115 (612)	2255 (52)
	3182 (31)	3182 (28)	2944 (74)	3184 (29)	3185 (21)	3129 (17)	3187 (26)	3187 (19)
	3184 (1)	3186 (4)	3169 (3)	3187 (1)	3193 (8)	3202 (16)	3190 (2)	3197 (9)
	3292 (0)	3294 (1)	3266 (4)	3294 (0)	3298 (4)	3207 (7)	3296 (0)	3300 (6)
	3310 (65)	3312 (68)	3287 (49)	3311 (60)	3318 (60)	3227 (4)	3314 (55)	3322 (56)
$r_{X\cdots L}$ (Å)	2.4884	3.2092	2.9080	2.1509	2.8520	1.4874	1.9032	2.6124
D_e (kJ/mol)	7.6 (0)	5.2 (0)	5.7 (1)	20.8 (0)	14.6 (0)	57.3 (0)	33.1 (0)	23.9 (0)
D_0 (kJ/mol)	6.5	3.9	4.6	17.7	11.6	37.8	31.1	21.4
ω_s (cm⁻¹)	79 (33)	81 (20)	59 (9)	119 (38)	123 (19)	652 (7)	134 (60)	138 (39)

Table 3. *(continued)* * stretch vibrations of CH_4; ** coupled C-H stretch modes of $C_2H_5^+$ and CH_4.

isomer	$a^+\cdots CO_2$	$a_1^+\cdots CO_2$	$d^+\cdots CH_4$	$e^+\cdots CH_4$	$a^+\cdots CH_4$
r_{12} (Å)	1.4752	1.4805	1.3741	1.3785	1.4928
r_{13} (Å)	1.0849	1.0868	1.0825	1.0825	1.0915
r_{14} (Å)	1.0849	1.0868	1.0825	1.0825	1.0815
r_{25} (Å)	1.0833	1.0823	1.0825	1.0826	1.0857
r_{26} (Å)	1.0833	1.0823	1.0825	1.0826	1.0852
r_{C7} (Å)	1.0949	1.0943	1.3150	1.2840 / 1.3306	1.0921
θ_{314} (deg)	114.0	113.2	119.0	119.0	111.0
θ_{526} (deg)	111.3	111.5	119.0	119.1	110.4
θ_{527} (deg)	108.0	107.2	105.5	105.6	107.7
ω_{CH} (cm⁻¹)	3075 (21) 3172 (0) 3180 (5) 3231 (0) 3277 (5)	3075 (21) 3162 (5) 3190 (2) 3209 (0) 3286 (9)	2135 (319) *3053 (27) **3184 (29) **3184 (6) 3187 (2) *3188 (8) *3214 (0) 3294 (0) 3311 (60)	2234 (49) *3066 (17) 3183 (25) 3188 (8) *3197 (10) *3198 (14) *3221 (2) 3296 (2) 3314 (63)	*2340 (250) 3089 (10) *3100 (20) 3133 (14) 3180 (7) 3220 (0) *3247 (17) 3259 (19) *3309 (17)
$r_{X\cdots L}$ (Å)	1.6609	1.6442	2.2626	3.0717	2.9184
D_e (kJ/mol) D_0 (kJ/mol)	31.0 (0) 17.3	31.0 (0) 16.9	17.7 (0) 15.0	11.2 (0) 8.4	33.2 (0) 18.0
ω_s (cm⁻¹)	436 (152)	456 (152)	143 (34)	116 (20)	310 (17)

shows the completely different fingerprint of a methylene group. The frequencies of the IR active C-H stretch vibrations of C_2H_4 are well matched by the IR active aliphatic stretch vibrations of c^+, showing that the perturbation caused by the attached proton is largely limited at the C=C bond. A typical effect of ionization or protonation is the significant increase in IR activity of the stretch vibrations; in the present case, the transition from C_2H_4 to the c^+ isomer of $C_2H_5^+$ results in a roughly fourfold increase of the IR intensity of the stretch vibrations.

7.2.2. $C_2H_5^+\cdots Ar$ dimers

As expected, the addition of an Ar atom changed almost nothing in the geometry of $C_2H_5^+$. The weak interaction of Ar with the $C_2H_5^+$ core is not able to change the stable geometry of $C_2H_5^+$. Figure 2 illustrates the relative stabilities of various investigated isomers and some TSs which are connecting them on the potential energy surface of $C_2H_5^+\cdots Ar$. It should be underlined that although the minima on the PES without the ZPE correction are comfortably separated by the TSs (black lines on Figure 2), the picture is more unclear when considering the ZPE-corrected PES (red lines on Figure 2). Like stated at the beginning of the *Quantum chemical calculations* chapter, the barrier will be derived from the uncorrected PES.

$a^+\cdots Ar$ Six possible geometries, derived from both staggered and eclipsed structures of C_2H_6, have been used for probing possible $a^+\cdots Ar$ dimers. For all these input geometries, the geometry optimization yielded only $c^+\cdots Ar$ dimers.

$b^+\cdots Ar$ By placing an Ar atom in the symmetry plane of isomer b^+ (plane $C_1C_2H_3H_4H_7$ on Figure 1), a number of stationary points were identified, but all of them retained the saddle point character seen for the monomer. Placing the Ar atom outside the symmetry plane of isomer b^+ means to drop the symmetry of the complex and the resulting unrestricted optimization yields again $c^+\cdots Ar$ dimers.

$c^+\cdots Ar$ Finally, for $c^+\cdots Ar$ dimers two minimum structures have been identified. In one case the Ar atom attaches directly to the bridging proton, resulting in a C_{2v} symmetric dimer; such an isomer will further be denoted as $d^+\cdots Ar$. In the second case the ligand is still located in the $C_1C_2H_7$ plane, but it is weakly bound directly to one C atom; this isomer will further be denoted as $e^+\cdots Ar$.

It can be seen that the two stable dimer structures are characterized by substantially different binding energies: $D_0^{d^+\cdots Ar} = 6.5$ kJ/mol while $D_0^{e^+\cdots Ar} = 3.9$ kJ/mol. The presently calculated $D_0^{d^+\cdots Ar}$ is in excellent agreement with the experimental result obtained via HPMS

by Hiraoka et al[17] (7.1 kJ/mol). These two minima are separated by a TS ($\mathbf{d^+}\cdots Ar \leftrightarrow \mathbf{e^+}\cdots Ar$), located in the $C_1C_2H_7$ plane, just 1.6 kJ/mol above the position of $\mathbf{e^+}\cdots Ar$ (0.8 kJ/mol when considering the fully harmonic ZPE correction); another TS ($\mathbf{e^+}\cdots Ar \leftrightarrow \mathbf{e^+}\cdots Ar$) separates the two possible $\mathbf{e^+}\cdots Ar$ sites. Together, these points fully describe the PES in the $C_1C_2H_7$ plane. The small height of the barrier separating $\mathbf{e^+}\cdots Ar$ from $\mathbf{d^+}\cdots Ar$ implies that the $\mathbf{e^+}\cdots Ar$ dimers are probably suppressed via isomerization following the supersonic expansion.

Figure 2. *Salient points on the PES of $C_2H_5^+\cdots Ar$ and their corresponding geometries. As reference for the energy scale is used $\mathbf{c^+} + Ar$; the unstable structure $\mathbf{b^+}$ lies almost 30 kJ/mol above the level of $\mathbf{c^+}$. Black lines show the uncorrected PES while red lines show the ZPE-corrected PES.*
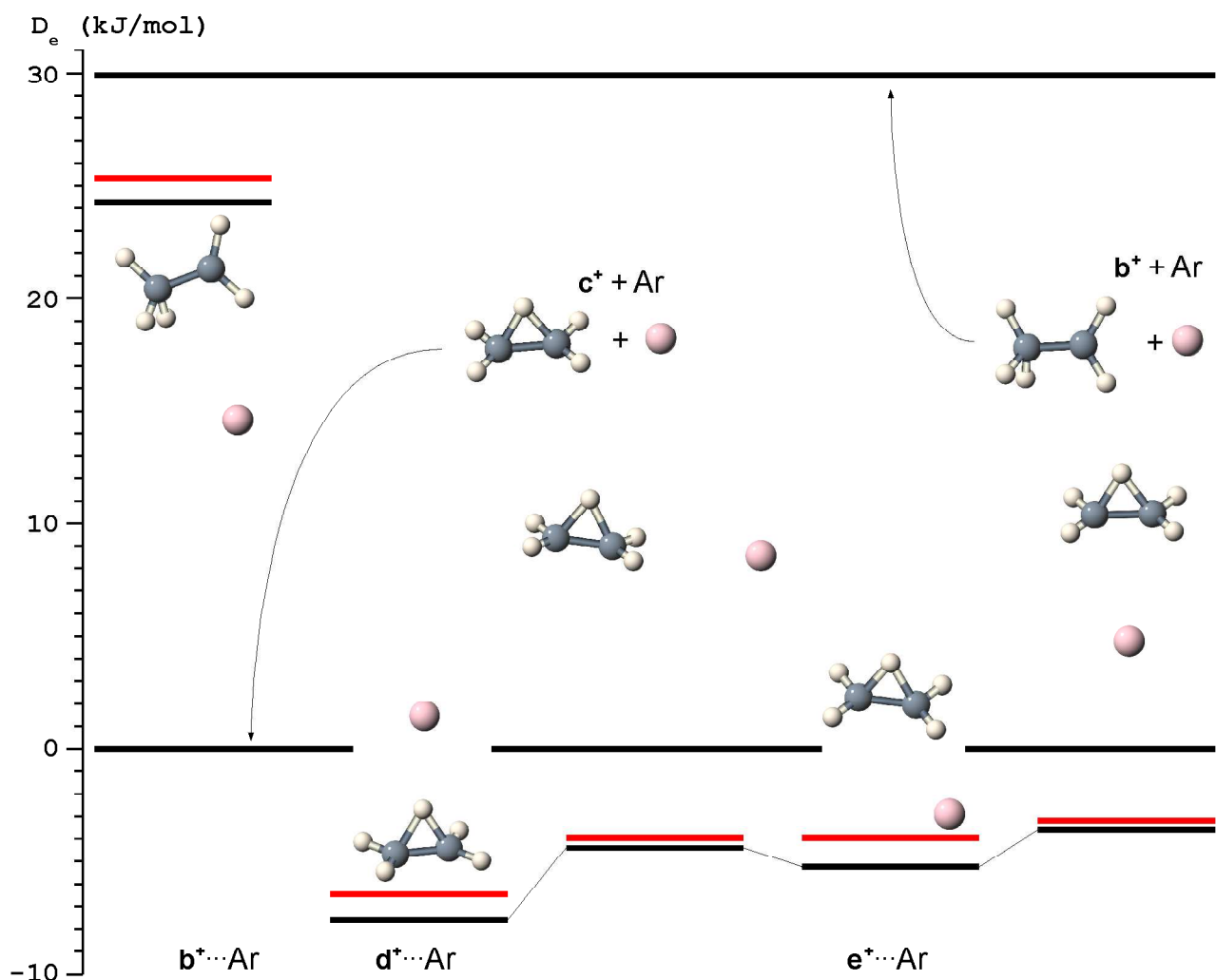
The position of $\mathbf{b^+}$ is also depicted in Figure 2, almost 30 kJ/mol above the level of the stable $\mathbf{c^+}$. From the possible $\mathbf{b^+}\cdots Ar$ structures, in Figure 2 is depicted the one identified as having the strongest intermolecular interaction. It can be seen that, while the intermolecular potential between $\mathbf{b^+}$ and Ar reaches a minimum for this structure, Ar is too

weak to stabilize the geometry of **b⁺**.

The stick spectra of the relevant dimers are plotted in Figure 7. There are shown the scaled C-H stretch vibrations (ν_{CH}) of the equilibrium structures **d⁺**···Ar and **e⁺**···Ar, of the **b⁺**···Ar dimer depicted in Figure 2, as well as the ones of the **b⁺** and **c⁺** monomers. It is easy to see that the spectra of both **d⁺**···Ar and **e⁺**···Ar dimers are virtually identical with the spectrum of **c⁺**, while the spectrum of the **b⁺**···Ar retains the fingerprint of the methyl and methylene groups stretch vibrations seen in the spectrum of **b⁺** (~2900 ... 3000 cm^{-1}).

7.2.3. $C_2H_5^+$···N_2 dimers

The PES of $C_2H_5^+$···N_2 is presented in Figure 3, where it can be seen that there are two main models which describe the intermolecular interaction. As discussed at the beginning of the **Quantum chemical calculations** chapter, the heights of the barriers separating various minima will be extracted from the uncorrected PES. Usually, the binding energy of a complex is equated with $D_0^{a^+\cdots L}$ which is extracted directly from the ZPE-corrected PES. In the present case however, a better estimate is that the binding energy lies between $D_e^{a^+\cdots L}$ and $D_0^{a^+\cdots L}$.

Optimization of the **c⁺** + N_2 system yields two stable dimers, similar in structure (ligand position with respect to the **c⁺** ion) with the stable $C_2H_5^+$···Ar complexes. In general, **c⁺** is almost unperturbed by the presence of the ligand. The parameters of the intermolecular bonds in the $C_2H_5^+$···N_2 dimers suggest a stronger intermolecular interaction (Table 3) than the one seen in the $C_2H_5^+$···Ar complexes. For both these stable dimers the intermolecular interaction is best described as a charge-quadrupole interaction, as suggested by the rather large intermolecular distance and the linear H···|N≡N| or C···|N≡N| geometries.

The largest geometrical change seen by the **d⁺**···N_2 dimer is the 0.0107 Å expansion of the $r_{17} \equiv r_{27}$ interatomic distance; following this bond expansion, the frequency of the stretching mode of the bridging proton is red-shifted by -106 cm^{-1}, while its IR intensity increases more than six times. The only affected part of the C_2H_4 core is the C=C bond which, as expected, is slightly shrinking. In contrast to these changes, the C-H bonds are basically unaffected: the frequencies of the C-H stretch modes are blue-shifted by at most +3 cm^{-1}, while their IR activities are marginally decreasing. Analysis of the same parameters of the **d⁺**···Ar dimer shows that although r_{27} expands by just 0.0040 Å and ω_{H7} is red-shifted by -46 cm^{-1}, the corresponding IR intensity is increasing almost four times. Overall, it can be seen that, as expected, the magnitude of the effects depends on the PA

of the ligand. It is relevant that even the stronger interaction of N_2 with the bridging proton of $\mathbf{c^+}$ is unable to open the nonclassical structure.

Figure 3. *Salient points on the PES of $C_2H_5^+\cdots N_2$ and their corresponding geometries. As reference for the energy scale is used $\mathbf{c^+} + N_2$. Black lines show the uncorrected PES while red lines show the ZPE-corrected PES.*
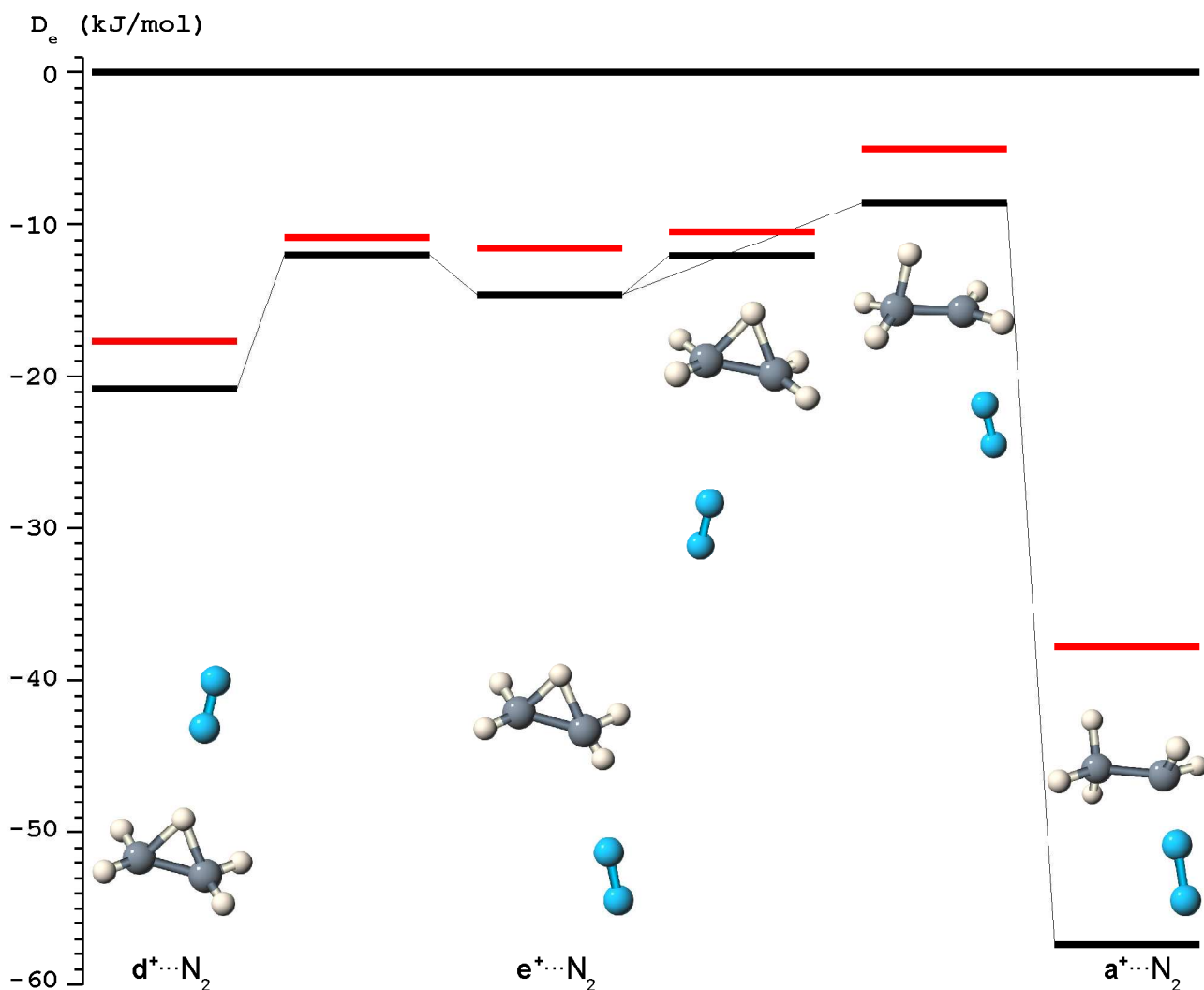
Attaching the ligand directly to one of the C atoms of the $\mathbf{c^+}$, thus forming an $\mathbf{e^+}\cdots L$ dimer, has as main effect the displacement of the bridging proton away from the C atom where the ligand binds and toward the other C atom of $C_2H_5^+$. Indeed, while r_{17} increases by 0.0138 Å for $\mathbf{e^+}\cdots Ar$ and by 0.0380 Å for $\mathbf{e^+}\cdots N_2$, r_{27} is decreasing by 0.0125 Å for $\mathbf{e^+}\cdots Ar$ and by 0.0299 Å for $\mathbf{e^+}\cdots N_2$. Although this change is not reflected in the ethylene geometry (the C=C bond and all aliphatic C-H bonds are essentially unchanged), it can be seen that the ω_{CH} vibrations are blue-shifted by up to +9 cm^{-1} for $\mathbf{e^+}\cdots N_2$ (+3 cm^{-1} for $\mathbf{e^+}\cdots Ar$).

In line with the increased PA of N_2 versus Ar, both $\mathbf{d^+}\cdots N_2$ and $\mathbf{e^+}\cdots N_2$ are characterized by stabilization energies which are almost 2.5 times larger than the

corresponding $C_2H_5^+\cdots Ar$ dimers. The calculated binding energy of the $C_2H_5^+\cdots N_2$ dimer characterized by the strongest intermolecular interaction is in very good agreement with the value obtained via HPMS[17]: $D_0^{d^+\cdots N_2} = 17.7$ kJ/mol, versus $D_{0,HPMS}^{C_2H_5^+\cdots N_2} = 15.5\pm1.3$ kJ/mol.

Aside from the dimers built around the c^+ geometry of $C_2H_5^+$, the calculations show that N_2 can also stabilize an open structure of the ethyl cation, by attaching directly to the atom C_1 of a^+. The strong interaction between C_1 and N_2 results in heavy reorganization of the $C_2H_5^+$ moiety: the $C=C$ bond breaks down and is replaced by a C-C bond while the bridging proton migrates to C_2. The change in hybridization of the two C atoms from sp^2 to sp^3 results in a structure which resembles the geometry of the staggered C_2H_6: the r_{CC} is just 0.0071 Å shorter, while the average value of r_{CH} for the methyl group is identical with the r_{CH} of the staggered C_2H_6. Apart from the $c^+\cdots N_2$ complexes, here the interaction takes place via the lone pair of the N_2 molecule, resulting in a nearly covalent bond between $H_3CCH_2^+$ and N_2. The spectral fingerprint of this $a^+\cdots N_2$ system is completely different from the one of the $d^+\cdots N_2$ and $e^+\cdots N_2$ dimers, making the analysis of the C-H stretch vibrational range a suitable method of identifying the ligand binding motif.

From Table 3 it can be seen that the interaction between the two fragments of the complex (a^+ and N_2) is exceptionally strong: $D_0^{a^+\cdots N_2} = 37.8$ kJ/mol and $D_e^{a^+\cdots N_2} = 57.3$ kJ/mol. As stated above, the binding energy of such complex should be considered to be bracketed by $D_0^{a^+\cdots N_2}$ and $D_e^{a^+\cdots N_2}$; even considering the minimum value ($D_0^{a^+\cdots N_2}$), the result is not compatible with the measured ethyl cation affinity of N_2, suggesting that the complexes measured in the HPMS experiments[17] were produced in conditions more favourable for the creation of $c^+\cdots N_2$ - type dimers.

7.2.4. $C_2H_5^+\cdots CO_2$ dimers

The PES of $C_2H_5^+\cdots CO_2$ is presented in Figure 4; like in the case of $C_2H_5^+\cdots N_2$, the intermolecular interaction is described by two largely different models.

Optimization of the c^+ + CO_2 system starting from various ligand positions yielded two stable dimers with structures similar to the ones seen for the $c^+\cdots Ar$ and $c^+\cdots N_2$ dimers, namely $d^+\cdots CO_2$ and $e^+\cdots CO_2$. In both dimer structures found, c^+ is almost unperturbed by the presence of the ligand: even the stronger interaction of CO_2 with the bridging proton of c^+ is unable to open the nonclassical structure. Optimization of $d^+\cdots CO_2$ geometries starting with the ligand tilted with respect to the C_2 axis of the c^+ moiety resulted in a linear $H\cdots|O=C=O|$ geometry. Few geometries were probed to identify minima of $e^+\cdots CO_2$ - type, including a c^+ + CO_2 dimer having the CO_2 molecule located under the C=C axis.

They all sled toward a stable equilibrium geometry closely mirroring the $e^+ \cdots N_2$ geometry. Thus, it seems that these weak interactions are of charge-quadrupole type.

Figure 4. *Salient points on the PES of $C_2H_5^+ \cdots CO_2$ and their corresponding geometries. As reference for the energy scale is used $c^+ + CO_2$. Black lines show the uncorrected PES while red lines show the ZPE-corrected PES.*
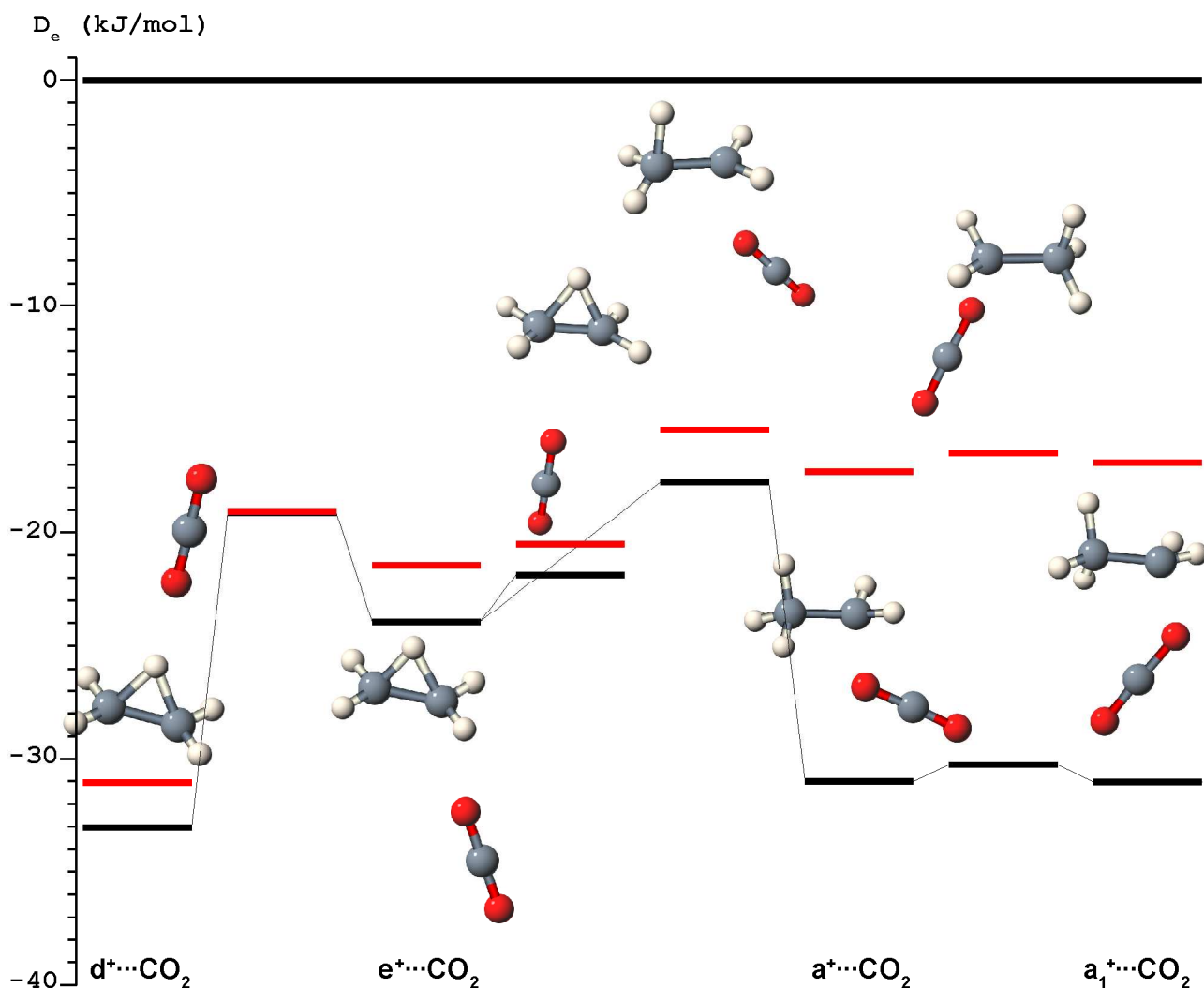
Owing to the fact that $PA_{CO_2} > PA_{N_2} > PA_{Ar}$, the intermolecular interaction in the $d^+ \cdots CO_2$ dimer is shown to be the strongest. However, the perturbation exerted by CO_2 shows up in an uneven manner: the geometry of c^+ in $d^+ \cdots CO_2$ is identical with the one calculated for $d^+ \cdots N_2$ and the most significant change is seen at the intermolecular level. Indeed, $r_{H \cdots CO2}$ drops to just 1.903 Å; to put this number in perspective, the contraction of the intermolecular bond from $d^+ \cdots N_2$ to $d^+ \cdots CO_2$ is almost as large as the one seen when going from $d^+ \cdots Ar$ to $d^+ \cdots N_2$. In line with the largely unpertubed geometry, the red-shift of the bridging proton's stretch vibration is only slightly larger ($\Delta\omega_{H7}$ = -113 cm^{-1} versus -106 cm^{-1}). Despite the only modest increase of the red-shift of ω_{H7}, its IR intensity shows a

dramatic increase (11 times larger than the monomer value). Simultaneously with the red-shift of ω_{H7}, all other ω_{CH} vibrations are blue-shifted by at most $+6 \, cm^{-1}$, while their IR intensities show only little decrease. The frequency of ω_s and its IR intensity increase dramatically, in line with the stronger intermolecular interaction.

At the level of the $C_2H_5^+$ moiety, the calculated $\mathbf{e^+} \cdots CO_2$ dimer is characterized by the same type of displacement of the brigding proton: while r_{17} is increasing by 0.0473 Å, r_{27} is decreasing by 0.0384 Å with respect to the isolated $\mathbf{c^+}$. The ethylene molecule is left unaffected at geometrical level (the C=C bond and all C-H bonds are essentially unchanged), but it can be seen that the ω_{CH} vibrations of $\mathbf{e^+} \cdots CO_2$ are blue-shifted by up to $+11 \, cm^{-1}$.

The stabilization energies of the $\mathbf{d^+} \cdots CO_2$ and $\mathbf{e^+} \cdots CO_2$ dimers exhibit a dramatic increase with respect to the equivalent N_2-based complexes, increasing by a factor ~1.8; at the same time, the calculated binding energy of the $\mathbf{c^+} \cdots CO_2$ dimer characterized by the strongest intermolecular interaction is in reasonable agreement with the value obtained via HPMS[19] ($D_0^{\mathbf{d^+} \cdots CO_2} = 31.1$ kJ/mol, versus $D_{0,HPMS}^{C_2H_5^+ \cdots CO_2} = 27.2 \pm 1.3$ kJ/mol).

Very much like N_2, CO_2 is also able to stabilize an open structure of the ethyl cation, by attaching directly to the atom C_1 of $\mathbf{a^+}$. Opposite to the weak interactions between $\mathbf{c^+}$ and CO_2, the intermolecular interaction in $\mathbf{a^+} \cdots CO_2$ takes place via one of the lone pairs of the CO_2 molecule. Indeed, the angle between the axis of CO_2 and the intermolecular bond ($\widehat{XO_1O_2}$, $X = H_7$ or C_1) decreases from $180°$ and $173.6°$ for $\mathbf{d^+} \cdots CO_2$ and $\mathbf{e^+} \cdots CO_2$, respectively, to just $126.6°$ for $\mathbf{a^+} \cdots CO_2$. It is then natural to search for another structure, in which the intermolecular bond creates similar angles with the $C_2 - C_1$ and with the $O_1 = C = O_2$ axis and has the ligand molecule located under the intramolecular C-to-C bond. The dimer thus found ($\mathbf{a_1^+} \cdots CO_2$ in Figure 4) indeed exhibits the predicted characteristics of the intermolecular bond; in particular, $\widehat{C_1O_1O_2}$ ($126.4°$) is, within the limits of the calculations, identical with the corresponding angle from $\mathbf{a^+} \cdots CO_2$.

While the spectral fingerprints of the two $\mathbf{a^+} \cdots CO_2$ dimers are basically indiscernible, they are largely different from the ones of the $\mathbf{c^+} \cdots CO_2$ dimers. This means that the analysis of the C-H stretch vibrational range can identify the observed species. On a side note, the intermolecular stretch vibrations of the two $\mathbf{a^+} \cdots CO_2$ dimers are lower in frequency as the one of $\mathbf{a^+} \cdots N_2$, but they exhibit an increase of their IR activities by a factor ~20.

Table 3 shows that the interaction between the two fragments of these classical complexes ($\mathbf{a^+}$ and CO_2) is weaker not only than the one in $\mathbf{a^+} \cdots N_2$, but also than the one of

$\mathbf{d^+}\cdots CO_2$. Indeed, the binding energies are somewhere between $D_0^{\mathbf{a^+}\cdots CO_2} = 16.9$ kJ/mol and $D_e^{\mathbf{a^+}\cdots CO_2} = 31.0$ kJ/mol, while the binding energy of the $\mathbf{d^+}\cdots CO_2$ complex is evaluated as $D_0^{\mathbf{d^+}\cdots CO_2} = 31.1$ kJ/mol. This finding is of major significance, as it implies that the dominant species visible in the $C_2H_5^+\cdots CO_2$ spectrum is supposed to be the weakly bound $\mathbf{d^+}\cdots CO_2$ and not the nearly covalent $\mathbf{a^+}\cdots CO_2$ species.

7.2.5. $C_2H_5^+\cdots CH_4$ dimers

The $C_2H_5^+\cdots CH_4$ complexes and its isomers are creating a mesh-like PES, with a large number of minima and TSs between them. This makes impossible the investigation of the $C_2H_5^+ - CH_4$ interaction without considering other $[C_3,H_9]^+$ moieties. Even the study of the weakly bound $C_2H_5^+\cdots CH_4$ complexes is complicated, as the CH_4 ligand is able to rotate with ease even while interacting with a cation. It is thus necessary to simplify the picture, by considering only a very limited number of isomers (as often as possible just one) for each class of geometries. The disadvantage of this approach comes from the fact that it is not possible to make sure that the considered isomer is the most energetically favorable of all structures sharing certain geometrical peculiarities. Figure 5 shows elements of the PES of $[C_3,H_9]^+$, starting from weakly bound $C_2H_5^+\cdots CH_4$ structures and ending with the elimination of a H_2 molecule to form $C_3H_7^+$; as origin of the energy scale was used $\mathbf{c^+} + CH_4$. The elements of the PES were computed without any BSSE correction. The advantage and, at the same time, the disadvantage of such an approach is that there is no need to freeze the charge on a certain component of the complex. In order to be able to do comparisons between various complexes, the interesting species were calculated also with BSSE correction (data in Table 3). Although the selected PES trajectory is considered to be representative, it is possible that the equilibrium structures identified here are not absolute minima or lowmost saddle points.

A large number of structures of type $\mathbf{c^+} + CH_4$, for which the intermolecular potential is described by the charge-octopole interaction, have been probed but only $\mathbf{d^+}\cdots CH_4$ and $\mathbf{e^+}\cdots CH_4$ have been found to be minima. All the input geometries have been modeled considering the CH_4 molecule as tetrahedron-shaped, resulting in C_s symmetric dimers. The following structures have been tested for the dimer having the ligand bound to the bridging proton ($\mathbf{d^+}\cdots CH_4$): CH_4 pointing with a tip toward the bridging proton of the $C_2H_5^+$ moiety and having an edge of the opposite face either perpendicular or parallel on the $C_1=C_2$ bond; CH_4 closing in with an edge toward the bridging proton of the $C_2H_5^+$ moiety and having this edge either perpendicular or parallel on the $C_1=C_2$ bond; CH_4 facing the

Figure 5. *Some significant points on the ZPE-corrected PES of $[C_3H_9]^+$ and their corresponding geometries. The green and blue lines show alternative paths connecting the nearly covalent bound $\mathbf{a}^+\cdots CH_4$ to the $C_3H_9^+$ systems.*

179
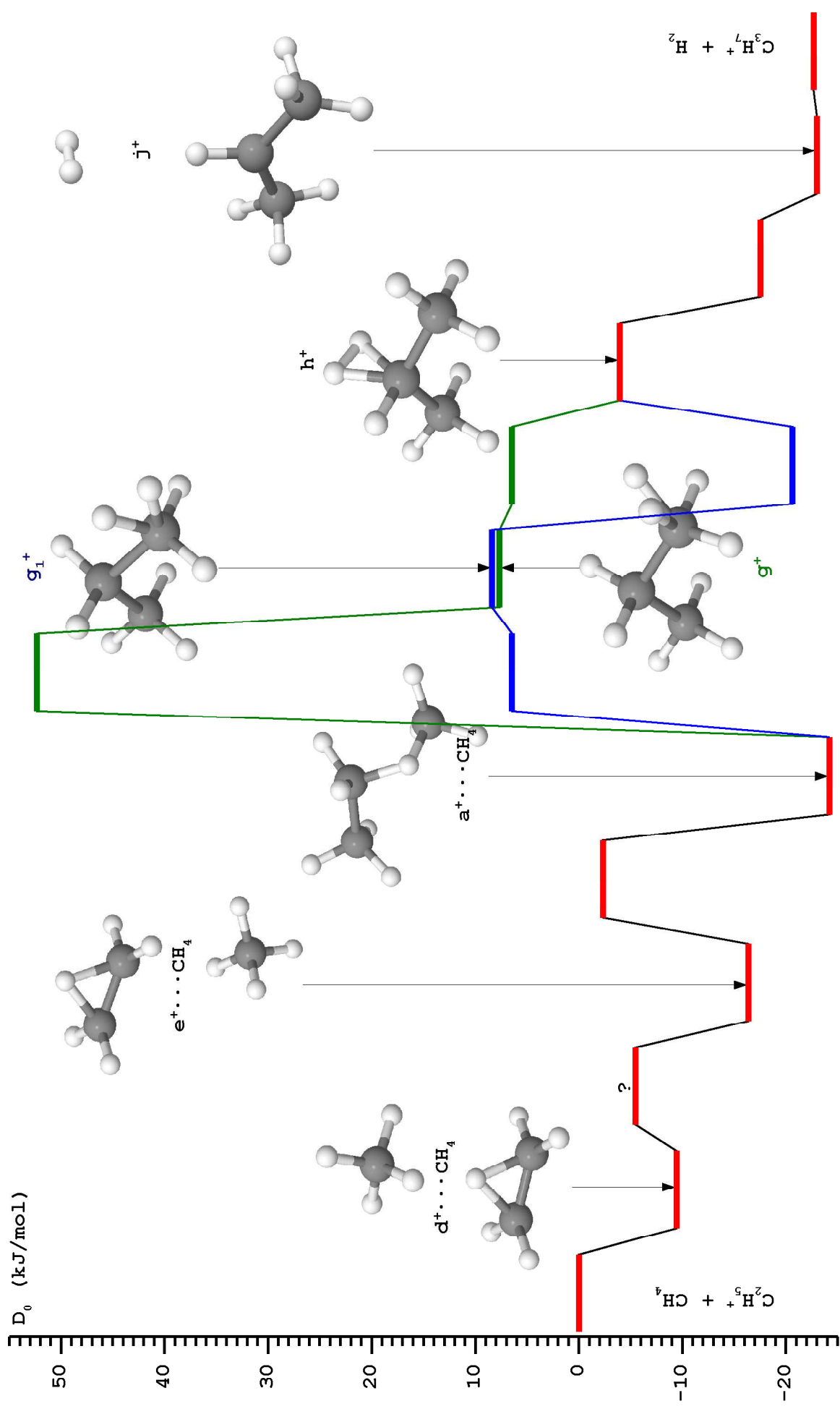
bridging proton of the $C_2H_5^+$ moiety and having an edge of this face either perpendicular or parallel on the $C_1=C_2$ bond. Only this last structure has been found to be a minimum on the PES ($\mathbf{d^+}\cdots CH_4$ on Figure 5). The same set of parameters have been considered in the search for a $\mathbf{e^+}\cdots CH_4$ - type stable equilibrium; the only minimum found is the one having a face of the CH_4 tetrahedron oriented toward a C atom of $C_2H_5^+$ and with the H atoms interlaced with the closest ones of $C_2H_5^+$ ($\mathbf{e^+}\cdots CH_4$ on Figure 5). The characteristics of the intermolecular interaction can be identified from the bond parameters: in both cases, the intermolecular distances are comparable with the ones of the corresponding $C_2H_5^+\cdots Ar$ complexes. (Here, the intermolecular distance is defined as the distance between the C atom of CH_4 and the closest atom of $C_2H_5^+$. If the definition of the intermolecular distance is changed to include the protons of CH_4, the values decrease toward the ones seen for the $C_2H_5^+\cdots CO_2$ and $C_2H_5^+\cdots N_2$ complexes, which are characterized by a much stronger intermolecular interaction: ~1.93 Å for $\mathbf{d^+}\cdots CH_4$ and ~2.88 Å for $\mathbf{e^+}\cdots CH_4$.) It should be noted that the binding energies of the $C_2H_5^+\cdots CH_4$ complexes (~17 kJ/mol) are similar with the ones of the $C_2H_5^+\cdots N_2$ complexes, at the same time being much lower than the experimental value of D_0 obtained via HPMS[20] (23 kJ/mol).

From all geometries considered as candidates for nearly covalent bound dimers of type $\mathbf{a^+}\cdots CH_4$, the most stable one is the one depicted in Figure 5. This minimum is characterized by long-distance direct bonding between the carbon atom of CH_4 and the carbon atom of the methylene group from $[H_3CCH_2]^+$. With respect to the C_1-C_2 bond, the C_1—C_8 bond is very long (2.0583 Å versus 1.4928 Å), showing that the two moieties - $C_2H_5^+$ and CH_4 - are keeping their identities. This intermolecular interaction is supplemented by a H bond between C_1 and the CH_4 ligand. Although $C_2H_5^+$ exerts a considerable pull on it, the bridging proton is clearly part of CH_4. Indeed, the distance between the bridging proton and C_8 is 1.1940 Å while the average distance between the other three protons of CH_4 and C_8 is 1.0841 Å; at the same time, the distance between the bridging proton and C_1 is 2.2346 Å while the average distance between the protons of $C_2H_5^+$ and the carbon atoms to which they bond is 1.0872 Å. It should be noted that at least one more minimum with a similar geometry can be found by rotating the $C_1C_8H_9$ plane around the C_1C_8 axis. The binding energy of this dimer (24.2 kJ/mol) is very much in line with the HPMS-derived value[20] (23 kJ/mol).

Structures derived from a propane backbone have also been investigated, although they are not supposed to dissociate in the present experimental conditions. Indeed, cleavage of a C-C bond in the propane backbone requires ~370 kJ/mol which equates to the simultaneous absorption of at least 9 photons from the investigated range. Such

multiple absorption is not possible here, as the energy density of the excitation laser beam is less than 200 kW/cm^2. Structures derived from a propane backbone are relevant for the chemistry of the EI source, as they are expected to be closer to the global minimum of $[C_3,H_9]^+$. Few such structures have been identified as minima on the global PES of $C_3H_9^+$ (**g$^+$**, **h$^+$**, and **j$^+$** on Figure 5):

- structure **g$^+$** is derived via protonating one of the methyl groups of propane;

- structure **h$^+$** is also an isomer of the protonated propane, having the proton attached to the center carbon atom;

- structure **j$^+$** is a weakly bound complex between $C_3H_7^+$ and H_2.

The assignment of the **g$^+$** and **h$^+$** structures to $C_3H_9^+$ isomers and not to $C_3H_7^+\cdots H_2$ complexes is supported by the large H-H distances ($r^{g^+}_{H-H}$ = 0.9232 Å and $r^{h^+}_{H-H}$ = 0.8824 Å versus $r^{H_2}_{H-H}$ = 0.7371 Å); in the case of the $C_3H_7^+\cdots H_2$ complex, $r^{j^+}_{H-H}$ = 0.7390 Å.

The only TS identified between **a$^+$** and **g$^+$** is a second order saddle point; at the same time the TS between **g$^+$** and **h$^+$** is placed lower than **g$^+$**, giving to **g$^+$** the appearance of a shoulder on the PES (green line in Figure 5). These abnormalities have prompted additional investigations of the protonation of one methyl group of propane. Another minimum (further denoted **g$_1$$^+$**) was thus identified. It was found to be similar with **g$^+$** in structure but slightly less stable. The characteristic of **g$_1$$^+$** is the alignment of the two closely-packed protons in the $C_1C_2C_8$ plane. Using this **g$_1$$^+$** structure, it was possible to find first order saddle points connecting the PES (blue line in Figure 5). However, both TSs obtained via quantum chemical calculations were found to be placed **lower** in energy than **g$_1$$^+$**. This means that **g$^+$** and **g$_1$$^+$** are rather unreliable elements of the $[C_3,H_9]^+$ PES.

Structure **j$^+$** seems to be the absolute minimum on the PES. The geometry of this complex has just C_2 symmetry, with the methyl groups twisted around the C-C bonds. The only saddle point found to connect **h$^+$** and **j$^+$** is a third order saddle point. It can be seen that the weakly bound $C_3H_7^+\cdots H_2$ complex requires very little energy to dissociate. Overall, the entire part of the $[C_3,H_9]^+$ PES which describes the propane backbone is unreliable and must be regarded only as an approximation.

The spectra of the **d$^+\cdots$CH$_4$** and **e$^+\cdots$CH$_4$** are quite similar with the ones of the other weakly bound systems investigated. The major differences result from the appearance of stretch vibrations specific to CH_4 which occur in the same range (marked with * in Table 3 and in Figure 11) and from the coupling between certain stretch modes of $C_2H_5^+$ with modes of CH_4 (marked with ** in Table 3 and in Figure 11). The spectra of **d$^+\cdots$CH$_4$** and **e$^+\cdots$CH$_4$** are indiscernible in the investigated range. In this case the assignment of

experimental bands to them must rely on the differences in the stabilization energy of the complexes. As the binding energy of **d⁺**···CH₄ is just half than the one of **e⁺**···CH₄, it results that **e⁺**···CH₄ is the only **c⁺**···CH₄ - type complex which should be considered.

In the case of the **a⁺**···CH₄ dimer, the spectra exhibit few remarkable characteristics. First, the contribution of the proton bridge to the intermolecular bond results in an exceptionally strong red-shift of the corresponding ω_{CH} vibration of the CH₄ ligand (2340 cm⁻¹, down circa -900 cm⁻¹ from its monomer position). The IR intensity is enhanced by more than a factor 10 with respect to the other ω_{CH} stretch vibrations. These remaining vibrations are spread over circa 200 cm⁻¹ and have roughly equal IR intensities.

7.3. Experimental details

The IRPD spectra of the mass-selected $C_2H_5^+$···L dimers (L = Ar, N₂, CO₂, CH₄) as well as of the $C_2H_5^+$···(N₂)ₙ (n = 1...6) complexes have been recorded in the quadrupole - octopole - quadropole tandem mass spectrometer, coupled with the electron ionization ion source and the OPO laser[23],[34] presented in the *Experimental setup* section. In the following only details specific to the production of $C_2H_5^+$···Lₙ complexes are described.

A mixture of CH₄ and ligand gas (Ar, N₂, CO₂, at a typical backing pressure of 3 bar and with a typical mixing ratio of 1:10) is sampled in the ion source. During the expansion, electron impact ionization of the Ar buffer gas occurs, followed by charge transfer from Ar⁺ to CH₄ and the elimination of a H atom; finally, the methyl cation (CH₃⁺) reacts with CH₄ and produces $C_2H_5^+$ via an elimination reaction:

$$Ar + e^- \rightarrow Ar^+ + 2 \cdot e^- \tag{1}$$

$$CH_4 + Ar^+ \rightarrow CH_3^+ + H + Ar \tag{2}$$

$$CH_3^+ + CH_4 \rightarrow C_2H_5^+ + H_2 \tag{3}$$

The complexation of $C_2H_5^+$ with Ar takes place in the supersonic expansion via three-body collisions:

$$C_2H_5^+ + Ar + M \rightarrow C_2H_5^+ \cdots Ar + M \qquad M = CH_4, Ar \tag{4}$$

The IRPD which takes place in the octopole results in the fragmentation of the complex:

$$C_2H_5^+ \cdots Ar + h \cdot \nu \rightarrow C_2H_5^+ + Ar \tag{5}$$

The production mechanisms are similar for all ligands; however, depending on the strength of the intermolecular bond, the IRPD process may differ considerably from (5). This is especially true for the strongly bound $\mathbf{a^+}\cdots N_2$, (and, maybe, for $\mathbf{d^+}\cdots CO_2$) for which D_0 is supposed to be larger than the energy of v_{CH}. In this case it is possible that the photodissociation spectrum of $C_2H_5^+\cdots L$, obtained via direct IR excitation, will show only hot bands.

Figure 6. *Typical ion source mass scan recorded for an Ar:CH$_4$ mixture ratio of 10:1, at 3 bar backing pressure. The right half is enlarged (X50) to better outline the complexes. The peaks at 20 u, 40 u and 41 u are attributed to Ar^{2+}, Ar^+ and ArH^+. The series marked by ▼ is assigned to $C_2H_5^+\cdots(CH_4)_n$ and the one marked by ● is assigned to $C_2H_5^+\cdots Ar_n$; $CH_5^+\cdots(CH_4)_n$ series, marked by ▲, can also be identified.*
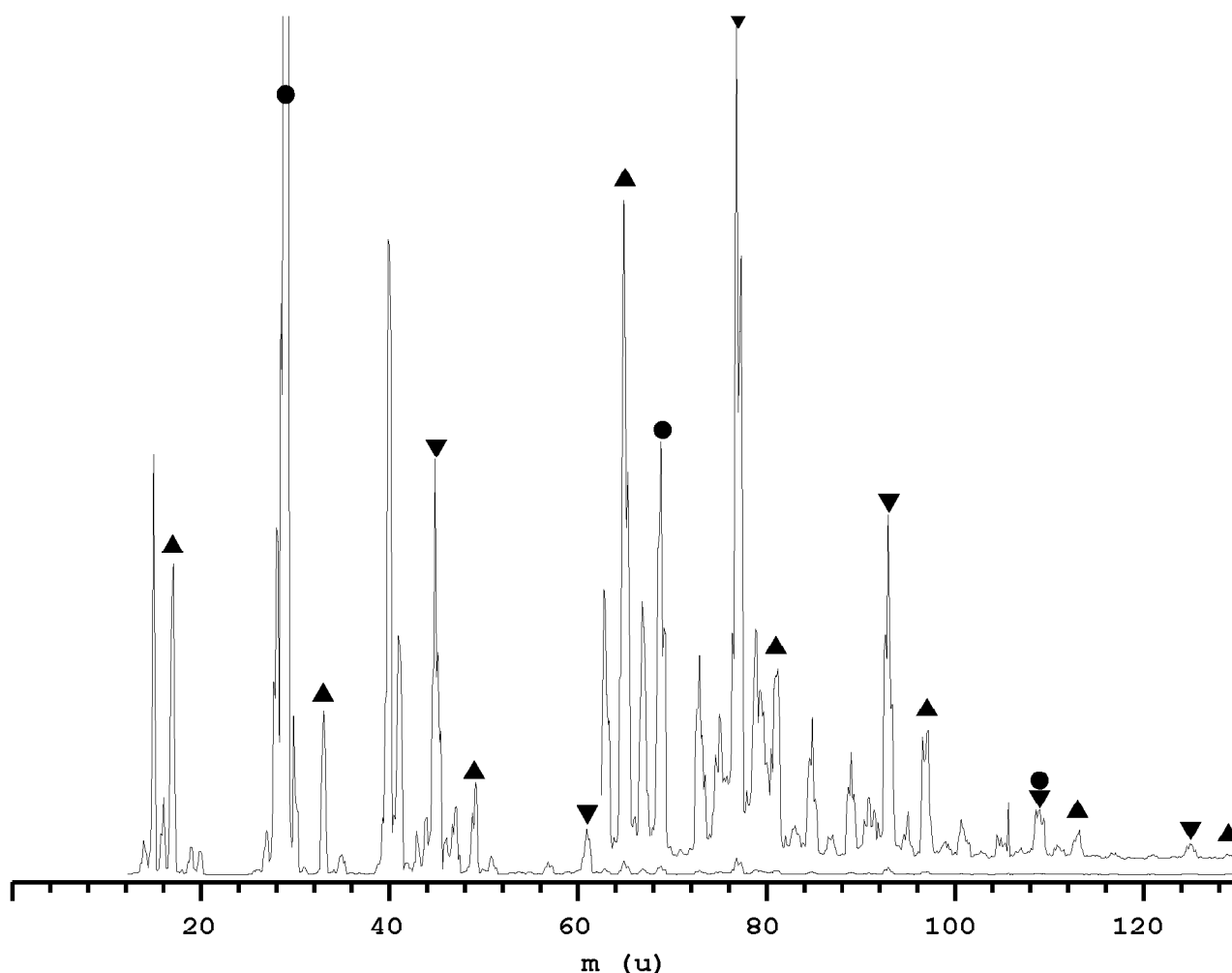
A typical mass spectrum of the output of the ion source is presented in Figure 6; in the right part of the picture is also presented an enlarged (X50) version of the scan, to facilitate the identification of weak components of the expansion. The largest feature of the

spectrum occurs at 29 u and is assigned to $C_2H_5^+$ and, maybe, to the N_2H^+ impurity. The peaks at 20 u, 40 u and 41 u are attributed to Ar^{2+}, Ar^+ and ArH^+. The series marked ▼ is assigned to $C_2H_5^+\cdots(CH_4)_n$ and the one marked ● is assigned to $C_2H_5^+\cdots Ar_n$; the feature appearing at 109 u is due to both $C_2H_5^+\cdots Ar_2$ and $C_2H_5^+\cdots(CH_4)_5$; the $CH_5^+\cdots(CH_4)_n$ series (▲) can also be easily identified.

As usual, a signal proportional with the laser power was recorded via an InSb detector simultaneous with the IR spectrum. The ion signal was linearly normalized on the resulting power trace in order to eliminate the ion signal' variations caused by fluctuating laser power. The calibration of the spectra was done using HDO as reference substance in the optoacoustic cell. By linearly resizing the interval between successive optoacoustic lines using literature tables,[35] accuracy better than 0.5 cm^{-1} was achieved.

7.4. Results and discussion

The IRPD spectra of the studied dimers, together with stick spectra derived from the quantum chemical calculations, are presented in Figure 7 ($C_2H_5^+\cdots Ar$), Figure 9 ($C_2H_5^+\cdots N_2$), Figure 10 ($C_2H_5^+\cdots CO_2$), and Figure 11 ($C_2H_5^+\cdots CH_4$) respectively. In order to better underline the similarities and the differences between them, a comparison of all IRPD spectra of the studied dimers is presented in Figure 12. Further experimental results are spectra of $C_2H_5^+\cdots(N_2)_n$ (n = 1...6), presented in Figure 13 and of $C_2H_5^+\cdots(CH_4)_n$ (n = 1...4), presented in Figure 14. The principal parameters of the observed bands (band center position, FWHM, proposed assignment) are shown in Table 4.

Table 4. *Band maxima (in cm^{-1}), their FWHM (in parentheses, in cm^{-1}), and proposed assignment for $C_2H_5^+\cdots Ar$, $C_2H_5^+\cdots(N_2)_n$, $C_2H_5^+\cdots(CO_2)_n$, and $C_2H_5^+\cdots(CH_4)_n$. For each complex, its fragmentation channel is listed as n→m.*

| n	m	Band	Position (FWHM) (cm^{-1})	Assignment	n	m	Band	Position (FWHM) (cm^{-1})	Assignment
			$C_2H_5^+\cdots Ar$					$C_2H_5^+\cdots(CO_2)_n$	
		A	3117 (30)	$\nu_{CH}^{d^+\cdots Ar}$			A	3122 (17)	$\nu_{CH}^{d^+\cdots CO_2}$
		B	3037 (25)	$\nu_{CH}^{d^+\cdots Ar}$	1	0	B	3042 (32)	$\nu_{CH}^{d^+\cdots CO_2}$
			$C_2H_5^+\cdots(N_2)_n$				G	2954 (30)	$\nu_{CH}^{a^+\cdots CO_2}$, $\nu_{CH}^{a_1^+\cdots CO_2}$
		A	3119 (30)	$\nu_{CH}^{d^+\cdots N_2}$			A	3125 (8)	$\nu_{CH}^{d^+\cdots CO_2}$
		B / C	3036 (10)	$\nu_{CH}^{d^+\cdots N_2}$, $\nu_{CH}^{a^+\cdots N_2}$	2	1	B	3039 (10)	$\nu_{CH}^{d^+\cdots CO_2}$

n	m				
1	0	D	3017	(15)	$\nu_{CH}^{a^+\cdots N_2}$
		E	2970	(14)	$\nu_{CH}^{a^+\cdots N_2}$
		F	2962	(14)	$\nu_{CH}^{a^+\cdots N_2}$
		G	2914	(10)	$\nu_{CH}^{a^+\cdots N_2}$
2	1	C	3034	(10)	$\nu_{CH}^{a^+\cdots N_2}$
		D	3017	(10)	$\nu_{CH}^{a^+\cdots N_2}$
		E	2970	(11)	$\nu_{CH}^{a^+\cdots N_2}$
		F	2960	(11)	$\nu_{CH}^{a^+\cdots N_2}$
		G	2925	(17)	$\nu_{CH}^{a^+\cdots N_2}$
3	1	C	3036	(7)	$\nu_{CH}^{a^+\cdots N_2}$
		D	3021	(10)	$\nu_{CH}^{a^+\cdots N_2}$
		E	2976	(8)	$\nu_{CH}^{a^+\cdots N_2}$
		F	2961	(10)	$\nu_{CH}^{a^+\cdots N_2}$
		G	2938	(10)	$\nu_{CH}^{a^+\cdots N_2}$
4	1	C	3036	(9)	$\nu_{CH}^{a^+\cdots N_2}$
		D	3020	(6)	$\nu_{CH}^{a^+\cdots N_2}$
		E	2974	(7)	$\nu_{CH}^{a^+\cdots N_2}$
		F	2959	(8)	$\nu_{CH}^{a^+\cdots N_2}$
		G	2938	(??)	$\nu_{CH}^{a^+\cdots N_2}$
5	2	C	3036	(7)	$\nu_{CH}^{a^+\cdots N_2}$
		D	3021	(5)	$\nu_{CH}^{a^+\cdots N_2}$
		E	2974	(9)	$\nu_{CH}^{a^+\cdots N_2}$
		F	2960	(9)	$\nu_{CH}^{a^+\cdots N_2}$
		G	2946	(10)	$\nu_{CH}^{a^+\cdots N_2}$

n	m				
		G	2949	(??)	$\nu_{CH}^{a^+\cdots CO_2}$, $\nu_{CH}^{a_1^+\cdots CO_2}$
3	1	A	3128	(8)	$\nu_{CH}^{d^+\cdots CO_2}$
		B	3041	(11)	$\nu_{CH}^{d^+\cdots CO_2}$
		G	2950	(13)	$\nu_{CH}^{a^+\cdots CO_2}$, $\nu_{CH}^{a_1^+\cdots CO_2}$

$C_2H_5^+\cdots(CH_4)_n$					
1	0	A	3118	(5)	$\nu_{CH}^{d^+\cdots CH_4}$
		C	3107	(20)	$\nu_{CH}^{a^+\cdots CH_4}$
		D	3084	(22)	$\nu_{CH}^{a^+\cdots CH_4}$
		E	2976	(22)	$\nu_{CH}^{a^+\cdots CH_4}$
		F	2948	(25)	$\nu_{CH}^{a^+\cdots CH_4}$
		G	2900	(24)	$\nu_{CH}^{a^+\cdots CH_4}$
		H	2885	(20)	$\nu_{CH}^{a^+\cdots CH_4}$
4	1	C_1	3101	(??)	$\nu_{CH}^{[C_3,H_9]^+}$
		D_1	3089	(11)	$\nu_{CH}^{[C_3,H_9]^+}$
		E_1	3075	(10)	$\nu_{CH}^{[C_3,H_9]^+}$
		F_1	3026	(9)	$\nu_3^{CH_4}$
		G_1	2998	(15)	$\nu_3^{CH_4}$
		H_1	2904	(11)	$\nu_1^{CH_4}$

Unidentified bands in the 29 + $(N_2)_n$ → 29+$(N_2)_m$ IRPD spectra					
2	1	X	2877	(21)	???
3	1	X	2917	(18)	???
4	2	X	2950	(14)	???
5	3	X	2973	(9)	???

7.4.1. The $C_2H_5^+\cdots$Ar dimer

The IRPD spectrum of $C_2H_5^+\cdots$Ar is presented in the upper part of Figure 7; in the lower part of the same figure are plotted the stick spectra of $d^+\cdots$Ar and $e^+\cdots$Ar. The computed frequencies plotted here have been corrected for anharmonicity by rescaling them so that the strongest vibration of d^+ overlaps with the most prominent band from the experimental spectrum. The value of the scaling factor (0.942) is typical for *ab initio*

185

calculations[36].

Figure 7. *The IRPD spectrum of* $C_2H_5^+\cdots Ar$ *and the stick spectra of* ***c⁺***, ***d⁺***, ***d⁺***···Ar, and ***e⁺***···Ar *monomers and complexes (calculated at the MP2/6-311G(2df,2pd) level and rescaled by 0.942).*
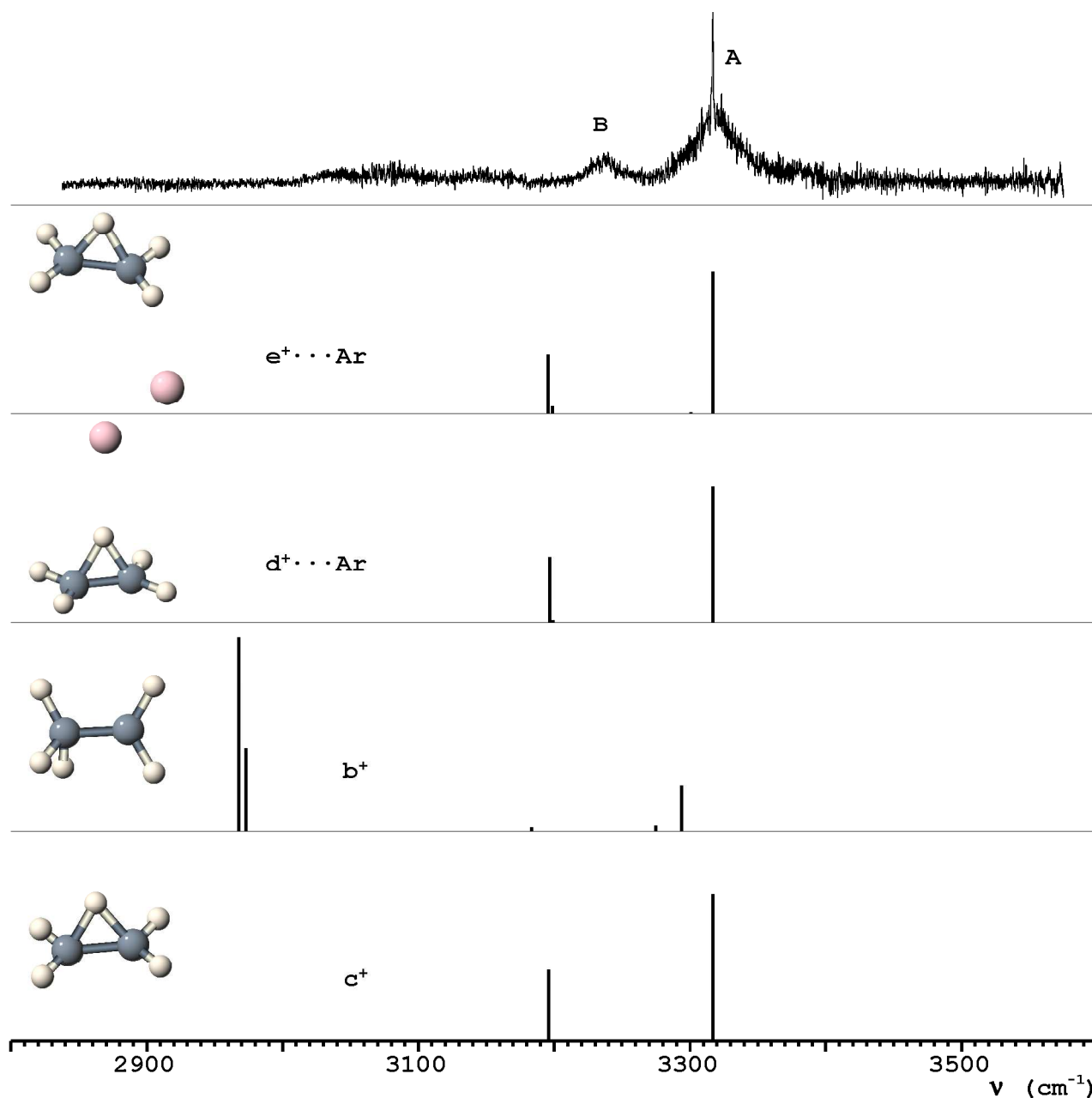
Although the investigated spectral domain (2650 cm⁻¹ ... 3375 cm⁻¹) is easily covering the ranges of sp³ C-H stretching frequencies (2850-3000 cm⁻¹), sp² C-H stretching frequencies (3020-3100 cm⁻¹) and even sp C-H stretching frequencies (~3300 cm⁻¹), the only two bands identified in the spectrum (band A at 3117 cm⁻¹ and band B at 3037 cm⁻¹), appear in the range of the sp² C-H stretching modes. Both bands are rather symmetric with respect to their absorption maxima, suggesting that the Ar ligand is not interacting

directly with any of the protons involved in the observed vibrations. This characteristic is compatible with both $c^+\cdots$Ar isomers. The ratio between the IR activities of the two bands (A:B $\cong$ 2:1) is in very good agreement with the intensity ratios of both $c^+\cdots$Ar - based dimers ($I_{IR}^A : I_{IR}^B$ = 2.3 : 1); however, the spacing between the observed bands (80 cm^{-1}) is not so well matched by the calculations (122 cm^{-1}). On one hand, it can be seen that the similarities between the simulated spectra of $d^+\cdots$Ar and $e^+\cdots$Ar render impossible the positive identification of the isomer(s) responsible for the observed bands. On the other hand, the relative stabilities of the two calculated dimers suggest that the dominant carrier for both observed bands is $d^+\cdots$Ar.

Figure 8. *High-resolution scan of band A (upper part, rights); simulation of the rotational contours of bands A and B (lower part), assuming the bridged geometry of $C_2H_5^+$ and that the ligand is attached to the bridging proton.*
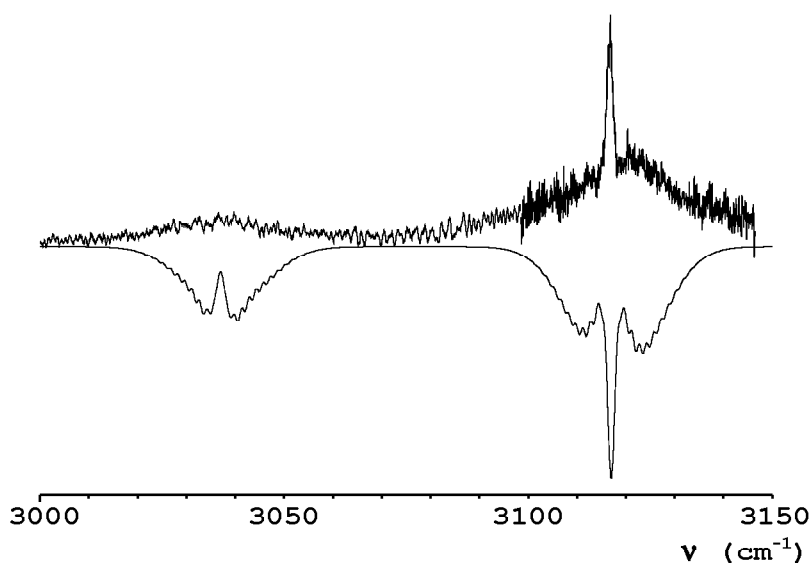
A higher resolution scan of band A (Figure 8, upper trace) reveals that the band is split into P, Q and R branches, but no further rotational structure can be resolved. In order to check the assignment of the bands, a rotational simulation for the two vibrations of $d^+\cdots$Ar has been done. The simulation was done by using the WANG program package, developed by Luckhaus[37]. The rotational constants of the ground vibrational state were calculated considering the equilibrium geometry. The dependence of the rotational constants on the vibrational excitation has been considered. This dependence results from the slight expansion of the C-H bonds upon vibrational excitation. It was considered that the C-H bonds expand by 0.5% with respect to the ground vibrational state values ($r_{CH}^{v=1}$ = 1.0840 Å versus $r_{CH}^{v=0}$ = 1.0835 Å), as derived from the measurements done by Oka et al on CH_3^{+}[38]. The resulting rotational constants are 24.0119072 GHz, 2.3144622 GHz, and 2.1747576 GHz for the ground state and 24.0052346 GHz, 2.3144142 GHz, and 2.1747221 GHz for the excited state. Band A is a c-type band whereas B is a b-type band. The simulated stick spectra were obtained considering a

Boltzmann distribution for the population of the first 50 rotational levels at a rotational temperature T_{rot} = 50 K; the centers of the experimental bands were considered as origins for the simulated bands. The computed lines were afterwards convoluted with Gaussian profiles having FWHM of 0.3 cm^{-1} and were used to generate the rotational contours plotted in the lower part of Figure 8. The two simulated rotational spectra were normalized considering the intensity ratio derived from the calculation. The resemblance of the simulated spectrum with the recorded one is striking and adds further weight to the assignment.

It should be noted that a partially-resolved rotational envelope was recorded at 3969 cm^{-1} by Yeh et al in their IR investigation of $C_2H_7^{+[39]}$ (see Figure 7 of their paper). At that time it was assigned to the H-H stretch fundamental of a weakly bound isomer of the classical $C_2H_5^+\cdots H_2$ (presented as a pentacoordinated carbonium ion). This assignment was supported by the presence of ripples on top of the P and R branches whose spacing was found to be consistent with the rotational constants of such a classical isomer. Further analysis done by other groups[10],[12] suggested alternative assignments for this band, still derived from classical isomers of $C_2H_7^+$: this band has been assigned to combination bands of the H-H stretch vibration with either an sp^2 C-H vibration or a complicated C-C stretch mode. Finally, East et al[11] have used the H-H stretch fundamental of a $d^+\cdots H_2$ complex to demonstrate via rotational profile simulation that not only open isomers of C_2H_7' are able to produce the observed rotational contour. However, in the end they have assigned this band not to the H-H stretch fundamental but to the first overtone of the bridging proton stretch vibration in the afore-mentioned complex. Independent of the precise assignment of this band, it is relevant the fact that there is previous spectroscopic evidence supporting the supposition that $C_2H_5^+$ has a nonclassical structure.

7.4.2. The $C_2H_5^+\cdots N_2$ dimer

Figure 9 shows the IRPD spectrum of $C_2H_5^+\cdots N_2$ together with the stick spectra of $d^+\cdots N_2$, $e^+\cdots N_2$, and $a^+\cdots N_2$. The computed frequencies plotted here have been corrected for anharmonicity using a factor (0.941) which brings in line the calculated frequency of the strongest ω_{CH} of $d^+\cdots N_2$ with the band A from the experimental spectrum. The value of the scaling factor is nearly identical to the one inferred for $d^+\cdots Ar$.

All the observed bands have rather symmetric shapes, suggesting that none of them is the result of a ligand-bound stretch vibration. The observed spectrum is completely different from the one of $C_2H_5^+\cdots Ar$: close to the position of band A in the spectrum of $C_2H_5^+\cdots Ar$ there is only a very weak absorption (3119 cm^{-1}), while close to the position of

band B there is a much stronger absorption (3036 cm^{-1}). Considering the calculated IR intensity ratio between bands A and B (circa 2 : 1) and the observed integrated band activity ratio (circa 1 : 2), it follows that the IR activity at 3036 cm^{-1} must have a strong

Figure 9. *The IRPD spectrum of $C_2H_5^+\cdots N_2$ and the stick spectra of $\mathbf{d^+}\cdots N_2$, $\mathbf{e^+}\cdots N_2$, and $\mathbf{a^+}\cdots N_2$ complexes (calculated at the MP2/6-311G(2df,2pd) level and rescaled by 0.941).*
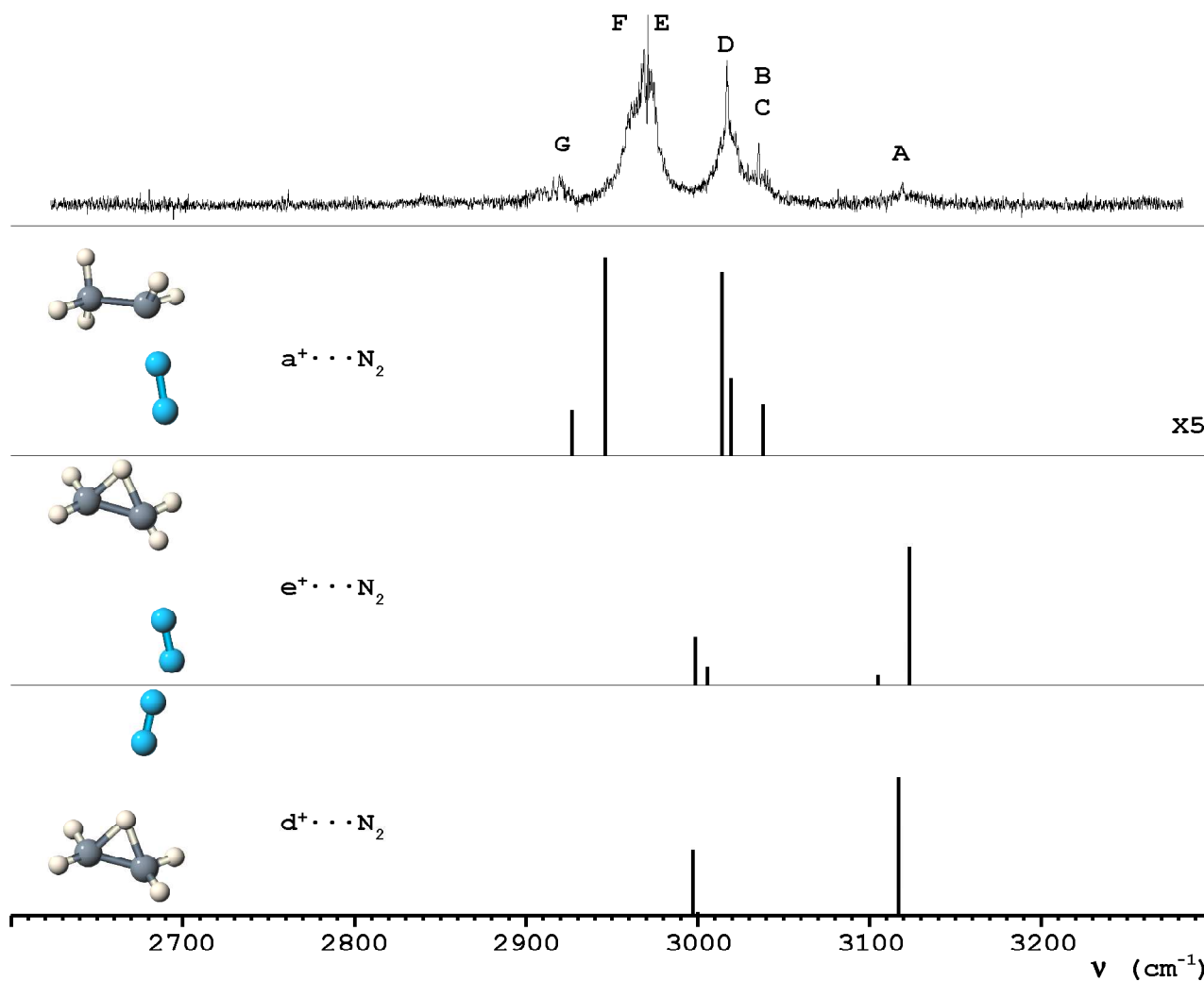
component from some different isomer. It can be seen that this band also sports a sharp Q branch component, which was absent from the simulated rotational contour done for $\mathbf{d^+}\cdots$Ar. Thus, the band at 3036 cm^{-1} will be given a double assignment, to band B of $\mathbf{d^+}\cdots N_2$ and to a band (further denoted C) of another isomer. Band A is blue-shifted by +2 cm^{-1} from the position recorded in the $\mathbf{d^+}\cdots$Ar spectrum; this slight shift is in line with the prediction of the calculations (+1 cm^{-1}). Same thing holds true also for band B, for which the predicted blue-shifts amounts to +2 cm^{-1}. The reason for this blue-shift is the redistribution of the charge in the $C_2H_5^+$ moiety driven by the intermolecular interaction. This results in strengthening of all C-H bonds, excepting the ones involving the bridging

proton.

The bands dominating the observed spectrum are largely corresponding to the open isomer $a^+ \cdots N_2$. It is remarkable that the correspondence between the observed IR absorption and the calculated vibrations is only loose. Indeed, the most obvious similarity between the calculations and the observed spectrum is the separation of the bands in two groups. However, the number of bands comprising each of these groups is not matched between the experiment and the calculations. This is probably the result of the strong intermolecular interaction specific to the $a^+ \cdots N_2$ dimer.

It should be noted that not only bands A and C exhibit rotational profile, but also band D. A simulation of the rotational profile is however not straightforward for these bands, as they are supposed to have both parallel and perpendicular transition characteristics.

The rather small FWHM of the observed bands suggests that they are results of fundamental transitions and not hot bands. This means that the dissociation energy of the complex is smaller than the IR excitation energy. The calculations done for $a^+ \cdots N_2$ have yielded binding energy of 4793 cm^{-1} without ZPE correction, or 3159 cm^{-1} including the ZPE correction, in line with the observed characteristics of the spectrum.

7.4.3. Larger $C_2H_5^+ \cdots (N_2)_n$ complexes (n = 2 ... 5)

All recorded spectra of $C_2H_5^+ \cdots (N_2)_n$ complexes (n = 1 ... 5) are presented in the left half of Figure 10. It can be seen that band A disappears completely from the spectrum of the trimer onwards, showing that, indeed, the $d^+ \cdots (N_2)_n$ complexes are much less stable than the $a^+ \cdots (N_2)_n$ ones. Bands C, D, E, and F behave in a similar fashion: they red-shift in the spectrum of the trimer by a small amount (~-2 cm^{-1}), then start to blue-shift. For the largest investigated cluster, these bands shift by ~+4 cm^{-1} with respect to the spectrum of the dimer. The remaining band (G) develops in a particular fashion: it continuously blue-shifts, appearing shifted by +32 cm^{-1} in the spectrum of $C_2H_5^+ \cdots (N_2)_5$ with respect to the position seen in the spectrum of $C_2H_5^+ \cdots N_2$. Considering that in all recorded spectra bands C, D, E, F, and G appear in the same photofragmentation channel, it is unlikely that band G is connected with other isomer but $a^+ \cdots (N_2)_n$. The general blue-shifting mirrors the global increase of the non-cooperative three-body interactions, which have as final result a weakening of the interaction between each $C_2H_5^+ \cdots N_2$ pair. The magnitude of these blue-shifts is in line with the known low acidity of the C-H bonds. While all bands are shifting toward higher frequencies at different paces, their FWHM are continuously decreasing. The decrease in FWHM of the observed bands signals the vibrational cooling of the complex and shows that, starting with the second ligand, their binding energies are

Figure 10. The IRPD spectra of $C_2H_5^+\cdots(N_2)_n$ ($n = 1 \ldots 5$) complexes (mass-selected as $29+n\cdot28\ u$), recorded in the $C_2H_5^+\cdots(N_2)_m$ ($m = 0 \ldots 3$) fragment channels (mass-selected as $29+m\cdot28\ u$). The evaporation channels are indicated at the left of each spectrum. The coloured stripes connect bands corresponding to the same vibration mode of the $C_2H_5^+$ moiety. The bands underlined in the right-hand of the picture are assigned to a vibrational mode of an impurity, most probably $C_2N_2H_5^+$ ($57+(n-1)\cdot28\ u \rightarrow 57+(m-1)\cdot28\ u$).
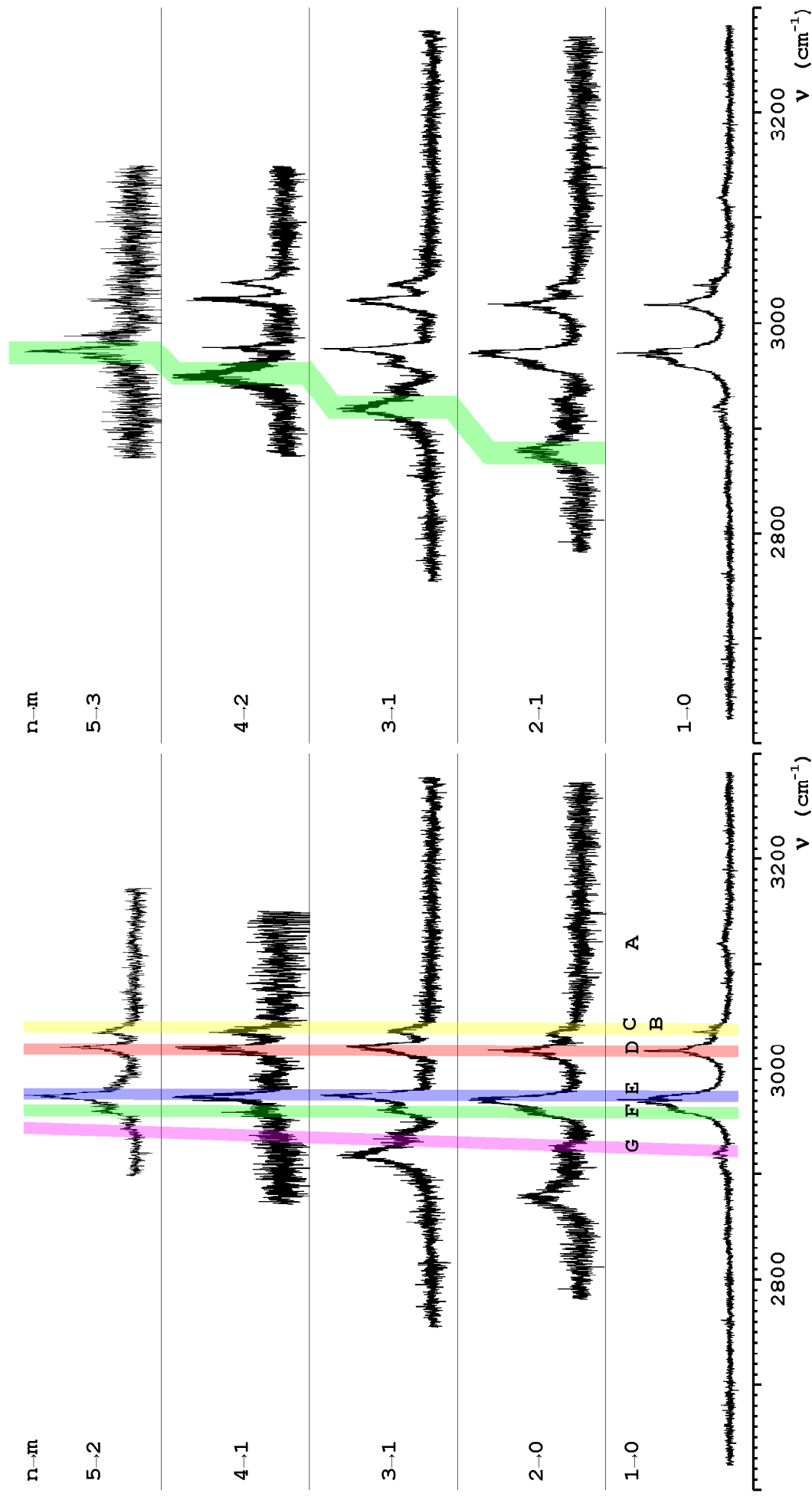
considerably lower than the one between the $C_2H_5^+$ moiety and the first ligand. This finding fits well the quantum chemical calculations which show that the most stable dimer structure is nearly covalently bound. A secondary effect of the decrease in FWHM of the bands is that they become more visible. This way it becomes obvious that the IR activity between 2940 cm^{-1} and 2990 cm^{-1} was correctly assigned to two independent bands.

One more highly active band (X) can be seen in the spectra of the trimer and the tetramer (2877 cm^{-1} and 2917 cm^{-1}, respectively). The disappearance of this band in the $4 \rightarrow 1$ and $5 \rightarrow 2$ fragmentation channels has prompted the analysis of the neighboring ones. Indeed, the band can again be found in the $4 \rightarrow 2$ and $5 \rightarrow 3$ fragmentation channels at 2949 cm^{-1} and 2973 cm^{-1} respectively. Backtracing the observed blue-shifts, it results that in the spectrum of the dimer, the corresponding band should appear somewhere between 2700 cm^{-1} and 2800 cm^{-1}. This position cannot be matched by any vibration of the dimers investigated via quantum chemical calculations. Another unusual characteristic is the strong blue-shifting of this band as the complexation increases. This signals that one ligand (probably the first one) is bound directly to the chromophore via an H-bond. Among the investigated dimer structures, the only H-bound dimer is $\mathbf{d^+ \cdots N_2}$ but the stretch vibration of the binding proton occurs no higher than 2122 cm^{-1} (this limit is set by the harmonic calculations). It results then that this band cannot be connected with any investigated dimer. Considering the specifics of the ion source used and the precursor substances, some tentative assignments can be made.

The simplest assignment is to N_2H^+ produced via the protonation of the carrier gas (N_2); indeed, N_2H^+ has the same mass (29 u) as $C_2H_5^+$. In this case, every $C_2H_5^+\cdots(N_2)_n$ mass channel would be contaminated with $N_2H^+\cdots(N_2)_n$. The fact that the magnitude of the complexation-induced blue-shifts is comparable with the one expected for a highly acidic N-H bond seems to support this assignment. However, both the theory and experiments are disproving this tentative assignment. Quantum chemical calculations done at the MP2/6-311G(2df,2pd) level yield $\omega_{NH} = 3430$ cm^{-1} for the N_2H^+ free proton stretch mode. The addition of a N_2 molecule to this system (thus obtaining [N≡N—H—N≡N]$^+$) shifts the harmonic frequency of the proton stretch mode down to $\omega_{NH} = 611$ cm^{-1}. Similar with previous investigations,[40] the only frequency matching the range of the recorded IRPD spectra is the one of the combination band between the proton stretch vibration ($\omega_{NH} = 611$ cm^{-1} and $I_{NH} = 5111$ km/mol) and the IR active mode of the N≡N stretches ($\omega_{NN} = 2219$ cm^{-1} and $I_{NN} = 239$ km/mol). This match is however only rough, as the anharmonicity of the system pushes the frequency of the combination mode much lower than the harmonic 2830 cm^{-1}. In the case of the trimer, the calculations reveal one possible

T-shaped structure. The proton stretch frequency in this case is $644\,cm^{-1}$ ($I_{NH} = 4721\,km/mol$) while the most IR active $N\equiv N$ stretch mode has a frequency of $2219\,cm^{-1}$ ($I_{NN} = 220\,km/mol$). It follows that the harmonic approximation of the combination band frequency is $2863\,cm^{-1}$, just below the observed position ($2877\,cm^{-1}$). Thus, the vibrational analysis infirms the $N_2H^+\cdots(N_2)_n$ tentative assignment. It is notable that this assignment seems to be supported by an analysis of the binding energies. Indeed, the energy required to evaporate one N_2 molecule from $[N_2HN_2]^+$ is much larger than the energy of the photons in the scanned range ($\sim 7080\,cm^{-1}$ - ZPE-corrected value versus maximum $3300\,cm^{-1}$); this find fits well with the absence of any vibration of $[N_2HN_2]^+$ in the spectrum. In the case of the presumed $(N_2)_3H^+$, the energy required to evaporate the added N_2 molecule is $1543\,cm^{-1}$, smaller than the energy of the excitation photon ($2877\,cm^{-1}$) and fitting with the observation of the unidentified band. In order to eliminate $(N_2)_{n+1}H^+$ as possible carrier, IRPD spectra of $(N_2)_{n+1}H^+$ have been recorded over the $2600 ... 3300\,cm^{-1}$ range. The $(N_2)_{n+1}H^+$ complexes have been obtained by replacing the CH_4 feed with a H_2 line; all other optimization elements have been left unchanged. Attempts have been made to record IRPD spectra in the following fragmentation channels: $(N_2)_2H^+ \rightarrow N_2H^+$, $(N_2)_3H^+ \rightarrow (N_2)_2H^+$, and $(N_2)_5H^+ \rightarrow (N_2)_3H^+$. While in all cases the CID suggesting that large amounts of the parent are present in the mixture, all three IRPD spectra have revealed no absorption.

Another molecular system which can easily be produced in the ion source is H_2CNH^+ (methanimine cation). Its N-H stretch mode was observed at $3263\,cm^{-1}$,[41] while presently done calculations are predicting it at $3595\,cm^{-1}$. Using the scaling factor resulting from these values, it can be predicted that the addition of a N_2 ligand to the N-H chromophore will shift the frequency of its stretch mode down to $2887\,cm^{-1}$. At the same time, the ZPE-corrected binding energy of this complex is calculated to be $2392\,cm^{-1}$, well under the excitation photon's energy. It results that, if produced in a sizeable amount, $H_2CNH^+\cdots N_2$ should dissociate and thus be visible even in the dimer spectrum. This means that also this tentative assignment must me discarded.

The absence of band X in the $57\,u \rightarrow 29\,u$ spectrum might signify that the smallest chemically bound species has an atomic mass of $57\,u$. There are five easily identifiable chemical formulas that have this atomic mass: $C_4H_9^+$, $C_3NH_7^+$, $C_2N_2H_5^+$, $CN_3H_3^+$, and N_4H^+. A previous study of a microwave discharge in a CH_4 and N_2 mixture has revealed that the dominant species at $m/z = 57$ is $C_2H_3N=NHH^+$.[42] Although no quantum chemical calculations have been attempted for this species, it will still be considered as the most probable origin of band X.

7.4.4. The $C_2H_5^+\cdots CO_2$ dimer

Figure 11 shows the IRPD spectrum of $C_2H_5^+\cdots CO_2$ together with the stick spectra of **d$^+$**$\cdots CO_2$, **e$^+$**$\cdots CO_2$, **a$^+$**$\cdots CO_2$, and **a$_1$$^+$**$\cdots CO_2$. The computed frequencies plotted here have been corrected for anharmonicity using a factor (0.942) which brings in line the calculated frequency of the strongest ω_{CH} of **d$^+$**$\cdots CO_2$ with the band A from the experimental spectrum. The value of the scaling factor fits very well the ones inferred for **d$^+$**$\cdots Ar$ and **d$^+$**$\cdots N_2$.

Figure 11. *The IRPD spectrum of $C_2H_5^+\cdots CO_2$ and the stick spectra of **d$^+$**$\cdots CO_2$, **e$^+$**$\cdots CO_2$, **a$^+$**$\cdots CO_2$, and **a$_1$$^+$**$\cdots CO_2$ complexes (calculated at the MP2/6-311G(2df,2pd) level and rescaled by 0.942).*
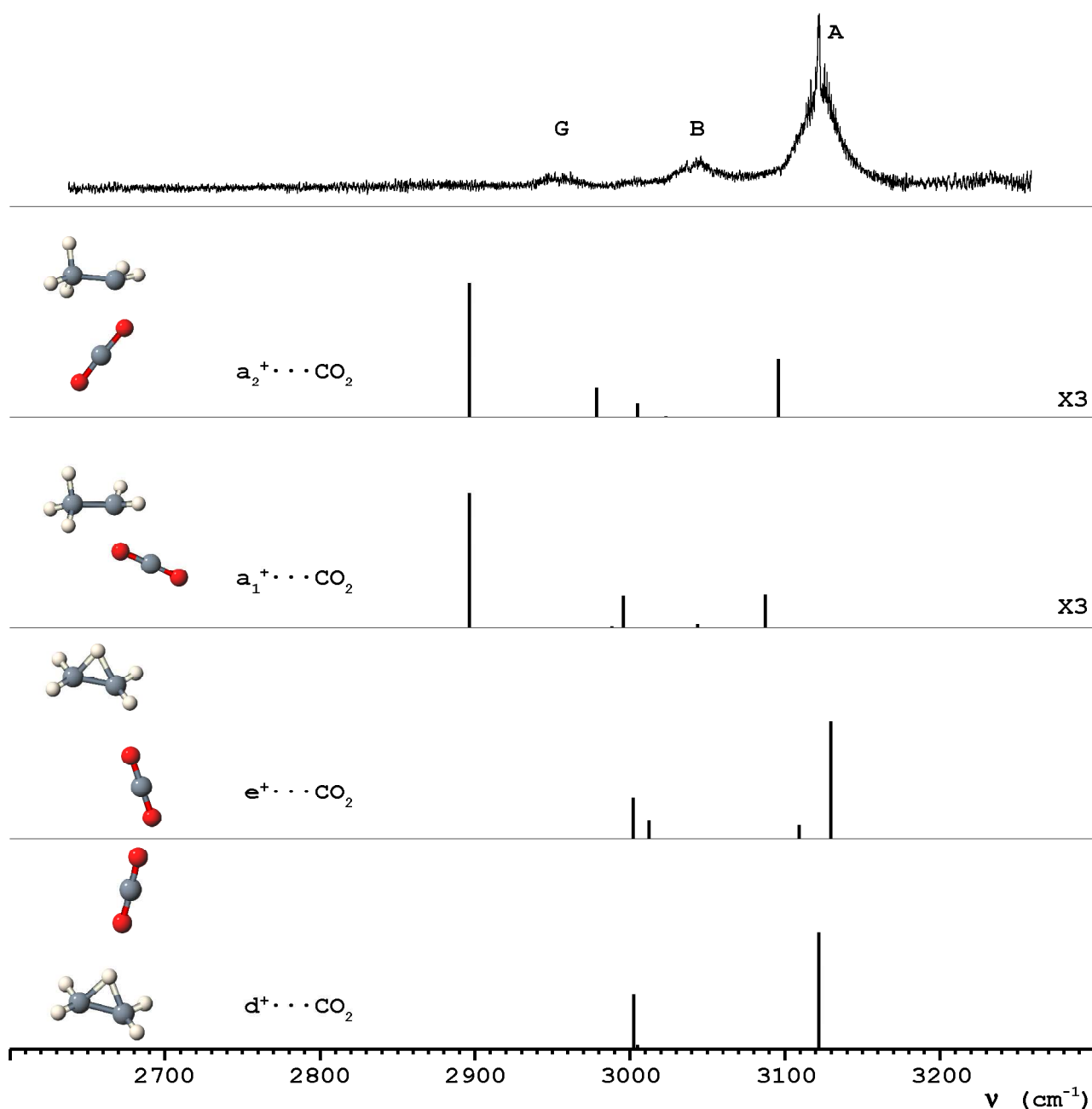
The main binding motif here seems to be $d^+\cdots CO_2$, as the spectrum largely reproduces the $C_2H_5^+\cdots Ar$ one. This trend is demonstrated by the number of observed bands, their positions and the ratio of their IR activities. Like all the other investigated spectra, the bands recorded here have the same symmetric shape, suggesting that the stretching modes from which they originate were not strongly affected by the presence of the ligand. Like in the case of $d^+\cdots N_2$, the observed bands are slightly blue-shifted with respect to the positions recorded in the $d^+\cdots Ar$ spectrum. In the present case, the blue-shifts are larger than the ones seen for $d^+\cdots N_2$, in line with the predictions of the calculations and with the larger D_0 obtained via HPMS. The IR activity ratio of bands A and B (obtained from the ratio of the integrated band contours) is diverging from the calculations (4 : 1 instead of 2 : 1).

While the position of band A confirms the nonclassical structure of the $C_2H_5^+$ moiety, its rotational profile defines the orientation of the ligand, giving information about the intermolecular interaction. Indeed, if the interaction would have taken place via a lone pair of the CO_2 molecule, this would have resulted in a rather strong deviation from linearity for $\overline{H\cdots O=C}$. Such a deviation would have resulted in skewing of the principal axis of the complex, thus altering the band profile.

Band G is associated with the nearly covalent bound isomers $a^+\cdots CO_2$ and $a_1^+\cdots CO_2$. Its position (2954 cm^{-1}) is in reasonable agreement with the calculated position, which was scaled considering the weak intermolecular interaction of $a^+\cdots CO_2$. As band G has a signal-to-noise ratio of just 2, it results that the other bands of the $a^+\cdots CO_2$ and $a_1^+\cdots CO_2$ complexes are too weak to be seen in the present experiment.

The ratio between the IR activities of bands A and G (10 : 1 - neglecting possible nonlinearities in the excitation laser intensity), together with the IR intensity ratio of the calculated vibrations to which they are assigned, allow an evaluation of the relative isomer abundance. Given the fact that there are two isomers possibly contributing to band G, the IR intensity ratio of the calculated vibrations will be considered to be 55 : (21+21) = 1.3 : 1. It results that the $d^+\cdots CO_2$ are at least 7 times more abundant than $a^+\cdots CO_2$ and $a_1^+\cdots CO_2$ together.

7.4.5. Larger $C_2H_5^+\cdots(CO_2)_n$ complexes (n = 2, 3)

All recorded spectra of $C_2H_5^+\cdots(CO_2)_n$ complexes (n = 1 ... 3) are presented in the Figure 12. Band A of $C_2H_5^+\cdots(CO_2)_3$ is shifted by just +6 cm^{-1} with respect to the position seen in the dimer spectrum. The other two bands are red-shifting in the spectrum of the

trimer, while in the one of the tetramer they shift by a tiny amount toward higher frequencies, mirroring the behavior seen for bands C, D, E, and F of $C_2H_5^+\cdots(N_2)_n$. The magnitude of the complexation-induced blue-shift fits well with the known weakly acidic C-H bonds. Both in the spectrum of the trimer and the ones recorded for the tetramer, the

Figure 12. *The IRPD spectra of $C_2H_5^+\cdots(CO_2)_n$ (n = 1, 2, 3) recorded in the dominant fragment channels as well as the spectrum of $C_2H_5^+\cdots(CO_2)_3$ recorded in the minor 3 → 2 fragment channel.*
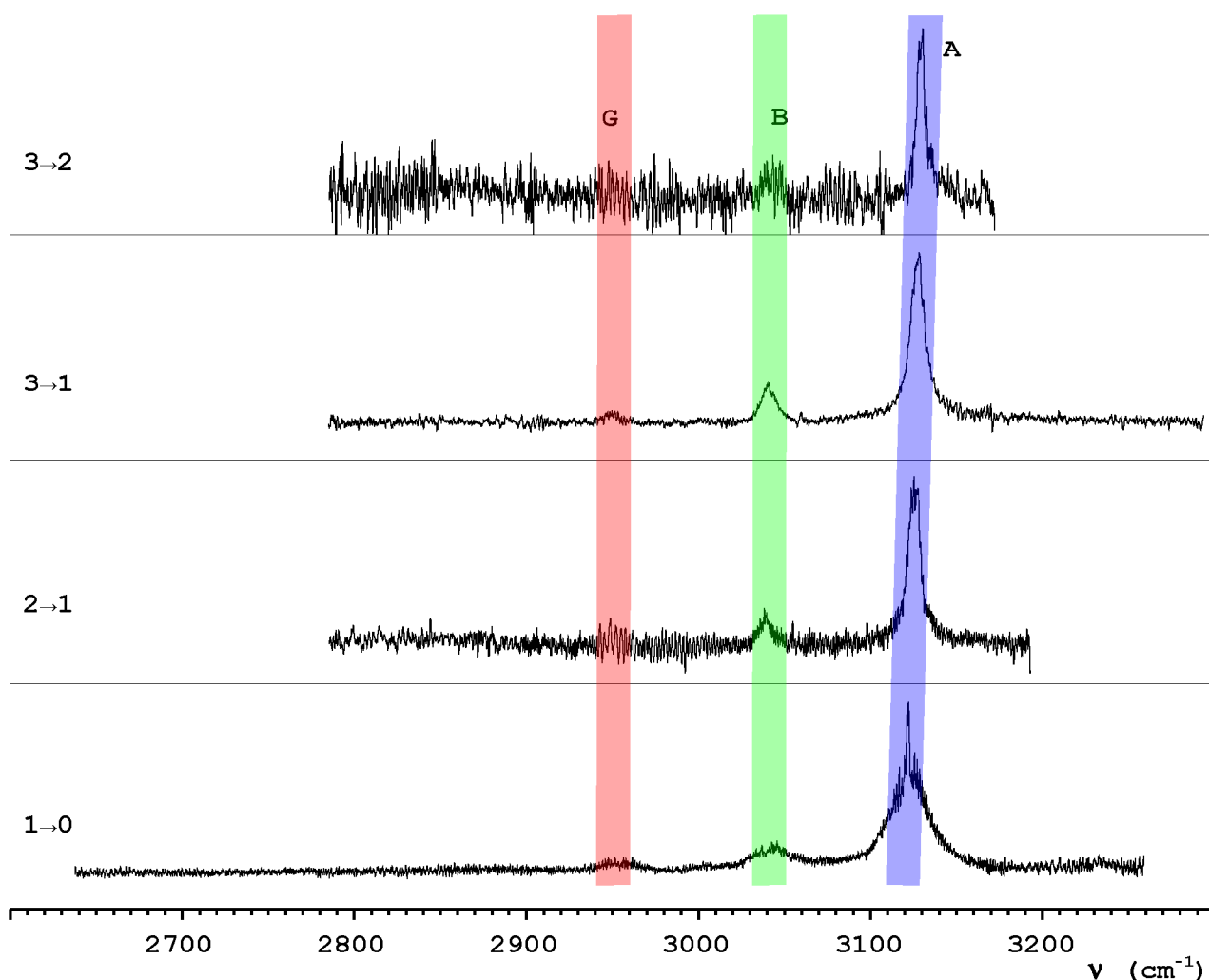
FWHM of band A is small, indicative for the good vibrational cooling of the complexes. It is significant that, apart from the case of the $C_2H_5^+\cdots(N_2)_n$, where IR absorption of the minor $d^+\cdots(N_2)_n$ complexes was suppressed starting from n = 2, here the band G assigned to the minor $a_{(1)}^+\cdots CO_2$ is visible in all spectra, bar the 3 → 2 fragmentation channel. This signals that the competition between the $d^+\cdots(CO_2)_n$ and the $a^+\cdots(CO_2)_n$ complexes is far less strong than the one seen in the case of $C_2H_5^+\cdots(N_2)_n$. The disappearance of band G from the 3 → 2 fragmentation channel shows that the complex from which it originates is

196

different in binding energy than the dominant $d^+ \cdots (CO_2)_n$ one.

It is interesting to qualitatively compare the signal-to-noise ratios (SNR) obtained in the recorded fragmentation channels. All spectra depicted in Figure 12 have been equally smoothed. In the case of the dimer, the good SNR can be seen as the result of good cooling of the complexes - which reduces the amount of metastable decay (MD), not very low dimer binding energy (low SNR driven mainly by low dimer binding energy has been seen in the case of $C_2H_5^+ \cdots Ar$), and reasonable IR activity of the investigated bands. In the case of the trimer, however, the decrease in production rate (specific to the incremental building of the complexes in the EI ion source) adds up to the slight decrease in binding energy of the ligands which favors an increase of the MD, precisely in the investigated fragmentation channel $(2 \rightarrow 1)$. The two spectra of the tetramer mirror the behavior of the dimer and the trimer ones. On one hand, although the absolute production rate of $C_2H_5^+ \cdots (CO_2)_3$ is just a fraction of the one of $C_2H_5^+ \cdots (CO_2)_2$, the SNR seen in the $3 \rightarrow 1$ channel is higher than the one seen in the $2 \rightarrow 1$ channel because the noise produced by the MD is insignificant. On the other hand, the $3 \rightarrow 2$ channel is both swamped by MD noise and not enough populated with IRPD fragments as it is not the channel corresponding to the largest internal energy expenditure. Overall, these spectra show a good example for the performances of the EI-IRPD technique: the sequential building of a complex, the evaporation of the maximum number of ligands, as well as its isomer selectivity.

7.4.6. The $C_2H_5^+ \cdots CH_4$ and $C_2H_5^+ \cdots (CH_4)_4$ complexes

The IRPD spectrum of $[C_3,H_9]^+$ recorded in the $C_2H_5^+$ fragment channel (top of Figure 13) is considerably more complex than any other investigated spectrum of $C_2H_5^+ \cdots L$, comprising three groups of bands situated between 2800 cm^{-1} and 3200 cm^{-1}. The calculations suggest that at least three types of $[C_3,H_9]^+$ complexes can fragment in the $C_2H_5^+$ channel; their stick spectra are also presented in Figure 13. The computed frequencies plotted here have been corrected for anharmonicity using a factor (0.942) which brings in line the calculated frequency of the strongest ω_{CH} of $d^+ \cdots CH_4$ with the band A from the experimental spectrum. Given the number of features observed in the experimental spectrum, it is obvious that the parent mass channel (45 u) is populated by at least two systems sharing the same $[C_3,H_9]^+$ formula.

Considering the nature of the ligand (CH_4), it is instructive to compare the calculated positions of the vibrations of the bare CH_4 with the ones of the $d^+ \cdots CH_4$ and $e^+ \cdots CH_4$ complexes. It can be seen that the IR inactive totally symmetric stretch of the CH_4

197

(3083 cm^{-1} in calculations, 2916.5 cm$^{-1[43]}$ in literature) becomes IR active and shifts by -30 cm^{-1} for $d^+\cdots CH_4$ and by -17 cm^{-1} for $e^+\cdots CH_4$. This shift has already been seen in the IRPD spectra of the benzene cation complexated with CH_4 molecules ($Bz^+\cdots(CH_4)_n$),[44] where a band centered at 2904 cm^{-1} was assigned to ν_1 of CH_4. Even more, in the same experiment it was seen that the triple degeneration of ν_3 of CH_4 (3019.5 cm$^{-1[43]}$) is partially lifted, resulting in the observation of two bands (3008 cm^{-1} and 3025 cm^{-1}). The change in degeneracy is caused by the charge induced dipole of CH_4.

Figure 13. *The IRPD spectrum of $[C_3,H_9]^+$ recorded in the $C_2H_5^+$ fragment channel and the stick spectra of $d^+\cdots CH_4$, $e^+\cdots CH_4$, and $a^+\cdots CH_4$ complexes (calculated at the MP2/6-311G(2df,2pd) level and rescaled by 0.942). The arrows on the experimental spectrum mark the frequencies of the stretch vibrations of the free CH_4; * stretch vibrations of the CH_4 moiety; ** stretch vibration modes coupled between $C_2H_5^+$ and CH_4.*
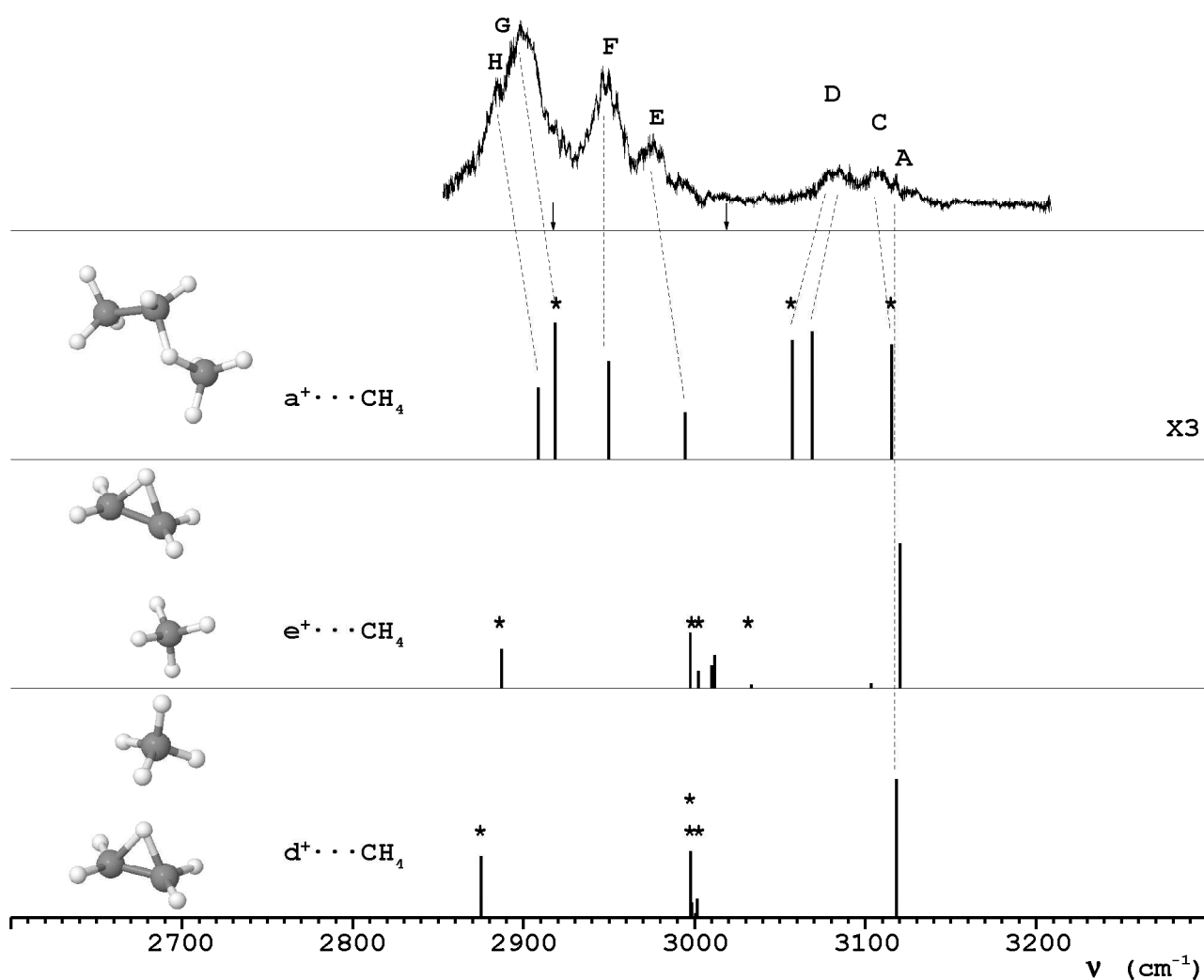
As the binding energy of $d^+\cdots CH_4$ is almost twice as large as the one of $e^+\cdots CH_4$, only the former will be considered for the discussion which follows. Analysis of the positions of

the observed bands suggests that band A (3118 cm^{-1}) is the result of IR absorption of $\mathbf{d^+}\cdots CH_4$ while the remaining bands are associated with $\mathbf{a^+}\cdots CH_4$. It is remarkable that the ratio between the IR activities around 2900 cm^{-1} and 3100 cm^{-1} is completely different from the one expected. A possible explanation would be a large change in the output power of the tunable IR source, which might escape detection as the sensitivity of the IR detector is strongly nonlinear in the investigated range. It is then sensible to consider just the positions of the bands and to discard their relative strength. Even so, the IR activity around 3100 cm^{-1} suggests that $\mathbf{a^+}\cdots CH_4$ is the dominant species in the ion beam.

Figure 14. *Comparison between the IR spectra obtained in the photodissociation channels $C_2H_5^+\cdots(CH_4)_n \rightarrow C_2H_5^+\cdots CH_4$ (lower part) and $[C_6,H_{21}]^+ \rightarrow [C_3,H_9]^+$ (upper part). The vertical lines mark the frequencies of the stretch vibrations of the free CH_4.*
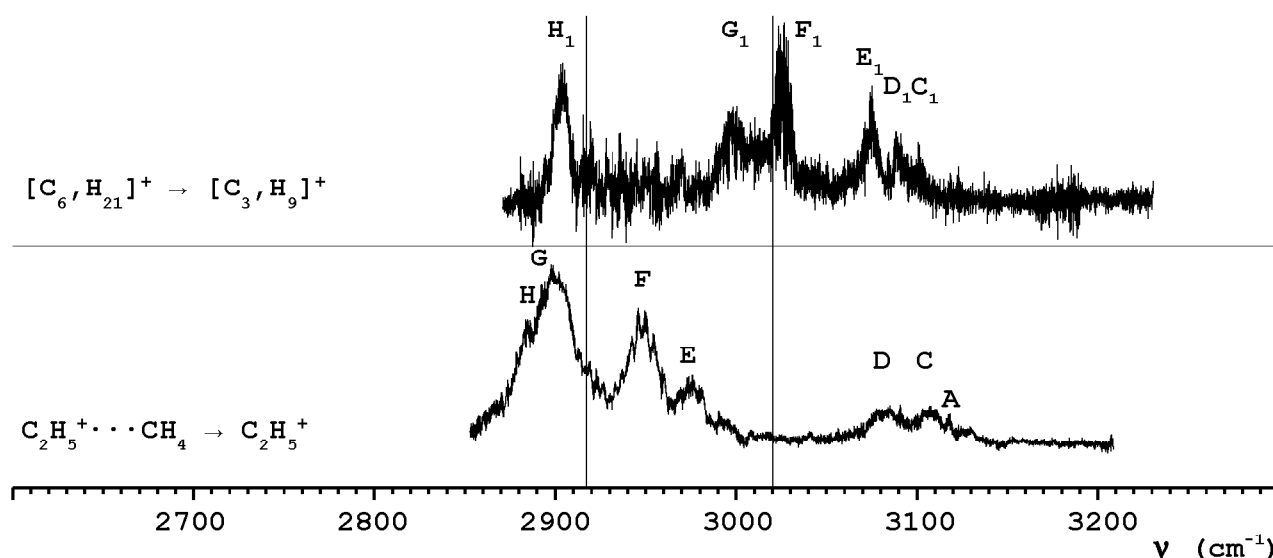
This tentative assignment can be verified by comparing the spectrum of $C_2H_5^+\cdots CH_4$ with the one of $C_2H_5^+\cdots(CH_4)_4$. Analysis of the photofragmentation data shows that the dominant fragmentation channel is $4 \rightarrow 1$. Here it is important to remember that the selection of the parent and fragment species is based on their mass. It follows that a correct description of the observed photofragmentation channel is 93 u $\rightarrow$ 45 u, which, considering the conditions of the EI and the precursor used (CH$_4$), is equivalent with $[C_6,H_{21}]^+ \rightarrow [C_3,H_9]^+$. This can be relevant, as the IR spectra of protonated propane isomers (C$_3$H$_9^+$) are different in the observed range from the one of C$_2$H$_5^+$. Figure 14 presents for comparison the IRPD spectrum of $C_2H_5^+\cdots CH_4$ and the one of $[C_6,H_{21}]^+$. It can be seen that the similarities between them are rather limited. Given their positions and rather large IR activities, bands F$_1$ (3026 cm^{-1}), G$_1$ (2998 cm^{-1}) and H$_1$ (2904 cm^{-1}) are assigned to stretch modes of CH$_4$. This is supported also by the assignment of similar bands (3025 cm^{-1},

3008 cm^{-1}, and 2904 cm^{-1}) also to CH_4 in the spectra of $Bz^+\cdots(CH_4)_n$.[44] The remaining three bands (3075 cm^{-1}, 3089 cm^{-1}, and 3101 cm^{-1}) will be considered to originate in $[C_3,H_9]^+$.

7.4.7. Ligand binding energies

The photofragmentation data, derived either from IRPD spectra or from laser-induced dissociation (LID), can provide information regarding the binding energies of the complexes. The available data will be presented in the following and compared with previous HPMS experiments (Table 1) and the results of the quantum chemical calculations (Table 3). The model described in **Chapter 4** will be used for evaluating the binding energies of the ligands.

The spectroscopic data available for $C_2H_5^+\cdots Ar$ is limited to just one photodissociation channel (1 → 0); the only information that can be extracted is that the stabilization energy must be < 36 kJ/mol. For comparison, the HPMS experiments yield ~7.1 kJ/mol,[17] which compares very well with the 6.5 kJ/mol derived from calculations.

The photofragmentation data for $C_2H_5^+\cdots(N_2)_n$ was extracted exclusively from IRPD spectra (Figure 10). The dominant photodissociation channels are: 1 → 0, 2 → 1, 3 → 1, 4 → 2, 5 → 2. It results that D_0 of the first ligand must be > 24 kJ/mol and that the following ligands are bound in average by 9 ... 12 kJ/mol. The former value fits well with the 37.8 kJ/mol obtained via quantum chemical calculations for the **a**$^+\cdots N_2$ isomer, supporting the spectroscopic assignment of the dominant species in the ion beam. At the same time, this value excedes the value obtained in HPMS experiments 15.5±1.3 kJ/mol.[17] The experimental value obtained for D_0 of the second and subsequent ligands is comparable with the 14.7±2 kJ/mol[17] obtained via HPMS, however, comparing these numbers might be misleading. Indeed, the sequential complex buildup used both in the presently used ion source and in the HPMS experiments ($C_2H_5^+\cdots N_2 + N_2 \rightarrow C_2H_5^+\cdots(N_2)_2$) implies that the structure of the $C_2H_5^+\cdots N_2$ parent will probably not be affected by further complexation. In this case it might be more appropriate to compare the D_0 obtained via HPMS with just the result of the calculation done for the **d**$^+\cdots N_2$ isomer (17.7 kJ/mol).

The photofragmentation data for $C_2H_5^+\cdots(CO_2)_n$ (n = 1 ... 7) was extracted from LID action. An overview of the LID results is summarized below.

n → m	0	1	2	3	4	5
1	100					
2		100				
3		50	50			
4			100			
5				100		
6				10	90	
7					10	90

Analysis of the data shows that the binding energy of the first ligand must be < 36 kJ/mol; quantum chemical calculations suggest that the most stable dimer ($\mathbf{d}^{+}\cdots CO_2$) is bound by 31.1 kJ/mol. These values are in good agreement with the HPMS experiments which show that D_0 = 27.2±0.8 kJ/mol.[19] The good match between the experimental and theoretical values lends support to the spectroscopic assignment of the dominant species in the ion beam. It can be seen that subsequent complexation seems to be characterized by binding energies of ~18 kJ/mol for a rather broad range of cluster sizes. This find is also in line with the HPMS experiments which show that the attachment of the second, third, and fourth ligands are characterized by the following stabilization energies: 20.5±4.4 kJ/mol,[19] 16.3±4.4 kJ/mol,[19] and 15.5±1.3 kJ/mol.[19]

As the fragment resulting from the photodissociation process $[C_{6,}H_{21}]^{+} \rightarrow [C_{3,}H_9]^{+}$ could not be clearly identified as an isomer of $C_2H_5^{+}\cdots CH_4$, it results that the only photofragmentation information available about $C_2H_5^{+}\cdots(CH_4)_n$ complexes is the $1 \rightarrow 0$ fragmentation. It results that the stabilization energy must be < 36 kJ/mol. In this case, the HPMS experiments yield 23.0±0.8 kJ/mol,[20] which is comparable with the 18.0 kJ/mol calculated for the dissociation of $\mathbf{a}^{+}\cdots CH_4$.

7.5. Conclusions

The equilibrium geometry of the ethyl cation has been probed by means of IRPD spectroscopy of $C_2H_5^{+}\cdots L$ (L = Ar, N_2, CO_2, CH_4) dimers. The IR spectra were recorded over the range of the C-H stretch fundamentals (covering possible sp^3 and sp^2 hybridization of C). Depending on the ligand species, the fingerprint of one or two largely different dimer geometries can be observed. Analysis of the $C_2H_5^{+}\cdots Ar$ spectrum reveals clearly shaped P, Q, and R branches for the band centered at 3117 cm^{-1}. The rotational profile of this band has been successfully simulated starting from quantum chemical data. It follows that the dimer consists of a nonclassical $C_2H_5^{+}$, with one proton bridging the double C=C bond of the C_2H_4 moiety, to which the Ar ligand is bound via this nonclassical proton. As no other type of $C_2H_5^{+}\cdots Ar$ complexes have been observed in the present IRPD experiment, it is sensible to consider the nonclassical $C_2H_5^{+}$ as the global minimum on the PES of $[C_2,H_5]^{+}$. The spectra of $C_2H_5^{+}\cdots N_2$ and $C_2H_5^{+}\cdots CO_2$ exhibit each one band similar in position and profile. The intensity of each of these bands, relative to the other features of each spectrum, are largely different. Thus, the spectrum of $C_2H_5^{+}\cdots N_2$ reveals that the complexes featuring weak bonds between the nonclassical proton of $C_2H_5^{+}$ and N_2 are present in just minor amounts in the ion beam, while the majority of the complexes are

almost covalently bonded $H_3CCH_2^+\cdots N_2$. The situation is reversed in the case of the $C_2H_5^+\cdots CO_2$ dimers: the dominant species in the ion beam are complexes based on the nonclassical $C_2H_5^+$, while the complexes featuring a strong intermolecular bond are in minor amounts. Finally, the spectrum of $C_2H_5^+\cdots CH_4$ reveals that, although the bulk of the complexes are derived from the classical $H_3CCH_2^+$, small amounts of nonclassical dimers are present in the ion beam. It was thus demonstrated that while the nonclassical $C_2H_5^+$ is the global minimum on the PES of the free $[C_2,H_5]^+$, the structure of the ethyl cation can be strongly influenced by the chemical properties of the environment.

References

[1] Surya Prakash G.K., Schleyer P.v.R., *Stable Carbocation Chemistry*, John Wiley & Sons (New York, 1997)

[2] Cravens T.E., Robertson I.P., Waite J.H., Yelle R.V., Kasprzak W.T., Keller C.N., Ledvina S.A., Niemann H.B., Luhmann J.G., McNutt R.L., Ip W.-H., De La Haye V., Mueller-Wodarg I., Wahlund J.-E., Anicich V.G., Vuitton V., *Geophys. Res. Lett.* **33** (2006) 7105

[3] Tsuji M., Arikawa T., Nishimura Y., *Bull. Chem. Soc. Jpn.* **72** (1999) 293

[4] Pacansky J., Dupuis M., *J. Am. Chem. Soc.* **104** (1982) 415

[5] Pacansky J., Dupuis M., *J. Chem. Phys.* **68** (1978) 4276

[6] Sears T.J., Johnson P.M., BeeBe-Wang J., *J. Chem. Phys.* **111** (1999) 9213

[7] Kim E., Yamamoto S., *J. Chem. Phys.* **120** (2004) 3265

[8] Sears T.J., Johnson P.M., Jin P., Oatis S., *J. Chem. Phys.* **104** (1996) 781

[9] Quapp W., Heidrich D., *J. Mol. Struct. (Theochem)* **585** (2002) 105

[10] Carneiro J.W.M., Schleyer P.v.R., Saunders M., Remington R., Schaefer H.F., Rauk A., Sorensen T.S., *J. Am. Chem. Soc.* **116** (1994) 3483

[11] East A.L.L., Liu Z.F., McCague C., Cheng K., Tse T.S., *J. Phys. Chem. A* **102** (1998) 10903

[12] Obata S. Hirao K., *Bull. Chem. Soc. Jpn.* **66** (1993) 3271

[13] Esteves P.M., Mota C.J.A., Ramirez-Solis A., Hernandez-Lamoneda R., *J. Am. Chem. Soc.* **120** (1998) 3213

[14] Houle F.A. Beauchamp J.L., *J. Am. Chem. Soc.* **101** (1979) 4067

[15] Dyke J.M., Ellis A.R., Keddar N., Morris A., *J. Phys. Chem.* **88** (1984) 2565

[16] Ruscic B., Berkowitz J.,Curtiss L.A., Pople J.A., *J. Chem. Phys.* **91** (1989) 114

[17] Cunje A., Hopkinson A. C., Yamabe S., Hiraoka K., Nakagawa F., Ishida M., Fujita K., Takao K., Wada A., and Hiizumi K., *J. Phys. Chem. A* **108** (2004) 11218

[18] Hiraoka K. and Kebarle P., *J. Am. Chem. Soc.* **98** (1976) 6119

[19] Hiraoka K., Shoda T., Kudaka I., Fujimaki S., Mizuse S., Yamabe S., Wasada H., Wasada-Tsutsui Y., *J. Phys. Chem. A* **107** (2003) 775

[20] Hiraoka K., Mori T., Yamabe S., *Chem. Phys. Lett.* **207** (1993) 178

[21] Hiraoka K., Fujita K., Ishida M., Hiizumi K., Nakagawa F., Wada A., Yamabe S. and Tsuchida N., *J. Am. Soc. Mass Spectrom.* **16** (2005) 1760

[22] Hunter E. P., Lias S. G., *J. Phys. Chem. Ref. Data* **27** (1998) 413

[23] Dopfer O., *Int. Rev. Phys. Chem.* **22** (2003) 437

[24] Frisch M.J., Trucks G.W., Schlegel H.B., Scuseria G.E., Robb M.A., Cheeseman J.R., Montgomery Jr. J.A., Vreven T., Kudin K.N., Burant J.C., Millam J.M., Iyengar S.S., J. Tomasi, V. Barone, B. Mennucci, M. Cossi, G. Scalmani, N. Rega, G.A. Petersson, H. Nakatsuji, M. Hada, M. Ehara, K. Toyota, R. Fukuda, J. Hasegawa, M. Ishida, T. Nakajima, Y. Honda, O. Kitao, H. Nakai, M. Klene, X. Li, J.E. Knox, H.P. Hratchian, J.B. Cross, V. Bakken, C. Adamo, J. Jaramillo, R. Gomperts, R.E. Stratmann, O. Yazyev, A.J. Austin, R. Cammi, C. Pomelli, J.W. Ochterski, P.Y. Ayala, K. Morokuma, G.A. Voth, P. Salvador, J.J. Dannenberg, V.G. Zakrzewski, S. Dapprich, A.D. Daniels, M.C. Strain, O. Farkas, D.K. Malick, A.D. Rabuck, K. Raghavachari, J.B. Foresman, J.V. Ortiz, Q. Cui, A.G. Baboul, S. Clifford, J. Cioslowski, B.B. Stefanov, G. Liu, A. Liashenko, P. Piskorz, I. Komaromi, R.L. Martin, D.J. Fox, T. Keith, M.A. Al-Laham, C.Y. Peng, A. Nanayakkara, M. Challacombe, P.M.W. Gill, B. Johnson, W. Chen, M.W. Wong, C. Gonzalez, J.A. Pople, *Gaussian 03, Revision D.01 Gaussian, Inc., Wallingford CT* (2004)

[25] Boys S.F., Bernardi F., *Mol. Phys.* **19** (1970) 553

[26] Chalasinski G., Szczesniak M.M., *Chem. Rev.* **94** (1994) 1723

[27] Martin J.M.L.,Taylor P.R., *Chem. Phys. Lett.* **248** (1996) 336

[28] Duncan J.L., McKean D.C., Mallinson P.D., *J. Mol. Spectr.* **45** (1973) 221

[29] Speirs G.K., Duncan J.L.,VanLerberghe D., *J. Mol. Spectr.* **51** (1974) 524

[30] Duncan J.L., *Mol. Phys.* **28** (1974) 1177

[31] Duncan J.L., Wright I.J., VanLerberghe D., *J. Mol. Spectr.* **42** (1972) 463

[32] Martin J.M.L., Lee T.J., Taylor P.R., Francois J.P., *J. Chem. Phys.* **103** (1995) 2589

[33] Duncan J.L., Hamilton E., Fayt A., VanLerberghe D., Hegelund F., *Mol. Phys.* **43** (1981) 737

[34] Dopfer O., *Z. Phys. Chem.* **219** (2005) 125

[35] Guelachvili G., Rao K. N., *Handbook of Infrared Standards,* Academic Press (London, 1993)

[36] Scott A. P., Radom L., *J. Phys. Chem.* **100** (1996) 16502

[37] Luckhaus D., Quack M., *Mol. Phys.* **68** (1989) 745

[38] Jagod M.-F., Gabrys C.M., Rosslein M., Uy D., Oka T., *Can. J. Phys.* **72** (1994) 1192

[39] Yeh L.I., Price J.M., Lee Y.T., *J. Am. Chem. Soc.* **111** (1989) 5597

[40] Dopfer O., Olkhov R.V., Maier J.P., *J. Phys. Chem. A* **103** (1999) 2982

[41] Hamada Y., Hashiguchi K., Tsuboi M., Koga Y., Kondo S., *J. Mol. Spectrosc.* **105** (1984) 70

[42] Kareev M., Sablier M., Fujii T., *J. Phys. Chem. A* **104** (2000) 7218

[43] Venuti E., Halonen L., Della Vale R.G., *J. Chem. Phys.* **53** (1975) 970

[44] Dopfer O., Olkhov R.V., Maier J.P., *J. Chem. Phys.* **111** (1999) 10754

8. Summary - Zusammenfassung

Conclusions specific to each investigated species are presented at the end of the section which bear the respective discussions. The following paragraphs are just summarizing the types of investigations performed and the most significant results. This section is presented in both English and German. Finally, a few investigations which will expand the field are suggested and some improvements of the experimental setup are outlined.

This work has presented a spectroscopic analysis of three types of hydrocarbon cations: two ionized aromatic hydrocarbons, two protonated aromatic hydrocarbons and the cation of a fundamental radical hydrocarbon. The experimental investigations were centered on the proton stretch vibrations of mass-selected complexes of these systems and polar (H_2O) and non polar (Ar, N_2, CO_2) ligands. The experimental results have been obtained in a tandem mass spectrometer coupled with an electron impact ionization ion source; an OPO laser system was used as tunable IR light source. All the proposed dimer structures have been also modeled using quantum chemical calculations. These calculations have consistently been matched with the experimental results and have enabled clear identification of the spectral features observed. Their match with the experimental results has also enabled the evaluation of thermochemical properties which could not be extracted directly from experiment.

The experiments done on complexes of ionized hydrocarbons (1-Np$^+$ in **Chapter 3**[1] and Im$^+$ in **Chapter 5**[2]) have allowed for the acidity of their various groups (C-H, N-H, O-H) to be probed. Indeed, the shifts in the frequency as well as the enhancement in the intensity of the O-H and N-H stretch vibrations (Δv_{OH} and Δv_{NH}) which resulted from the complexation have yielded dependences on both the species of the ligands (L) and the number of ligands (n). For the first time, the O-H bound 1-Np$^+\cdots$Ar has been detected, showing that the REMPI-IRPD method previously used for investigating this dimer is severely limited with respect to the production of the most stable isomer of a given cationic

205

complex. The detection of c-1-Np$^+$···(N$_2$)$_n$ corresponds to the first observation of c-1-Np$^+$ complexes and enables thus direct comparison of both 1-Np$^+$ rotamers. The $\Delta\nu_{NH}$ shift of Im$^+$···N$_2$(H) yielded a first experimental estimate for the PA of the imidazyl radical of $\cong$ 890 ± 30 kJ/mol. It was also found that the most stable 1-Np$^+$···Ar and Im$^+$···Ar structures (H-bound isomers) differ qualitatively from that of the corresponding neutral dimers (π-bound structure), emphasizing the large impact of ionization on the interaction potential and the preferred recognition motif between acidic aromatic molecules (A) and nonpolar ligands. The ionization induced $\pi \rightarrow$ H switch in the preferred binding type in A$^{(+)}$···Ar complexes has now been established for a large variety of A$^{(+)}$ molecules with acidic functional YH$_k$ groups (Y = O, N) and seems to be a general phenomenon. The IRPD spectra of 1-Np$^+$···L$_n$ and Im$^+$···L$_n$ yielded spectroscopic information about the ν_{CH}, ν_{NH} and ν_{OH} vibrations of bare 1-Np$^+$ and Im$^+$. The dependence of the shifts in the frequency of the O-H and N-H stretch vibrations ($\Delta\nu_{OH}$ and $\Delta\nu_{NH}$) have allowed for microsolvation models to be created. For both cations, their microsolvation in N$_2$ was found to start with the complexation of the highest acidic proton, the dimer thus created being further solvated by π-bound ligands.

The spectroscopic results obtained on size-selected 1-NpH$^+$···L$_n$ (**Chapter 4**) show that, in the output of the presently used ion source, three classes of 1-NpH$^+$ isomers can be identified: oxonium ions (1-Np protonated at the O atom); carbenium ions obtained by protonation in the *para* and *ortho* positions with respect to the OH functional group; carbenium ions obtained by the addition of a proton to well-defined sites on the second naphthalene ring. The spectral identification of these three classes of protonation sites is supported by their different photofragmentation patterns.

It was demonstrated that the spectroscopic monitoring of the microsolvation of ImH$^+$ in Ar and N$_2$ (**Chapter 6**) together with the quantum chemical calculations paint a very detailed picture of the microsolvation process, evidencing clear differences between the microsolvation models as function of the PA of the ligands. Important differences have also been identified between the various binding sites, enabling the creation of a clear scale of priorities for occupation of the binding sites during microsolvation. The application of IRPD to the study of microhydrated ImH$^+$ provided for the first time direct spectroscopic information on the properties of the N-H bonds of this biomolecular building block under controlled microhydration.[3] It was demonstrated that, as protonation enhances the acidity of the N-H groups, the ability for proton conductivity of ImH$^+$ increases. More work must be done to identify the interactions between the proton stretch vibrations and other vibration

modes of ImH⁺(···L).

A very important result is derived from the IRPD spectroscopy of $C_2H_5^+$···L (L = Ar, N₂, CO₂, CH₄) dimers (**Chapter 7**). The equilibrium geometry of the ethyl cation has long been debated. Now, IRPD spectra were recorded over the range of the C-H stretch fundamentals (covering possible sp³ and sp² hybridization of C). Depending on the ligand species, the spectra are found to be dominated by the fingerprint of two largely different dimer geometries. Using the experimental $C_2H_5^+$···Ar spectrum and the corresponding quantum chemical calculations, the structure of the (weakly perturbed) ethyl cation was found to be the nonclassical one, with one proton straddling across the C=C bond of the ethylene moiety. On the other hand, ligands like N₂ and CH₄ are strongly influencing the geometry, as seen in the spectral signatures of the $C_2H_5^+$···N₂ and $C_2H_5^+$···CH₄, which correspond to the classical $[H_2CCH_3]^+$. It was thus demonstrated that while the nonclassical $C_2H_5^+$ is the global minimum on the PES of the free $[C_2,H_5]^+$, the structure of the ethyl cation can be strongly influenced by the chemical properties of the environment.

It can thus be seen that IR spectroscopy of cluster ions can be used to probe thermochemical properties of transient radicals as well as fundamental properties of isolated ions (messenger technique).

It is important to note that the used experimental setup is a suitable tool for preparing beams of well-specified isomeric ions, because of the double mass selection coupled with the spectral analysis. Even more, the method sets a certain upper limit for the internal energy of the selected species. This means that cations which are fundamentally unstable in condensed phase can be selected and their spectral, thermodynamic, or kinetic properties can be observed.

The mechanism for clusters generation was shown to be of paramount importance: the spectral features observed on complexes produced in the EI cluster ion source are qualitatively different from the ones produced via REMPI. Indeed, while it has been demonstrated that the EI cluster ion source predominantly produces the most stable structure of a given cluster ion, it can be seen that the REMPI cluster ion source is usually producing charged complexes with structures similar to the most stable structures of the corresponding neutral clusters. This demonstrates that the EI source is more generally applicable than photoionization for the spectroscopic characterization of global minima of cation complexes.

Gegenstand dieser Arbeit ist die Spektralanalyse von drei Arten von Kohlenwasserstoffkationen: zwei ionisierten aromatische Kohlenwasserstoffen (1-Np⁺,

Im⁺), zwei protonierten aromatischen Kohlenwasserstoffen (1-NpH⁺, ImH⁺) und vom eines Radikal-Kohlenwasserstoff-Kation (C₂H₅⁺). Die experimentellen Untersuchungen wurden auf die Proton-Streckschwingungen der massenselektierten Komplexe dieser Systeme mit angehängtem polaren (H₂O) und unpolaren (Ar, N₂, CO₂) Liganden fokussiert. Die experimentellen Resultate wurden in einem Tandem-Massenspektrometer, das mit einer Elektronstoßionisationsquelle verbunden ist, erzielt. Als abstimmbare IR-Lichtquelle wurde ein OPO-Laser-System benutzt. Alle vorgeschlagenen Dimerstrukturen sind auch mit Quantenchemieberechnungen modelliert worden. Diese Berechnungen stimmen mit den experimentellen Ergebnisse überein und haben die eindeutige Identifizierung der beobachteten Schwingungsstrukturen erlaubt. Die Übereinstimmung mit den experimentellen Resultaten ermöglichte auch die Auswertung der thermochemischen Eigenschaften, die nicht direkt aus dem Experiment zugänglich waren.

Die Experimente, die an Komplexen der ionisierten Kohlenwasserstoffe durchgeführt wurden (1-Np⁺ im **Kapitel 3** *und Im⁺ in* **Kapitel 5***), haben die Untersuchung der Azidität der verschiedenen Gruppen (C-H, N-H, O-H) erlaubt. Frequenzverschiebung sowie die Erhöhung der Intensität der O-H- und der N-H-Streckschwingungen ($\Delta\nu_{OH}$ und $\Delta\nu_{NH}$), als Folge der Komplexbildung hängen sowohl von der Sorte der Liganden (L) als auch der Zahl der Liganden (n) ab. Zum ersten Mal wurde das O-H gebundene 1-Np⁺···Ar detektiert. Das zeigt, dass die REMPI-IRPD Methode, welche vorher für die Untersuchung dieses Dimers verwendet wurde, in Bezug auf die Produktion des stabilsten Isomers eines gegebenen kationischen Komplexes streng begrenzt ist. Die Entdeckung von c-1-Np⁺···(N₂)ₙ stimmt mit der ersten Beobachtung des c-1-Np⁺ Komplexes überein und ermöglicht den direkten Vergleich beider 1-Np⁺ Rotameren. Aus der Frequenzverschiebung $\Delta\nu_{NH}$ von Im⁺···N₂(H) konnte die erste experimentelle Abschätzung der Protonaffinität des Imidazyl-Radikals zu 890 ± 30 kJ/mol ermittelt werden. Es wurde auch gefunden, dass die stabilsten 1-Np⁺···Ar und Im⁺···Ar Strukturen (H-gebundene Isomere) sich qualitativ vom entsprechenden neutralen Dimer (π-gebundene Struktur) unterscheiden. Dies zeigt den großen Einfluss der Ionisierung auf das Wechselwirkungspotential und das bevorzugte Erkennungsmotiv zwischen sauren aromatischen Molekülen (A) und nichtpolaren Liganden. Die ionisierungsinduzierte Umlagerung von π→H an der bevorzugten Bindungsseite im A⁽⁺⁾···Ar Komplex ist inzwischen für eine große Vielzahl A⁽⁺⁾-Moleküle mit säuren funktionalen Gruppen YHₖ (Y = O, N) etabliert und scheint ein allgemeines Phänomen zu sein. Die IRPD-Spektren von 1-Np⁺···Lₙ und Im⁺···Lₙ erbrachten spektralanalytische Hinweise über die ν_{CH}-, ν_{NH}- und ν_{OH}- Schwingungen des isolierten 1-Np⁺ und Im⁺. Die*

Frequenzverschiebungsabhängigkeit der O-H- und N-H-Streckschwingungen (Δv_{OH} und Δv_{NH}) konnte zur Aufstellung von Microsolvationsmodellen genutzt werden. Es wurde gefunden, dass für beide Kationen die Mikrosolvatation im N_2 mit der N_2-Komplexbildung am saurersten Protons beginnt. Das so entstandene Dimer solvatisiert dann weiter durch Ausbildung von π-Bindungen mit den Liganden.

Die spektralanalytischen Resultate an größenselektierten 1-NpH$^+$···L$_n$-Kationen (**Kapitel 4**) zeigen dass, mit der hier verwendeten Ionenquelle, drei 1-NpH$^+$-Isomere entstehen: Oxonium-Ionen (1-Np protoniert am O Atom); Carbenium-Ionen, die durch Protonierung in para- und ortho-Position bezüglich der OH-Gruppe und Carbenium-Ionen, die durch die Protonierung an einer definierten Position am zweiten Naphthalinring gebildet werden. Die spektrale Identifizierung dieser drei Kategorien von Protonierungsstellen wird durch ihre unterschiedlichen Photofragmentationsmuster gestützt.

Es wurde gezeigt, dass die spektralanalytische "Abfrage" der Mikrosolvatation von ImH$^+$ in Ar und N_2 (**Kapitel 6**) zusammen mit den Quantenchemischen Berechnungen ein sehr detailliertes Bild des Solvatationsprozesses beschreibt und belegt deutliche Unterschiede zwischen Mikrosolvationsmodellen als Funktion der PA der Liganden. Wichtige Unterschiede sind auch zwischen den verschiedenen Bindungsstellen identifiziert worden unter Ermöglichung der Schaffung einer klaren Prioritäten-Skala für die Besetzung der Bindungsposition während der Mikrosolvatation. Die Anwendung von IRPD zur Studie von mikrohydratisiertem ImH$^+$ verschafft zum ersten Mal direkte spektralanalytische Informationen über die Eigenschaften der N-H Bindungen dieses biomolekularen Bausteins unter kontrollierter Mikrohydratisierung. Es wurde gezeigt, dass, mit der Protonierung die Azidität der N-H Gruppen erhöht wird und damit die Fähigkeit für die Protonleitfähigkeit in ImH$^+$ steigt. Mehr Arbeit muss erledigt werden, um die Wechselwirkung zwischen den Proton-Streckschwingungen und anderen Schwingungsmoden von ImH$^+$(···L) zu identifizieren.

Ein sehr wichtiges Resultat wird von der IRPD-Spektroskopie des Dimers $C_2H_5^+$···L, mit L = Ar, N_2, CO_2, CH_4 (**Kapitel 7**) abgeleitet. Die Gleichgewichtgeometrie des Ethylkations ist lange Zeit diskutiert worden. Jetzt wurden IRPD-Spektren über den Bereich der C-H-Streckschwingungen aufgenommen (Abdeckung sp^3 und sp^2 Hybridisierung von C). Abhängig von der Ligandenart wurde gefunden, dass die Spektren durch den Fingerabdruck von zwei sehr unterschiedlichen Dimergeometrien dominiert werden. Mit dem experimentellen $C_2H_5^+$···Ar Spektrum und den entsprechenden quantenchemischen Berechnungen konnte bewiesen werden, dass das schwach gestörte

Ethylkations in der nicht-klassischen H-überbrückten Struktur vorliegt. Andererseits beeinflussen Liganden wie N_2 und CH_4 stark die Geometrie, wie die spektralen Signaturen des $C_2H_5^+ \cdots N_2$ und des $C_2H_5^+ \cdots CH_4$ zeigen, die dem klassischen $[H_2CCH_3]^+$ entsprechen. Es wurde auch gezeigt, dass während das nicht-klassische $C_2H_5^+$ das globale Minimum auf der PES vom freien $[C_2,H_5]^+$ repräsentiert, die tatsächliche Struktur des Ethylkations durch die chemischen Eigenschaften des Umgebung stark beeinflußt werden kann.

Man kann sehen, dass die IR-Spektroskopie an Clusterionen verwendet werden kann, um thermochemische Eigenschaften kurzlebiger Radikale sowie fundamentale Eigenschaften der isolierten Ionen (Messengertechnik) zu prüfen.

Es ist wichtig zu anmerken, dass der verwendete experimentelle Aufbau aufgrund der Verbindung von doppelter Massenselektivität und spektraler Analyse ein angemessenes Werkzeug für das Herstellen eines Ionenstrahls aus gut-spezifizierten Isomeren dargestellt. Außerdem setzt die Methode eine bestimmte obere Grenze für die interne Energie der selektierten Ionensorte. Dies heißt, dass Kationen, die in der kondensierten Phase instabil sind, selektiert werden können und ihre spektralen, thermodynamischen oder kinetischen Eigenschaften charakterisiert werden können.

Der Mechanismus der Clustererzeugung war hierbei von höchster Wichtigkeit: die spektralen Eigenschaften, beobachtet bei Komplexen, die in der EI-Clusterionenquelle produziert wurden, unterscheidet sich qualitativ von den, die über REMPI produziert wurden. Es konnte tatsächlich gezeigt werden, dass die EI-Clusterionenquelle überwiegend die stabilste Struktur eines gegebenen Clusterions produziert, während die REMPI-Clusterionenquelle normalerweise geladene Komplexe mit den Strukturen produziert, die den stabilsten Strukturen der entsprechenden Neutralcluster ähnlich sind. Dieses zeigt, dass die EI-Quelle sich im Allgemeinen besser als die Photoionisation eignet, um das globale Minimums der Kationkomplexe spektroskopisch zu beschreiben.

Apart from the results presented in this work, a number of other experimental investigations have been carried out on the same experimental setup. For the first time, the spectra of the protonated carbonic acid and of its isomeric $H_3O^+ \cdots CO_2$ have been recorded.[4] The investigation has been done via tagging the charged species with a weakly bound Ar ligand. The microsolvation of the protonated carbonic acid and of $H_3O^+ \cdots CO_2$ in Ar and CO_2 has also been investigated and the results are currently prepared for publication. Also the weakly bound complexes of phenol cation and Kr have been investigated in the range of the O-H stretch vibration.[5] Like for all other $Ph^+ \cdots L$ complexes previously investigated, it was found that the REMPI-IRPD allows for only limited amounts

of OH-bound complexes to be produced. The ligand-specific frequency shift of the O-H stretch vibration (Δv_{OH}) was found to be in line with the prediction based on a linear dependence of the Δv_{OH} on the PA of the ligand.

Keeping in mind the results of the IRPD investigations previously done as well as the ones presented in this works and, few directions of possible future studies are suggested in the following.

It might be interesting to further expand the IRPD studies of mass-selected $1\text{-Np}^{+}\cdots L_n$ (reported in *Chapter 3*) and $\text{Ph}^{+}\cdots L_n$ (L = Ar, N_2) with similar studies of $2\text{-Np}^{+}\cdots L_n$, $\text{resorcinol}^{+}\cdots L_n$, and $\text{hidroquinone}^{+}\cdots L_n$. Such an investigation is accessible with the present experimental setup and might give further insight in the solvation mechanisms and the competition between two similarly acidic groups. Similar studies on the protonated 2-Np, resorcinol, and hidroquinone would also enable further testing of the ISA theory used in *Chapter 4*.

Probing the acidity of the ionized and protonated imidazole (*Chapter 5* and *Chapter 6*) must be considered as valuable steps in understanding chemical reactions involving biologically relevant systems containing such a molecular building block. As the interaction of Im(H)^{+} with water is of large biological interest, further IRPD studies might shed light on its microhydration and, maybe, on the proton transfer between water clusters and Im. The expansion of these studies to other biomolecular building blocks (like 7-azaindole, pyrrole, furan) will lead to a collection of experimental results which can probably be combined into a comprehensive picture of spectroscopically-derived properties of fundamental biomolecules (DNA bases, amino acids, etc.).

The present IRPD investigations, done in a tandem mass spectrometer coupled with an electron impact ionization ion source, have underlined few limitations of the experimental apparatus used. Maybe the most important limitation is the inability of producing high enough densities of biologically relevant species in the gas phase. Indeed, given the low vapor pressure of the most interesting biomolecules (DNA bases like adenine or guanine), it is essential to use different mechanisms for bringing them in gas phase and ionizing / protonating them. Thus, the use of an electrospray ion source or of a laser ablation ion source can open a lot of new opportunities for investigating interesting biomolecules. Another improvement which will increase the efficiency of observing ions of low-vapor pressure substances is the modification of the octopole ion guide into an ion trap. Along the same line, the replacement of the integrators used for recording the IRPD signals with event counters might give another boost to the sensitivity of the setup. Finally,

the extension of the operating range of the OPO laser system (down to under 1800 cm^{-1}) might allow for observation not only of proton stretch vibrations, but also of other vibrational modes.

References

[1] Andrei H.S., Solca N., Dopfer O. *Phys. Chem. Chem. Phys.* **6** (2004) 3801

[2] Andrei H.S., Solca N., Dopfer O. *J. Phys. Chem. A* **109** (2005) 3598

[3] Andrei H.S., Solca N., Dopfer O. *Chem. Phys. Chem.* **7** (2006) 107

[4] Andrei H.S., Nizkorodov S.A., Dopfer O. *Angew. Chem. Int. Ed.* **46** (2007) 4754

[5] Takeda A., Andrei H.S., Miyazaki M., Ishiuchi S.-I., Sakai M., Fujii M., Dopfer O. *Chem. Phys. Lett.* **443** (2007) 227

List of acronyms

ADIR	Autoionization Detected Infrared	PIE	Photoionization Efficiency
AIM	Atoms in Molecules	PIRI	Photoinduced Rydberg Ionization
BSSE	Basis Set Superposition Error	REMPI	Resonance Enhanced Multiphoton Ionization
CID	Collision Induced Dissociation	RFO	Rational Function Optimization
EI	Electron Impact	UV	Ultraviolet
FEL	Free Electron Laser	ZEKE	Zero Electron Kinetic Energy
FC	Franck-Condon	ZPE	Zero-point Energy
FWHM	Full Width Half Maximum		
IR	Infrared		
IRPD	Infrared Photodissociation	$A^{(+)}$	aromatic molecule (cation)
ISA	Independent Substituent Approximation	AH^+	protonated aromatic molecule
KTP	Potassium Titanyl Phosphate	L	ligand atom or molecule
LID	Laser Induced Dissociation	$An^{(+)}$	aniline (cation)
MALDI	Matrix Assisted Laser Desorption / Ionization	$Bz^{(+)}$	benzene (cation)
MATI	Mass Analyzed Treshold Ionization	BzH^+	protonated benzene
MD	Metastable Decay	His	histidine
MO	Master Oscillator	Im	imidazole
Nd:YAG	Neodym Yttrium Aluminium Granat	ImH^+	protonated imidazole
NRO	Non Resonant Oscillator	$In^{(+)}$	indole (cation)
OG	Octopole Guide	$Ph^{(+)}$	phenol (cation)
OPA	Optical Parametric Amplifier	PhH^+	protonated phenol
OPO	Optical Parametric Oscillator	Rg	rare gas atom
PA	Proton Affinity	$1\text{-}Np^{(+)}$	1-naphthalenole (cation)
PD	Photodissociation	$1\text{-}NpH^+$	protonated 1-naphthalenole
PES	Potential Energy Surface		

Acknowledgement

I would like to express my gratitude to those who have influenced, directly or indirectly, my course during my PhD.

I would thus like to thank to Prof. Dr. Otto Dopfer for allowing me to work as part of his group. These years will never be forgotten. The financial support of Prof. Dopfer's project came from DFG and must also be acknowleged.

Many thanks have to go to Prof. Dr. Ingo Fischer and to his students (Dr. Thomas Schüßler, Dr. Mattias Zierhut, Stefan Dümmler, Michael Schneider, and many, many others) who have kindly provided me with laboratory equipments which were essential for the good operation of the experimental setup. Dr. Wolfgang Roth was also one the most helpful persons when having to deal with practical aspects of the quantum chemical calculations.

Valuable lessons (not only regarding quantum chemistry) I have received from Prof. Dr. Volker Engel and his students. Thank you Stefanie, thank you Marco, thank you Philipp.

A big nod to Dr. Roland Colditz for his support related to the undergraduate students' laboratory practice.

Many thanks to Dr. Judith Langer who kindly reviewed the German translation of the summary of this work.

Mrs. Ursula Müller, Mrs. Andrée Meyer, Mrs. Gudrun Mühlrath, and Ms. Stefanie Schaubert were not only permanent employees of the Institute but also permanent stops in my never-ending quest to solve administrative problems. Thank you, thank you very much!

Mr. Jürgen Zimmermann and Mr. Rainer Eck in the electronic workshop as well as Mr. Wolfgang Libler, Mr. Gerhard Bömmel, Mr. Thomas Schreckling, Mr. Ralf Kohrmann, AND Mr. Peter Lang in the mechanic workshop were more than helpful in solving the problems which have appeared in the laboratory.

Dr. Nicola Solca proved to really be a friend and helped me understand some of the 'mysteries' of the experiments we were working on during his time in Würzburg. Many thanks, Dottore!

Biggest grin of them all goes to Bernd Küstner, for all the beer and the chats we had together. They helped me figure out many things.

Arguably the most important people I have to thank to are my mother and my wife. They have both been supportive and tolerant, even when things have gone astray.

Lebenslauf

Persönliche Daten

Name	**Horia-Sorin ANDREI**
Staatsangehörigkeit	rumänisch
Alter	33
Anschrift	Universität Bukarest - Facultät für Physik Fachbereich Optik, Spektroskopie, Plasma und Lasers Postfach MG-11 077125 Bukarest-Magurele, Rumänien
Telefon	+49 163 1586094
Fax	+40 21 4208625
E-Mail	hsandrei@phys-chemie.uni-wuerzburg.de horiandrei@yahoo.com

Schulausbildung und Studium

seit 04/2003	**Doktorand** Institut für Physikalische Chemie, Universität Würzburg / Institut für Optik und Atomare Physik, Technische Universität Berlin Thema: *Infrared photodissociation spectroscopy of ionic hydrocarbons: microsolvation and protonation sites*
10/1997 - 02/1999	**Master of Science** Universität Bukarest, Fachbereich Physik Schwerpunkt: Optik, Spektroskopie, Plasma und Lasers Dissertation: *Electron Energy Distribution Function. Modeling.*
10/1992 - 06/1997	**Bachelor of Science** Universität Bukarest, Fachbereich Physik Schwerpunkt: Optik, Spektroskopie, Plasma und Lasers Diplomarbeit: *White-Light Lasers.*
10/1988 - 06/1992	"Octav Onicescu" Oberschule, Bukarest, Rumänien

Berufserfahrung

seit 04/2006	Wissenschaftlicher Mitarbeiter Institut für Optik und Atomare Physik, Technische Universität Berlin
04/2003 - 03/2006	Wissenschaftlicher Mitarbeiter Institut für Physikalische Chemie, Universität Würzburg
09/2000 - 03/2003	Assistant Professor II, Universität Bukarest, Facultät für Physik
10/1998 - 08/2000	Teaching Assistant, Universität Bukarest, Facultät für Physik

Publications list

papers

IR spectra of phenol$^+$···Kr_n (n = 1, 2) cluster cations: evidence for photoionization-induced $\pi \rightarrow$H isomerization
A. Takeda, H.-S. Andrei, M. Miyazaki, S. Ishiuchi, M. Sakai, M. Fujii, O. Dopfer
Chem. Phys. Lett. **443** (2007) 227-231

IR spectra of protonated carbonic acid and its isomeric H_3O^+···CO_2 complex
H.-S. Andrei, S. A. Nizkorodov, O. Dopfer
Angew. Chem. Int. Ed. **46** (2007) 4754-4756

Microhydration of protonated biomolecular building blocks: IR spectra of protonated imidazole-(water)$_n$ clusters
H.-S. Andrei, N. Solcà, O. Dopfer
Chem. Phys. Chem. **7** (2006) 107-110

Interaction of ionic biomolecular building blocks with nonpolar solvents: Acidity of the imidazole cation (Im^+) probed by IR spectra of Im^+···L_n complexes (L = Ar, N_2, n < 4)
H.-S. Andrei, N. Solcà, O. Dopfer
J. Phys. Chem. A **109** (2005) 3598-3607

Ionization-induced switch in aromatic molecule-nonpolar ligand recognition: Acidity of 1-naphthol$^+$ (1-Np$^+$) rotamers probed by IR spectra of 1-Np$^+$···L_n complexes (L = Ar, N_2, n≤5)
H.-S. Andrei, N. Solcà and O. Dopfer
Phys. Chem. Chem. Phys. **6** (2004) 3801-3810

posters

Spectroscopic Studies of Ionic Hydrogen Bonds of Biophysical Interest
N. Solcà, H.-S. Andrei, and **O. Dopfer**
XVth International Conference on Horizons in Hydrogen Bond Research
Berlin, 16.09 - 21.09.2003

Spectroscopic Characterization of Protonated Imidazole Clusters
N. Solcà, **H.-S. Andrei** und O. Dopfer
Frühjahrstagung der Deutschen Physikalischen Gesellschaft
München, 22.03. - 26.03.2004

Struktur elementarer Reaktionsintermediate: IR Spektroskopie protonierter Aromaten unter kontrollierten Solvatationsbedingungen
O. Dopfer, N. Solcà, H.-S. Andrei
103. Hauptversammlung der Deutschen Bunsen-Gesellschaft für Physikalische Chemie e. V.
Dresden, 20.05 - 22.05.2004

Hydration of Protonated Biomolecular Building Blocks: IR spectra of Protonated Imidazole Clusters

H.-S. Andrei, N. Solcà, **O. Dopfer**
104. Hauptversammlung der Deutschen Bunsen-Gesellschaft für Physikalische Chemie e.V.
Frankfurt, 05.05 - 07.05.2005

IR spectrum of the ethyl cation: nonclassical versus classical structure
H.-S. Andrei, H. Kuchelmeister, N. Solcà, **O. Dopfer**
105. Hauptversammlung der Deutschen Bunsen-Gesellschaft für Physikalische Chemie e. V.
Erlangen, 25.05 - 27.05.2006

IR spectrum of the ethyl cation ($C_2H_5^+$): nonclassical versus classical structure
H.-S. Andrei, H. Kuchelmeister, N. Solcà and **O. Dopfer**
XXVIIIth European Congress on Molecular Spectroscopy
Istanbul, 03.09 - 08.09.2006

oral presentations

IR spectrum of the ethyl cation: nonclassical versus classical structure
H.-S. Andrei, H. Kuchelmeister, N. Solcà, and Otto Dopfer
Frühjahrstagung der Deutschen Physikalischen Gesellschaft
Frankfurt, 13.03. - 17.03.2006

Solvation of Protonated Biomolecular Building Blocks: IR spectra of Protonated Imidazole Clusters
H.-S. Andrei, N. Solcà, and O. Dopfer
Frühjahrstagung der Deutschen Physikalischen Gesellschaft
Berlin, 04.03. - 09.03.2005

IR Spektren von (protonierten) Naphthol Clustern
N. Solcà, H.-S. Andrei und O. Dopfer
Frühjahrstagung der Deutschen Physikalischen Gesellschaft
München, 22.03. - 26.03.2004

Erklärung

Hiermit erkläre ich an Eides statt, dass ich die Dissertation
Infrared photodissociation spectroscopy of ionic hydrocarbons: microsolvation and protonation sites
selbständig angefertigt und keine anderen als die von mir angegebenen Quellen und Hilfsmittel benutzt habe.

Ich erkläre außerdem, dass diese Dissertation weder in gleicher oder anderer Form bereits in einem Prüfungsverfahren vorgelegen hat.

Ich habe früher außer den mit dem Zulassungsgesuch urkundlich vorgelegten Graden keine weiteren akademischen Grade erworben oder zu erwerben versucht.

Würzburg, den 15. August 2007

_____

(Horia - Sorin ANDREI)